Theoretical analysis of the electrostatic interactions between charged polarisable particles



Eric Brazil Lindgren

Department of Theoretical and Physical Chemistry,

University of Nottingham

This thesis is submitted for the degree of

Doctor of Philosophy

October 2017

To my grandfather, Nelio Brazil,

and to the memory of my father, David C. Lindgren.

Acknowledgements

First and foremost, I would like to thank my supervisor, Prof. Elena Besley, for the opportunity of being part of her research group and for the exceptional support and guidance over the past four years. I am also grateful to current and former members of our electrostatics group: Prof. Tony Stace, Dr Ho-Kei Chan and Dr Ivan Derbenev; thank you very much for the productive meetings and conversations. A very special thanks goes to Prof. Benjamin Stamm and Prof. Yvon Maday for the invaluable scientific collaboration and for hosting me in their research institutes in three different occasions. I also would like to thank the School of Chemistry and the University of Nottingham for providing a productive and pleasant studying and working environment, and the CAPES Foundation for the fully funded PhD scholarship, through the Science Without Borders programme. Finally, I am deeply grateful to my wife, Tatiana, for being such an amazing life partner, to my family, and especially to my mother for providing me unfailing support and excellent education throughout my life.

Abstract

Theoretical approaches to calculating electrostatic interactions between charged particles of dielectric materials are presented and applied to diverse examples of electrostatic behaviour. The accuracy of numerical predictions based on the multipole expansion used in calculations of the electrostatic force is discussed. Strict corresponding convergence criteria are established, particularly when addressing problems involving materials with high dielectric constants, large differences in particles size and short inter-particle separation distances. An extensive study of various types of electrostatic interactions is undertaken, with greater stress on the circumstances in which rather counterintuitive events might exist, namely the attraction between like-charged particles, generally dependant on certain degrees of asymmetry in charge density and charge distribution on the surface of the interacting particles, and the repulsion between oppositely charged particles, which involves magnitudes of charge that are below some critical limit and the presence of a sufficiently polarisable medium. Several examples addressing experimental problems, notably the growth mechanism of aerosols in the atmosphere of Saturn's moon Titan, and electrostatic self-assembly processes, are included. Many-particle dynamics simulations of electrostatically driven systems are finally presented through some selected scenarios.

Peer-reviewed publications

The author has contributed to the following related publications:

- H.-K. Chan, **E. B. Lindgren**, A. J. Stace, E. Besley. A general geometric representation of sphere-sphere interactions. *Progress in Theoretical Chemistry and Physics* 29, 29-36 (2015).
  DOI: http://dx.doi.org/10.1007/978-3-319-14397-2.

- **E. B. Lindgren**, H.-K. Chan, A. J. Stace, E. Besley. Progress in the theory of electrostatic interactions between charged particles. *Physical Chemistry Chemical Physics* 18, 5883-5895 (2016).
  DOI: http://dx.doi.org/10.1039/C5CP07709E.

- **E. B. Lindgren**, B. Stamm, H.-K. Chan, Y. Maday, A. J. Stace, E. Besley. The effect of like-charge attraction on aerosol growth in the atmosphere of Titan. *Icarus* 291, 245-253 (2017).
  DOI: http://dx.doi.org/10.1016/j.icarus.2016.12.013.

- C. Harris, J. Baptiste, **E. B. Lindgren**, E. Besley, A. J. Stace. Coulomb fission in multiply charged molecular clusters: Experiment and theory. *Journal of Chemical Physics* 146, 164302 (2017).
  DOI: http://dx.doi.org/10.1063/1.4981918.

Table of contents

List of figures **xv**

List of tables **xxxv**

Nomenclature **xxxvii**

1 Introduction **1**

1.1 An electromagnetic world 1

1.2 Electrostatics and polarisation of matter 3

2 Electrostatic interactions in two-body systems **11**

2.1 Theoretical background 11

2.2 General numerical results 18

2.2.1 Electrostatic force 18

2.2.2 A point charge distribution parallel 24

2.2.3 Electrostatic potential energy 27

2.3 The effects of system's parameters on electrostatic interactions . 29

2.4 Electrostatic interactions with respect to the geometry of the system 33

2.4.1 The scaled surface-to-surface separation parameter 34

2.4.2 Electrostatic force and the scaled surface-to-surface separation parameter 38

2.4.3 Large sphere approximation to an infinite planar surface . 40

2.5 Dimension and scaling of results 41

2.6 Convergence rates 45

2.7 The growth of charged aerosol particles in Titan's atmosphere . . 51
2.7.1 Experimental data and the Cassini–Huygens mission . . . 52
2.7.2 The potential contribution of like-charge attraction 53

3 Electrostatic interactions in the presence of a dielectric medium 61
3.1 Theory for implementing the presence of a medium 62
3.2 General numerical results 64
3.3 The significance of the medium in electrostatic self-assembly processes 71
3.3.1 Current state of research 71
3.3.2 A self-assembly case involving neutral and charged objects 72
3.3.3 A self-assembly case involving oppositely charged objects . 75

4 Electrostatic interactions in many-body systems 81
4.1 Theory 83
4.1.1 Representation in terms of integral equations 85
4.1.2 Discretisation 88
4.1.3 Electrostatic potential energy 91
4.1.4 Electrostatic force 92
4.2 General numerical results 95
4.3 Nonadditivity of the electrostatic force in many-body systems . . 100
4.4 Calculations for systems with a larger number of particles 103
4.4.1 Halite lattice and estimation of Madelung constant 103
4.4.2 Electrostatic self-assembly of polystyrene microspheres . . 105
4.5 Newtonian particle dynamics 110
4.5.1 Physics engine 110
4.5.2 Bouncing frequency of attracting particles 111
4.5.3 A dynamics example of electrostatic self-assembly 114
4.5.4 Effusion through a charged array 124

5 Outlook 129

References **135**

Appendix A **147**

A.1 Matrix solution for the multipole moment coefficients 147

A.2 Benchmark of the two-body formalism related computer program 151

Appendix B **155**

B.1 Effective electric dipole moment of a polarised particle 155

Appendix C **159**

C.1 Benchmark of the many-body formalism related computer program 159

List of figures

1.1 (a) Classical view of a neutral and unperturbed atom, consisted of a positive nucleus surrounded by a negative cloud of electrons. (b) Same atom, polarised by an electric field **E**, created by an external positive point charge. Note the creation of a dipole **p**, aligned and pointing in the same direction of the electric field. 6

1.2 (a) Illustration of a neutral and unperturbed object made of a dielectric material. (b) View of the same object, polarised by an external electric field **E**. Note that, while in the bulk (shaded in grey) the opposite charges corresponding to adjacent dipoles tend to cancel each other out, at the surfaces there is no cancellation, which leads to the accumulation of a special type of charge known as *bound charges*. 7

2.1 A general geometric representation of two interacting spherical dielectric particles suspended in vacuum. Dielectric constants, charges, radii, and the polar angles of particles 1 and 2 are denoted as k_1, q_1, a_1, β_1 and k_2, q_2, a_2, β_2, respectively. The centre-to-centre separation is defined as h and the corresponding surface-to-surface separation is given by $s = h - a_1 - a_2$. 12

2.2 (a) Plot of the electrostatic force F as function of the surface-to-surface separation s for a case of charged particle − neutral particle interaction. The first particle has a nominal charge of +10, whilst the second particle is neutral. The two particles are equal-sized, with a nominal radii of 1 and each curve corresponds to a distinct value of the particles's dielectric constants, $k_1 = k_2$. (b) Plot of the total surface charge densities σ_i $(i = 1, 2)$ as function of the polar angles β_i, corresponding to the curve where $k_1 = k_2 = 20$ and $s = 0.1$. Inset shows a geometrical representation of the problem, with the total surface charge density (charge per unit area) mapped out for each of the particles. Blue tones denote positive charge densities, and red tones denote negative charge densities. 19

2.3 (a) Plot of the electrostatic force F as function of the surface-to-surface separation s for a case of opposite-charge interaction. The first particle has a nominal charge of +10, whilst the second particle has an opposite charge of -10. The two particles are equal-sized, with a nominal radii of 1 and each curve corresponds to a distinct value of the particles's dielectric constants, $k_1 = k_2$. (b) Plot of the total surface charge densities σ_i $(i = 1, 2)$ as function of the polar angles β_i, corresponding to the curve where $k_1 = k_2 = 20$ and $s = 0.1$. Inset shows a geometrical representation of the problem, with the total surface charge density mapped out for each of the particles. Blue tones denote positive charge densities, and red tones denote negative charge densities. 20

2.4 (a) Plot of the electrostatic force F as function of the surface-to-surface separation s for a case of like-charge interaction. The two particles are identical, having a nominal charge of $+10$ and a nominal radii of 1. Each curve corresponds to a distinct value of the particles's dielectric constants, $k_1 = k_2$. (b) Plot of the total surface charge densities σ_i $(i = 1, 2)$ as function of the polar angles β_i, corresponding to the curve where $k_1 = k_2 = 20$ and $s = 0.1$. Inset shows a geometrical representation of the problem, with the total surface charge density mapped out for each of the particles. . 21

2.5 (a) Plot of the electrostatic force F as function of the surface-to-surface separation s for a case of like-charge interaction, where it exists an asymmetry in the given free charge. The first particle has a nominal charge of $+10$ while the second particle has a nominal charge of $+20$. Both particles have a nominal radii of 1, and each curve corresponds to a distinct value of the particles's dielectric constants, $k_1 = k_2$. (b) Plot of the total surface charge densities σ_i $(i = 1, 2)$ as function of the polar angles β_i, corresponding to the curve where $k_1 = k_2 = 20$ and $s = 0.1$. Inset shows a geometrical representation of the problem, with the total surface charge density mapped out for each of the particles. Blue tones denote positive charge densities, and red tones denote negative charge densities. . 22

2.6 (a) Plot of the electrostatic force F as function of the surface-to-surface separation s for a case of like-charge interaction, where it exists an asymmetry in size. Both particles carry the same nominal charge of $+10$ but the second one is two times larger than the first, with a nominal radius of 2. Each curve corresponds to a distinct value of the particles's dielectric constants, $k_1 = k_2$. (b) Plot of the total surface charge densities σ_i $(i = 1, 2)$ as function of the polar angles β_i, corresponding to the curve where $k_1 = k_2 = 20$ and $s = 0.1$. Inset shows a geometrical representation of the problem, with the total surface charge density mapped out for each of the particles. Blue tones denote positive charge densities, and red tones denote negative charge densities. 23

2.7 (a) Plot of the electrostatic force F, given in piconewtons (pN), as function of the distance h between the centre of the circular distribution of positive charges and the positive test charge q_{t}, given in nanometres (nm). (b) Schematic illustration of the problem, where each point charge is visually of finite size, for clarity, and coloured in blue. 25

2.8 (a) Plot of the electrostatic force F (pN), as function of the distance h (nm) between the centre of the circular distribution of charges and the test charge q_{t}. (b) Schematic illustration of the problem, where each point charge is visually of finite size, the point charges with magnitude $+3$ e are grey coloured, the ones with magnitude $+1$ e are coloured in blue, and the ones with magnitude -1 e are coloured in red. 26

2.9 (a) Plots of the electrostatic potential energy U, and (b) electrostatic force F, as function of the surface-to-surface separation s between two interacting particles, for cases of stable (solid line; $a_2 = 3$, $q_1 = 30$), metastable (dashed line; $a_2 = 2$, $q_1 = 20$) and unstable (dotted line; $a_2 = 1$, $q_1 = 10$) interactions. The dielectric constant of both particles, the radius particle 1, and the charge of particle 2 are maintained fixed at $k_1 = k_2 = 20$, $a_1 = 1$ and $q_2 = 10$, respectively. The presented results are dimensionless. Note that the scale of the x-axis is different on each plot. 28

2.10 Contour maps of the electrostatic force (pN) as a function of the charge ratio q_2/q_1, and radius ratio a_2/a_1, for a pair of like-charged particles separated by a fixed distance of $s = 0.01$ μm and with different values of the dielectric constant: (a) $k_1 = k_2 = 2$, (b) 5, (c) 10, (d) 40, (e) 80 and (f) 1000. The radius of particle 1 is fixed at $a_1 = 1$ μm and its charge at $q_1 = 10^3$ e. Black coloured curves denote the points where the electrostatic force is zero. Equivalent zero force curves for two conducting particles are also shown in light blue colour. 30

2.11 Contour maps of the electrostatic force (pN) as a function of the charge ratio q_2/q_1, and radius ratio a_2/a_1, for a pair of like-charged particles at various surface-to-surface separations: (a) $s = 5$ μm, (b) 1, (c) 0.1, (d) 0.01, (e) 0.001 and (f) 0.0001. The value of the dielectric constant of the particles, the radius of particle 1 and its charge are held fixed at $k_1 = k_2 = 1000$, $a_1 = 1$ μm and $q_1 = 10^3$ e, respectively. Zero force curves are shown in black, and equivalent zero force curves for two conducting particles are shown in blue. . 32

2.12 The six different possible geometric combinations of pairwise interactions involving point particles, spheres and planes. 34

2.13 The bispherical coordinate system. (a) Illustration of how the various length quantities, c_1, c_2, d_1 and d_2 are related to the inter-focal separation 2a, centre-to-centre separation h, and surface-to-surface separation s, and (b) how the position of an arbitrary point X in space is described with reference to the two foci. 35

2.14 Three-dimensional plot of the scaled surface-to-surface separation s^*, as function of the radii of the spheres divided by the surface-to-surface separation s. It can be noted that, as the radius of both spheres becomes much larger than s, the value of s^* approaches zero. Conversely, as the spheres's radii become much smaller than s, the value of s^* approaches unity. 37

2.15 A geometric representation of two spheres with radii (a) $a_1 = a_2 = 5$ mm, (b) $a_1 = 5$ μm and $a_1 = 7.5$ μm, and (c) $a_1 = a_2 = 5$ nm, separated by a fixed surface-to-surface separation $s = 10$ μm. The bar in the bottom represents the scale of the scaled surface-to-surface separation, s^*, and the corresponding value of this parameter is given for each of the three cases. 38

2.16 Contour maps of the electrostatic force (pN) between a pair of equal-sized, like-charged particles, with dielectric constants (a) $k_1 = k_2 = 1000$ and (b) $k_1 = k_2 = 10$. The force is plotted as a function of the scaled surface-to-surface separation s^* and the charge ratio q_2/q_1, with $a_1 = a_2 = 1$ μm and $q_1 = 10^3$ e. The regions of attractive and repulsive forces are separated by a thin black solid line, which denotes the cases of zero force. 39

2.17 (a) Calculated electrostatic force (pN) as function of the radius ratio between a small charged particle with fixed radius $a_1 = 1$ μm and charge $q_1 = 10^3$ e, and a larger neutral particle (that should mimic an infinite planar surface) with varying radius a_2, separated by a distance of $s = 1$ μm. The line with hollow circle markers denotes the force obtained by the formalism based on bispherical coordinates, considering an actual (neutral) infinite planar surface. (b) Percentage error between the forces given in (a) as function of the radius ratio. 41

2.18 Plots of the (a) electrostatic force (pN) and (b) interaction energy (eV) as function of the radius ratio a_2/a_1, where $a_1 = 1$ μm and a_2 accounts for the only variable of the system. The other parameters are held fixed at $k_1 = k_2 = 10$, $q_1 = q_2 = 10^3$ e and $s = 0.01$ μm. Inset shows the total surface charge density ($\mathrm{e} \cdot \mu\mathrm{m}^{-2}$) mapped out for each of the particles, corresponding to the point where $a_2/a_1 = 1.5$. 43

2.19 Plots of the (a) electrostatic force (pN) and (b) interaction energy (eV) as function of the radius ratio a_2/a_1, for the same case addressed in Figure 2.18, with the difference that quantities related to the geometry of the system, a_1 and s, have been multiplied by a factor $\alpha = 10$. 44

2.20 Plots of the (a) electrostatic force (pN) and (b) interaction energy (eV) as function of the charge ratio q_2/q_1, where $q_1 = 10^3$ e and q_2 accounts for the only variable of the system. The other parameters are held fixed at $k_1 = k_2 = 10$, $a_1 = a_2 = 10$ μm and $s = 0.01$ μm. Inset shows the total surface charge density ($\mathrm{e} \cdot \mu\mathrm{m}^{-2}$) mapped out for each of the particles, corresponding to the point where $q_2/q_1 = 1.5$. 44

2.21 Plots of the (a) electrostatic force (pN) and (b) interaction energy (MeV) as function of the charge ratio q_2/q_1, for the same case addressed in Figure 2.20, with the difference that q_1 has been multiplied by a factor $\alpha = 10$. 45

2.22 Plots of the minimum number of terms N in the multipole expansion of Equation 2.16, required to obtain a converged electrostatic force between two particles with a precision of ten significant figures, as function of the (a) surface-to-surface separation s, (b) radius ratio a_2/a_1, and (c) and (d) dielectric constants $k_1 = k_2$, determined using the solution based on spherical coordinates (curves with hollow circle markers) and the equivalent solution based on bispherical coordinates (curves with hollow square markers). In all instances, the particles's parameters are fixed at $k_1 = k_2 = 40$, $a_1 = 2$, $a_2 = 1$, $q_1 = 2 \times 10^3$, $q_2 = 1 \times 10^3$, and $s = 0.1$, unless the respective parameter is being considered as a variable in the plot. In (b), a_1 is still fixed and a_2 is allowed to vary. 47

2.23 Vector plots of the electric field related to an interaction between two equal-sized and oppositely charged particles, with dielectric constants (a) $k_1 = 1$, $k_2 = 80$, (b) $k_1 = 10$, $k_2 = 1000$, and (c) $k_1 = 20$, $k_2 = 10^6$. Note that the size of the arrows is proportional to the magnitude of the field at the corresponding point and the particle $i = 1$ is placed at the bottom. As can be seen, as the dielectric constant of a particle increases, the arrow in its interior and, hence, the magnitude of the corresponding electric field, diminishes. 49

2.24 Plot of the minimum number of terms N in the multipole expansion, required to obtain a converged electrostatic force between two particles with a precision of ten significant figures, as function of the charge ratio q_2/q_1, where $q_1 = 2 \times 10^3$. The remaining parameters are fixed at $k_1 = k_2 = 40$, $a_1 = 2$, $a_2 = 1$, and $s = 0.1$. Inset shows an expanded y-axis. Only data points taken from the solution based on spherical coordinates are shown, due to a great similarity to its counterpart in this case. 50

2.25 Plot of the percentage error in the calculated electrostatic force with respect to the reference value (with a precision of ten significant figures) as a function of the number of terms N in the multipole expansion of Equation 2.16. 51

2.26 (a) Maxwell-Boltzmann distribution of the kinetic energy of the particles at the upper and lower Titan's thermosphere average temperatures. (b) Probability (%) that particles, with a thermal energy of kT, will overcome the barrier as function of the latter's magnitude, evaluated for the two extreme temperatures. In the second plot, any point after the maximum value for the x-axis has a corresponding probability that is always lower than 0.5 %. . . . 56

2.27 Plot of the dielectric constant as function of hydrogen cyanide molar fraction for methane/hydrogen cyanide (solid line) and ethane/hydrogen cyanide (dotted line) mixtures. 59

3.1 Electrostatic maps showing regions of repulsive (light purple) and attractive (white) interactions. The electrostatic force has been calculated as a function of the charge ratio, q_2/q_1 and the radius ratio, a_2/a_1, with the radius and charge of particle 1 fixed at $a_1 = 1$ and $q_1 = 1$. The dielectric constants of the particles are $k_1 = k_2 = 10$ and the calculations have been undertaken at a fixed separation distance of $s = 0.1\,a_1$; k_m in each diagram denotes the dielectric constant of the solvent or medium, and the solid deep purple line denotes points where the electrostatic force is zero. . . 65

3.2 (a1−3) Plot of the electrostatic force F as function of the surface-to-surface separation s for cases of neutral particle − charged particle interaction, corresponding to different values of k_m that are lower than that of the particles, as explicit in the figure. The first particle is neutral whilst the second particle has a nominal charge of +10. The two particles are equal-sized, with a nominal radii of 1 and dielectric constants $k_1 = k_2 = 10$. (b1−3) Corresponding plots of the total surface charge densities σ_i $(i = 1, 2)$ as function of the polar angle β_i at a separation of $s = 0.1$. Inset shows a geometrical representation of the problem, with the total surface charge density (charge per unit area) mapped out for each of the particles. Blue tones denote positive charge densities, and red tones denote negative charge densities. 67

3.3 Plots of the electrostatic force and total surface charge density for the same scenario described in Figure 3.2, but corresponding to different values of k_m that are now equal or greater than that of the particles ($k_1 = k_2 = 10$), as explicit in the figure. 69

3.4 Vector plots of the electric field, generated by a positively charged particle, at the vicinity of a neutral particle, for three different values of the dielectric constant of the medium: (a) $k_{\mathrm{m}} = 1$, (b) $k_{\mathrm{m}} = 10$, and (c) $k_{\mathrm{m}} = 80$. In each plot, the size of the arrows is proportional to the magnitude of the field at the corresponding point, and the charged particle (not shown) is situated above the region plotted. The particles are equal-sized, with a nominal radii of 1, dielectric constants $k_1 = k_2 = 10$, and separated by a distance of $s = 1.0$. 71

3.5 Plot of the electrostatic force F (nN) as a function of the surface-to-surface separation s between a neutral alumina spherical particle and a charged nano-diamond surface, immersed in a solvent with dielectric constant (a) $k_{\mathrm{solvent}} = 1.86$, and (b) $k_{\mathrm{solvent}} = 20$. The particle has a radius of 25 nm and a dielectric constant $k_{\mathrm{particle}} = 9.9$. The surface charge density of the planar surface is $+1\,\mathrm{e}\cdot\mathrm{nm}^{-2}$, and the dielectric constant is $k_{\mathrm{surface}} = 5.3$. 73

3.6 Illustration of the electrostatic interactions presented in Figure 3.5, showing equipotential lines, the electric field, the effective dipole moment in the neutral alumina particle, values of the effective surface charge density at selected points, and values of the electric potential at selected points away from the surface. Note the switch in the direction of the effective dipole moment when the dielectric constant of the solvent changes from (a) $k_{\mathrm{solvent}} = 1.86$ to (b) $k_{\mathrm{solvent}} = 20$. 74

3.7 Schematic illustration of the POM − surface interaction. In (a) the medium/solvent has a dielectric constant of 1 (vacuum) and in (b) the medium/solvent has a dielectric constant of 20. The planar surface has a surface charge density of $0.05\,\mathrm{e}\cdot\mathrm{nm}^{-2}$ and the POM particle has a net charge of -12 e. The total charge density on the planar surface, $\sigma_{\mathrm{surface}}$ (dashed curve), and on the POM particle, σ_{POM} (solid curve), are also shown for each interaction case: for $\sigma_{\mathrm{surface}}$, the x-axis denotes the radial position y, with $y = 0$ indicating the centre of POM projected on the surface; for σ_{POM}, the x-axis denotes the polar angle (β), where $\beta = 0$ represents the nearest point to the plane. The colour shades on both objects reflect qualitatively the calculated charge distribution, however the colour scale is different in each example. 77

4.1 Geometric representation of the system comprised of M non-overlapping spherical particles $\Omega_1, \ldots, \Omega_M$ with radius a_i, dielectric constant k_i, and centred at $\mathbf{r}_i$, surrounded by a homogeneous medium of dielectric constant k_0. 83

4.2 Plot of the total electrostatic force F acting on the left-hand particle as function of the surface-to-surface separation s, for a case of charged particle − neutral particle interaction. The particle in the centre has a nominal charge of +1, whilst the left- and right-hand particles are neutral. The three particles are equal-sized, with nominal radii of 1 and each curve corresponds to a distinct value of the particles's dielectric constants, $k_1 = k_2 = k_3$. Also shown is a geometrical representation of the problem, with the total surface charge density (charge per unit area) mapped out for each of the particles, corresponding to the curve where $k_1 = k_2 = k_3 = 20$ and $s = 0.2$. 96

4.3 Plot of the total electrostatic force F acting on the left-hand particle as function of the surface-to-surface separation s, for a case of opposite-charge interaction. In (a) the particle at the centre has a nominal charge of +1, while the left- and right-hand particles have nominal charges of -1. In (b) the particle at the centre has a nominal charge of +0.01, whilst the left and right particles have nominal charges of -10. In all cases the particles are equal-sized, with nominal radii of 1 and each curve corresponds to a distinct value of the particles's dielectric constants, $k_1 = k_2 = k_3$. Inset shows a geometrical representation of the problem, with the total surface charge density mapped out for each of the particles, corresponding to the curve in (b) where $k_1 = k_2 = k_3 = 20$ and $s = 0.2$. 97

4.4 Plot of the total electrostatic force F acting on the left-hand particle as function of the surface-to-surface separation s, for a case of like-charge interaction. In (a) all particles are identical, with a nominal charge of +1 and nominal radius of 1. In (b) all particles have a nominal charge of +1, the central particle has a nominal radius of 3, whilst the left- and right-hand particles have a nominal radius of 1. Each curve corresponds to a distinct value of the particles's dielectric constants, $k_1 = k_2 = k_3$, and the inset shows a geometrical representation of the problem, with the total surface charge density mapped out for each of the particles, corresponding to the curve in (b) where $k_1 = k_2 = k_3 = 20$ and $s = 0.2$. Note that the visual scale differs from that employed in the two previous figures. 98

4.5 Plot of the total electrostatic force F acting on the left-hand particle as function of the surface-to-surface separation s, for another case of like-charge interaction. In (a) all particles are identical, with a nominal charge of $+1$ and nominal radius of 1. In (b) all particles have a nominal radius of 1, but the left-hand particle has a nominal charge of $+3$, whilst the particles on the right-hand each have a nominal charge of $+1$. Each curve corresponds to a distinct value of the particles's dielectric constants, $k_1 = k_2 = k_3$, and the inset shows a geometrical representation of the problem, with the total surface charge density mapped out for each of the particles, corresponding to the curve in (b) where $k_1 = k_2 = k_3 = 20$ and $s = 0.2$. 99

4.6 Schematic illustration of the electrostatic interaction between three non-polarisable particles placed at the vertices of an equilateral triangle of side $h = 3$. The three upper diagrams represent an isolated pairwise interaction in the absence of the third particle, whose phantom location is shown as a dashed circle, and the bottom diagram represents the overall interaction, involving all three particles. The x and y components of the force are shaded in grey, while the total force is denoted in black. Accordingly, the arrows represent unit vectors (not in the same scale of the other length quantities, for clarity), portraying the direction of each force, whose corresponding absolute magnitude is displayed right below in each case. 101

4.7 Schematic illustration of the same system considered in Figure 4.6, but with the key difference that the particles are polarisable, with dielectric constants $k_1 = k_2 = k_3 = 20$. Clearly shown is the total surface charge density, mapped out for the particles, assuming a different distribution for each of the depicted diagrams. Values within brackets denote absolute force magnitudes that would be obtained if such interaction obeyed the principle of superposition, while values without brackets denotes the real force. 102

4.8 Halite ('rock-salt') structure of sodium chloride (NaCl), where the sodium cation is depicted in yellow and the chlorine anion in blue. Shown are the first three possible cubic structures starting with the unit cell. 103

4.9 (a) Semi-log plot of the estimated lattice energy and (b) estimated Madelung constant, as function of the number of particles M in the structure. The sodium cation is represented by a sphere of radius 1.02 Å carrying a positive elementary charge, and the chlorine anion is represented by a sphere of radius 1.81 Å carrying a negative elementary charge. Unlike some previous calculations, these results are not dimensionless, hence, the actual value of Coulomb's constant has been used. The lattice energy is presented as the Coulomb interaction added by the Born forces component from Born-Landé equation. 104

4.10 Plot of the interaction energy U (J) as function of the amount of charge q_{1layer} (nC) on each of the 339 10 μm-radius microspheres that constitute the particles layer, for three different degrees N of spherical harmonics utilised in the truncated series. Placed on the right is an illustration of the system, with the total surface charge density mapped out for each of the particles. 107

4.11 Interaction potential energy U (J) surfaces, calculated as function of the amount of charge, q_{1layer} and q_{2layer}, on each particle that constitutes the first and second layer, respectively, for three different degrees N of spherical harmonics utilised in the truncated series. Shown are only the regions of surfaces where the energy is negative, so accordingly the flat parts represent regions of positive energy that have been clipped out, for clarity. Placed on the centre-right is an illustration of the system, with the total surface charge density mapped out for each of the particles. 109

4.12 Plot of the interaction energy U as function of simulation time t for distinct values of the particles's dielectric constants, $k_1 = k_2$. Each collision is treated as being perfectly elastic, where CR = 1. Diagram on the right shows a geometrical representation of the bouncing cycle. 112

4.13 Plot of the interaction energy U as function of simulation time t for distinct values of the particles's dielectric constants, $k_1 = k_2$. Each collision is treated as being partially elastic, where CR = 0.9. Diagram on the right shows a geometrical representation of the bouncing cycle. 114

4.14 Geometric representation of a system comprised of a 500 nm-radius particle fixed at the centre of a volume contained by a closed box, and eight surrounding 100 nm-radius free to move particles, placed initially at the vertices and half-sides of a virtual square situated on the $x - y$ plane and whose centre coincides with the one of the box. 116

4.15 Snapshots of a 1000 μs dynamics simulation involving a 500 nm-radius particle with 25 e of charge, and eight 100 nm-radius particles, each with -1 e of charge. Diagram in the bottom right corner shows the path traced by the particle that is initially placed at the origin. The spectrum of colours goes from deep blue to bright yellow, respectively representing the smallest and largest value of surface charge density in each frame. 118

4.16 Plots of the (a) electrostatic interaction energy U (eV), and (b) RMS speed (m/s), as function of time t (μs) for the simulation presented in Figure 4.15. 119

4.17 Snapshots of a 1000 μs dynamics simulation involving a 500 nm-radius particle with 25 e of charge, and eight neutral 100 nm-radius particles. Diagram in the bottom right corner shows the path traced by the particle that is initially placed at the origin. The spectrum of colours goes from deep blue to bright yellow, respectively representing the lowest and highest value of surface charge density in each frame. 120

4.18 Plots of the (a) electrostatic interaction energy U (eV), and (b) RMS speed (m/s), as function of time t (μs) for the simulation presented in Figure 4.17. 120

4.19 Snapshots of a 1000 μs dynamics simulation involving a 500 nm-radius particle with 25 e of charge, and eight 100 nm-radius particles, each with 1 e of charge. Diagram in the bottom right corner shows the path traced by the particle that is initially placed at the origin. The spectrum of colours goes from deep blue to bright yellow, respectively representing the lowest and highest value of surface charge density in each frame. 121

4.20 Plots of the (a) electrostatic interaction energy U (eV), and (b) RMS speed (m/s), as function of time t (μs) for the simulation presented in Figure 4.19. 122

4.21 Snapshots of a 1000 μs dynamics simulation involving a 500 nm-radius polarisable particle with 1 e of charge, and eight 100 nm-radius particles, each with 4 e of charge. Diagram in the bottom right corner shows the path traced by the particle that is initially placed at the origin. The spectrum of colours goes from deep blue to bright yellow, respectively representing the lowest and highest value of surface charge density in each frame. 123

4.22 Plots of the (a) electrostatic interaction energy U (eV), and (b) RMS speed (m/s), as function of time t (μs) for the simulation presented in Figure 4.21. 123

4.23 Geometric representation of a system comprised of a box with an opening in its far right side, a two-dimensional fixed array consisted of nine 200 nm-radius particles, and 4 different, free to move 100 nm-radius particles, initially positioned at the innermost side of the box. 125

4.24 Selected snapshots of a 1000 μs dynamics simulation involving an unmovable array of equally spaced 200 nm-radius non-polarisable particles, each carrying 4 e of charge, and a set of four different 100 nm-radius polarisable particles, with constituents carrying -1, 0, 0.1, and 1 e of charge, all placed in a box with an opening in its far right side. Diagram in the bottom right corner shows the path traced by the particle that is initially placed at a position that is closest to the origin. The spectrum of colours goes from deep blue to bright yellow, respectively representing the lowest and highest value of surface charge density in each frame. 126

4.25 Plots of the (a) electrostatic interaction energy U (eV), and (b) RMS speed (m/s), as function of time t (μs) for the simulation presented in Figure 4.24. 127

A.1 (a) Plot of the wall time (s) as function of the number of terms N in the multipole expansion. (b) Equivalent log-log plot, showing the approximately quadratic scaling behaviour. 153

A.2 Plot of the wall time (s) to compute each component and solve the linear system (Equation A.19). The y-axis in the right-hand side reflects the percentage of computation time with respect to the total wall time. 153

B.1 Geometric representation of the various relevant quantities to the calculation of the effective dipole moment of a polarised spherical particle. 156

C.1 (a) Plot of the wall time (s) as function of the number of particles M in the system. Although visually indistinguishable, the elapsed time in the FMM calculation varies from ≈ 0.8 to 1.2 seconds. (b) Log-log plot of the calculation performed without the FMM, showing its quadratic scaling profile. 160

C.2 (a) Plot of the wall time (s) as function of the number of particles M in the system, for various curves representing different Tree Heights in the FMM calculation. (b) Log-log plot of the piecewise composition of parabolic profiles, each corresponding to a particular value of Tree Height, showing that a regular effective linear scaling can be obtained. 160

C.3 (a) Plot of the wall time (s) as function of the degree of spherical harmonics N utilized in the truncated series. Although visually indistinguishable, the elapsed time in the axisymmetric calculation varies from ≈ 0.03 to 3 seconds. (b) Log-log plot of both curves, showing that an imposition of symmetry reduces the scaling profile from $\approx N^4$ to N^2. 161

List of tables

2.1 Calculated energy barriers (eV) between two interacting like-charged, dielectric particles, for a range of radii (nm) and charge (e). White, light and dark grey shades denote stable, metastable, and unstable interactions, respectively. The charge q_1 and q_2 can be simultaneously regarded as either positive or negative. 55

2.2 Energy barrier (eV) for the case of two interacting dielectric particles as depicted in Table 2.1(b), but with a lower dielectric constant of $k_1 = k_2 = 3$. 57

3.1 The electrostatic force (pN) calculated for the experimental case of an interaction between a Eu-POM and an oppositely charged planar surface at a surface-to-surface separation distance of 1 nm. Calculations have been undertaken using different combinations of charge density on the planar surface (σ_{surface}) and dielectric constant of the solvent (k_{solvent}). The POM particle has a radius of 0.5 nm and an estimated dielectric constant of $k_{\text{POM}} = 10^{\dagger}$. The planar surface has an outer coating of poly(ethylenimine)/poly(styrenesulfonate)/poly(allylamine hydrochloride), with an estimated dielectric constant of $k_{\text{surface}} = 5$. The charge density on the planar surface is in units of $\text{e} \cdot \text{nm}^{-2}$. . 76

Nomenclature

Acronyms / Abbreviations

CR	Coefficient of restitution
FMM	Fast multipole method
PAH	Polycyclic aromatic hydrocarbon
POM	Polyoxometalate
RMS	Root-mean-square
SAM	Self-assembled monolayer

Symbols

α	Polarisability
β	Polar angle
χ_e	Electric susceptibility
ϵ	Permittivity (absolute)
ϵ_0	Permittivity of free space (vacuum)
Γ	Denomination of a particle surface in the many-body formalism
$\mathcal{D}$	Double layer boundary operator
$\mathcal{S}$	Single layer boundary operator

$\mathcal{Y}_{\ell m}$	Spherical harmonics, where $l = 0, 1, 2, \ldots$ and $m = -l, -(l-1), \ldots, 0, \ldots, l-1, l$
Ω	Denomination of a particle in the many-body formalism
Φ	Electric potential
σ	Total surface charge density
σ_b	Surface bound (polarisation) charge density
σ_f	Surface free charge density
$\mathbf{a}$	Acceleration
$\mathbf{D}$	Electric displacement field
$\mathbf{E}$	Electric field
$\mathbf{F}$	Electrostatic force
$\mathbf{r}$	Position
$\mathbf{v}$	Velocity
$\tilde{\mathcal{S}}$	Single layer potential
φ	Azimuthal angle
a	Radius
$A_{i,l}$	Multipole moment coefficients, where $i = 1, 2$ and $l = 0, 1, 2, \ldots$
c	Speed of light
h	Centre-to-centre separation
i	Subscript that denotes particle i, where $i = 1, 2, \ldots$
K	Coulomb's constant

k	Dielectric constant (relative permittivity)
M	Number of particles
m	Mass
N	Number of terms
P_l	Legendre polynomials, where $l = 0, 1, 2, \ldots$
q	Charge
R	Gas constant
s	Surface-to-surface separation
T	Temperature
t	Time
U	Electrostatic potential energy

Chapter 1

Introduction

1.1 An electromagnetic world

There are only four fundamental types of force known in nature. In order of decreasing magnitude, they are: strong, electromagnetic, weak, and gravitational. [1, 2] The first and third types are restricted to the nuclei of atoms and have extremely short range, therefore being essentially encountered only in the study of nuclear physics. The last one is quite familiar to everyone, being responsible for governing the motion of celestial bodies, like planets, stars, galaxies, etc., and also, in a more usual aspect, for many phenomena that are part of daily life, like the fall of an apple from a tree, and the fact that we are bound to the ground, and not suspended in space. It may not be evident to an uninformed person at first, but the second type of force, i.e. the electromagnetic force, is responsible for many other phenomena. Its existence is quite obvious when a lighting bolt strikes, when a comb attracts small pieces of paper after being used, or even when crackling sounds can be heard when one takes a shirt off. But the extent of the electromagnetic force is, in fact, considerably more wide. Ultimately, such force is largely responsible for the structure and behaviour of matter at many different levels. [1, 3]

A good part of the universe, at least the known world, is made of baryonic (ordinary) matter [4] which, in turn, is composed of discrete constituents—the atoms. These are basically formed by a positive nucleus, with a particular number of neutrons and protons, and a negative cloud of electrons that surrounds the nucleus.[1] As suggested by its name, neutrons have no electric charge, but protons and electrons carry one positive and one negative elementary charge, respectively. Evidently, if the core of matter is made of particles that are electrically charged, it is not by accident that effects of these charges affect the macroscopic world.

Gravitational force happens between any two bodies with mass, but it requires the presence of massive amounts of matter to be significant, at least in one of the interacting bodies. A good example would be the interaction of the Earth, a massive body, with any other body in the presence of the former's gravitational field. Electromagnetic force occurs between electrically charged particles and, differently, can be significant even when only small quantities of charge are involved. More specifically, it is manifested through two components: the electric force and the magnetic force. The first is always present where there are charges, while the latter manifest itself through elementary particles with their intrinsic magnetism, and also when charges are moving. At the atomic and molecular level, however, the former is so dominant that the effects of the latter can be considered to be negligible in most circumstances.

Of all fundamental forces, the electromagnetic is the only one that is completely understood at the present, being fully described by the branch of physics named electromagnetism. [3] The electromagnetic theory was gradually developed through the work of great names of science, such as Coulomb, Ampère, Faraday and Ørsted, until Maxwell, in the 19th century, presented an unified and consistent form of the theory, with the publication of a series of four papers entitled *On*

[1] An electron is in reality a lepton (therefore not a baryon), but it shall be considered here as a constituent of "ordinary" matter, for convenience and because it has an insignificant contribution to the mass of an atom. [4]

Physical Lines of Force, [5–8] where its fundamentals were formulated in a set of four partial differential equations, commonly known as Maxwell's equations.[2]

The work that is subject of this thesis only relates to situations where distributions of charges are stationary and, for all intents and purposes, its applicability is essentially restricted to length scales that are greater than the atomic one. As a consequence of charges being stationary, consideration of magnetic force is not required and, therefore, only one of Maxwell's equations, namely Gauss's law, appears in the subsequent discussions. In addition, quantum effects do not needed to be accounted for, since they are generally not relevant at the considered length scales, or at least their disregard can be justified as a good approximation. Electrostatics, a sub-field of the electromagnetic theory, provides then the basic theoretical background necessary for the developed of the work presented in this thesis, thus some of its relevant aspects are addressed next.

1.2 Electrostatics and polarisation of matter

The effects of static electricity are ubiquitous, impacting on many natural phenomena and human activities. A few examples drawn from the first category include the formation of clouds on Earth, [10, 11] the behaviour of volcanic ash, [12, 13] the aggregation of dust particles in space, [14, 15] and the stability of casein micelles in milk, [16] whilst in the latter category, electrostatic gas cleaning such as in coal-fired power stations, [17] food processing, [18] powder coating, [19] inkjet and laser printing, [20] and electronic ink, [21] can be included in a long list of applications where particles are deliberately charged in order to facilitate particular industrial processes or operations. [22] Underpinning all these examples is the need of a quantitative understanding of electrostatic interactions that exist between charged particles of widely varying composition.

[2]On a historical note, Maxwell ended up with not four but twenty equations. It was Oliver Heaviside in Great Britain and Heinrich Hertz in Germany who combined such equations into a set of only four equations via vector notation, during the two decades after Maxwell's death. [9]

It has been over two centuries since Charles Augustin de Coulomb published his famous law, which fundamentally asserts that the force exerted by a point charge on another is directly proportional to the product of their magnitudes, and inversely proportional to the square of the distance between them: [3]

$$\mathbf{F}_{12} = K\frac{q_1 q_2}{h^2}\,\hat{\mathbf{h}}, \qquad \text{Coulomb's law} \tag{1.1}$$

where $K = 1/(4\pi\epsilon_0)$ is the Coulomb's constant, ϵ_0 is the permittivity of free space (vacuum), and $\hat{\mathbf{h}}$ is an unit vector directed from the first point charge to the second one. Similarly, according to Newton's third law, the force on the first point charge due to the second one is given by $\mathbf{F}_{21} = -\mathbf{F}_{12}$. Considering that the electric field $\mathbf{E}$ generated by a point charge is spherically symmetric, it can be seen that Coulomb's law, in fact, follows directly from Gauss's law:

$$\oint_S \mathbf{E}\cdot d\mathbf{A} = \mathbf{E}(\mathbf{h})\cdot 4\pi h^2\,\hat{\mathbf{h}} = \frac{q_1}{\epsilon_0} \implies \mathbf{E}(\mathbf{h}) = K\frac{q_1}{h^2}\,\hat{\mathbf{h}} \quad \therefore \quad \mathbf{F}_{12} = \mathbf{E}(\mathbf{h})\,q_2\ , \tag{1.2}$$

where $d\mathbf{A}$ is the infinitesimal area element, and the integral is performed over a spherical surface S of radius h, centred at the point charge q_1.

However, interactions involving a charged finite-sized particle, i.e. a physical body with an unbalance of positive and negative charges, cannot be, in general, accurately described by a simple application of Coulomb's law, the reason being that, under influence of an electric field created by an external source, charges in a finite-sized particle might be redistributed before assuming an static equilibrium position. It's only when and if such static configuration of charges is known that Coulomb's law can be applied.

Particularly, the response of a certain material to an external electric field **E** created, for instance, by a point charge or a collection of point charges in a charged object, generally depends on the nature of such material. Accordingly, most of ordinary matter can be essentially classified in two categories: conductors or dielectrics, [3], where the main difference between the two is that, while in the former electric current can flow freely through the material, in the latter charges are bound to its constituent atoms. As an example, consider a solid object made of gold placed in an electric field. As it is a metal, outer electrons are loosely bound to its atoms, so they move under influence of the electric field until the whole object becomes an equipotential, with **E** vanishing in its interior.

Dielectrics, in contrast, respond to an electric field in a more subtle way. In fact, their response is closely related to the behaviour of each of its constituents atoms. In an isolated state, an atom can be classically described as being consisted of a positive nucleus surrounded by a spherical negative cloud of electrons. When such atom is placed in the vicinity of a positive point charge, however, its structure gets disturbed in a way that the positive nucleus is slightly displaced away from such external point charge, as both exert a repulsive force on each other and, oppositely, the electrons in the cloud are, in average, slightly displaced towards the external point charge, as there is an attractive interaction between them. The effective outcome of this phenomenon, as illustrated in Figure 1.1, is that an electric dipole is created as the average centres of the positive and negative charges in the atom no longer coincide with each other and, therefore, the atom is regarded as being polarised. If the external point charge was negative, the response would be identical, but oppositely symmetric. Regardless, an electric dipole with the same magnitude and aligned in the direction of the field would be observed in both cases. Accordingly, the polarisability α of atoms or molecules is defined according to the strength of the electric dipole moment **p** induced on them by an external electric field **E**, as follows: [23]

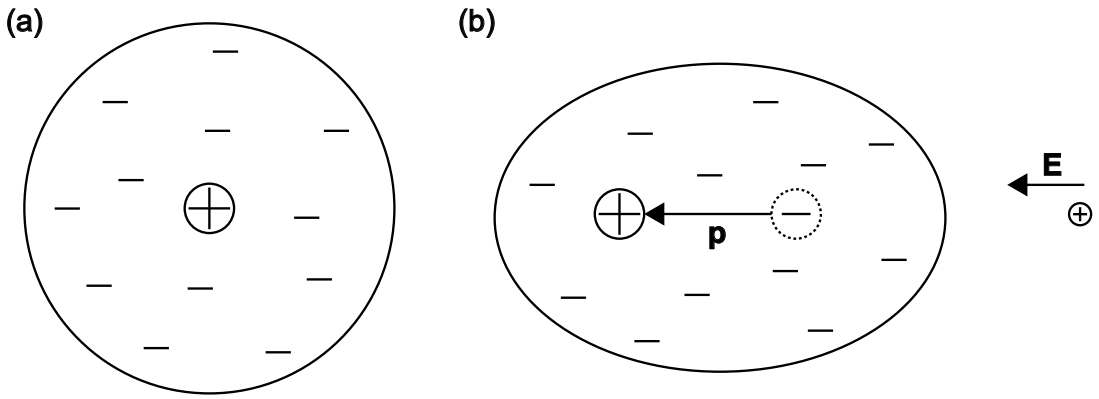


Fig. 1.1 (a) Classical view of a neutral and unperturbed atom, consisted of a positive nucleus surrounded by a negative cloud of electrons. (b) Same atom, polarised by an electric field **E**, created by an external positive point charge. Note the creation of a dipole **p**, aligned and pointing in the same direction of the electric field.

$$\mathbf{p} = \alpha\,\mathbf{E}. \tag{1.3}$$

For polar molecules, however, there are other contributions to the polarisability, particularly from their intrinsic dipole, that results from the arrangement coupled with differences in electronegativity of its constituents atoms.

Consider now an object made of a dielectric material such as glass, for instance. When such object is placed under influence of an external electric field, each of its constituents atoms gets polarised in the way described above, and every corresponding tiny induced dipole, created across the bulk and extending to the surface of the material, effectively adds up so that the object as a whole becomes polarised, resulting in the creation of bound charges at the surface of the object, as depicted in Figure 1.2. A convenient description of such effect can be given in terms of the polarisation **P**, defined as *dipole moment per unit volume*, and related to the applied electric field, **E**, as:[3]

$$\mathbf{P} = \epsilon_0\,\chi_e\,\mathbf{E}, \tag{1.4}$$

[3]Provided **E** is not too strong.

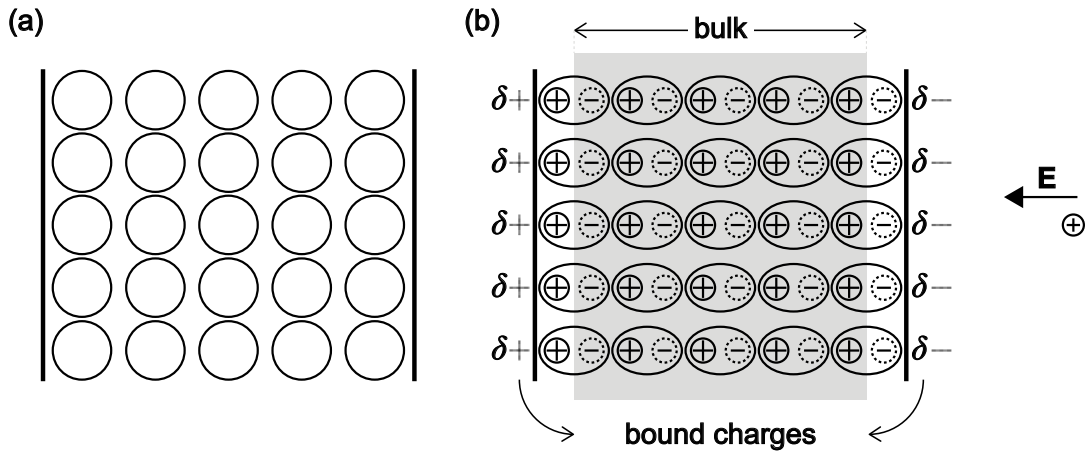


Fig. 1.2 (a) Illustration of a neutral and unperturbed object made of a dielectric material. (b) View of the same object, polarised by an external electric field **E**. Note that, while in the bulk (shaded in grey) the opposite charges corresponding to adjacent dipoles tend to cancel each other out, at the surfaces there is no cancellation, which leads to the accumulation of a special type of charge known as *bound charges*.

where χ_e is the electric susceptibility, a dimensionless constant of proportionality that effectively indicates the degree of polarisation of a material in response to an electric field. The electric susceptibility is more commonly expressed in terms of the relative permittivity, also known as dielectric constant k of the material:

$$k = \chi_e + 1, \tag{1.5}$$

where k is defined as the ratio between the absolute permittivity of the material and the permittivity of free space, i.e. $k = \epsilon/\epsilon_0$. A material that has a dielectric constant equal to unity does not become polarised by an external electric field, as can be inferred by substituting $k = 1$ in Equations 1.5 and 1.4, respectively. A good example of a non-polarisable material would be vacuum[4], whose dielectric constant is, by definition, exactly equal to unity. An example of an approximately non-polarisable material would be air under normal conditions, as its gaseous constituents are sparsely dispersed. If a non-polarisable material is also neutral, i.e. if it contains the same amount of positive and negative charges, it does

[4]Strictly speaking, vacuum is not a material, but any particular volume in space that is void of matter.

not respond in any way to an applied electric field, as no bound charges are created and, consequently, the electric field propagates unperturbedly through the material. Materials with low dielectric constants are generally nonpolar in nature, getting only weakly polarised under influence of an electric field. Examples of such materials include, oils, plastics, dust and wood. Conversely, materials with moderate to high dielectric constants are generally of polar character, being constituted by molecules with an intrinsic, permanent electric dipole moment. When placed in an electric field, the already present dipoles become slightly enhanced and also tend to align with such field, effectively polarising the material, which then becomes more strongly able to counterbalance the magnitude of the electric field through the extent of the material itself. Water, certain ceramics and nitrogen-substituted compounds such as ammonia and hydrogen cyanide, are just few examples of considerably polarisable materials, with moderate to high dielectric constants.

It should be noted, however, that the dielectric constant is a bulk property and when used in the context of a very small particle, especially molecules and atoms, it may lose its significance. Instead, it can take the form of a parameter, which reflects the total polarisability of the corresponding particle by treating it as a sphere of dielectric constant k and radius a, as given by Clausius-Mossotti relation: [23]

$$\alpha = \left(\frac{k-1}{k+2}\right) 4\pi\,\epsilon_0\,a^3. \tag{1.6}$$

For instance, the smallest object addressed in this thesis corresponds to a polyoxometalate particle; a spherical macromolecule with 1 nm of diameter and an estimated dielectric constant $k = 10$. Accordingly, its corresponding polarisability is equal to $93.7 \times (4\pi\epsilon_0)10^{-30}$ m^3 according to Equation 1.6, a value relatively higher than the usual tabulated polarisabilities, [24] which corresponds to smaller chemical species.

Early research on models to describe the interaction between charged particles was aided by comparatively simple boundary conditions and driven by a desire to better understand the emerging field of electrostatics. It was also focused primarily on conducting spheres, deriving from the work of W. Thomson (also known as Lord Kelvin). [25, 26] A complete solution to the interaction between two conducting spheres did not appear until 1964, when Davis used a bispherical coordinate system to derive an expression for the electrostatic force; [27] research that has subsequently seen extensive application in the field of cloud physics. The high dielectric constant of water means that a conducting sphere solution remains effective to this date. [11] However, the vast majority of materials from which charged particles are composed, for example, volcanic ash, [12, 13] cosmic dust grains, [14, 15] printer toner, [20] food coatings, [18] colloids, [28] etc., are not conducting and therefore require a formalism that is more universally applicable. To this end, a solution to the more difficult problem of how charged dielectric particles interact with one another has been sought for many years.

Recently, a series of new and more sophisticated solutions to the problem of calculating the electrostatic interactions between charged particles, dielectric or conducting, have been presented literature. In particular, a number of the proposed solutions that target the dielectric particle interaction problem have built on the early conducting sphere solution and used the image charge approach. [29–36] Furthermore, a number of studies have alternatively adopted a multipole approach, whereby each particle possesses a defined set of electrostatic multipoles, the sum of which describe the total interaction force or energy. [37–40] An advantage of this latter approach is that it can provide a physical picture of the extent to which the charge on both particles is polarised through a mutual interaction. When reduced to a point charge − charged sphere configuration, these theories can provide the classical electrostatic multipole terms, i.e. ion − induced dipole, ion − induced quadrupole etc.

The work presented in this thesis starts with a deep investigation of the intrinsic aspects and outcomes of the multipole approach, more specifically the proposed two-body solution by Bichoutskaia et al., [37] where the theory is extensively tested and developed further. Emphasis is given to the fundamentals of a two-body electrostatic interaction, focusing on the development of a certain intuition regarding the physics of the problem, that might possibly help in the understanding of more complicated scenarios. The crucial treatment of the presence of a dielectric medium (solvent) is introduced, making the theory suitable for treating not only the restricted cases where interaction between charged particles happens in vacuum, but also the vast majority of problems where the particles are immersed in a medium. Finally, a solution to the more general problem of calculating the electrostatic interactions between many particles, with arbitrary properties, namely size, charge, dielectric constant and position in the three-dimensional space, also immersed in a dielectric medium, is presented. Analysis of the many-body theory starts with the consideration of systems containing a small number of particles, where the fundamentals underlined for the two-body case can be readily extrapolated. Larger systems are addressed afterwards, culminating in an adaptation of the model as a force field for Newtonian dynamics comprising a limited number of particles. Additionally, application of the theoretical methods in the comprehension of experimental problems are given throughout the thesis, at relevant points.

Chapter 2

Electrostatic interactions in two-body systems

2.1 Theoretical background

This chapter builds upon the solution introduced by Bichoutskaia et al. [37] to the problem of calculating electrostatic interactions between charged particles of dielectric materials. The model [37] describes the electrostatic interaction between a pair of spherical particles suspended in vacuum, with net charges q_1 and q_2 (contributed solely by the presence of free charges on the surface of each particle), radii a_1 and a_2, and dielectric constants k_1 and k_2. The particles are assumed to be electrically non-conducting, where electrical conductivity is defined as the product of carrier mobility and charge density. [3] Therefore, a non-conducting case implies either the absence of free charge in the system or, if free charge is present, no mobility for the free charge carriers. For a homogeneous polarisable material with a bulk polarisability described by the dielectric constant, Gauss's law states that the volume densities of free charge, bound (polarisation) charge, and total charge (the sum of free and bound charge) are proportional. [3, 41] At the surface of a dielectric particle, the density of free and total charge can be described by a set of field discontinuities accounted by boundary conditions, which

involve dielectric constants from both sides of the surface. It is assumed that the free charge is uniformly distributed on the surface of a charged dielectric particle, which corresponds to the lowest-energy configuration, and remains immobile during interaction; the latter assumption is justified by the zero mobility of free charge carriers. This condition also implies in an absence of free charge inside the particle, so that only charge on the surface needs to be considered. The total surface charge density σ on a particle can be written as a sum of contributions from the bound charge density σ_b and the free charge density σ_f, i.e. $\sigma = \sigma_b + \sigma_f$, where the bound charge is a dynamic quantity that varies as a function of the separation between the interacting particles, amongst other factors.

Figure 2.1 gives a geometric representation of the problem being addressed. The dielectric constants (relative permittivities) of the particles are defined as $k_i = \epsilon_i/\epsilon_0$ $(i = 1, 2)$, where ϵ_0 is the permittivity of free space (vacuum), and ϵ_i is the absolute permittivity of particle i.

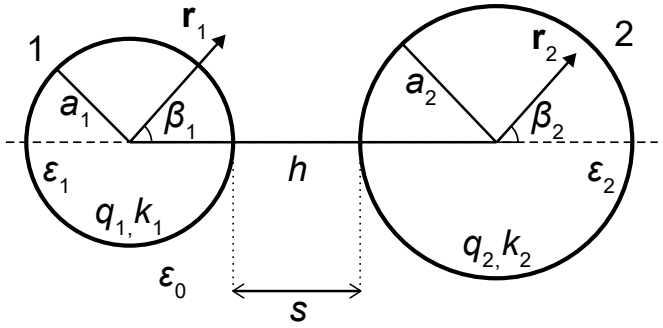


Fig. 2.1 A general geometric representation of two interacting spherical dielectric particles suspended in vacuum. Dielectric constants, charges, radii, and the polar angles of particles 1 and 2 are denoted as k_1, q_1, a_1, β_1 and k_2, q_2, a_2, β_2, respectively. The centre-to-centre separation is defined as h and the corresponding surface-to-surface separation is given by $s = h - a_1 - a_2$.

The electric potential at a designated point $\mathbf{r}_i$ $(i = 1, 2)$ due to the presence of charge on the particles is represented through a multipole expansion in terms of Legendre polynomials about the centre of each particle, resulting in the following expressions for the potential inside and in the vicinity of each respective particle:

$$\Phi(\mathbf{r}_1) = \sum_{l=0}^{\infty} A_{1,l} \frac{r_1^l}{a_1^{2l+1}} P_l(\cos\beta_1) + \sum_{l=0}^{\infty}\sum_{m=0}^{\infty} A_{2,m} \frac{(l+m)!}{l!m!} \frac{r_1^l}{h^{l+m+1}} P_l(\cos\beta_1) \quad \text{for} \quad r_1 < a_1, \tag{2.1}$$

$$\Phi(\mathbf{r}_1) = \sum_{l=0}^{\infty} A_{1,l} \frac{1}{r_1^{l+1}} P_l(\cos\beta_1) + \sum_{l=0}^{\infty}\sum_{m=0}^{\infty} A_{2,m} \frac{(l+m)!}{l!m!} \frac{r_1^l}{h^{l+m+1}} P_l(\cos\beta_1) \quad \text{for} \quad r_1 > a_1, \tag{2.2}$$

$$\Phi(\mathbf{r}_2) = \sum_{l=0}^{\infty} A_{2,l} \frac{r_2^l}{a_2^{2l+1}} P_l(\cos\beta_2) + \sum_{l=0}^{\infty}\sum_{m=0}^{\infty} A_{1,m} \frac{(l+m)!}{l!m!} \frac{r_2^l}{h^{l+m+1}} P_l(\cos\beta_2) \quad \text{for} \quad r_2 < a_2, \tag{2.3}$$

$$\Phi(\mathbf{r}_2) = \sum_{l=0}^{\infty} A_{2,l} \frac{1}{r_2^{l+1}} P_l(\cos\beta_2) + \sum_{l=0}^{\infty}\sum_{m=0}^{\infty} A_{1,m} \frac{(l+m)!}{l!m!} \frac{r_2^l}{h^{l+m+1}} P_l(\cos\beta_2) \quad \text{for} \quad r_2 > a_2, \tag{2.4}$$

where P_l are the Legendre polynomials, and $A_{i,(l\vee m)}$ $(i = 1, 2)$ are the multipole moment coefficients (expressions given below).

With the knowledge of the electric potential, the following standard boundary conditions in the theory of electrostatics [3, 41, 42] can be imposed:

i. The electric potential Φ, on the surface of each particle is continuous due to the continuity of the tangential component of the electric field $\mathbf{E}$:

$$\frac{1}{r_i}\frac{\partial \Phi}{\partial \beta}\bigg|_{r_i=a_i^+} - \frac{1}{r_i}\frac{\partial \Phi}{\partial \beta}\bigg|_{r_i=a_i^-} = 0 \; ; \tag{2.5}$$

ii. The normal component of the electric field is discontinuous due to the presence of a net charge on the surface of each particle:

$$4\pi K \sigma_i = \frac{\partial \Phi}{\partial r_i}\bigg|_{r_i=a_i^+} - \frac{\partial \Phi}{\partial r_i}\bigg|_{r_i=a_i^-} \; ; \tag{2.6}$$

iii. The normal component of the electric displacement field $\mathbf{D}$ is discontinuous due to the presence of a free charge on the surface of each particle:

$$4\pi K \sigma_{f,i} = \frac{\partial \Phi}{\partial r_i}\bigg|_{r_i=a_i^+} - k_i \frac{\partial \Phi}{\partial r_i}\bigg|_{r_i=a_i^-} \; ; \tag{2.7}$$

where $i = 1, 2$ and the subscripts a_i^+ and a_i^- respectively denote radial positions in the outside and the inside of the surface of the ith particle. The electric displacement field is related to the electric field as $\mathbf{D} = k_i\, \epsilon_0\, \mathbf{E} = \epsilon_i\, \mathbf{E}$.

Application of the boundary conditions (Equations 2.5−2.7) to the set of equations for the electric potential (2.1-2.4) results in the following expressions for the total surface charge density:

$$\sigma_i\,(\beta) = \frac{1}{4\pi K}\sum_{l=0}^{\infty} A_{i,l}\frac{2l+1}{a_i^{l+2}} P_l\,(\cos\beta_i) \qquad \text{for} \quad i = 1, 2 \; ; \tag{2.8}$$

and the multipole moment coefficients:

$$4\pi K a_1 \sigma_{f,1}\delta_{l,0} = \frac{A_{1,l}}{a_1^{l+1}} + \frac{(k_1-1)l}{(k_1+1)l+1}\sum_{m=0}^{\infty} A_{2,m}\frac{(l+m)!}{l!\,m!}\frac{a_1^l}{h^{l+m+1}} \tag{2.9}$$

for particle 1, and

$$4\pi K a_2 \sigma_{f,2} \delta_{l,0} = \frac{A_{2,l}}{a_2^{l+1}} + \frac{(k_2 - 1)l}{(k_2 + 1)l + 1} \sum_{m=0}^{\infty} A_{1,m} \frac{(l+m)!}{l!\, m!} \frac{a_2^l}{h^{l+m+1}} \tag{2.10}$$

for particle 2. The complementary expressions for the multipole moment coefficients (Equations 2.9 and 2.10) account for the mutual polarisation experienced by the two interacting particles as a function of their dielectric constants (k_1 and k_2), radii (a_1 and a_2), charges (q_1 and q_2), and the centre-to-centre separation, h.

The electrostatic force due to the presence of a total charge on the surface of each particle is calculated from a generalisation of Coulomb's law for point charges and is given by

$$\mathbf{F}_{12} = K \int dq_1(\mathbf{r}_1) \int dq_2(\mathbf{r}_2) \frac{\mathbf{r}_1 - \mathbf{r}_2}{|\mathbf{r}_1 - \mathbf{r}_2|^3}, \tag{2.11}$$

where $\mathbf{r}_1$ and $\mathbf{r}_2$ are position vectors on the surface of each respective particle, $dq_1(\mathbf{r}_1)$ and $dq_2(\mathbf{r}_2)$ are the corresponding charge elements, and K is the Coulomb's constant. The first integral in Equation 2.11 takes into account the total charge residing on particle 1 and the second integral is the electric field generated by the total charge residing on particle 2. By symmetry and according to Newton's third law, an equivalent expression, $\mathbf{F}_{21} = -\mathbf{F}_{12}$, would take into account the total charge residing on particle 2 and the electric field generated by the total charge residing on particle 1. Throughout this thesis, it has been adopted the convention that a negative magnitude of the force denotes an attractive interaction and a positive magnitude denotes a repulsive interaction.

Integration of the total charge (Equation 2.8) over the surface of each particle in Equation 2.11 results, after futher mathematical developments, in the following analytical expression for the electrostatic force:

$$F_{12} = K\frac{q_1 q_2}{h^2} + \left(-q_1 \sum_{m=1}^{\infty} \sum_{l=0}^{\infty} A_{1,l} \frac{(k_2 - 1)m(m+1)}{(k_2 + 1)m + 1} \right.$$
$$\left. \times \frac{(l+m)!}{l!\, m!} \frac{a_2^{2m+1}}{h^{2m+l+3}} - \frac{1}{K} \sum_{l=1}^{\infty} A_{1,l} A_{1,l+1} \frac{(k_1 + 1)(l+1) + 1}{(k_1 - 1)a_1^{2l+3}} \right), \tag{2.12}$$

which gives a simple and well-behaved solution for the electrostatic force between two charged polarisable particles as a function of the input parameters of the system, namely the particles's dielectric constants, radii, (given free) charges, and the centre-to-centre separation. The first expression in Equation 2.12 corresponds to Coulomb's law and, therefore, accounts for the force due to the uniformely distributed free charges on the surface of each particle. The second expression (inside parentheses) in Equation 2.12 derives from the multipole expansion of the electric potential, being consisted then of an infinite series of multipole terms, that accounts for the contribution polarisation makes to the overall electrostatic force. This second expression is always negative and, consequently, contributes as an attractive component of the force. If the particles are non-polarisable, i.e. in the limit of $k_1 = k_2 \to 1$, the sum of the multipole terms in Equation 2.12 goes to zero, so the interaction is naturally and fully described by the first term, i.e. Coulomb's law. If the particles have dielectric constants that are greater than unity, however, then the attractive multipole terms gain in magnitude, weakening the repulsion between the particles if these are like-charged, or strengthening the attraction if the particles are oppositely charged. As presented, the formalism [37] is able to treat and differentiate a broad range of dielectric materials, ranging from oils ($k \approx 2$) through to water ($k \approx 80$), and on to particles of metallic character ($k \gtrsim 1000$). At the limit $l = 0$, Equation 2.12 is reduced to represent the electrostatic force between a charged polarisable particle and a non-polarisable particle (or a point charge), and if taken a step further with $q_2 = 0$, the following

classical textbook [43] expression that describes the attraction between a point charge ($i = 1$) and a neutral polarisable particle ($i = 2$) is obtained:

$$F_{12} = K\frac{q_1^2}{h^2}\sum_{m=1}^{\infty}\frac{(1-k_2)\,m\,(m+1)}{(k_2+1)\,m+1}\frac{a_2^{2m+1}}{h^{2m+1}}. \tag{2.13}$$

Since Equation 2.12 contains an infinite series, if at least one of the particles is polarisable ($k_i > 1$, where $i = 1 \vee 2$), only an approximate solution to the problem can be obtained. As the series is convergent, then in practice it only needs to be evaluated to an upper bound N, that fulfils a determined convergence criterion, so that Equations 2.9, 2.10 and 2.12 can be rewritten as

$$4\pi K a_1 \sigma_{f,1}\delta_{l,0} = \frac{A_{1,l}}{a_1^{l+1}} + \frac{(k_1-1)l}{(k_1+1)l+1}\sum_{m=0}^{N} A_{2,m}\frac{(l+m)!}{l!\,m!}\frac{a_1^l}{h^{l+m+1}}, \tag{2.14}$$

$$4\pi K a_2 \sigma_{f,2}\delta_{l,0} = \frac{A_{2,l}}{a_2^{l+1}} + \frac{(k_2-1)l}{(k_2+1)l+1}\sum_{m=0}^{N} A_{1,m}\frac{(l+m)!}{l!\,m!}\frac{a_2^l}{h^{l+m+1}}, \tag{2.15}$$

and

$$F_{12} = K\frac{q_1 q_2}{h^2} + \left(-q_1\sum_{m=1}^{N}\sum_{l=0}^{N} A_{1,l}\frac{(k_2-1)m(m+1)}{(k_2+1)m+1} \times \frac{(l+m)!}{l!\,m!}\frac{a_2^{2m+1}}{h^{2m+l+3}} - \frac{1}{K}\sum_{l=1}^{N} A_{1,l}A_{1,l+1}\frac{(k_1+1)(l+1)+1}{(k_1-1)a_1^{2l+3}}\right), \tag{2.16}$$

respectively. Once the input parameters of the system are given and the multipole moment coefficients (Equations 2.14 and 2.15) determined, the electrostatic force between two interacting spherical particles can be straightforwardly obtained through Equation 2.16. A solution based on matrix algebra for efficiently computing the multipole moment coefficients (Equations 2.14 and 2.15) has been

developed and its details are presented in Appendix A, along with an assessment of the performance of the computer program written in the implementation of the model.

An alternative solution based on the same considerations underlined above, but derived using the bispherical coordinate system, which makes it suitable for treating spherical particles and planar surfaces (but not point particles), has also been developed [38]. It has been proved later, though, that this approach does not converges when free charge is imputed to a plane and that, in virtually all other situations, it converges more slowly than its counterpart solution, [37] based on the spherical coordinate system. Nonetheless, this alternative solution stands as the most indicated for calculating the electrostatic interaction between a charge spherical particle and a neutral planar surface.

2.2 General numerical results

2.2.1 Electrostatic force

Next it is presented a series of cases where it is investigated how the electrostatic interaction between a pair of charged particles can be influenced by the value of their dielectric constants. In all these initial calculations the various physical quantities are considered to be dimensionless, for simplicity. Consequently, Coulomb's constant has been replaced by unity.

The first example concerns a case where the first particle carries a positive charge and the second particle is neutral, such that the existence of an electrostatic interaction depends upon the neutral particle being polarisable. As shown in Figure 2.2(a), when the particles have a dielectric constant equal to unity, i.e. when they are non-polarisable, no bound charges are induced, especially on the neutral particle, so there is a complete absence of electrostatic interaction. However, as the value of their dielectric constants increases, i.e. as the particles become more polarisable, bound charges are induced, and the interaction becomes

progressively more attractive. Fundamentally, the electric field created by the positive free charges on the first particle induces the appearance of negative bound charges on the second particle, particularly on the side that is adjacent to the former, as shown in Figure 2.2(b). Since the second particle is neutral, its total charge must remain zero, hence positive bound charges emerge on the side that is farthest from the first particle. As it is an iterative process, the electric field created by the induced bound charges on the second particle also polarises the first particle, which then becomes more positively charged at the end closest to the neutral particle. The ability of the particles to be polarised is in practice, then, translated to an effective displacement of opposite charges towards one another and, similarly, an effective displacement of like charges away from one another, so the overall effect is that, when all charges on the surface of each particle are integrated and each pairwise interaction computed, the total electrostatic force becomes attractive.

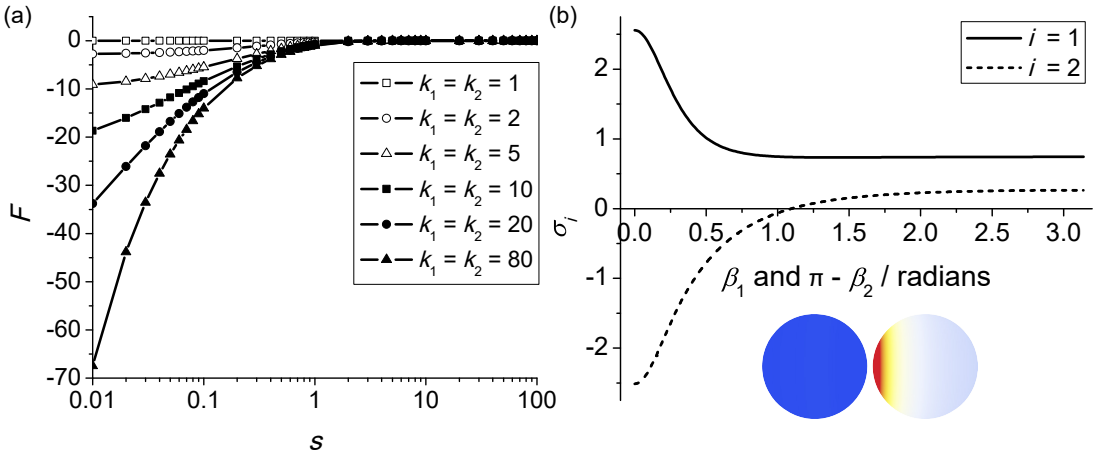


Fig. 2.2 (a) Plot of the electrostatic force F as function of the surface-to-surface separation s for a case of charged particle − neutral particle interaction. The first particle has a nominal charge of $+10$, whilst the second particle is neutral. The two particles are equal-sized, with a nominal radii of 1 and each curve corresponds to a distinct value of the particles's dielectric constants, $k_1 = k_2$. (b) Plot of the total surface charge densities σ_i $(i = 1, 2)$ as function of the polar angles β_i, corresponding to the curve where $k_1 = k_2 = 20$ and $s = 0.1$. Inset shows a geometrical representation of the problem, with the total surface charge density (charge per unit area) mapped out for each of the particles. Blue tones denote positive charge densities, and red tones denote negative charge densities.

The second example addresses a case where the particles are oppositely charged. As shown in Figure 2.3(a) when the particles are non-polarisable ($k_1 = k_2 = 1$), the electrostatic interaction is always attractive and described entirely by Coulomb's law. In this particular example, attraction is due to an opposite-charge interaction between the positive free charges on the first particle and the negative free charges on the second particle. When the dielectric constants of the particles become larger than unity, bound charges are induced on the particles in a manner similar to the case depicted in Figure 2.2, as can be seen from Figure 2.3(b), such that as the value of $k_1 = k_2$ increases, the interaction becomes more attractive. Here, the practical effect of polarisation is then to enhance the already existing attractive interaction between the oppositely charged particles.

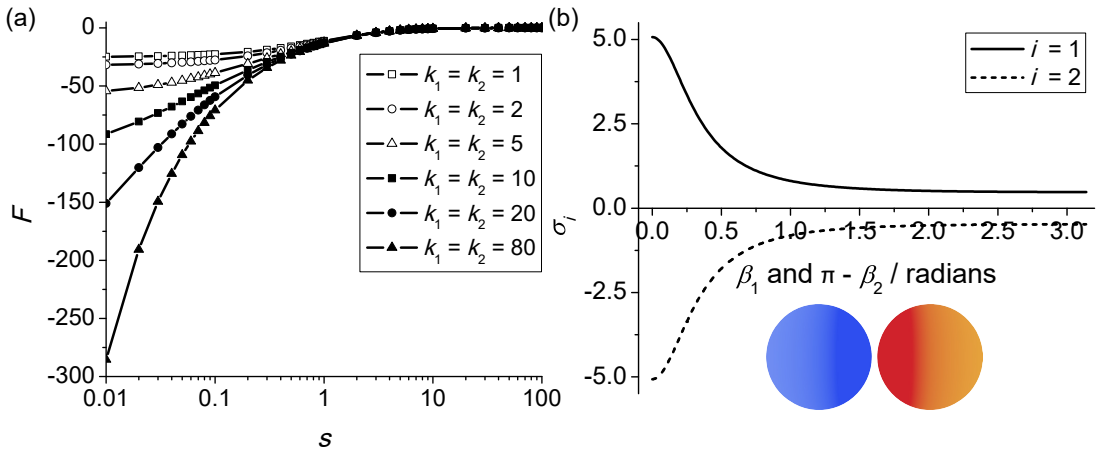


Fig. 2.3 (a) Plot of the electrostatic force F as function of the surface-to-surface separation s for a case of opposite-charge interaction. The first particle has a nominal charge of +10, whilst the second particle has an opposite charge of -10. The two particles are equal-sized, with a nominal radii of 1 and each curve corresponds to a distinct value of the particles's dielectric constants, $k_1 = k_2$. (b) Plot of the total surface charge densities σ_i $(i = 1, 2)$ as function of the polar angles β_i, corresponding to the curve where $k_1 = k_2 = 20$ and $s = 0.1$. Inset shows a geometrical representation of the problem, with the total surface charge density mapped out for each of the particles. Blue tones denote positive charge densities, and red tones denote negative charge densities.

In the third example, a case where the particles are like-charged is investigated. Figure 2.4(a) shows that when the particles are identical, which includes a consideration of the magnitude and sign of charge, the electrostatic interaction will always be repulsive, no matter how polarisable the particles are. Polarisation

effects, in this case, merely serve to weaken the electrostatic repulsion between the particles, so as the value of $k_1 = k_2$ increases, the magnitude of the repulsive force decreases. Since such particles have equivalent electrostatic properties (they are identical), there exists a balance between the mutual repulsive and polarising effects they exert on each other and, as a result, the particles present mirror-symmetric surface charge distributions, as illustrated in Figure 2.4(b).

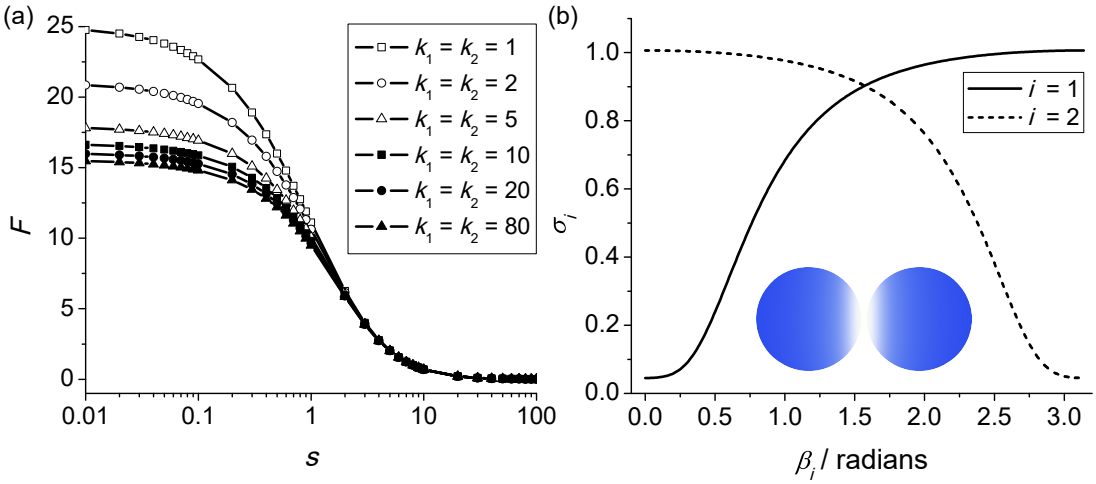


Fig. 2.4 (a) Plot of the electrostatic force F as function of the surface-to-surface separation s for a case of like-charge interaction. The two particles are identical, having a nominal charge of $+10$ and a nominal radii of 1. Each curve corresponds to a distinct value of the particles's dielectric constants, $k_1 = k_2$. (b) Plot of the total surface charge densities σ_i $(i = 1, 2)$ as function of the polar angles β_i, corresponding to the curve where $k_1 = k_2 = 20$ and $s = 0.1$. Inset shows a geometrical representation of the problem, with the total surface charge density mapped out for each of the particles.

Interestingly, it can been seen from the fourth example that, in the case of like-charged particles, a rather counterintuitive effect can be achieved by the introduction of asymmetry in one of the parameters of the particles, namely the given free charge. As depicted in Figure 2.5(a), two times more charge has been assigned to the second particle, compared to the first one, such that they now have different surface charge densities. As in the previous case, when the particles are non-polarisable, the electrostatic interaction can be described entirely by Coulomb's law. Similarly still, as the value of $k_1 = k_2$ increases, the polarisation effects start to weaken the electrostatic repulsion between particles but, as the dielectric constants of the particles reach a particular value (in this

case, $k_1 = k_2 \geq 20$), the polarisation effects become strong enough to overcome the Coulomb repulsion. Equivalently, the multipole terms become larger than the monopole term (Coulomb's law) in Equation 2.16, which results in the onset of an overall attractive interaction at short inter-particle separation distances, even though the particles are like-charged. As the second particle has the highest charge density, it is the first particle that gets polarised in a way that negative bound charges are induced on it, specifically on the side that is closest to former, and not the contrary, as suggested by Figure 2.5(b).

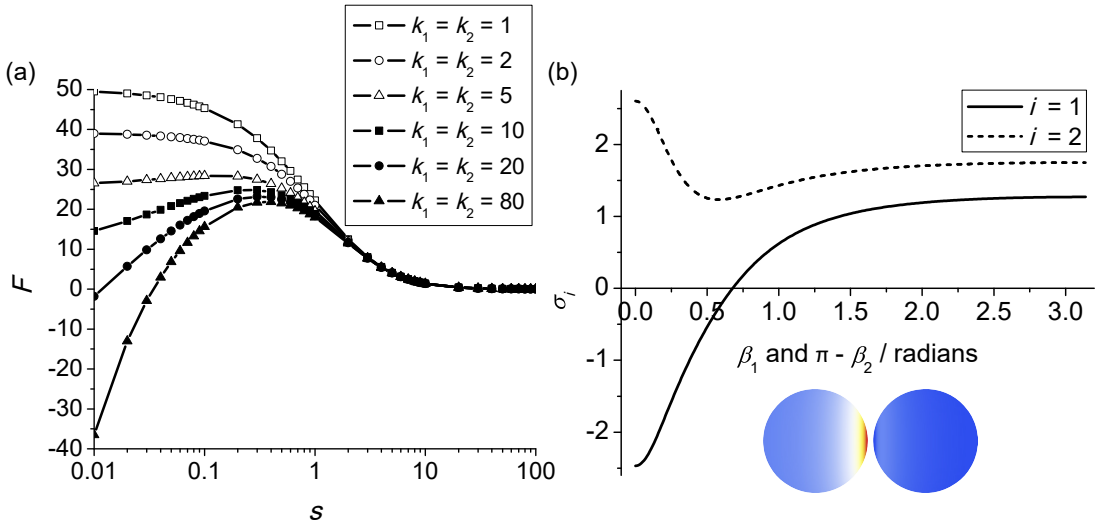


Fig. 2.5 (a) Plot of the electrostatic force F as function of the surface-to-surface separation s for a case of like-charge interaction, where it exists an asymmetry in the given free charge. The first particle has a nominal charge of $+10$ while the second particle has a nominal charge of $+20$. Both particles have a nominal radii of 1, and each curve corresponds to a distinct value of the particles's dielectric constants, $k_1 = k_2$. (b) Plot of the total surface charge densities σ_i $(i = 1, 2)$ as function of the polar angles β_i, corresponding to the curve where $k_1 = k_2 = 20$ and $s = 0.1$. Inset shows a geometrical representation of the problem, with the total surface charge density mapped out for each of the particles. Blue tones denote positive charge densities, and red tones denote negative charge densities.

Attraction between like-charged particles can also be achieved by introducing another sort of asymmetry, this time regarding the radii. In the case illustrated in Figure 2.6, the particles are equally charged but differ in size, with the second particle being twice as large as the first one. In a similar manner to the previous case (Figure 2.5), it can be seen from Figure 2.6(a) that, at sufficiently short

inter-particle separation distances, an attractive regime can occur if the dielectric constants of the interacting particles are at least equal to 20. Since it is the first particle that has a higher charger density in this example, for it bears the same amount of surface charge as the second particle, but smeared over a smaller surface area, it is the latter that gets polarised in a way that negative bound charges are induced on the side that is closest to former, and not the contrary, as suggested by Figure 2.6(b).

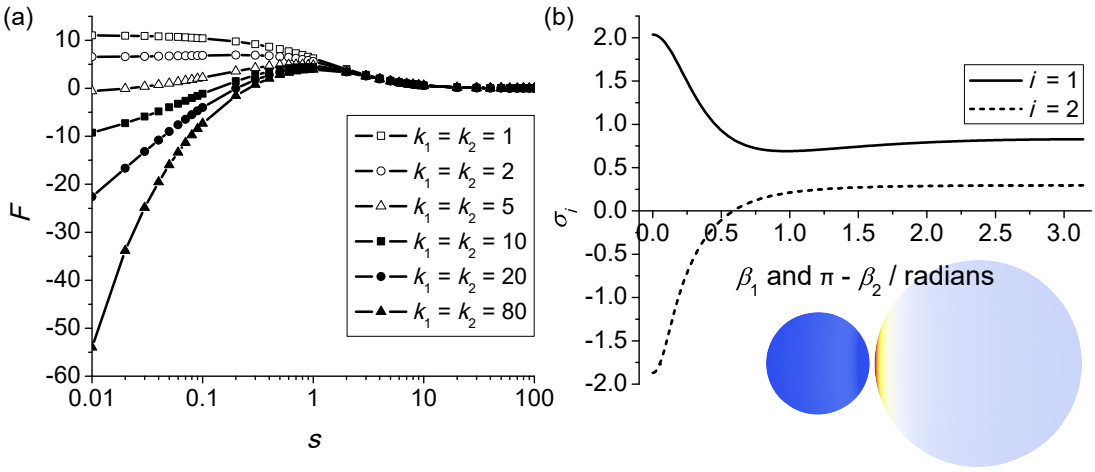


Fig. 2.6 (a) Plot of the electrostatic force F as function of the surface-to-surface separation s for a case of like-charge interaction, where it exists an asymmetry in size. Both particles carry the same nominal charge of $+10$ but the second one is two times larger than the first, with a nominal radius of 2. Each curve corresponds to a distinct value of the particles's dielectric constants, $k_1 = k_2$. (b) Plot of the total surface charge densities σ_i $(i = 1, 2)$ as function of the polar angles β_i, corresponding to the curve where $k_1 = k_2 = 20$ and $s = 0.1$. Inset shows a geometrical representation of the problem, with the total surface charge density mapped out for each of the particles. Blue tones denote positive charge densities, and red tones denote negative charge densities.

It can be noticed in all of the examples discussed above that the various force-separation curves converge at large surface-to-surface separation. The reason being that induced multipoles, namely the dipole, quadrupole, octupole, etc., diminish in magnitude more rapidly than the permanent monopole, as the separation between particles increases. Whilst the Coulomb (monopole) contribution to the force is inversely proportional to the square of the distance between interacting particles, as described in Equation 2.16, the multipole terms have higher inverse orders of relation with this variable. As a consequence, polarisation effects are only

significant at short inter-particle separation distances and, therefore, it can be inferred that the dielectric constant of a particle will only have an important role in a two-body electrostatic interaction (in vacuum) if this geometrical requirement is met.

2.2.2 A point charge distribution parallel

It has already been shown in Section 1.2 how Coulomb's law can be used to calculate the electrostatic force between two point charges. However, since Coulomb's law obeys the principle of superposition, the electrostatic force on a third point charge can be also obtained by a simple vector sum of the forces exerted on it by the first two point charges: $\mathbf{F}_3 = \mathbf{F}_{13} + \mathbf{F}_{23}$. Indeed, the force on a test charge q_t due to n point charges can be generalised as: [3]

$$\begin{aligned}\mathbf{F}_{q_t} &= K\frac{q_1\ q_\mathrm{t}}{\left|\mathbf{r}-\mathbf{r}_1^{'}\right|^2}\frac{(\mathbf{r}-\mathbf{r}_1^{'})}{\left|\mathbf{r}-\mathbf{r}_1^{'}\right|} + K\frac{q_2\ q_\mathrm{t}}{\left|\mathbf{r}-\mathbf{r}_2^{'}\right|^2}\frac{(\mathbf{r}-\mathbf{r}_2^{'})}{\left|\mathbf{r}-\mathbf{r}_2^{'}\right|} + \dots \\ &= Kq_\mathrm{t}\sum_{i=1}^{n}\frac{q_i}{\left|\mathbf{r}-\mathbf{r}_i^{'}\right|^2}\frac{(\mathbf{r}-\mathbf{r}_i^{'})}{\left|\mathbf{r}-\mathbf{r}_i^{'}\right|}\end{aligned} \tag{2.17}$$

where $\mathbf{r}$ is the position vector corresponding to the test charge q_t and $\mathbf{r}_i^{'}$ is the position vector of the ith point charge q_i, so that the last fraction on Equation 2.17 corresponds to a unit vector pointing from q_i to q_t.

The inverse distance-square character of Coulomb's law is a remarkable feature that can actually explain why particles carrying the same sign of charge can be attracted to one another in some circumstances. As an illustration, consider a set of elementary charges q_i $(i = 1, 2, \dots, 36)$ displaced in a circular manner, and a test charge q_t placed at a distance h from the geometric centre of the set. Figure 2.7 gives a plot of the electrostatic force acting on q_t as function of h, easily obtained from Equation 2.17, for the case where all charges are positive and have the same magnitude of +1 e, q_t inclusive. As expected, the force is always repulsive and its magnitude increases as h shortens.

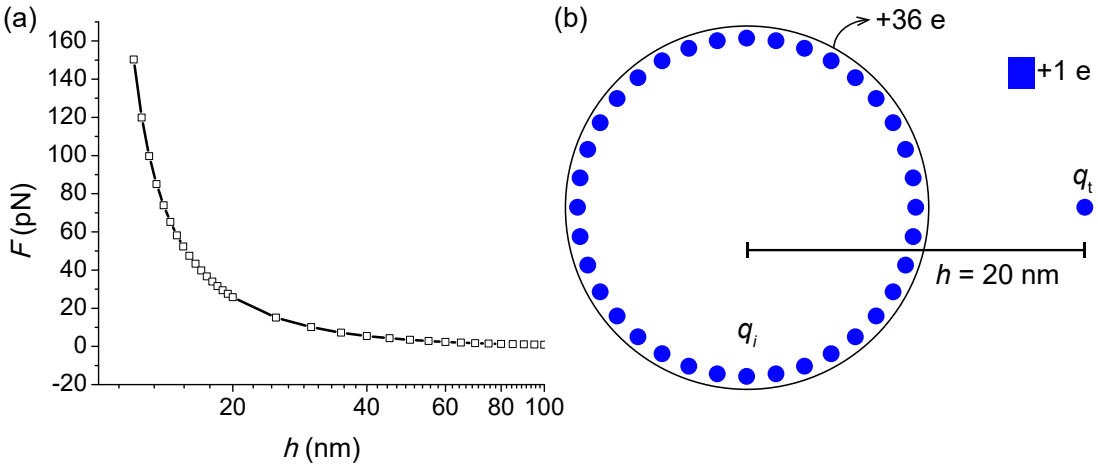


Fig. 2.7 (a) Plot of the electrostatic force F, given in piconewtons (pN), as function of the distance h between the centre of the circular distribution of positive charges and the positive test charge q_t, given in nanometres (nm). (b) Schematic illustration of the problem, where each point charge is visually of finite size, for clarity, and coloured in blue.

Consider now a similar case where the only difference is that the three point charges in the circular distribution that are closest to the test charge are negative, with a magnitude of -1 e each, and the three point charges in the circular distribution that are farthest to the test charge are positive, but with a magnitude of +3 e each, so that the net charge in the set remains the same, i.e. equal to +36 e. A plot of the electrostatic force acting on the test charge q_t for this scenario (Figure 2.8) shows that, if the magnitude of h is sufficiently small, the interaction changes from repulsive to attractive. Because of the inverse distance-square character of Coulomb's law, when the positive test charge is close enough to the three negative point charges in the set, the magnitude of the attractive force felt by the former due to the latter is sufficiently large so it overcomes the repulsive force exerted by all other positive point charges. As the magnitude of h increases, however, the distances between each point charge in the set and the test charge become asymptotically equal, so that the force acting on the latter can be effectively approximated by the force that would be exerted by a point charge with magnitude +36 e placed at nearly the centre of the charge distribution. For an equivalent spherical distribution, this position would be exactly at the centre, as predicted by Gauss's law.

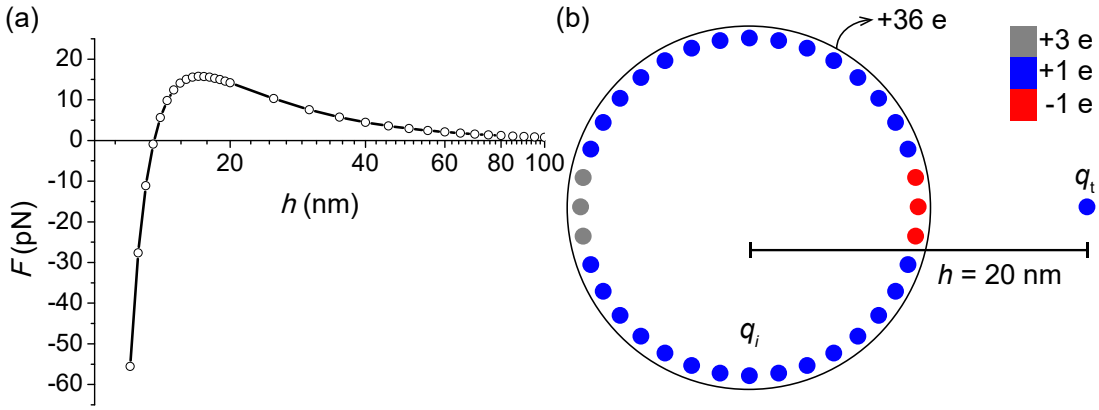


Fig. 2.8 (a) Plot of the electrostatic force F (pN), as function of the distance h (nm) between the centre of the circular distribution of charges and the test charge q_t. (b) Schematic illustration of the problem, where each point charge is visually of finite size, the point charges with magnitude +3 e are grey coloured, the ones with magnitude +1 e are coloured in blue, and the ones with magnitude -1 e are coloured in red.

This case of like-charge attraction between the positive set of charges and the positive test charge (Figure 2.8) is in fact comparable to the cases of attraction between like-charged dielectric particles described earlier in Figures 2.5 and 2.6. When a dielectric particle is polarised, bound charges are displaced, which leads to the creation of regions with different charge densities on the surface of the particle. In a similar way, it could be considered that the circular distribution of point charges depicted in Figure 2.8 is a "polarised" version of the one shown in Figure 2.7, for there is also creation of regions with different density of charges, while the net charge in the set is unchanged. Apart from the dissimilar geometries, the difference between these two cases where like-charge attraction occurs, namely the circular distribution of point charges with a test charge (Figure 2.8) and the dielectric spherical particles (Figures 2.5 and 2.6), is that while in the former the pairwise interaction between each relevant point charge is computed explicitly, in the latter the pairwise interactions are computed through integration of charge densities over the surface of the corresponding particles, in a generalisation of Coulomb's law (Equation 2.11). Nonetheless, it is the inverse distance-square character of Coulomb's law that is responsible for the advent of an attractive

regime in both instances, given that the appropriate separation distances are sufficiently short.

2.2.3 Electrostatic potential energy

The electrostatic potential energy of an interaction between two charged particles can be accurately obtained through a numerical integration of the electrostatic force over the inter-particle separation distance. By definition, infinity is the point of reference where the energy of interaction between two charged particles is zero. In practice, then, the integration must be performed from a sufficiently large separation where the interaction energy can be considered to be negligible, where the criteria of negligibility can be defined as the obtained energy or corresponding force being smaller than a threshold of choice. The criterion adopted in this chapter for all numerical calculations of the energy considers the integration starting point as the separation where the electrostatic force is smaller than 10^{-6} (in the considered force unit).

In a two-body system there exist essentially three possible types of interaction between like-charge particles from the perspective of energy, as illustrated in Figure 2.9. When particles repel one another at all values of inter-particle separation distance, the potential energy increases continuously as the particles approach each other. As a consequence, the interaction energy reaches a maximum at the minimum possible separation, i.e. at the touching point, where the surface-to-surface separation $s = 0$, so the electrostatic interaction can be classified as *unstable*, since the particles would be at a lower energy level at any other point.

However, if a like-charge attractive interaction occurs at sufficiently short inter-particle separation distances, then the location where the energy is maximum happens before the touching point. Accordingly, the magnitude of this maximum energy can be identified as a potential energy barrier that needs to be overcome by approaching particles if they are to get closer. The barrier happens exactly at the point where the electrostatic force between the interacting particles is

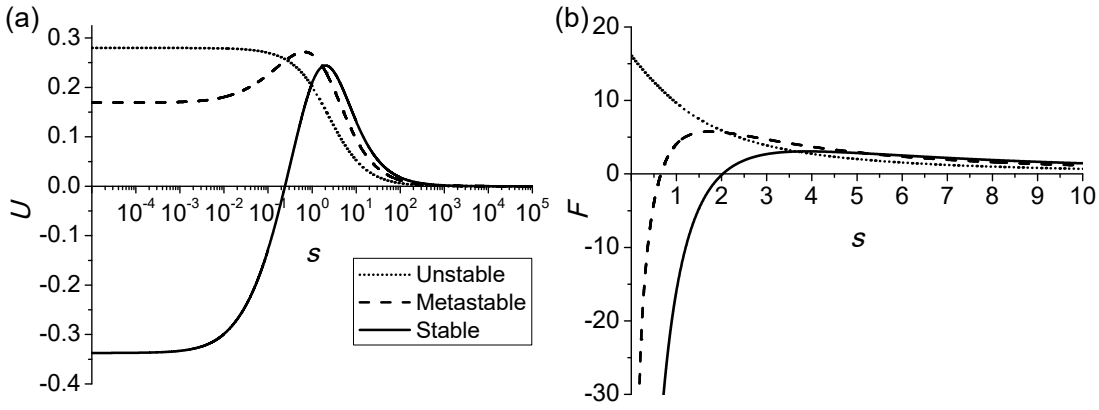


Fig. 2.9 (a) Plots of the electrostatic potential energy U, and (b) electrostatic force F, as function of the surface-to-surface separation s between two interacting particles, for cases of stable (solid line; $a_2 = 3$, $q_1 = 30$), metastable (dashed line; $a_2 = 2$, $q_1 = 20$) and unstable (dotted line; $a_2 = 1$, $q_1 = 10$) interactions. The dielectric constant of both particles, the radius particle 1, and the charge of particle 2 are maintained fixed at $k_1 = k_2 = 20$, $a_1 = 1$ and $q_2 = 10$, respectively. The presented results are dimensionless. Note that the scale of the x-axis is different on each plot.

zero, i.e. at the inflection point that marks the division between the attractive and repulsive regimes. When the energy over the barrier, towards the touching point, is just a local minimum, the interaction can be classified as *metastable*. If the energy over the barrier eventually reaches a value that corresponds to the global minimum energy, however, then the interaction can be classified as *stable*. Equivalently, a reverse energy barrier can be defined as the difference between the global maximum energy and the local minimum energy at shorter separations, which can also be global or not, and that would correspond to an energy barrier that needs to be overcome by touching particles if they are to get separated from each other.

The interaction between two oppositely charged particles or a charged particle and a neutral particle is naturally classified as stable, since it is always attractive, at least when the interaction happens in vaccum.

2.3 The effects of system's parameters on electrostatic interactions

In this section, a more detailed investigation into cases where dielectric particles carrying the same sign of charge interact and the conditions under which like-charge attraction occurs are presented, in the form of a series of calculations that examine how the nature of electrostatic interactions depends on the parameters of the system, namely the dielectric constants, radii and charges of the interacting particles, and the separation between them.

For six different values of dielectric constant of the particles ($k_1 = k_2$), the magnitude of the electrostatic force has been determined as a function of charge ratio (q_2/q_1), ranging from 0 to 10, with $q_1 = 10^3$ e, and radius ratio (a_2/a_1), also ranging from 0 to 10, with $a_1 = 1$ μm. These results are plotted in Figure 2.10. For the purpose of comparison, analytical zero force curves obtained from Lekner's model, [44] which describes the electrostatic interactions between equivalent charged conducting spherical particles, are also plotted in light blue colour.

Essentially, each of the diagrams shown in Figure 2.10 can be divided into three regions: (i) when $a_2 \gg a_1$, the scale of the attractive interaction is dominated by the ability of the particle with higher charge density to polarise the other; this can be achieved even under circumstances where the charge ratio q_2/q_1 is also increasing; (ii) as the ratio a_2/a_1 decreases, the contribution polarisation makes to the interaction diminishes and the force between particles becomes dominated by Coulomb repulsion; (iii) as a_2/a_1 decreases still further, particle polarisation again begins to dominate the strength of the interaction, particularly as the ratio q_2/q_1 increases. For dielectric particles of any composition, this latter combination of a_2/a_1 and q_2/q_1 would appear to provide the most favour conditions for a strong attractive interaction. As Figure 2.10 shows, the dielectric response of each particle makes a significant contribution to the nature of the mutual interaction they experience in close proximity. Even particles composed of

weakly polarisable materials, for example oils, plastics, and dust, as represented by plot (a) in Figure 2.10, can be attracted to one another at certain values of size and/or charge ratios; large differences in charge can lead to particularly strong attraction. As the dielectric constant increases towards the values appropriate for water droplets, [11, 45] a very significant fraction of the contour plot denotes the presence of an attractive interaction between particles.

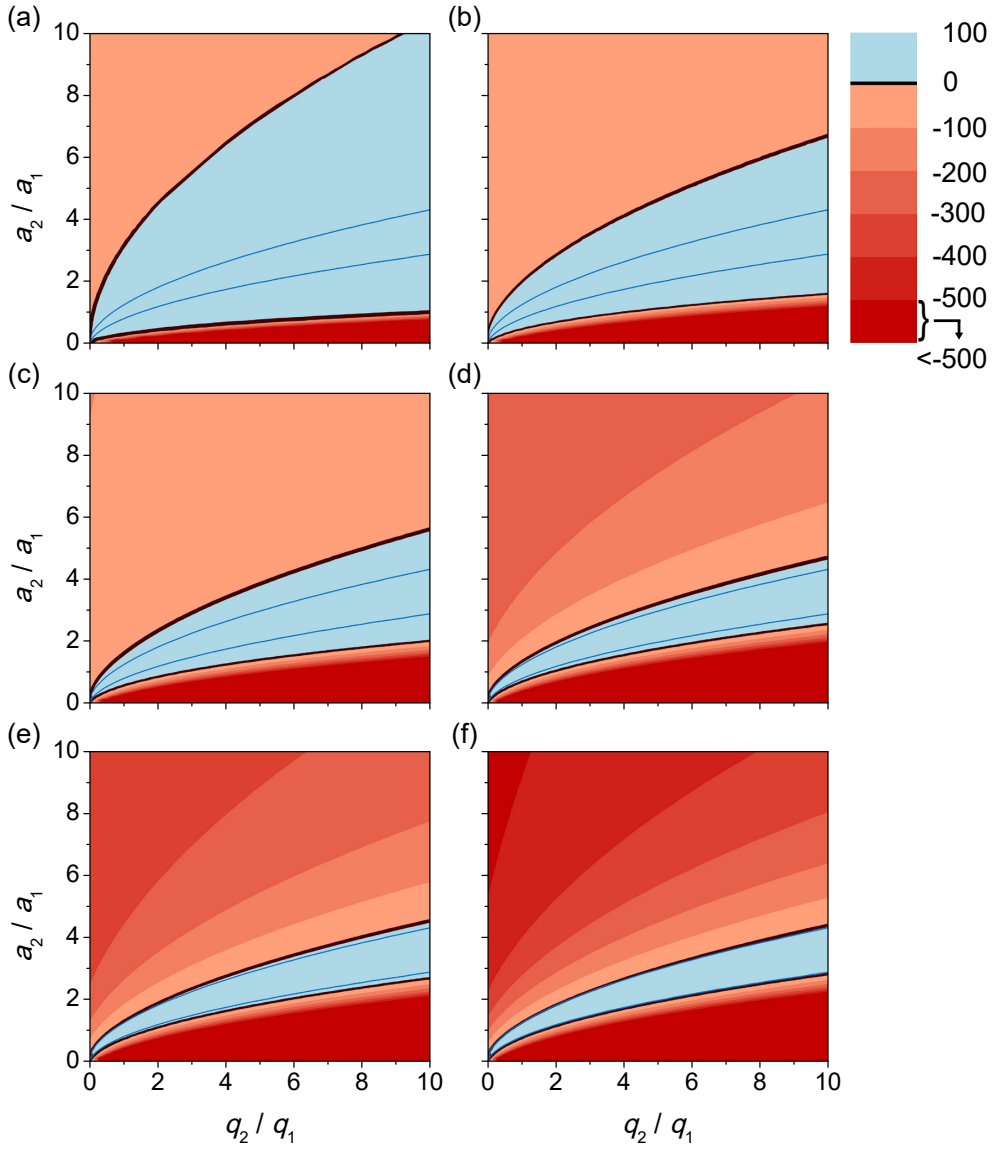


Fig. 2.10 Contour maps of the electrostatic force (pN) as a function of the charge ratio q_2/q_1, and radius ratio a_2/a_1, for a pair of like-charged particles separated by a fixed distance of $s = 0.01$ μm and with different values of the dielectric constant: (a) $k_1 = k_2 = 2$, (b) 5, (c) 10, (d) 40, (e) 80 and (f) 1000. The radius of particle 1 is fixed at $a_1 = 1$ μm and its charge at $q_1 = 10^3$ e. Black coloured curves denote the points where the electrostatic force is zero. Equivalent zero force curves for two conducting particles are also shown in light blue colour.

Figure 2.10 also shows that Lekner's model [44] agrees almost exactly with results obtained from the dielectric model [37] when $k_1 = k_2 = 1000$. Indeed, an increase in the dielectric constants of the particles should enhance their electric susceptibility, so it might be reasonable to assume that, with such high value of dielectric constant, the particles can be so strongly polarised that they effectively adopt a metallic character, consequently being able to mimic the behaviour of a metallic particle when exposed to an external electric field (further details are given later in this chapter).

As Figures 2.2−2.6 would suggest, changing the separation between particles can alter the balance between contributions to the force from the long-range Coulomb repulsion component and the short-range attractive multipole terms. Therefore, the next few examples focus on how the degree of attraction between like-charged particles varies as a function of their separation. For six values of the surface-to-surface separation s, the magnitude of the electrostatic force has been determined as a function of q_2/q_1, again ranging from 0 to 10 with $q_1 = 10^3$ e, and a_2/a_1, likewise ranging from 0 to 10 with $a_1 = 1$ μm. These results are plotted in Figure 2.11. To better illustrate the effect of polarisation and, consequently, the attractive component of the force, the dielectric constants have been fixed at a value of $k_1 = k_2 = 1000$. Analytical zero force curves (in blue) obtained from Lekner's model for conducting particles [44] are once again superimposed in each diagram.

As Figure 2.11 shows, there are clearly defined circumstances where like-charged particles are attracted to one another, even when the separations involved are comparable to their size. For example, particles separated by 1 μm could coalesce if they carry the same amount of charge, but have a radii ratio of 4:1. Both Figures 2.10 and 2.11 show that the attraction between particles can become markedly stronger if there is a large disparity in the amount of charge they carry. The latter effect becomes amplified when it is also accompanied by an increase in the value of the dielectric constant of the interacting particles. It is interesting

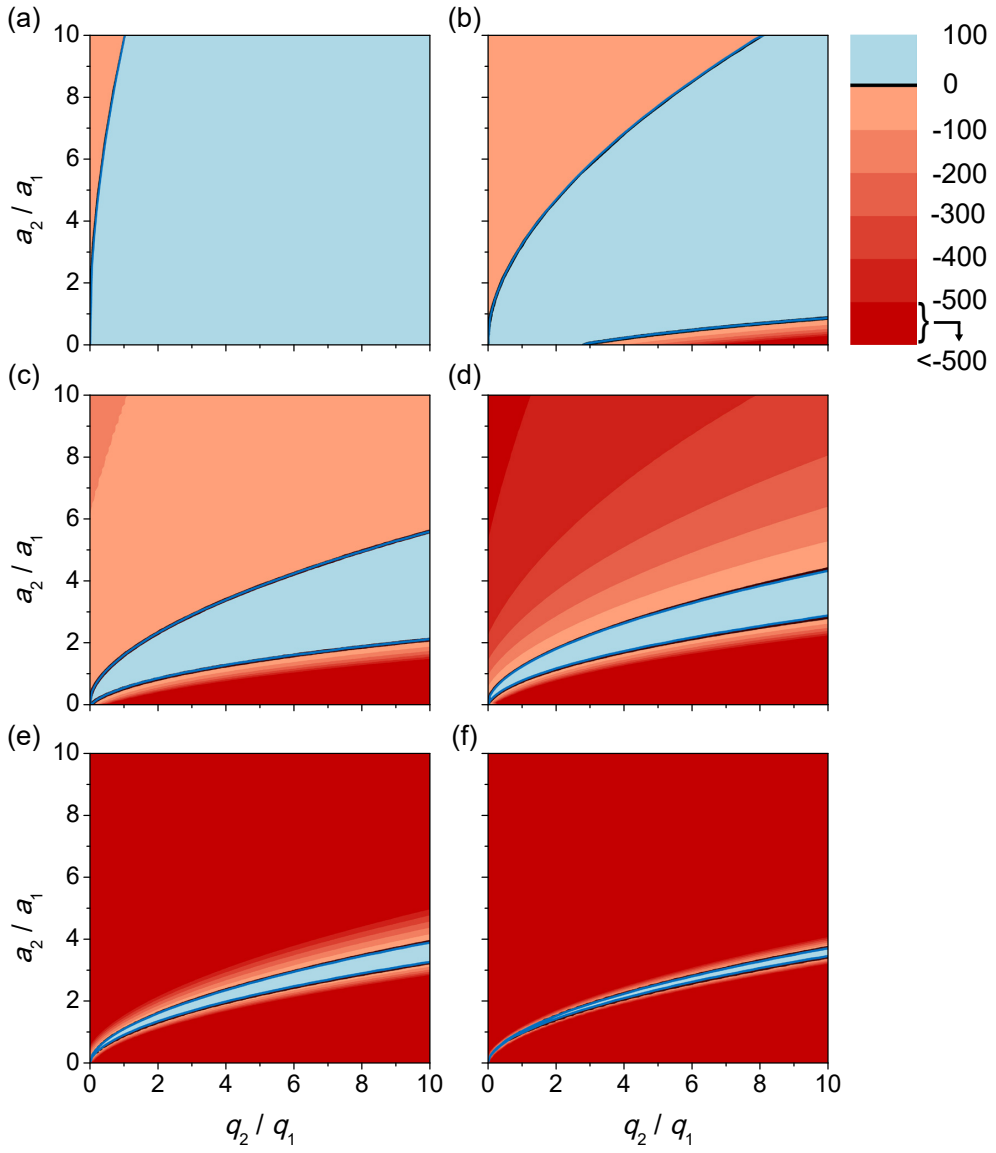


Fig. 2.11 Contour maps of the electrostatic force (pN) as a function of the charge ratio q_2/q_1, and radius ratio a_2/a_1, for a pair of like-charged particles at various surface-to-surface separations: (a) $s = 5$ μm, (b) 1, (c) 0.1, (d) 0.01, (e) 0.001 and (f) 0.0001. The value of the dielectric constant of the particles, the radius of particle 1 and its charge are held fixed at $k_1 = k_2 = 1000$, $a_1 = 1$ μm and $q_1 = 10^3$ e, respectively. Zero force curves are shown in black, and equivalent zero force curves for two conducting particles are shown in blue.

to note that the results in Figure 2.11(a) would suggest that particles of radius 1 μm and 10 μm, both composed of a material of high dielectric constant and carrying a similar amount of charge, would be attracted to one another over a distance of 5 μm. Since these effects scale up, it is straightforward to see how physical processes, such as charge scavenging, [11, 17, 46] can operate quite readily under conditions where one of the particles may have a radius of 1 μm or

more. Also, the good agreement between Lekner's model for conducting particles and the dielectric model with $k_1 = k_2 = 1000$ suggests that results from the latter converge to the correct limit when the theory is applied to particles with very high dielectric constants.

2.4 Electrostatic interactions with respect to the geometry of the system

Much of the research carried out on pair interactions in the field of electrostatics describes the interacting bodies as point particles, spheres or planes. As shown in Figure 2.12, the possible geometries of a two-body interaction include a pair of point particles (which can be described by Coulomb's law in the case of two point charges), the interaction between two spheres, as well as four other geometric combinations drawn from the set of point particles, spheres and planes. Accordingly, a point particle and a plane can be defined as a sphere of infinitely small and infinitely large radius, respectively, as in Lie sphere geometry [47]. However, while the absolute geometry of an indiviual object is mathematically well defined, the geometry of a pair of interacting objects can only be described with respect to their surface-to-surface separation s, for an alternative description based on the centre-to-centre separation h distance would be ambiguous if one of the interacting objects is a plane.

It has already been shown in this chapter that the nature of the electrostatic interaction between two dielectric spherical particles can change markedly depending on the separation between them. If the separation is sufficiently short, the total electrostatic force (obtained from Equation 2.16) deviates from the Coulomb force (obtained from Coulomb's law). However, as the separation increases, the first type of force becomes asymptotically equal to the the latter, irrespective of the particles's dielectric constants. Clearly this change in the geometry of the system seems to have an influence in the nature of the electrostatic interaction.

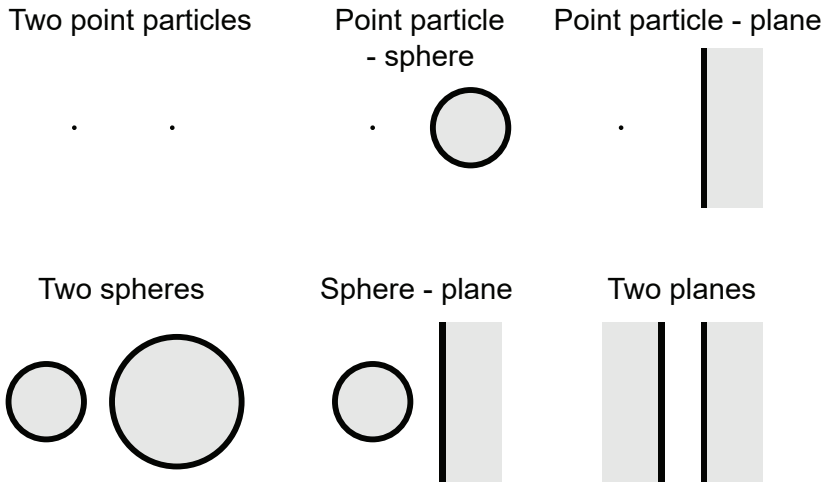


Fig. 2.12 The six different possible geometric combinations of pairwise interactions involving point particles, spheres and planes.

The fact that the force between two finite size dielectric particles can be virtually described by Coulomb's law at sufficiently large separations is already a hint that they might have approached a geometrical limit that is equivalent to two point charges at such condition, i.e. they might effectively "perceive" each other as being point charges instead of finite size particles, if the separation between them is sufficiently large. But the question of how much "sufficiently large" is remains. Therefore, to address this problem, a dimensionless length-scale independent parameter based on the bispherical coordinate system, that describes all possible combinations of sphere size and surface-to-surface separation distance in a two-body system, is introduced next.

2.4.1 The scaled surface-to-surface separation parameter

The bispherical coordinate system, illustrated in Figure 2.13, was first introduced by Jeffery [48] in the derivation of a solution of Laplace's equation in a form that is suitable for a system made of two interacting spheres. In this unusual coordinate system, the position of a point X in space is described with reference to a pair of foci, which are separated by a distance of 2a. The foci are defined as

inverse points of each other such that

$$c_1 d_1 = a_1^2 \tag{2.18}$$

and

$$c_2 d_2 = a_2^2, \tag{2.19}$$

where c_1 and d_1 are inverse-point separations with respect to sphere 1, and c_2 and d_2 are inverse-point separations with respect to sphere 2. The centre-to-centre separation is given by

$$h = s + a_1 + a_2 = 2a + c_1 + c_2. \tag{2.20}$$

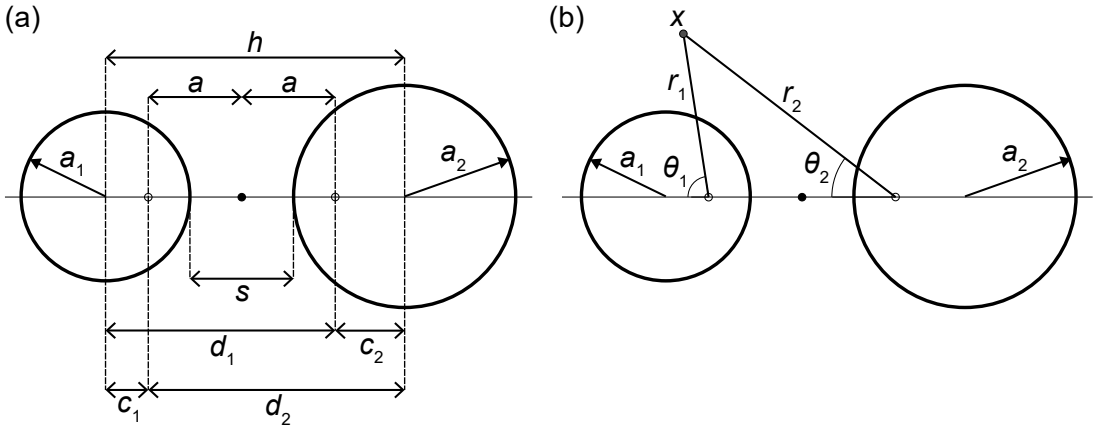


Fig. 2.13 The bispherical coordinate system. (a) Illustration of how the various length quantities, c_1, c_2, d_1 and d_2 are related to the inter-focal separation 2a, centre-to-centre separation h, and surface-to-surface separation s, and (b) how the position of an arbitrary point X in space is described with reference to the two foci.

The bispherical coordinates (η, ξ, φ) are defined as: [48, 49]

$$\eta \equiv -\ln\left(\frac{r_1}{r_2}\right), \quad \xi \equiv \theta_1 - \theta_2,$$

where r_1 and r_2, θ_1 and θ_2 are respectively the distances and angular positions of a point X relative to the two foci. The third coordinate, φ, is the azimuthal angle

about the axis that joins the centres of the spheres. The cartesian coordinates are related as follows:

$$x = \frac{a \sin\xi \cos\varphi}{\cosh\eta - \cos\xi}, \quad y = \frac{a \sin\xi \sin\varphi}{\cosh\eta - \cos\xi}, \quad z = \frac{a \sinh\eta}{\cosh\eta - \cos\xi}.$$

Consideration of equations 2.18−2.20, together with

$$d_1 = c_1 + 2a \tag{2.21}$$

and

$$d_2 = c_2 + 2a \tag{2.22}$$

allows the geometric quantity a, which corresponds to half of the interfocal separation, to be expressed in terms of input paramters of the system, namely the centre-to-centre separation h and the radii a_1 and a_2:

$$a = \sqrt{\frac{h^4 + \left(a_1^2 - a_2^2\right)^2 - 2h^2\left(a_1^2 + a_2^2\right)}{4h^2}}, \tag{2.23}$$

but since h can be written as function of the sphere's radii and the surface-to-surface separation s as $h = a_1 + a_2 + s$, Equation 2.23 becomes

$$a = \sqrt{\frac{\left(a_1 + a_2 + s\right)^4 + \left(a_1^2 - a_2^2\right)^2 - 2\left(a_1 + a_2 + s\right)^2\left(a_1^2 + a_2^2\right)}{4\left(a_1 + a_2 + s\right)^2}}. \tag{2.24}$$

Equation 2.24 diverges only if the radius of both spheres approach infinity, which suggests that this quantity can be used as a parameter to distinguish between geometries of sphere-plane and plane-plane interactions. Accordingly, a scaled surface-to-surface separation $s^* \equiv s/2a$ can be defined, where

$$\lim_{(a_1,a_2)\to(0,0)} s^* = 1 \tag{2.25}$$

for the interaction between two point charges (spheres of infinitely small radius),

$$\lim_{(a_1,a_2)\to(0,\infty)} s^* = \frac{1}{2} \tag{2.26}$$

for an interacting point charge and plane (the latter being a sphere of infinitely large radius), and

$$\lim_{(a_1,a_2)\to(\infty,\infty)} s^* = 0 \tag{2.27}$$

for two interacting planes. For any possible combination of sphere size and separation distance, the value of the parameter s^* lies within the range [0, 1]. A value of s^* close to unity indicates that the system has approached the geometric limit of two point particles, and a value of s^* close to zero indicates that the system has approached the geometric limit of two planes, as depicted in Figure 2.14.

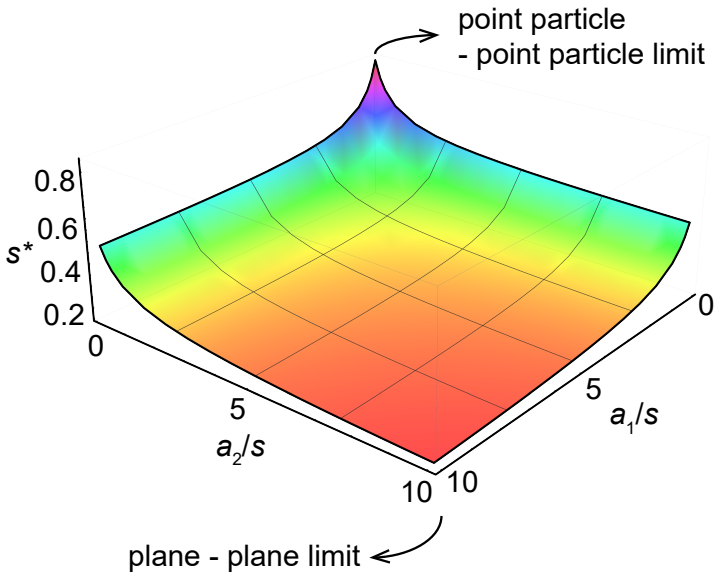


Fig. 2.14 Three-dimensional plot of the scaled surface-to-surface separation s^*, as function of the radii of the spheres divided by the surface-to-surface separation s. It can be noted that, as the radius of both spheres becomes much larger than s, the value of s^* approaches zero. Conversely, as the spheres's radii become much smaller than s, the value of s^* approaches unity.

The parameter s^* proves to be useful in discerning when the distance between two interacting charged particles is sufficiently large, so that the electrostatic interaction can be accurately calculated by Coulomb's law, or oppositely, when

such distance is sufficiently small, which would imply that an accurate computation of the electrostatic interaction must take into account the effects of polarisation. As an example, consider the case where two particles are separated by a fixed distance of $s = 10$ μm. As shown in Figure 2.15, if the radius of both particles are equal to 5 nm, s^* assumes a value that is approximately equal to unity, which indicates that such configuration has approached the geometric limit of two point charges and can be accurately treated only by Coulomb's law. However, for the other configurations in Figure 2.15, the particles's radii are either comparable or much larger than the fixed separation $s = 10$ μm, so the corresponding values of s^* are distant from unity, and so polarisation effects must be accounted for. Similar results could be achieved by varying the surface-to-surface separation s while the radius of both particles are maintained fixed. The key factor here is how the radii of the particles compare to the separation between them.

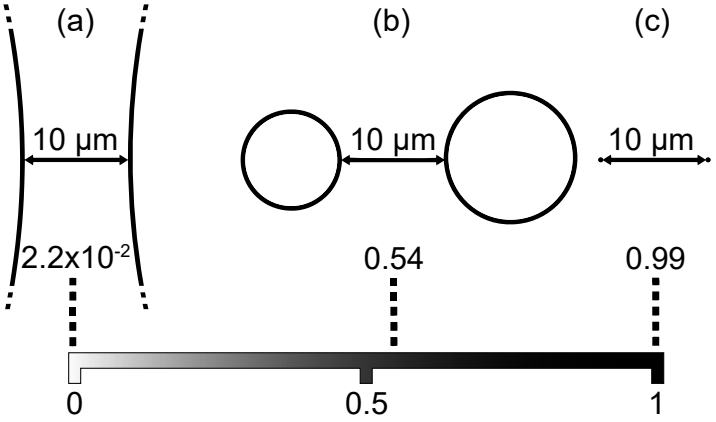


Fig. 2.15 A geometric representation of two spheres with radii (a) $a_1 = a_2 = 5$ mm, (b) $a_1 = 5$ μm and $a_1 = 7.5$ μm, and (c) $a_1 = a_2 = 5$ nm, separated by a fixed surface-to-surface separation $s = 10$ μm. The bar in the bottom represents the scale of the scaled surface-to-surface separation, s^*, and the corresponding value of this parameter is given for each of the three cases.

2.4.2 Electrostatic force and the scaled surface-to-surface separation parameter

For any given charge ratio q_2/q_1, the electrostatic force can now be studied as a function of s^* with respect to any given geometric configuration. As an

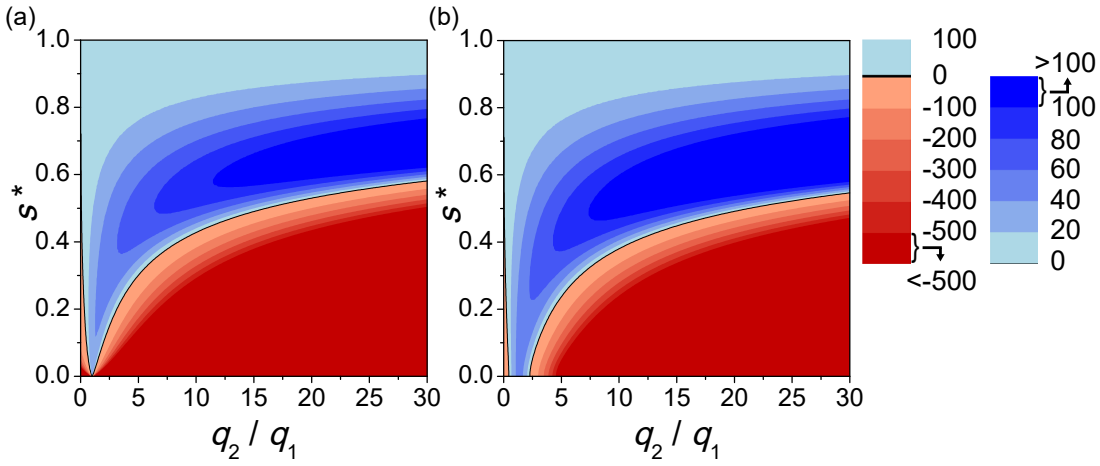


Fig. 2.16 Contour maps of the electrostatic force (pN) between a pair of equal-sized, like-charged particles, with dielectric constants (a) $k_1 = k_2 = 1000$ and (b) $k_1 = k_2 = 10$. The force is plotted as a function of the scaled surface-to-surface separation s^* and the charge ratio q_2/q_1, with $a_1 = a_2 = 1$ μm and $q_1 = 10^3$ e. The regions of attractive and repulsive forces are separated by a thin black solid line, which denotes the cases of zero force.

example, consider a pair of like-charged particles with radius $a_1 = a_2 = 1$ μm. Let the free charge on particle 1 be fixed at $q_1 = 10^3$ e such that the free charge on particle 2 and the surface-to-surface separation account for the only two variables in the system, which can be expressed as the charge ratio q_2/q_1 and the scaled surface-to-surface separation s^*. Figure 2.16 shows how the electrostatic force depends on these two parameters, for two cases: (a) $k_1 = k_2 = 1000$; and (b) $k_1 = k_2 = 10$. For (a), at the limit $s^* = 0$, which can correspond to either two planar surfaces or two large spheres in very close proximity, the repulsive force vanishes completely apart from when $q_2/q_1 \to 1$; as the charge ratio approaches unity from either direction, the magnitude of the repulsive Coulomb term (see Equation 2.12) increases gradually until it balances the attractive multipole terms of the force. However, under all circumstances other than $q_2/q_1 \to 1$, two like-charged equal-sized spherical particles at the limit of $s^* = 0$ will always be attracted to one another if they are of metallic nature. This result is consistent with Lekner's [44] conclusion regarding the behaviour of charged metallic spheres in close proximity. One can note a marked difference at the limit of $s^* \to 0$ for case (b), where the particles have considerably lower dielectric constants and

are therefore less polarisable. The range of q_2/q_1 values over which the particles will repel each other is much larger than for case (a) and, overall, the attractive polarisation contributions to the force are smaller, which means that the region of repulsion is more pronounced. Towards the other geometric limit of $s^* = 1$, for two point particles, the attractive contributions to the total force become increasingly less significant and at some point are overtaken by a more pronounced repulsive Coulomb component. Consequently, the forces in both case (a) and (b) are dominated by the Coulomb term for two point charges and the corresponding contour plots become very similar.

2.4.3 Large sphere approximation to an infinite planar surface

As already mentioned in Section 2.1, a solution to the problem of calculating electrostatic interactions between a pair of objects, made from a combination of dielectric spherical particles and planar surfaces, has also been presented. [38] Further developments demonstrated, however, that this approach does not converge when it considers a charged planar surface. Notwithstanding, any given case involving a sphere − planar surface geometry can still be accurately treated by the formalism based on spherical coordinates [37] as a small particle interacting with a larger particle, provided the ratio involving their radii is sufficiently large.

For instance, consider the case where a small particle with fixed radius $a_1 = 1$ μm and charge $q_1 = 10^3$ e interacts with a neutral particle of increasing radius a_2 that is supposed to mimic a planar surface. Figure 2.17 shows that as the radius of the second particle increases, the difference between the calculated force and the real force between the same small particle and an actual neutral planar surface, obtained from the model based on bispherical coordinates [38], becomes negligible. Hence, this approximation of an infinite planar surface as a sufficiently large sphere provides a mechanism for treating infinite dielectric surfaces that also carry a charge.

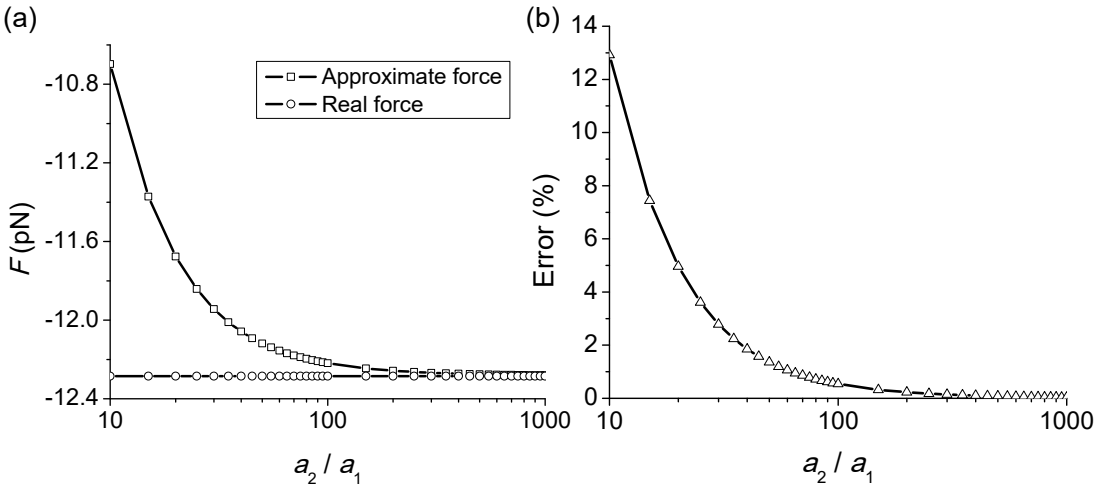


Fig. 2.17 (a) Calculated electrostatic force (pN) as function of the radius ratio between a small charged particle with fixed radius $a_1 = 1$ μm and charge $q_1 = 10^3$ e, and a larger neutral particle (that should mimic an infinite planar surface) with varying radius a_2, separated by a distance of $s = 1$ μm. The line with hollow circle markers denotes the force obtained by the formalism based on bispherical coordinates, considering an actual (neutral) infinite planar surface. (b) Percentage error between the forces given in (a) as function of the radius ratio.

The exact geometry of the target configuration considered in Figure 2.17, namely a particle of radius equal to 1 μm and a planar surface (sphere of infinitely large radius) separated by a distance of $s = 1$ μm, corresponds to a scaled surface-to-surface separation value of $s^* = 0.288675$. In the approximation involving a small and a larger particle, when $a_2/a_1 = 10$, such parameter assumes the value of $s^* = 0.315244$, hence corresponding to an error in s^* of approximately 9.2% when compared to the real planar surface − spherical particle case. When the ratio between the radii increases to $a_2/a_1 = 1000$, however, s^* becomes equal to 0.288964, and the error in s^* drops to less than 0.1%.

2.5 Dimension and scaling of results

In some of the calculations presented in this chapter, e.g. Figures 2.2−2.6, one can note that no units were imputed to the physical quantities, while in others, e.g. Figures 2.7 and 2.8, results were given in particular units, with Coulomb's constant being equated to its reference value of $K \approx 8.987 \times 10^9$ N$\cdot$m$^2\cdot$C^{-2}. Units

can be straightforwardly assigned to a dimensionless result, however. Consider the electrostatic force, for example. Since it is obtained from a generalisation of Coulomb's law (Equation 2.11), units can be imputed to a dimensionless force through multiplication of its value by Coulomb's constant and the appropriate units of charge and distance. For instance, if lengths (surface-to-surface separation and radii of particles) and charges in Figure 2.6 were to be given in micrometres (μm) and elementary units (e), respectively, then a dimensioneless force of -10 would correspond to a force of:

$$\begin{aligned} F &= -10 \times \left(8.987 \times 10^{9}\ \mathrm{N \cdot m^{2} \cdot C^{-2}} \frac{(1.602 \times 10^{-19}\ \mathrm{C})^{2}}{(10^{-9}\ \mathrm{m})^{2}} \right) \\ &= -2.31 \times 10^{-9}\mathrm{N} = -2.31\ \mathrm{nN}. \end{aligned}$$

A similar rationale can be also applied to a dimensioneless energy or surface charge density. Such generality in the results allows for a scaling to be performed with very little restriction. For instance, if the quantities related to the geometry of the system, namely the radii of both particles and their separation, are all scaled by an arbitrary factor α, the electrostatic force will change by a factor of $1/\alpha^2$, in accordance with the inverse distance-square character of Coulomb's law (recall that the force is obtained from a generalisation of Coulomb's law, Equation 2.11). Note that the particles's radii must also be multiplied by the factor α in order to keep the geometry of the system unchanged, which translates to a constant value of the scaled surface-to-surface separation s^*, before and after the scaling. Similarly, the surface charge density of each particle also changes by a factor of $1/\alpha^2$ when such geometric scaling is performed, but the reason is purely geometric. Since it is defined as "charge per surface area" and the area of a spherical particle is equal to $4\pi a_i^2$ $(i = 1, 2)$, it follows that the surface charge density assumes an inverse radius-square character. The interaction energy, on the other hand, only changes by a factor of $1/\alpha$ when the particles's radii and their separation are scaled by α. This comes from the fact that the energy is

inversely proportional to the separation between charges, as evidenced by its definition:

$$U = -\int F dh = -K\, q_1 q_2 \int \frac{1}{h^2} dh = K\frac{q_1 q_2}{h}.$$

An illustration of such scaling process involving the geometric quantities of the system is given in Figures 2.18 and 2.19. Additionally, a scaling can also be performed with respect to the particles's charges, as illustrated in Figures 2.20 and 2.21. It follows directly from the definition of the electrostatic force, energy and surface charge density that, if the charges of each particle are scaled by an arbitrary factor α, the three above-mentioned quantities will change by a factor of α^2, α^2 and α, respectively.

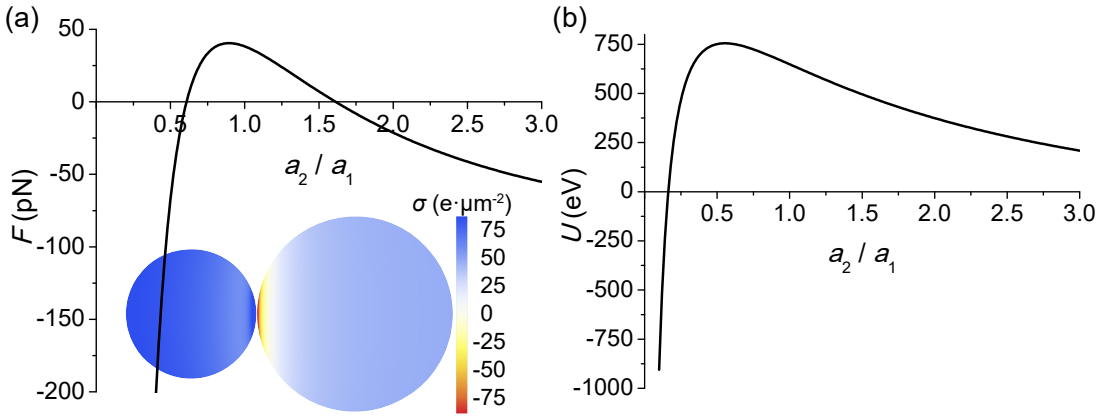


Fig. 2.18 Plots of the (a) electrostatic force (pN) and (b) interaction energy (eV) as function of the radius ratio a_2/a_1, where $a_1 = 1$ μm and a_2 accounts for the only variable of the system. The other parameters are held fixed at $k_1 = k_2 = 10$, $q_1 = q_2 = 10^3$ e and $s = 0.01$ μm. Inset shows the total surface charge density $(\mathrm{e} \cdot \mu\mathrm{m}^{-2})$ mapped out for each of the particles, corresponding to the point where $a_2/a_1 = 1.5$.

These observations suggest a certain degree of generality of the results, in the sense that values for the physical quantities can be scaled up or down to any desired order of magnitude. For example, in the results shown in Figure 2.10 and 2.11, the values of force, length (radii and separation distances) and charge are given respectively in units of piconewtons, micrometres and orders of 10^3 e; however, the same contour maps would be obtained if these same values were

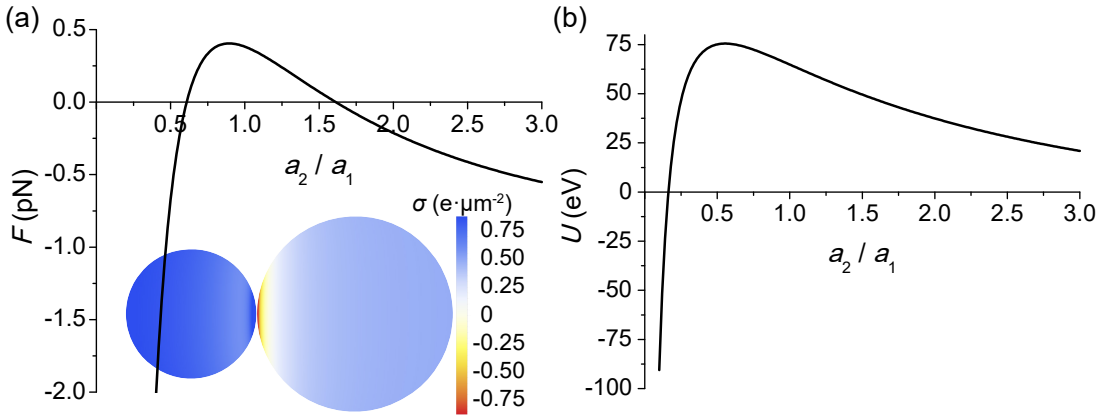


Fig. 2.19 Plots of the (a) electrostatic force (pN) and (b) interaction energy (eV) as function of the radius ratio a_2/a_1, for the same case addressed in Figure 2.18, with the difference that quantities related to the geometry of the system, a_1 and s, have been multiplied by a factor $\alpha = 10$.

given in micronewtons, millimetres and orders of 10^9 e. The only restriction one needs to be aware of when performing a scaling of results is that if, for instance, a geometric scaling is to be executed, then all geometric quantities must be involved. Equivalently, if a scaling is with respect to the charges on the particle, then the charges of both interacting particles must be involved.

Although the model [37] is mathematically indifferent to numbers and units imputed to it, so one could easily determine, for instance, the electrostatic

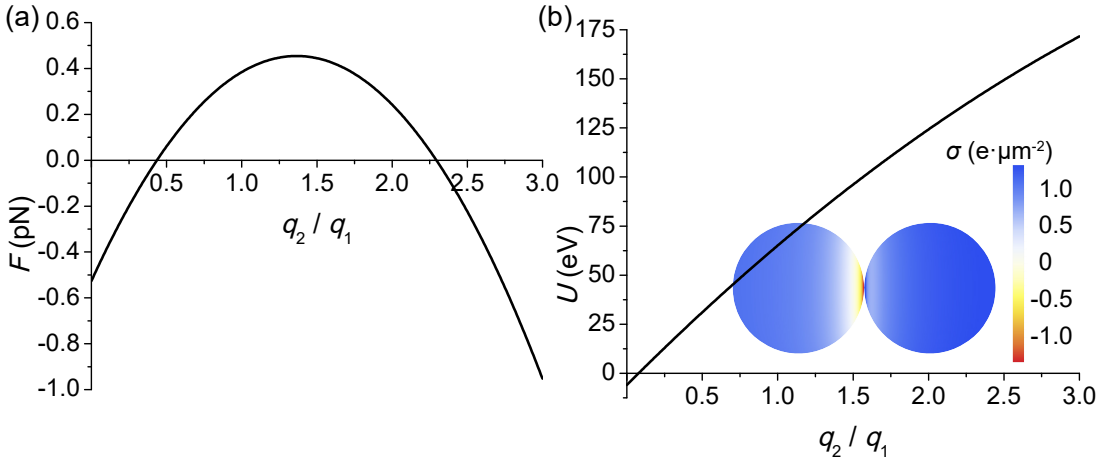


Fig. 2.20 Plots of the (a) electrostatic force (pN) and (b) interaction energy (eV) as function of the charge ratio q_2/q_1, where $q_1 = 10^3$ e and q_2 accounts for the only variable of the system. The other parameters are held fixed at $k_1 = k_2 = 10$, $a_1 = a_2 = 10$ μm and $s = 0.01$ μm. Inset shows the total surface charge density $(\mathrm{e} \cdot \mu\mathrm{m}^{-2})$ mapped out for each of the particles, corresponding to the point where $q_2/q_1 = 1.5$.

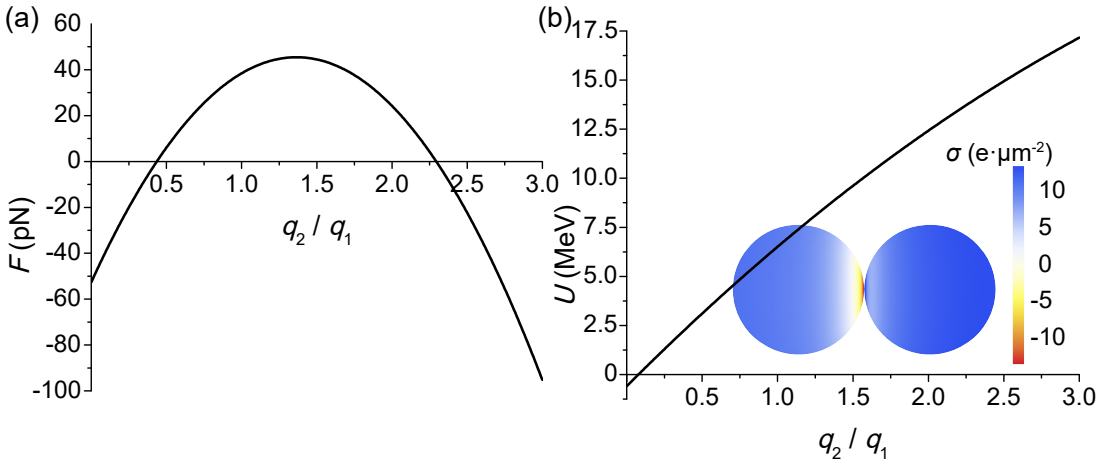


Fig. 2.21 Plots of the (a) electrostatic force (pN) and (b) interaction energy (MeV) as function of the charge ratio q_2/q_1, for the same case addressed in Figure 2.20, with the difference that q_1 has been multiplied by a factor $\alpha = 10$.

interaction between two dielectric particles with radii equal to 1 femtometres (fm), the result would have no physical significance, since at this order of magnitude the calculation looses its validity. Therefore, one should always have good judgement regarding the choice of parameters in a calculation, so that the results are in accordance with the physics of the problem.

2.6 Convergence rates

Since the electrostatic force between two dielectric particles, given by Equation 2.16, is represented as a sum of a Coulomb (monopole) term and a convergent expansion of several (N) multipole terms, it is instructive to examine how rapidly such expression converges. Presented next then is a series of convergence tests, where is also investigated the differences between the solution based on spherical coordinates [37] and the equivalent solution based on bispherical coordinates [38].

Figure 2.22 shows the results of calculations, where the number of terms in the multipole expansion that is required to achieve a precision of ten significant figures in the calculated electrostatic force has been explored in terms of three variables of the system: surface-to-surface separation s, radius ratio a_2/a_1, and dielectric constants, $k_1 = k_2$. The influence of the charge ratio q_2/q_1 is considered

separately in Figure 2.24. Since the effects of polarisation are manifested through multipole terms, the results in Figures 2.10 and 2.11 would suggest that considerable differences might be expected in the number of terms required to achieve convergence when the ratios of particle size and charge are different from unity and/or when there are variations in particle−particle separation.

According to Figure 2.22(a), it appears that the number of necessary terms responds to the surface-to-surface separation s as would be expected; the result reflects the distance-dependence of the multipole terms that appear in the expansion, which vary as a combination of increasing inverse powers of h. The first few multipole terms contributing to the force are monopolar, dipolar, and quadrupolar in nature and, at sufficiently large distances, namely where the system is close to the limit of two point charges ($s^* \to 1$), Figure 2.22(a) would imply that only the monopole term prevails (also see Figures 2.2−2.6). However, as the particle−particle separation decreases, there is a very evident and rapid increase in the number of terms required to achieve convergence. In some respects, the number of terms in the expansion can be considered as an indirect measure of the level of induced polarisation taking place between the two interacting particles. At very large values of s, there is virtually no polarisation and therefore a minimum number of terms is required; however, close to the touching limit of $s = 0$, the degree of induced polarisation is very high. As can also be seen, for small values of s, the solution based on spherical coordinates [37] converges with fewer terms than the equivalent bispherical solution [38].

Figure 2.22(b) shows how the convergence of the multipole series depends on the radius ratio a_2/a_1 where, to simplify the problem, the geometric variables a_1 and s have been fixed and only a_2 has been allowed to vary. As can be seen, the number of terms required to achieve convergence increases as the ratio a_2/a_1 moves away from unity in either direction; however, for $a_2/a_1 > 1$ there is a particularly dramatic increase seen in the number of terms required. As in the discussions for Figures 2.5, 2.6, 2.10 and 2.11, the occurrence of like-charge

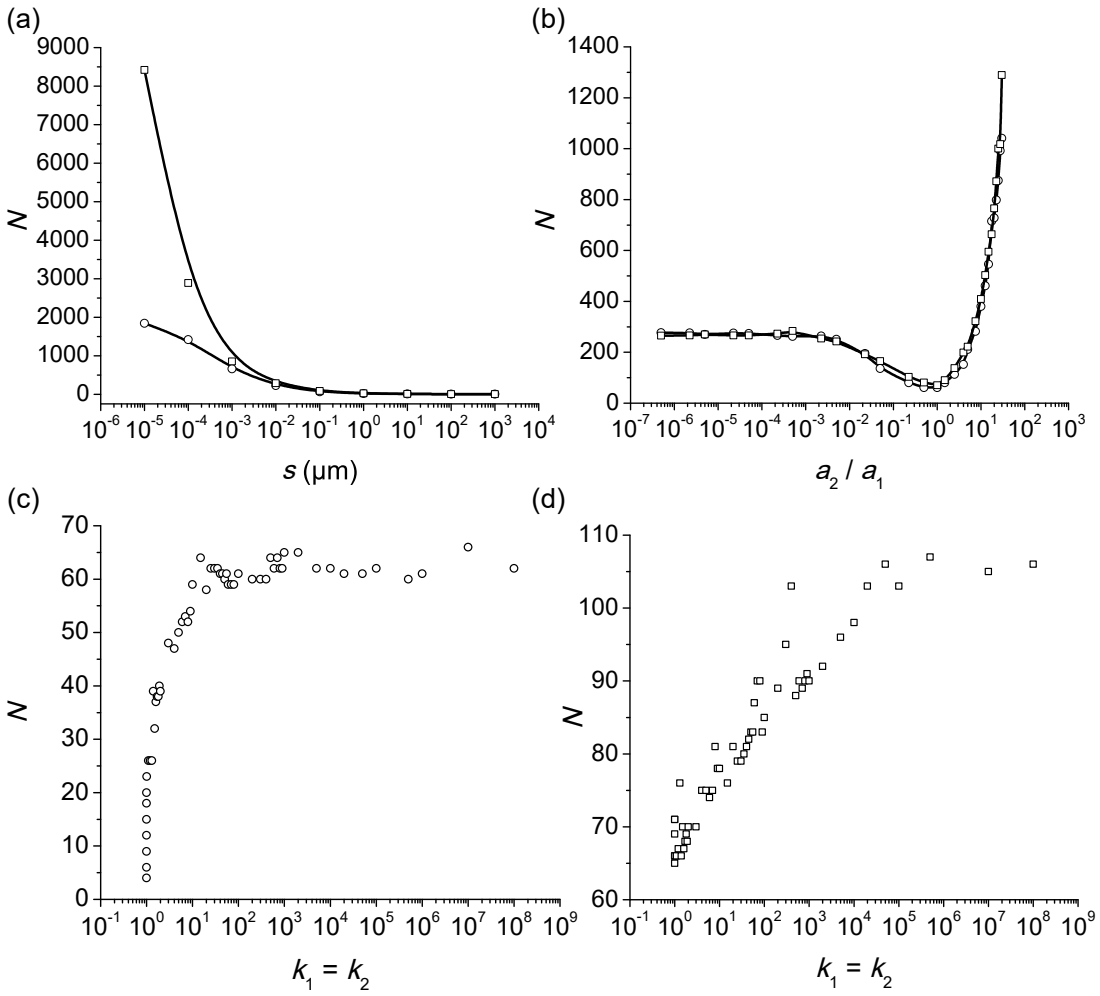


Fig. 2.22 Plots of the minimum number of terms N in the multipole expansion of Equation 2.16, required to obtain a converged electrostatic force between two particles with a precision of ten significant figures, as function of the (a) surface-to-surface separation s, (b) radius ratio a_2/a_1, and (c) and (d) dielectric constants $k_1 = k_2$, determined using the solution based on spherical coordinates (curves with hollow circle markers) and the equivalent solution based on bispherical coordinates (curves with hollow square markers). In all instances, the particles's parameters are fixed at $k_1 = k_2 = 40$, $a_1 = 2$, $a_2 = 1$, $q_1 = 2 \times 10^3$, $q_2 = 1 \times 10^3$, and $s = 0.1$, unless the respective parameter is being considered as a variable in the plot. In (b), a_1 is still fixed and a_2 is allowed to vary.

attraction is conditional upon either a sufficiently large asymmetry with respect to the particles's radius or charge. In the situation where $a_2/a_1 \approx 1$, neither of these conditions is met, and therefore the number of terms required to describe the effects of polarisation reaches a minimum. With a progressive decrease in a_2, the system begins to resemble the point charge − spherical particle case, where mutual polarisation no longer occurs and the number of terms needed to account

for the behaviour of (a fixed radius) particle 1 rapidly reaches an upper limit. In contrast, a progressive increase in the radius of particle 2, such that $a_2/a_1 > 1$, moves the system towards the planar surface − spherical particle limit. Hence, as a_2 increases (whilst maintaining fixed values for a_1 and s) the polarisable volume available within particle 2 increases rapidly, and this is reflected in the number of terms required to achieve convergence.

The behaviour of the two mathematical solutions in response to changes in the value of the dielectric constant assigned to each particle is illustrated in Figures 2.22(c) and (d). While there is a marked difference between the two cases for relatively low values of the dielectric constant, in both cases the number of terms required for convergence approaches a constant value for increasing dielectric constant, and it eventually flattens out. Indeed, a particle i in an external electric field has an electric susceptibility that is proportional to $(k_i - 1)$, and for high values of the dielectric constant k_i, a dielectric particle will have a great degree of freedom to counterbalance an external electric field and so minimise the system's electrostatic energy by means of an induced bound charge. At the theoretical limit of infinite k_i, a particle will enjoy complete freedom to polarise itself to achieve energy minimisation. This is analogous to the case of a charged metallic particle, where its charge is free to redistribute virtually instantaneously in response to an electric field, effectively minimising its energy. Zettergren et al. have shown theoretically [30] that a charged spherical particle of infinite dielectric constant will achieve the same lowest-energy charge distribution as a charged metallic sphere, if they are placed in the neighbourhood of a point charge. Moreover, Figure 2.23 depicts vector plots of the electric field relative to two interacting particles, where it is shown that, as the dielectric constant of a particle increases, the electric field in its interior fades away, and for a particle with sufficiently high dielectric constant, the electric field in its interior goes to zero; behaviour similar to that observed in a particle of metallic nature. So it becomes clear to understand that the number of terms required for convergence eventually

flattens out at high values of $k_1 = k_2$ in Figures 2.22(c) and (d) once the charge distribution corresponding to the lowest electrostatic energy is achieved. Also, while the difference between Figures 2.22(c) and (d) would imply that fewer terms are needed in the solution based on spherical coordinates to provide an accurate representation of the polarisation of a particle, from either solution it is evident that a considerable number of terms is required to provide an accurate description of the interaction between highly polarisable particles, such as two water droplets. [11] As noted earlier, although slower to converge, the strength of the bispherical solution lies in the ability to model charged particle - neutral surface interactions.

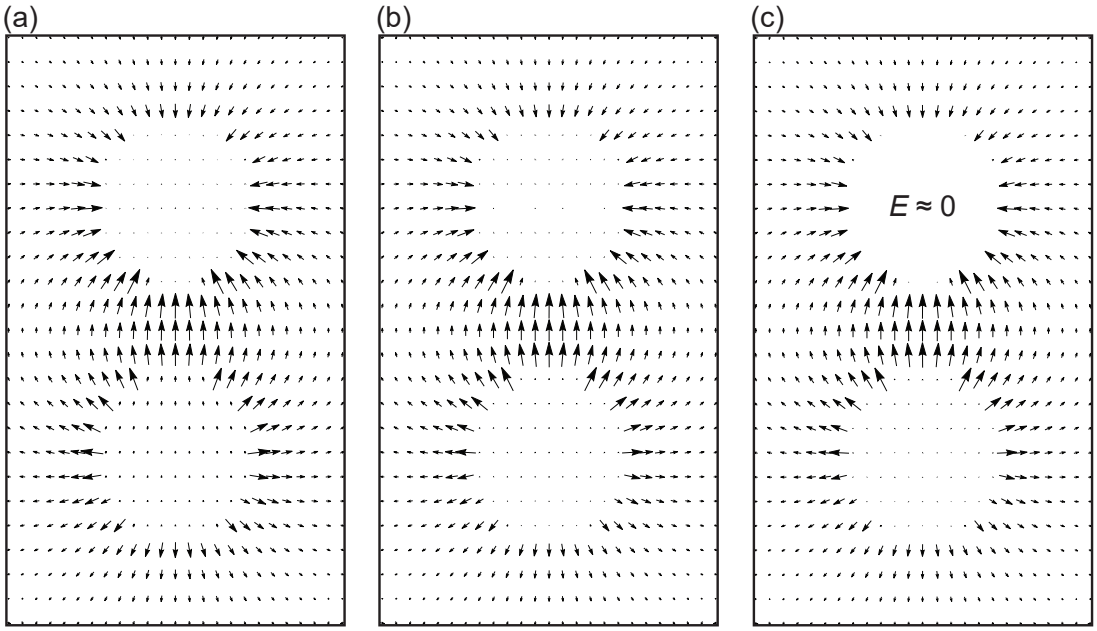


Fig. 2.23 Vector plots of the electric field related to an interaction between two equal-sized and oppositely charged particles, with dielectric constants (a) $k_1 = 1$, $k_2 = 80$, (b) $k_1 = 10$, $k_2 = 1000$, and (c) $k_1 = 20$, $k_2 = 10^6$. Note that the size of the arrows is proportional to the magnitude of the field at the corresponding point and the particle $i = 1$ is placed at the bottom. As can be seen, as the dielectric constant of a particle increases, the arrow in its interior and, hence, the magnitude of the corresponding electric field, diminishes.

The convergence profile with respect to the charge ratio q_2/q_1 is shown in Figure 2.24. In contrast to the previous tests, depicted in Figure 2.22, the number of terms in the multipole series only fluctuates as the charge ratio changes. Since polarisation effects depend on the size of the interacting particles, the fixed radii (limited volume) mean that the level of polarisation of both particles becomes

saturated, even if they continuously acquire more charge. The y-axis on Figure 2.24 is deliberately set to be the same as that for Figure 2.22(b) in order to show that the response of the multipole expansion to changes in q_2/q_1 is reduced significantly from that seen for changes in particle separation, radius and dielectric constant. Nevertheless, as already mentioned above, there are fluctuations in the conditions necessary for series convergence and these can be seen on an expanded scale in the inset to Figure 2.24. In response to changes in q_2/q_1, there is no significant difference between the two mathematical solutions.

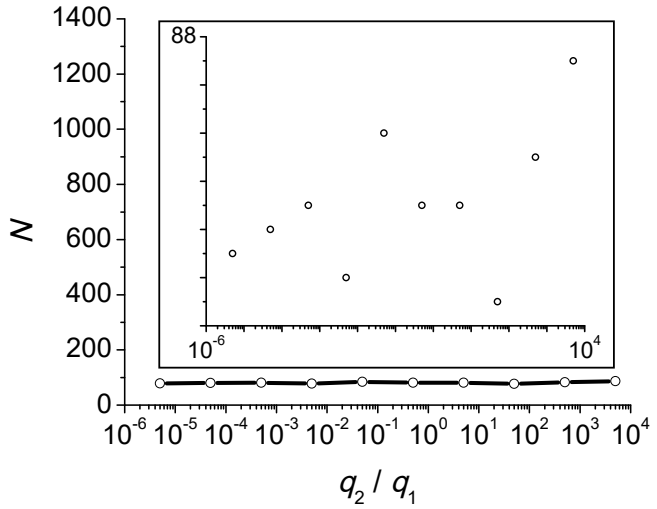


Fig. 2.24 Plot of the minimum number of terms N in the multipole expansion, required to obtain a converged electrostatic force between two particles with a precision of ten significant figures, as function of the charge ratio q_2/q_1, where $q_1 = 2 \times 10^3$. The remaining parameters are fixed at $k_1 = k_2 = 40$, $a_1 = 2$, $a_2 = 1$, and $s = 0.1$. Inset shows an expanded y-axis. Only data points taken from the solution based on spherical coordinates are shown, due to a great similarity to its counterpart in this case.

In a number of applications, particularly when used in conjunction with water droplets, the equivalent point charge − spherical particle series expansion is often truncated after the first few terms. [11]. To verify if such approximation is justified, the consequences on the calculated force of neglecting higher order terms in the multipole expansion is examined next, in a few practical examples where two dielectric particles interact. Figure 2.25 gives the percentage error in the calculated force obtained by truncating the number of terms at N, corresponding to four different sets of parameters, where two possible values for the particles's

dielectric constants are considered: $k_1 = k_2 = 5$, a value that might be appropriate for an interaction between charged oil droplets, and $k_1 = k_2 = 80$, matching the conditions of the charge scavenging mechanism used to describe the growth of water droplets in clouds. [11] According to Figure 2.25, if a calculation of the electrostatic force between two water droplets separated by 1 μm just used the first 10 terms in the multipole expansion, then the final result would be in error by $\approx 35\%$. To maintain the same percentage error when the surface-to-surface separation is reduced to 0.1 μm it would require over 20 terms. Even for materials with a low dielectric constant, there would appear to be a need for significantly more terms than just the usual charge − induced dipole to give a quantitative account of a particle−particle interaction.

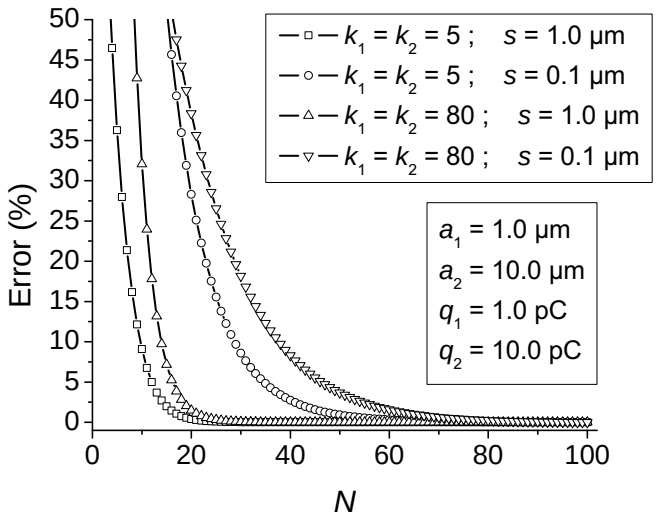


Fig. 2.25 Plot of the percentage error in the calculated electrostatic force with respect to the reference value (with a precision of ten significant figures) as a function of the number of terms N in the multipole expansion of Equation 2.16.

2.7 The growth of charged aerosol particles in Titan's atmosphere

In the last section of this chapter, a direct application of the two-body formalism [37] to an experimental case is presented, where it is investigated the

role certain types of charged particles might have in the formation of aerosols in the atmosphere of Titan.

2.7.1 Experimental data and the Cassini–Huygens mission

Titan is Saturn's largest moon and the only satellite in the Solar System known to display a dense atmosphere [50], harbouring several organic compounds and particular conditions that led some authors to even consider the presence of different life forms [51–54]. Over the past few decades, a significant amount of new information about Titan has been acquired, especially with the arrival of the Cassini-Huygens spacecraft in 2004 at Saturn and its moons, which allowed Titan's atmosphere and surface to be studied in greater detail, through *in situ* measurements made by the lander Huygens and the Cassini orbiter.

The atmosphere of Titan is presently known to stage a series of chemical and physical processes that are ultimately responsible for the formation of its characteristic orange haze. Composed primarily of nitrogen (N_2) and methane (CH_4) [50, 55, 56], Titan's atmosphere is constantly bombarded by sources of energy such as solar ultraviolet radiation and energetic particles from Saturn's magnetosphere. Such events trigger the dissociation and ionisation of these simple primordial molecules and subsequently leads, through a series of chemical and physical processes, to the formation of charged aerosol particles with an average mass of 500 Da [57] at altitudes between 950 and 1150 km (upper atmosphere) [55, 56, 58–60]. With decreasing altitude, these particles grow spherically until they reach the detached haze layer at 520 km in Titan's mesosphere, from where they start to form fractal aggregates [56, 61–63].

Several studies have already shown the crucial role of ion-neutral chemistry and physical aggregation in the production of aerosols in Titan's atmosphere [56–58, 61–70]. However, in all of them, it was broadly assumed that like-charged particles will always repel one another and so any such interactions will make no contribution to the growth of aerosols [57]. Whilst this concept is generally true,

it has been shown through this chapter that, if certain circumstances are met, attraction between particles with the same sign of charge can occur due to effects of polarisation.

In the following, calculations for the interaction between a range of particles of various radius and charge, representative of the aerosols found in Titan's atmosphere, are presented. Interactions between neutral and charged particles as well as between oppositely charged particles are not considered, though, since these are already taken to be attractive under similar conditions. The calculations also examine how differences in the dielectric constants of particles could lead to a preferential concentration of nitrogen-containing aerosols in the lower atmosphere of Titan.

2.7.2 The potential contribution of like-charge attraction

Depending on the assumed mass density, particles produced in the upper atmosphere of Titan have an estimated radius of either 0.6 nm or 6 nm if 1 elementary charge per particle and densities of 1000 kg $\cdot$m^{-3} [57] or 1 kg $\cdot$m^{-3} [71, 72], respectively, are considered. Regardless of their initial size, these particles grow as they sink towards lower altitudes eventually forming large particles with radii of 40-50 nm, which have been identified as being present in the detached haze layer [61, 62, 73, 74]. Since the amount of charge on the embryonic particles cannot be independently measured, actual sizes could be larger than those estimated above [55, 58]. For example, a particle bearing 5 elementary charges would have a radius approximately 1.7 greater than the same particle carrying just 1 charge. To take into account this degree of uncertainty, the calculations presented here consider charge per particle values that range from 1 to 5 e.

Table 2.1 shows values of potential energy barriers (eV) calculated for different cases where two like-charged particles interact. These examples have been chosen to represent the process of particle growth that occur in Titan's upper atmosphere, leading to the production of aerosol monomers in the detached haze layer. In each

sub-table, the radius a_2 and charge q_2 of particle 2 have been allowed to vary from 5 to 50 nm and 1 to 5 e, respectively, whilst the equivalent parameters a_1 and q_1 for particle 1 have remained fixed. Each particle has been assigned a dielectric constant of $k_i = 20$, since this value is comparable to that of many hydrocarbon-nitrile compounds [45], and so should be representative of nitrile-rich aerosols. It is worth noting that the spherical geometry of the particles in the model [37] is in accordance with the spherical nature of the particles that are present at the region considered in the calculations, i.e. from the upper atmosphere to the detached haze layer. [56, 61–63].

As can be seen from Table 2.1, examples of unstable interactions occur at or near the point where the interacting particles have identical characteristics, i.e. $a_1 = a_2$ and $q_1 = q_2$, and in general they extend across points where a_2/a_1 and q_2/q_1 increase concurrently. Cases of stable interaction occur when the particles have sufficiently dissimilar sizes, and are more generally favoured when the smaller of the two particles carries more charge. Metastable interactions fall between these two scenarios. The magnitude of the energy barrier varies inversely with particle radii and increases with the amount of charge. Broadly speaking, as interacting particles increase in size, the free charge on one becomes, on average, more distant from the free charge on the second particle, which then contributes to a decrease in Coulomb repulsion and, consequently, a decrease in the energy barrier. In contrast, for a fixed particle size, an increase in the amount of free charge on one or both particles means that more charge occupies a fixed area, which then contributes to an increase in Coulomb repulsion and, consequently, an increase in the magnitude of the energy barrier.

Figure 2.26(a) shows a Maxwell-Boltzmann distribution of the kinetic energy of particles, calculated for the upper and lower average temperatures, 112 K and 175 K [75], as identified for Titan's thermosphere. The calculations presented in Table 2.1 suggest that at the beginning of the aerosol growth process, when particles are particularly small, the Coulomb repulsion barrier, generally greater than kT,

Table 2.1 Calculated energy barriers (eV) between two interacting like-charged, dielectric particles, for a range of radii (nm) and charge (e). White, light and dark grey shades denote stable, metastable, and unstable interactions, respectively. The charge q_1 and q_2 can be simultaneously regarded as either positive or negative.

(a) $a_1 = 5$; $q_1 = 1$; $k_1 = k_2 = 20$

q_2										
5	0.49	0.43	0.33	0.25	0.20	0.17	0.14	0.13	0.11	0.10
4	0.41	0.35	0.25	0.19	0.16	0.13	0.11	0.097	0.086	0.078
3	0.33	0.26	0.18	0.14	0.11	0.092	0.079	0.069	0.062	0.055
2	0.24	0.17	0.11	0.086	0.069	0.057	0.049	0.043	0.038	0.034
1	0.13	0.074	0.049	0.037	0.030	0.025	0.021	0.019	0.016	0.015
a_2	**5**	**10**	**15**	**20**	**25**	**30**	**35**	**40**	**45**	**50**

(b) $a_1 = 10$; $q_1 = 1$; $k_1 = k_2 = 20$

q_2										
5	0.24	0.24	0.24	0.21	0.19	0.16	0.14	0.12	0.11	0.10
4	0.21	0.21	0.20	0.17	0.15	0.13	0.11	0.097	0.086	0.078
3	0.17	0.17	0.15	0.13	0.11	0.092	0.079	0.069	0.062	0.055
2	0.13	0.12	0.10	0.084	0.068	0.057	0.049	0.043	0.038	0.034
1	0.074	0.064	0.048	0.037	0.030	0.025	0.021	0.019	0.016	0.015
a_2	**5**	**10**	**15**	**20**	**25**	**30**	**35**	**40**	**45**	**50**

(c) $a_1 = 20$; $q_1 = 1$; $k_1 = k_2 = 20$

q_2										
5	0.12	0.12	0.12	0.12	0.12	0.12	0.11	0.11	0.10	0.094
4	0.10	0.10	0.10	0.10	0.10	0.098	0.093	0.087	0.080	0.074
3	0.084	0.084	0.084	0.083	0.081	0.076	0.071	0.065	0.059	0.054
2	0.063	0.063	0.062	0.061	0.057	0.052	0.047	0.042	0.038	0.034
1	0.037	0.037	0.036	0.032	0.028	0.024	0.021	0.018	0.016	0.015
a_2	**5**	**10**	**15**	**20**	**25**	**30**	**35**	**40**	**45**	**50**

(d) $a_1 = 30$; $q_1 = 1$; $k_1 = k_2 = 20$

q_2										
5	0.081	0.081	0.081	0.081	0.081	0.081	0.081	0.080	0.079	0.077
4	0.069	0.069	0.069	0.069	0.069	0.069	0.068	0.067	0.065	0.063
3	0.056	0.056	0.056	0.056	0.056	0.056	0.055	0.053	0.051	0.048
2	0.042	0.042	0.042	0.042	0.041	0.040	0.039	0.037	0.034	0.032
1	0.025	0.025	0.025	0.024	0.023	0.021	0.020	0.018	0.016	0.015
a_2	**5**	**10**	**15**	**20**	**25**	**30**	**35**	**40**	**45**	**50**

(e) $a_1 = 40$; $q_1 = 1$; $k_1 = k_2 = 20$

q_2										
5	0.061	0.061	0.061	0.061	0.061	0.061	0.061	0.061	0.061	0.060
4	0.052	0.052	0.052	0.052	0.052	0.052	0.052	0.052	0.051	0.051
3	0.042	0.042	0.042	0.042	0.042	0.042	0.042	0.042	0.041	0.040
2	0.031	0.031	0.031	0.031	0.031	0.031	0.031	0.030	0.029	0.028
1	0.019	0.019	0.019	0.018	0.018	0.018	0.017	0.016	0.015	0.014
a_2	**5**	**10**	**15**	**20**	**25**	**30**	**35**	**40**	**45**	**50**

is high enough to reduce the coagulation rates between like-charged particles. Hence growth is restricted to oppositely charged interactions, and notably the

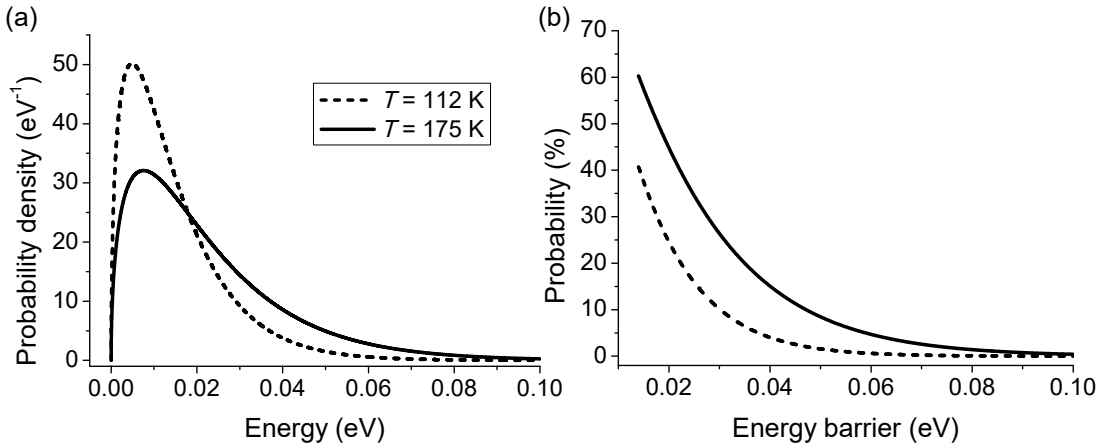


Fig. 2.26 (a) Maxwell-Boltzmann distribution of the kinetic energy of the particles at the upper and lower Titan's thermosphere average temperatures. (b) Probability (%) that particles, with a thermal energy of kT, will overcome the barrier as function of the latter's magnitude, evaluated for the two extreme temperatures. In the second plot, any point after the maximum value for the x-axis has a corresponding probability that is always lower than 0.5 %.

absorption of positive ions by the large negatively charged particles [57], or even neutral-charged particle interactions. However, as particle growth continues, the charge density drops and the corresponding Coulomb barrier decreases in magnitude, eventually becoming comparable to or even smaller than kT. In which case, a colliding pair of like-charged particles could interact under stable or metastable conditions and contribute to the growth process. For example, taking the case shown in Table 2.1(c) where $a_1 = 20$ nm, $a_2 = 10$ nm and $q_1 = q_2 = 1$ e, the interaction is predicted to be metastable with a barrier height of 0.037 eV. According to Figure 2.26(b), there is, at the above temperatures, an $8-18$ % probability that the particles will have sufficient energy to overcome the barrier. Any barrier higher than 0.1 eV is unlikely to be overcome.

In cases that involve low Coulomb barriers it can be considered that like-charged interactions, especially those between the more abundant negatively charged particles, can contribute to growth via a scavenging mechanism, similar to that identified for the formation of clouds on Earth [10, 76, 46]. In that case, sufficiently large aerosol droplets will grow by assimilating smaller particles even when they are like-charged. This mechanism should then be regarded as a

potential component of the whole aerosol growth process, along with the usually considered interactions between oppositely charged particles and neutral-charged particle collisions. Table 2.1 also suggests that an increase in the Coulomb repulsion barrier with the amount of charge residing on particles should prevent large departures from neutrality with respect to the growing aggregates. Therefore, the absorption of positive ions by large negatively charged particles and a charge scavenging mechanism are very likely to operate synergistically. The presence of positively charged particles would act to keep a low net charge on growing particles, whilst a charge scavenging mechanism would be highly favourable due to the higher abundance of negatively charged particles. It is worth mentioning that this mechanism operates irrespective of the sign of particle's charge. That is, if there is an initial bias towards, for instance, the production negative ions, as suggested by experimental evidence to be the case for Titan [57, 77–79], then the mechanism will act to enhance the growth of such particles until possibly reaching an upper limit to the amount of charge each growing particle can carry when Coulomb repulsion becomes the dominant interaction. Similarly, if the initial bias is towards the production of positive ions then the mechanism would operate identically, since the magnitude of electrostatic interactions is independent of sign of charge (*vide* Coulomb's law). As already noted elsewhere [71], the preferential formation of negatively charged particles seems understandable considering the electron affinity of the molecules that compose Titan's upper atmosphere.

Table 2.2 Energy barrier (eV) for the case of two interacting dielectric particles as depicted in Table 2.1(b), but with a lower dielectric constant of $k_1 = k_2 = 3$.

q_2										
5	0.30	0.30	0.26	0.23	0.20	0.17	0.15	0.13	0.12	0.11
4	0.25	0.25	0.21	0.18	0.16	0.14	0.12	0.11	0.095	0.085
3	0.20	0.19	0.16	0.14	0.12	0.10	0.087	0.077	0.069	0.062
2	0.15	0.13	0.11	0.090	0.075	0.064	0.055	0.049	0.043	0.039
1	0.085	0.068	0.053	0.042	0.034	0.029	0.025	0.022	0.019	0.017
a_2	**5**	**10**	**15**	**20**	**25**	**30**	**35**	**40**	**45**	**50**

Table 2.2 shows the consequences of like-charged particles interacting under circumstances identical to those given in Table 2.1(b), but with a dielectric

constant of $k_1 = k_2 = 3$. Such a value would be appropriate for many hydrocarbon and polycyclic aromatic hydrocarbon (PAH) compounds [45]. As can be seen from Table 2.2, there are no interactions where the outcome of a collision would be a larger, stable particle. There are a few metastable interactions, but the majority of collisions would take place on a repulsive energy surface and lead to an immediate separation of particles. In general, energy barriers are also higher than those calculated when $k_1 = k_2 = 20$. Consequently, it could be inferred that an enrichment in nitrogen content of Titan's atmospheric aerosols might be favoured as a consequence of a charge scavenging mechanism operated by the abundant large negatively charged particles. Critical to the effectiveness of this enrichment mechanism is the large difference in dielectric constant that exists between hydrocarbon-based particles and those where the constituent molecules predominantly include nitrogen atoms. Ergo, a lack of nitrogen atoms in the constituent molecules of a particle, for example, a droplet that is mostly composed of methane or ethane, would lead to a considerable reduction in dielectric constant, which in turn, would make attractive or stabilising like-charge interactions much less likely. Pure hydrocarbons generally have low dielectric constants due to their non-polar character. Methane (CH_4) and ethane (C_2H_6), compounds that are presented at an early stage of aerosol formation in Titan's atmosphere, have dielectric constant values of just 1.6761 and 1.9356, respectively [45]. Polar-substituted hydrocarbons naturally have higher dielectric constants, so that the incorporation of a functional group containing nitrogen, for example, usually increases the dielectric constant of the substituted hydrocarbon. Hydrogen cyanide (HCN), one of the main nitrogen-substituted compounds found in Titan's atmosphere, has a particular high dielectric constant value of 114.9 [45]. Figure 2.27 shows estimated values (according to [80]) for the dielectric constant of a mixture consisting of methane/hydrogen cyanide, and ethane/hydrogen cyanide, both as function of the molar fraction of hydrogen cyanide (x_{HCN}). As can be seen, a mixture that contains at least about 20 percent of molar fraction of HCN

will have a dielectric constant of 20 or greater in both cases; stressing the assertion that the incorporation of nitrogen by the growing aerosol particle favours the scavenging mechanism.

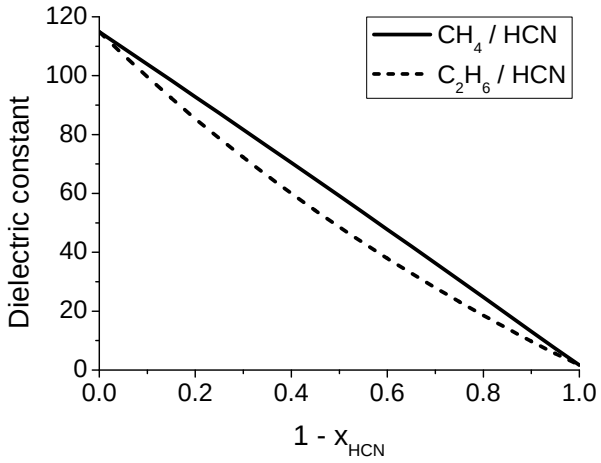


Fig. 2.27 Plot of the dielectric constant as function of hydrogen cyanide molar fraction for methane/hydrogen cyanide (solid line) and ethane/hydrogen cyanide (dotted line) mixtures.

As part of this growth process, it should be noted that all other factors which contribute towards the calculation of collision efficiencies, i.e. Reynolds number, terminal velocity, etc., will be identical for all particles with the same radius, mass and charge, irrespective of composition [81]. Hence, the only quantity that will differentiate collision efficiencies and, as a result, the degree of enrichment for each of the cases in Tables 2.1 and 2.2, is the dielectric constant.

Chapter 3

Electrostatic interactions in the presence of a dielectric medium

In many occasions where electrostatic interactions play an important role, especially those involving technological applications, the interacting particles are immersed in a dielectric medium. A couple of examples are charged colloidal systems [28] and electrostatic self-assembly processes. [82–84] As already thoroughly discussed in the previous chapters, the electrostatic force between any pair of point charges in vacuum is universally expressed by Coulomb's law. However, if the charges are immersed in a homogeneous medium or solvent of dielectric constant k_{m}, the Coulomb force is attenuated by a factor equal to k_{m}, as a result of polarisation being induced in the medium. [3, 23] In these circumstances, the presence of a medium does not actually alter the nature of the electrostatic interaction, i.e. the sign of the force remains the same. Notwithstanding, describing electrostatic interactions becomes much more complicated when finite-sized bodies are involved, besides potentially unveiling non-trivial situations; [23] a notable example being the counterintuitive like-charge attraction between polarisable particles in vacuum, as described earlier in this thesis and elsewhere [37, 85]. Most self-assembly processes, for example, take place in aqueous solution [86], but there is also a growing realisation that for many of newer materials, such

as magnetic nanoparticles [87] and quantum dots, [88] assembly in a non-polar solvent would offer distinct advantages. [89, 90] In all cases, nevertheless, it is of fundamental importance to acquire a greater quantitative understanding of how interactions between charged, polarisable, finite-sized objects are influenced by the presence of a medium. From such considerations then arises the question whether attenuation by k_{m} still apply or does the force, and possibly the very nature of the interaction, depend critically on the dielectric constants of the various materials involved.

The two-body formalism [37], presented and discussed in the previous chapter, was originally designed to treat only particles in vacuum. However, it will be demonstrated in the following that, through mathematical manipulation of the boundary conditions without actually changing them, therefore maintaining the physics of the problem consistent, it is possible to adapt the original solution for two particles in vacuum and obtain an equivalent solution able of treating two interacting particles immersed in a dielectric medium.

3.1 Theory for implementing the presence of a medium

The boundary condition that relates the presence of free charge on the surface of each particle to a discontinuity in the normal component of the electric displacement field, Equation 2.7, can be rewritten in a more general form, by considering that the dielectric constant of the material outside the particles, namely the medium, is not necessarily equal to unity, but actually equal to an arbitrary value k_{m}:

$$4\pi K\sigma_{f,i} = k_{\mathrm{m}}\frac{\partial\Phi}{\partial r_i}\bigg|_{r_i=a_i^+} - k_i\frac{\partial\Phi}{\partial r_i}\bigg|_{r_i=a_i^-} . \tag{3.1}$$

Additionally, since multiplication of both the left-hand and right-hand sides by a factor of $1/k_{\mathrm{m}}$ does not alter Equation 3.1, it can be expressed as:

$$\frac{4\pi K\sigma_{f,i}}{k_{\mathrm{m}}} = \left.\frac{\partial\Phi}{\partial r_i}\right|_{r_i=a_i^+} - \frac{k_i}{k_{\mathrm{m}}}\left.\frac{\partial\Phi}{\partial r_i}\right|_{r_i=a_i^-} . \tag{3.2}$$

When the particles are immersed in a medium, the total surface charge on each dielectric boundary includes free and bound charges related to both the particles and the medium. Therefore, by conveniently introducing an effective dielectric constant $k_i' = k_i/k_{\mathrm{m}}$, and an effective free charge $q_{f,i}' = q_{f,i}/k_{\mathrm{m}}$ for each particle, which yields an identical electric potential (or field) that satisfies Equations 2.6 and 2.7, it becomes possible to adapt the original two-body formalism [37] for the treatment of electrostatic interactions in the presence of a medium with dielectric constant k_{m}. Implementation of this new defined quantities in Equation 3.2 results in:

$$4\pi K\sigma_{f,i}' = \left.\frac{\partial\Phi}{\partial r_i}\right|_{r_i=a_i^+} - k_i'\left.\frac{\partial\Phi}{\partial r_i}\right|_{r_i=a_i^-} . \tag{3.3}$$

Accordingly, the boundary condition that relates the presence of a net charge on the surface of each particle to a discontinuity in the normal component of the electric field, namely Equation 2.6, becomes:

$$4\pi K\sigma_i' = \left.\frac{\partial\Phi}{\partial r_i}\right|_{r_i=a_i^+} - \left.\frac{\partial\Phi}{\partial r_i}\right|_{r_i=a_i^-} . \tag{3.4}$$

However, this latter condition means that the total charge integrated over the surface of a particle i gives $q_{f,i}'$, and not $q_{f,i}$. Consequently the corresponding force,

$$\mathbf{F}_{12}' = K\int dq_1'(\mathbf{r}_1)\int dq_2'(\mathbf{r}_2)\frac{\mathbf{r}_1-\mathbf{r}_2}{|\mathbf{r}_1-\mathbf{r}_2|^3},$$

is not actually the real force, but a hypothetical force that describes the interaction between two particles with dielectric constants k_1' and k_2', and given charges $q_{f,1}'$

and $q'_{f,2}$, interacting in vacuum. To transform such hypothetical force into a real force, the total charge should be multiplied by k_{m}, corresponding then to $q_i = k_{\mathrm{m}}\, q'_i$. With the above considerations in mind, the electrostatic force between two particles immersed in a medium can be likewise obtained from a generalisation of Coulomb's law, attenuated by a factor of k_{m} to account for the presence of the medium:

$$\begin{aligned} \mathbf{F}_{12} &= \frac{1}{k_{\mathrm{m}}}\, K \int k_{\mathrm{m}}\, dq'_1(\mathbf{r}_1) \int k_{\mathrm{m}}\, dq'_2(\mathbf{r}_2) \frac{\mathbf{r}_1 - \mathbf{r}_2}{|\mathbf{r}_1 - \mathbf{r}_2|^3} \\ &= k_{\mathrm{m}}\, \mathbf{F}'_{12}, \end{aligned} \tag{3.5}$$

effectively extending the vacuum solution [37] to the case of two charged dielectric particles immersed in a polarisable medium.

3.2 General numerical results

Having already an understanding of how electrostatic interactions occur in vacuum, especially regarding the conditions required for allowing non-trivial interactions to happen, as underlined in Figures 2.10 and 2.11, it becomes instructive to examine now the natural extension of these results to situations where the particles can be oppositely charged and also immersed in a medium of dielectric constant k_{m}. Figure 3.1 presents a series of calculations, where the electrostatic force has been computed for six different values of k_{m}, as a function of the charge ratio (q_2/q_1) and radius ratio (a_2/a_1), covering both opposite- and like-charged interactions, and size ratios which span from particles of equal size through to differences in size that are almost representative of a particle − planar surface interaction (*vide* Section 2.4.3).

Given that each particle has a dielectric constant of 10, it can be seen that the most dramatic changes take place as the dielectric constant of the medium shifts from 9 through to 11. At $k_{\mathrm{m}} = 5$ and $k_{\mathrm{m}} = 9$, all interactions where

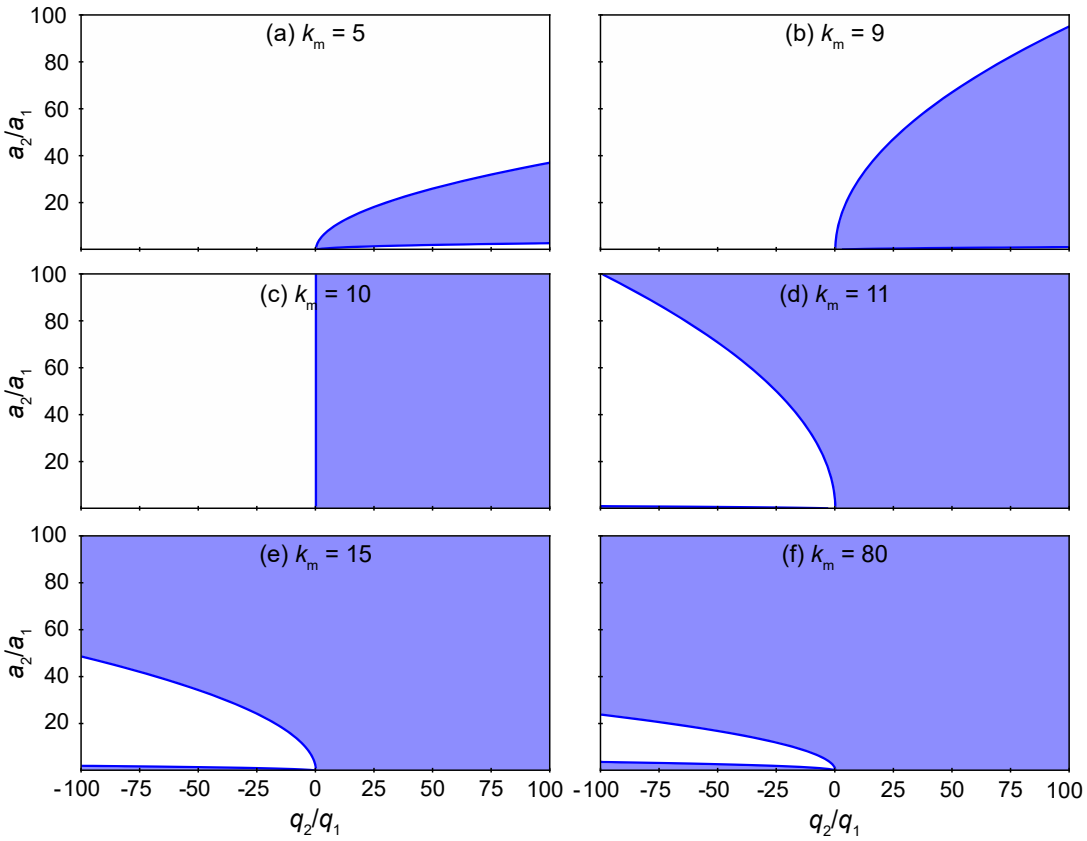


Fig. 3.1 Electrostatic maps showing regions of repulsive (light purple) and attractive (white) interactions. The electrostatic force has been calculated as a function of the charge ratio, q_2/q_1 and the radius ratio, a_2/a_1, with the radius and charge of particle 1 fixed at $a_1 = 1$ and $q_1 = 1$. The dielectric constants of the particles are $k_1 = k_2 = 10$ and the calculations have been undertaken at a fixed separation distance of $s = 0.1\,a_1$; k_m in each diagram denotes the dielectric constant of the solvent or medium, and the solid deep purple line denotes points where the electrostatic force is zero.

the particles are oppositely charged are attractive, as are a significant fraction of those between like-charged particles, but under two quite distinct sets of conditions; similarly to the vacuum case (Figures 2.10 and 2.11), attraction between like-charged particles occurs when there are either a sufficiently large difference with respect to their sizes or charge. As k_m switches to 10, the cases where like-charged particles attract each other cease to exist and, as would be normally expected, all interactions where the particles are oppositely charged continue to be attractive. However, a remarkable phenomenon happens when k_m changes to 11; not only all like-charged interactions are repulsive, but also a portion of the oppositely-charged interactions become repulsive, revealing yet

another type of counterintuitive electrostatic interaction, namely opposite-charge repulsion. As the dielectric constant of the medium keeps increasing in magnitude, to 15 and on to 80, the region of attraction between oppositely charged particles diminishes markedly, remaining, in contrast, predominantly dependent on not so large differences in charge density between the interacting particles.

The results given by Figure 3.1 strongly suggest that the ratio between the dielectric constants of the interacting particles and the medium, k_i/k_m $(i = 1, 2)$, can be viewed as a critical parameter for the interaction. Accordingly, if $k_i/k_\mathrm{m} \approx 1$, the classical assumption regarding electrostatic interactions, which is independent of the presence of a medium, seems to apply, i.e. like-charged particles repel and oppositely charged particles attract. In contrast, when $k_i/k_\mathrm{m} \ll 1$ or $k_i/k_\mathrm{m} \gg 1$, the nature of the electrostatic force unusually changes in some circumstances, switching from attractive to repulsive and *vice versa*. Since polarisation effects are responsible for these changes, next it is examined in more details how the dielectric constant of the medium affects quantitatively the magnitude and direction of the force, as well the distribution of induced bound charges on the surface of the interacting particles.

Consider the interaction between a neutral and a positively charged, equal-sized particles with dielectric constants $k_1 = k_2 = 10$, immersed in a medium of dielectric constant k_m. Figure 3.2 shows the calculated electrostatic forces and surface charge densities for cases where $k_i/k_\mathrm{m} > 1$ $(i = 1, 2)$. The first case, where the interaction happens in vacuum $(k_\mathrm{m} = 1)$, in fact corresponds to one of the scenarios presented in Figure 2.2, where the interaction becomes progressively more attractive as polarisation effects become stronger with decreasing inter-particle separation distance. In addition, it can be seen from Figure 3.2(a1) that the effective electric dipole[1] calculated for the neutral particle is aligned with and points in the same direction of the electric field generated by the positive charges on the second particle, as would be expected. When $k_\mathrm{m} = 2$, the profile of the

[1]The methodology to calculate effective electric dipoles from the information about the distribution of surface charges is given in Appendix B.

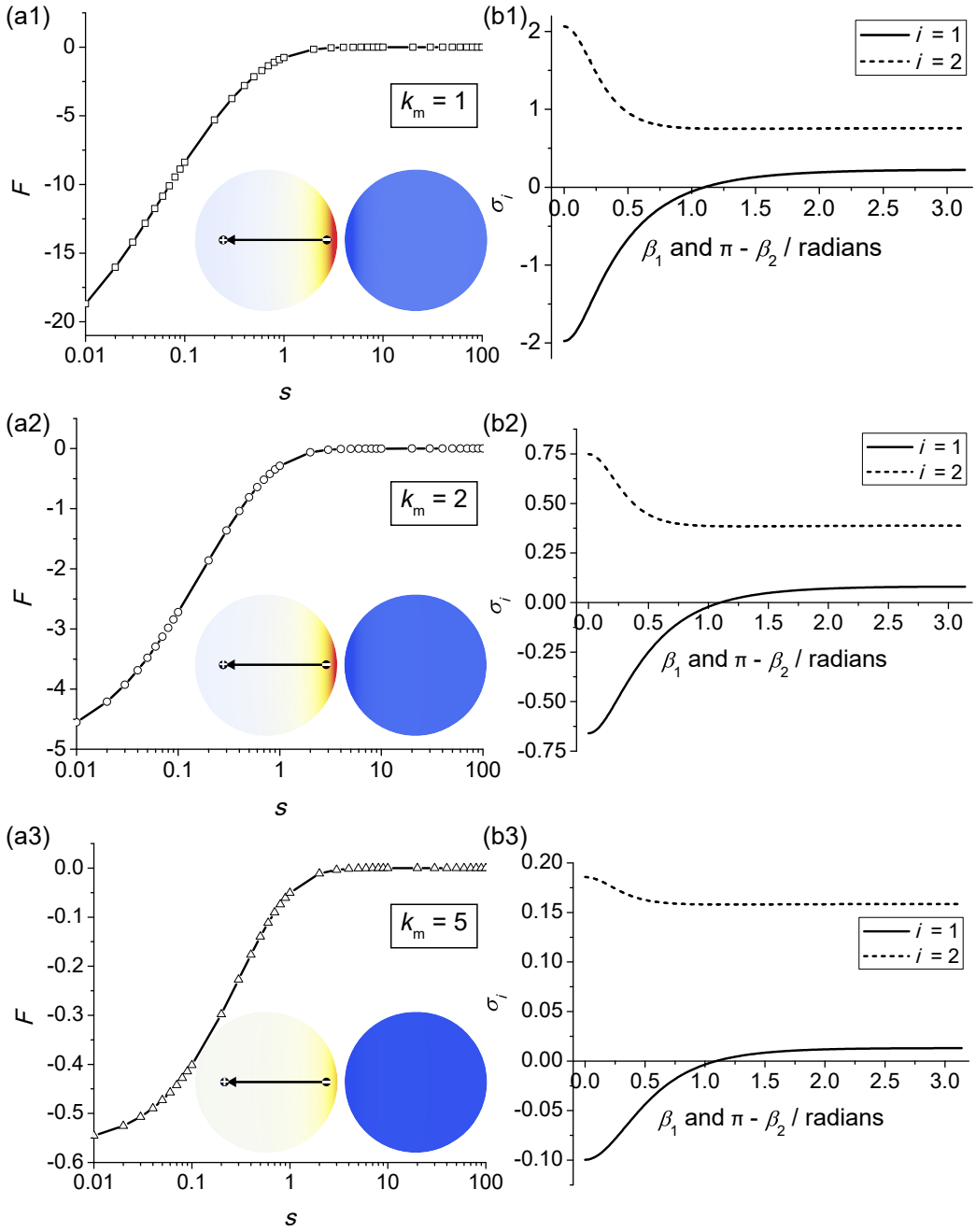


Fig. 3.2 (a1−3) Plot of the electrostatic force F as function of the surface-to-surface separation s for cases of neutral particle − charged particle interaction, corresponding to different values of k_{m} that are lower than that of the particles, as explicit in the figure. The first particle is neutral whilst the second particle has a nominal charge of +10. The two particles are equal-sized, with a nominal radii of 1 and dielectric constants $k_1 = k_2 = 10$. (b1−3) Corresponding plots of the total surface charge densities σ_i $(i = 1, 2)$ as function of the polar angle β_i at a separation of $s = 0.1$. Inset shows a geometrical representation of the problem, with the total surface charge density (charge per unit area) mapped out for each of the particles. Blue tones denote positive charge densities, and red tones denote negative charge densities.

interaction remains similar but, unlikely what would be predicted by a simple application of Coulomb's law in a medium, the electrostatic is not attenuated by a factor of 2. Here, polarisation effects influence not only the particles but also the dielectric medium, so that the total charge at the interface particle − medium includes contributions from both the bound charges induced in the medium and on the particle, besides the free charge on the surface of the particle, when present. The consequence is that the force effectively diminishes by a factor that is actually greater than k_{m}, as the total charge at the interface particle − medium becomes smaller due to contribution of bound charges originated from the medium. In a similar way, when k_{m} increases to 5, the force is effectively attenuated by a factor greater than k_{m} and the distribution of total charge on the surface of the particles becomes more closer to uniform.

Correspondingly, Figure 3.3 shows the calculated electrostatic forces and surface charge densities for the interaction between the same neutral and positively charged particles, with the difference that $k_i/k_{\mathrm{m}} \leq 1$ $(i = 1, 2)$. Right in the first case, where the dielectric constants of both the medium and particles are identical, a singular outcome is obtained; there is an absence of electrostatic interaction despite both particles being polarisable and at least one of them being charged. In this particular situation, the lack of dielectric discontinuity between the neutral particle and the medium means that no bound charge is induced on the former, which can be seen by the absence of an electric dipole on it. Effectively, the charged particle does not "see" the neutral one, so the electrostatic force acting on both is zero and the distribution of surface charge on the charged particle is uniform. This scenario is analogous to cases of a neutral and a charged, non-polarisable particles (see corresponding curve in Figure 2.2) or a single point charge, all in vacuum. The key factor present in these cases is that there is no induction of bound charges, which implies that only one body in the system is charged, so no electrostatic interaction can exist. As anticipated in Figure 3.1, when $k_i/k_{\mathrm{m}} < 1$ $(i = 1, 2)$, the nature of a neutral particle − charged particle

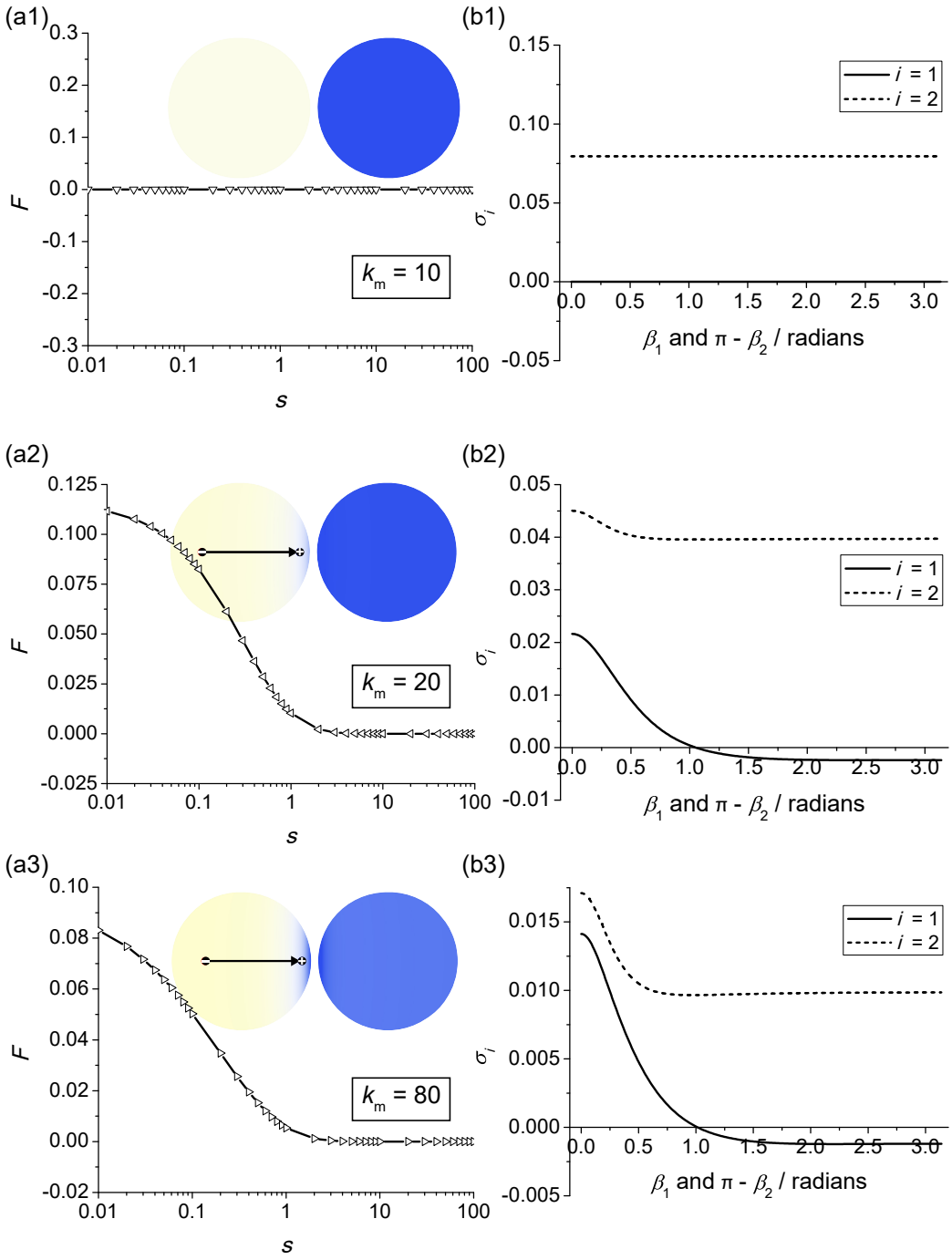


Fig. 3.3 Plots of the electrostatic force and total surface charge density for the same scenario described in Figure 3.2, but corresponding to different values of k_m that are now equal or greater than that of the particles ($k_1 = k_2 = 10$), as explicit in the figure.

interaction changes completely, becoming always repulsive. Now, the medium is the component of the system with the highest dielectric constant, having then an ability to be polarised more strongly than both particles. So, in the presence of the electric field created by the charged particle, bound charges are induced in a

greater degree in the medium when compared to the neutral particle, so that an effective reverse polarisation of the latter occurs, producing an effective dipole moment that is aligned with the electric field but points contrarily to it, as shown in Figure 3.3, which implies in a constant repulsive regime. As the dielectric constant of the medium increases to 20 and then 80, it can also be seen that the magnitude of the force decreases, but now with a factor that is smaller than k_{m}. Since the charged particle is the only component of the system with a net charge and, therefore, also the primary source of electric field, neither changing its dielectric constant nor the magnitude of its charge will change qualitatively the results presented in Figures 3.2 and 3.3.

A more comprehensive perspective of the three fundamental states of a neutral particle − charged particle interaction in a dielectric medium can be obtained by examining the behaviour of electric field at the vicinity of the neutral particle, as given in Figure 3.4, which addresses the same system considered in Figures 3.2 and 3.3. When such interaction happens in vacuum, negative bound charges are induced in the area of the neutral particle that is closest to the charged one, as can be noted from Figure 3.2(a1) and (b1), so field lines that are originated from the latter ends up in these areas of negative surface charge of the former, as depicted in 3.4(a). Accordingly, positive bound charges appear in the corresponding opposite area of the neutral particle, so that a net zero amount of charge is maintained, and field lines can be seen originating and pointing away from these positive areas. When the dielectric constant of the medium has the same magnitude of that of the particles, a lack of dielectric discontinuity is established in the system, so no bound charges are induced. Consequently, the electric field, originated in the charged particle, passes unperturbed through the neutral particle as if such particle was not present; situation that is illustrated in Figure 3.4(b). An effective reverse polarisation of the neutral particle occurs when the medium becomes the most polarisable component of the system. In this case, a total positive bound charge is induced at the neutral particle − medium interface that is closest to the

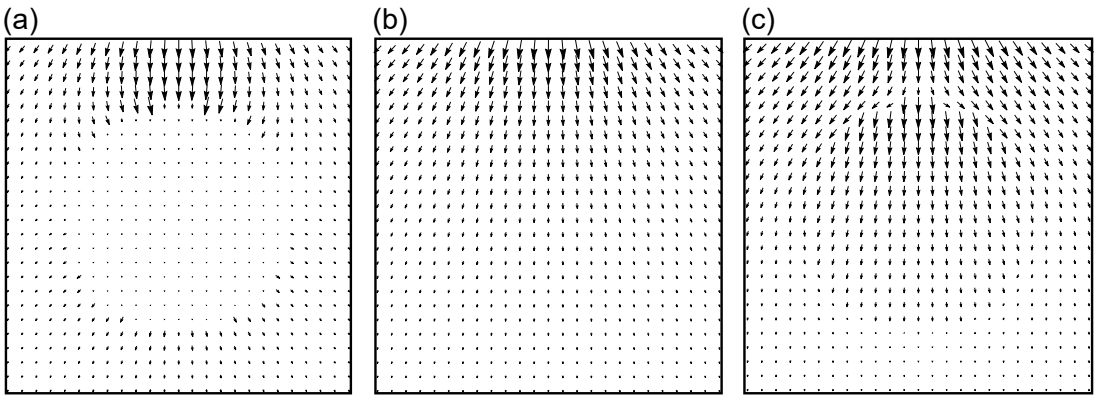


Fig. 3.4 Vector plots of the electric field, generated by a positively charged particle, at the vicinity of a neutral particle, for three different values of the dielectric constant of the medium: (a) $k_{\mathrm{m}} = 1$, (b) $k_{\mathrm{m}} = 10$, and (c) $k_{\mathrm{m}} = 80$. In each plot, the size of the arrows is proportional to the magnitude of the field at the corresponding point, and the charged particle (not shown) is situated above the region plotted. The particles are equal-sized, with a nominal radii of 1, dielectric constants $k_1 = k_2 = 10$, and separated by a distance of $s = 1.0$.

charged particle, so the electric field lines that is originated from the latter curves around the neutral particle, as can be seen from Figure 3.4(c). Additionally, it can also be noted that the magnitude of the field inside the latter becomes stronger as k_{m} increases.

3.3 The significance of the medium in electrostatic self-assembly processes

In the following it is presented an application of the formalism [37], that has been adapted to treat also the presence of a dielectric medium, to two cases of great experimental relevance, where it is investigated the role of the solvent and how modulation of characteristics of the system can be used to control outcomes in self-assembly processes that are driven by electrostatic forces.

3.3.1 Current state of research

The effective use of electrostatic forces in the self-assembly and fabrication of nano-materials is rapidly gaining significance in the technological development

of new devices and processes. [91] Examples of electrostatic self-assembly range from isolated nanoscale structures, [92–94] through patterned [95, 96] and layered surfaces [89] to macroscopic crystals consisting of millimetre diameter spherical polymer particles. [97] In many assembly processes, particularly with reference to the fabrication of new devices, an important component in the initial stage is the self-assembled monolayer (SAM). A SAM acts as a template that enables surface characteristics to be fine-tuned for the purpose of accommodating either individual nanoparticles or multilayers in the form of layer-by-layer structures. [86, 98] SAMs can be either polar or non-polar, or they can be induced to attract or release protons, all of which influence the electrostatic forces experienced by nanoparticles when forming a layered surface: this electrostatic constituent is central to almost all significant developments in the field of thin film fabrication. [99] As previously discussed, if described in terms of point charges (e.g. H^+ and O^-) located on self-assembly components, the fabrication mechanism would be, at first sight, straightforward, as the electrostatic force between any pair of point charges can be universally expressed by Coulomb's law attenuated by the dielectric constant of the solvent. [3, 23] However this simple description becomes invalid when the interacting objects are polarisable and of finite size, as has been extensively demonstrated in this chapter. To date there is only qualitative evidence for a "solvent effect" in electrostatic self-assembly; [99–101] therefore, the following quantitative analysis of such behaviour contributes to a more rigorous evaluation of the role of the solvent.

3.3.2 A self-assembly case involving neutral and charged objects

A straightforward example of how the properties of the solvent could either facilitate or suppress electrostatic fabrication, can be seen from experiments [83] involving the interaction of neutral spherical alumina particles of approximately 50 nm diameter and dielectric constant $k_{\text{particle}} = 9.9$, with a charged nano-

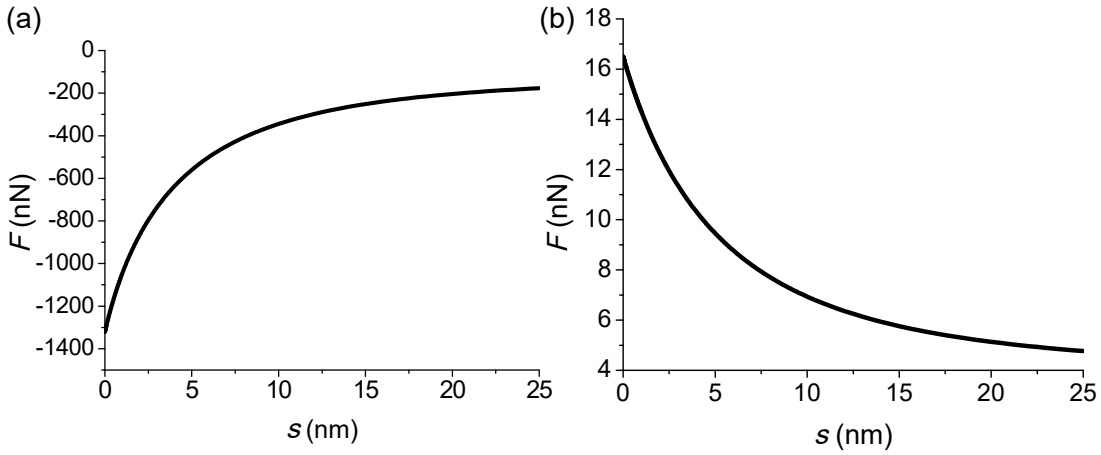


Fig. 3.5 Plot of the electrostatic force F (nN) as a function of the surface-to-surface separation s between a neutral alumina spherical particle and a charged nano-diamond surface, immersed in a solvent with dielectric constant (a) $k_{\text{solvent}} = 1.86$, and (b) $k_{\text{solvent}} = 20$. The particle has a radius of 25 nm and a dielectric constant $k_{\text{particle}} = 9.9$. The surface charge density of the planar surface is $+1\,\text{e} \cdot \text{nm}^{-2}$, and the dielectric constant is $k_{\text{surface}} = 5.3$.

diamond surface of dielectric constant $k_{\text{surface}} = 5.3$. The expectation is that a neutral particle will be attracted to a surface with a given charge density of $\sigma_{\text{surface}} = +1\,\text{e} \cdot \text{nm}^{-2}$, and that is exactly what the experiments show if the particles are immersed in a liquid solvent of dielectric constant $k_{\text{solvent}} = 1.86$ (insulating fluorocarbon solution, fluorinert FC-90). Figure 3.5(a) reinforces this observation by showing that the computed electrostatic force is attractive at all separation distances up to touching point. However, further calculations show that the nature of the interaction can switch markedly from being attractive to repulsive if a solvent with a dielectric constant, $k_{\text{solvent}} = 20$, for example, acetone, were to be used instead, as suggested by Figure 3.5(b).

This transition from attractive to repulsive electrostatic behaviour occurs at $k_{\text{solvent}} = k_{\text{particle}} = 9.9$, where the lack of a dielectric discontinuity at the interface between the particle and the solvent implies an absence of bound charge, resulting in the elimination of any electrostatic interaction between the particle and the surface. At $k_{\text{solvent}} = 1.86$, where the solvent is less polarisable than both the alumina particle and the nano-diamond surface, the positively charged planar surface can induce an effective dipole on the neutral particle which, as shown in

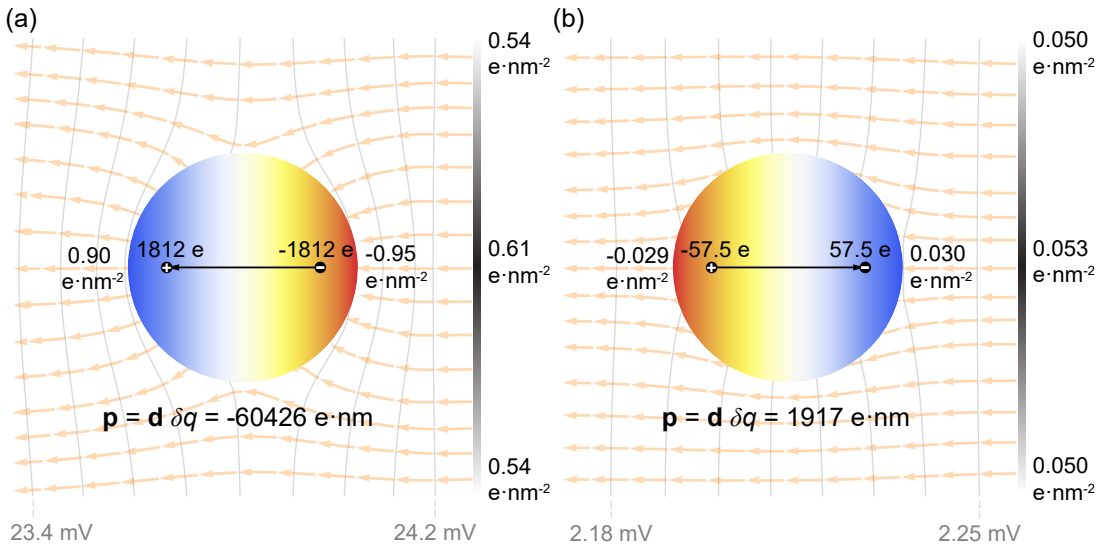


Fig. 3.6 Illustration of the electrostatic interactions presented in Figure 3.5, showing equipotential lines, the electric field, the effective dipole moment in the neutral alumina particle, values of the effective surface charge density at selected points, and values of the electric potential at selected points away from the surface. Note the switch in the direction of the effective dipole moment when the dielectric constant of the solvent changes from (a) $k_{\text{solvent}} = 1.86$ to (b) $k_{\text{solvent}} = 20$.

Figure 3.6(a), points away from the surface. Since the negative component of the dipole is adjacent to the positively charged surface, the overall interaction between the particle and the surface is dominated by an attractive electrostatic force. However, if a solvent with a higher dielectric constant is chosen, for instance $k_{\text{solvent}} = 20$, the solvent is now more polarisable than either the particle or the surface and, as shown in Figure 3.6(b), there is a corresponding switch in the direction of the induced dipole. The result is a net repulsive interaction between the particle and the surface, which would not be predicted from a simple application of Coulomb's law. Note also that, although a charge density of $+1\text{e} \cdot \text{nm}^{-2}$ has been imposed on the surface, the effective charge experienced by the neutral particle is severely depleted in the presence of a highly polarisable solvent. The observed repulsive interaction between a neutral particle and a charged planar surface will persist with solvents of higher dielectric constant, such as water ($k_{\text{solvent}} \approx 80$), that are increasingly more polarisable than the components offered for electrostatic self-assembly. It is worth remembering that

neither changing the sign of the charge on the planar surface nor changing its magnitude can change these circumstances.

3.3.3 A self-assembly case involving oppositely charged objects

As a second illustration of the importance of the solvent in influencing fabrication processes, the assembly of thin films from polyoxometalate (POM) nanoclusters is examined next. Nanostructured materials containing POMs are increasingly seen as an attractive route to the development of functional materials and devices; [82, 102] however, to achieve these objectives, it is necessary to develop a strategy for creating coherent thin-film structures. Most POMs are soluble in water, [103] but it is widely recognized that from such a polar solvent it is not possible to fabricate layers without first creating a charged substrate. [82] The following calculations have been designed to model deposition of the quasi-spherical Eu-POM onto a layer of positively charged macromolecules in the form of a planar substrate. [82] Liu et al. have subsequently shown that this particular combination of materials can form the base of an electrochromic device. [102] The Eu-POM is an anion, $[Eu(H_2O)P_5W_{30}O_{110}]^{12-}$, and a polyelectrolyte layer residing on a quartz or silicon substrate provides the positive charge. The charge density associated with the substrate is unknown, and it is this quantity that is explored here in terms of the minimum density required to promote the surface deposition of POMs in a solvent with a given dielectric constant. Although the presence of an electrolyte (NaCl) does improve surface coverage, it has been shown that fabrication can proceed in the absence of sodium chloride[2]. [82]

Table 3.1 shows the variation of the calculated electrostatic force between the Eu-POM particle, $[Eu(H_2O)P_5W_{30}O_{110}]^{12-}$, and an uniform polyelectrolyte

[2]It is assumed that any considered solvent is not acting as or does not contain an electrolyte. Nonetheless, it is acknowledged that pure water ($k_{\text{solvent}} \approx 80$), for example, is itself a very weak electrolyte providing screening from H^+ and OH^- in equilibrium, but it has a Debye length that far exceeds the discussed length scales ($\lambda_D \approx 1$ micron, at room temperature.)

layer as a function of both the charge density on the substrate and the dielectric constant of the solvent in which the Eu-POM is suspended. As can be seen, at very low surface charge densities, the two interacting objects are only attracted to one another in vacuum ($k_{\text{"solvent"}} = 1$) and in all other types of solvent a layered structure would fail to form. The reason for this failure is related to the observations accompanying Figure 3.3, in that for constituents with the dielectric constants $k_{\text{POM}} = 10$ and $k_{\text{surface}} = 5$ in the presence of a solvent where $k_{\text{solvent}} \geq 10$, there will be a weakly repulsive electrostatic force preventing assembly. However, as Table 3.1 shows, a gradual increase in surface charge density reveals the existence of a critical density, $\sigma_{\text{critical}} = 0.1\ \text{e} \cdot \text{nm}^{-2}$, beyond which layer formation is assured for all solvents, including water.

Table 3.1 The electrostatic force (pN) calculated for the experimental case [82, 102] of an interaction between a Eu-POM, $[\text{Eu}(\text{H}_2\text{O})\text{P}_5\text{W}_{30}\text{O}_{110}]^{12-}$, and an oppositely charged planar surface at a surface-to-surface separation distance of 1 nm. Calculations have been undertaken using different combinations of charge density on the planar surface (σ_{surface}) and dielectric constant of the solvent (k_{solvent}). The POM particle has a radius of 0.5 nm and an estimated dielectric constant of $k_{\text{POM}} = 10^{\dagger}$. The planar surface has an outer coating of poly(ethylenimine)/poly(styrenesulfonate)/poly(allylamine hydrochloride), with an estimated dielectric constant of $k_{\text{surface}} = 5$. [104] The charge density on the planar surface is in units of $\text{e} \cdot \text{nm}^{-2}$.

$k_{\text{solvent}} \downarrow$ / $\sigma_{\text{surface}} \rightarrow$	0.001	0.005	0.01	0.05	0.1	0.5	1
1	-2510.4	-2649.6	-2823.7	-4216.2	-5957.1	-19889.0	-37317.1
10	118.8	105.0	87.7	-50.2	-222.7	-1602.2	-3326.6
20	108.4	101.5	92.9	23.8	-62.7	-753.9	-1617.9
30	86.4	81.8	76.0	29.8	-27.8	-489.4	-1066.2
40	70.7	67.2	62.9	28.2	-15.1	-361.6	-794.6
50	59.6	56.8	53.3	25.6	-9.1	-286.5	-633.1
60	51.4	49.1	46.2	23.0	-5.9	-237.1	-526.1
70	45.1	43.2	40.7	20.8	-4.0	-202.3	-450.1
80	40.2	38.5	36.3	19.0	-2.7	-176.3	-393.2

†There do not appear to be any reliable data on the dielectric constants of POMs. A value of 10 is based on values for metal oxides. [105], and metal-containing nanoparticles [106].

To demonstrate the consequence of introducing a solvent in terms of changes that take place in the distribution of charge, Figure 3.7 gives a graphical illustration of an example taken from Table 3.1. For a net charge of -12 e on the POM

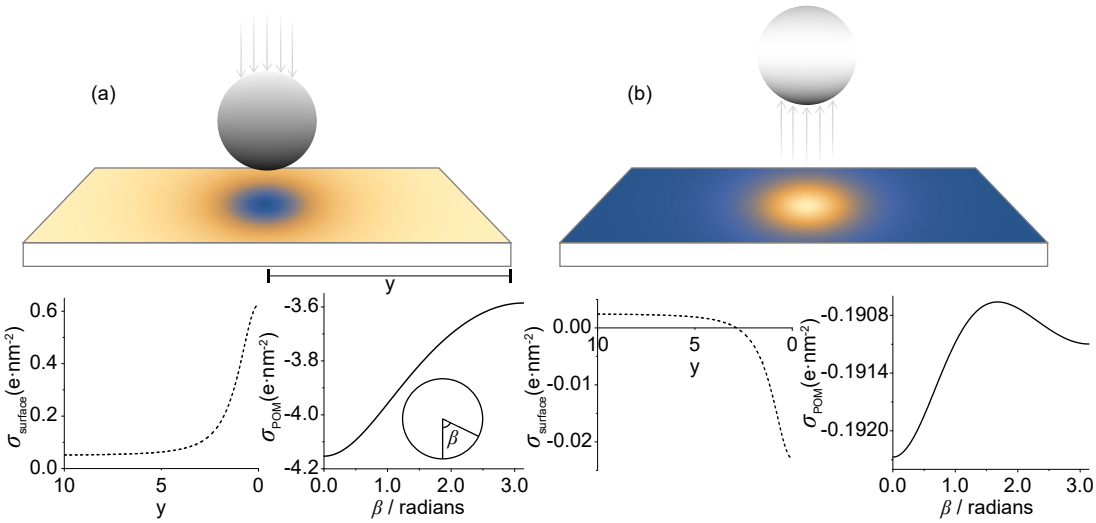


Fig. 3.7 Schematic illustration of the POM − surface interaction. In (a) the medium/solvent has a dielectric constant of 1 (vacuum) and in (b) the medium/solvent has a dielectric constant of 20. The planar surface has a surface charge density of $0.05\,\mathrm{e}\cdot\mathrm{nm}^{-2}$ and the POM particle has a net charge of -12 e. The total charge density on the planar surface, $\sigma_{\mathrm{surface}}$ (dashed curve), and on the POM particle, σ_{POM} (solid curve), are also shown for each interaction case: for $\sigma_{\mathrm{surface}}$, the x-axis denotes the radial position y, with $y = 0$ indicating the centre of POM projected on the surface; for σ_{POM}, the x-axis denotes the polar angle (β), where $\beta = 0$ represents the nearest point to the plane. The colour shades on both objects reflect qualitatively the calculated charge distribution, however the colour scale is different in each example.

and a planar surface charge density of $0.05\,\mathrm{e}\cdot\mathrm{nm}^{-2}$, changes in density as the two interacting objects approach one another have been calculated for vacuum (Figure 3.7(a)) and for a solvent with a dielectric constant of 20 (Figure 3.7(b)). For the vacuum case, Figure 3.7(a) also shows how charge density on the surface changes from $\sigma_{\mathrm{surface}} = 0.05\,\mathrm{e}\cdot\mathrm{nm}^{-2}$, at a radial distance of 10 nm from the POM, to $\sigma_{\mathrm{surface}} \approx 0.6\,\mathrm{e}\cdot\mathrm{nm}^{-2}$ immediately below the POM. A comparable change in negative charge density is seen on the POM, and the net result is that oppositely charged bodies attract. With the introduction of a solvent, the transition in behaviour is dramatic. The POM retains a negative charge and the presence of the surface has minimal effect on how it is distributed. In contrast, the planar surface is, as expected, positively charged at a radial distance of 10 nm from the POM, but as Figure 3.7(b) shows, in close proximity to the POM, the charge on the surface changes sign to become $\sigma_{\mathrm{surface}} \approx -0.25\,\mathrm{e}\cdot\mathrm{nm}^{-2}$ at the point of

closest contact. The net result now is that the two interacting objects repel one another. As demonstrated in Figure 3.6, polarisation of the solvent leads to a dramatic attenuation of charge density; however, in that example, it was the neutral particle that switched density, whereas in Figure 3.7, it is the charge on the planar surface that is most influenced by the choice of solvent.

There are several examples in the literature of deposition processes where there is evidence of a critical charge density being required for the growth of layers. [98, 107] The exact numbers in Table 3.1 are specific to the model system being studied; however, it is instructive to see what the values equate to in molecular terms: given that a Eu-POM has a diameter of approximately 1 nm, which would give it a projected surface coverage of 3.14 nm^2, the required critical surface charge density is less than one proton per POM. If, however, the attractive force needs to be greater than the minimum, then at $\sigma_{\text{plane}} = 0.5\,\text{e} \cdot \text{nm}^{-2}$, for example, the surface coverage would need to be closer to two protons per POM. Some of the experimental evidence for a critical charge density in layer-by-layer assembly is complicated by the need to invert surface charge in order to accommodate subsequent layers; [108] however, there is supporting evidence for such an effect when, under aqueous conditions, polystyrene nanoparticles with varying degrees of negative charge are adsorbed onto the surface of a positively charged polymer film. [109]

There are important differences between the two examples of self-assembly discussed above. In the first case, any attractive interaction between the charged nano-diamond surface and the neutral alumina particle is due entirely to polarisation effects, and these are readily suppressed when the dielectric constant of the medium exceeds that of the interacting particles. In contrast, the second example represents a case where oppositely charged bodies should experience an interaction, which Coulomb's law would describe as being attractive under all circumstances (vacuum and solvent). However, that is clearly not the case, and the calculations reveal the existence of a critical charge density that is required to

be present on a substrate in order to overcome polarisation effects in a medium that may serve to suppress any attraction.

In summary, a consistent message to emerge from these calculations is that electrostatic self-assembly is more likely to proceed if undertaken in a solvent with a low dielectric constant. [89] Although such conditions make it more difficult for particles and surfaces to acquire charge, the calculations show that assembly can proceed at significantly lower levels of charge than are typical for an aqueous medium. The absence of strong screening also means that low charge levels can be effective over large distances, which again should be important for self-assembly.

Chapter 4

Electrostatic interactions in many-body systems

In the previous chapters, a solution to the problem of calculating electrostatic interactions between pairs of charged particles, of dielectric or effectively metallic character, has been extensively analysed and also further developed to accurately describe de presence of a dielectric medium. Such solution has proved to be an excellent platform for understanding the fundamentals of the physics behind the problem besides generating predictive results that can be applied to the interpretation of experimental observations. However, there are many situations where a knowledge of two-body interactions is not sufficient for a quantitative description of a problem, and under those circumstances a solution to more complex systems where more than two particles interact would appear necessary. Examples where the latter may be appropriate include concentrated colloidal solutions [110], Coulombic crystals [97], electrostatic self-assembly and, more recently, super lattices [111]. In general terms, a two-body electrostatic interaction involving polarisation arises when the presence of electric charge in one of the particles creates an electric field that induces the redistribution of surface charge and/or the polarisation of bound charge on a second particle, which, in turn, generates its own electric field, that prompts the same effect on the first particle.

This iterative process results in an equilibrium state where both particles acquire a static charged configuration that can promote attraction, repulsion or even a null force between them. It is straightforward to anticipate then, that if a third particle is now introduced, the aforementioned iterative process will take place between all three particles, potentially altering the global state of the system.

A number of solutions to calculating electrostatic interactions in many-body systems can be found in the literature, with the majority relying on image charge methods [32, 35, 112, 113] and a few others on a multipole expansion approach. [40, 114, 115] However, an accurate description of a particular problem by such methods often becomes prohibited in terms of computation time, particularly when the configuration of the system requires use of a large number of corresponding "images" or multipole terms. Indeed, describing electrostatic interactions in many-body systems is an intrinsically more complex problem, as the induction of bound charges due to polarisation effects in one particle is coupled with the same process in all others; as a consequence, each pairwise interaction cannot be resolved independently. In addition, simplification based on symmetry assumptions, that can be naturally imposed in a two-body system, is rarely allowed if three or more particles are involved.

As an alternative to the current available methods, a numerical solution to the problem of calculating electrostatic interactions between many dielectric particles is presented in the following. This new development, based on an integral equation approach, is comparable to the multipole expansion, considering that it can also provide an accurate quantitative description about the various physical quantities of the problem, but with the advantage of being very computationally efficient. The solution is able to treat a number M of particles with arbitrary size, charge, dielectric constant, and position in a three-dimensional space, embedded in a homogeneous medium of arbitrary dielectric constant. As presented, it constitutes an effective generalisation of the two-body solution, perfectly agreeing with latter in terms of the numerical results for any calculated physical quantity. Additionally,

it converges up to the point where particles touch and therefore can be readily adapted as a force field for particle dynamics simulations.

4.1 Theory

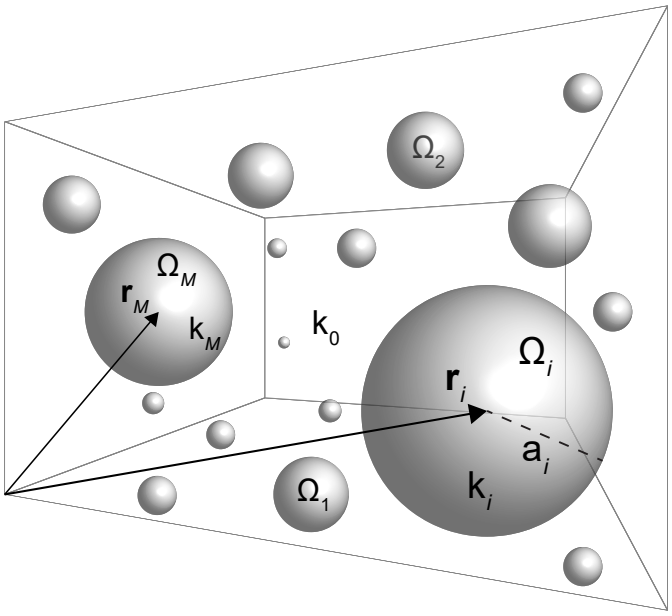


Fig. 4.1 Geometric representation of the system comprised of M non-overlapping spherical particles $\Omega_1, \ldots, \Omega_M$ with radius a_i, dielectric constant k_i, and centred at $\mathbf{r}_i$, surrounded by a homogeneous medium of dielectric constant k_0.

The considered system, illustrated in Figure 4.1, can be described in terms of a collection of M non-overlapping spherical particles $\Omega_1, \ldots, \Omega_M$ in a three-dimensional space, whereby each Ω_i $(i = 1, 2, \ldots, M)$ has radius a_i, and position $r_i = (r_{i,x}, r_{i,y}, r_{i,z})$. The dielectric constant within each particle Ω_i is denoted by $k_i \geq 1$ and, correspondingly, the dielectric constant of the surrounding medium is denoted by $k_0 \geq 1$. Accordingly, the dielectric constant as a function of space is given by

$$k(r) = k_0 + \sum_{i \in \{1,\ldots,M\}} (k_i - k_0) \mathbb{1}_{\Omega_i}(r), \qquad r \in \mathbb{R}^3, \tag{4.1}$$

where $\mathbb{1}_{\Omega_i}$ denotes the characteristic function of Ω_i. The function k is the piecewise relative permittivity of the system. Let $\Omega_0 = \mathbb{R}^3 \setminus \cup_{i=1}^{M} \overline{\Omega}_i^c$ be the complementary

part to the particles and set $\Gamma_i = \partial\Omega_i$ for $i = 0, 1, \ldots, M$. Note that

$$\overline{\Omega}_0^c = \Omega_1 \cup \ldots \cup \Omega_M,$$
$$\Gamma_0 = \Gamma_1 \cup \ldots \cup \Gamma_M.$$

Each particle Ω_i carries a free charge $\sigma_{f,i} = q_i/(4\pi a_i^2)$ that is completely supported at its boundary Γ_i, such that a global function can be defined:

$$\sigma_f(r) = \begin{cases} \sigma_{f,i} & \text{if } r \in \Gamma_i, \\ 0 & \text{otherwise.} \end{cases}$$

If the electric potential Φ created by a free charge $\sigma_{f,i}$ residing on each particle can be determined, then the electrostatic potential energy U follows directly from: [3, 41]

$$U = \frac{1}{2} \int_{\Gamma_0} \sigma_f(s)\Phi(s)ds, \tag{4.2}$$

where, exclusively in this section, s denotes a point on the surface of a particle, and not a surface-to-surface separation.

In order to use an approach that allows for a representation in terms of integral equations, [116, 117] the problem is formulated as an interface problem, where a potential Φ needs to be determined such that, in a similar way to the two-body problem, the standard set of boundary conditions are observed; in particular:

$$\Delta\Phi = 0 \qquad \text{in each } \Omega_i, i = 0, 1, \ldots, M, \tag{4.3}$$
$$[\![\Phi]\!] = 0 \qquad \text{on } \Gamma_0, \tag{4.4}$$
$$[\![k\nabla\Phi]\!] = 4\pi K\sigma_f \qquad \text{on } \Gamma_0, \tag{4.5}$$

where $[\![\Phi]\!]$ and $[\![k\nabla\Phi]\!]$ are the discontinuities defined by

$$[\![\Phi]\!]|_{\Gamma_i}(r) = \Phi|_{\Omega_0}(r)n_0(r) + \Phi|_{\Omega_i}(r)n_i(r),$$
$$[\![k\nabla\Phi]\!]|_{\Gamma_i}(r) = (k\nabla\Phi)|_{\Omega_0}(r)\cdot n_0(r) + (k\nabla\Phi)|_{\Omega_i}(r)\cdot n_i(r),$$

for all $r \in \Gamma_i$, $i = 1, \ldots, M$, where $n_0(r)$ denotes the outward pointing normal to Ω_0, and $n_i(r)$ denotes the outward pointing normal to Ω_i.

4.1.1 Representation in terms of integral equations

At a local level, i.e., for each interface Γ_i with $i = 1, \ldots, M$, a local single layer potential $\tilde{\mathcal{S}}_i$ is defined by

$$(\tilde{\mathcal{S}}_i\nu)(r) := \int_{\Gamma_i} \frac{\nu(s)}{|r-s|}\, ds, \qquad \forall r \in \mathbb{R}^3\backslash\Gamma_i.$$

Further, any harmonic function w in $\Omega_i \cup \overline{\Omega}_i^c$ that is continuous across the interfaces Γ_i can be represented by the discontinuity in its normal derivative on Γ_i across the interface by the local single layer potential

$$w = \tilde{\mathcal{S}}_i\nu_i \qquad \text{with } \nu_i = \frac{1}{4\pi}[\![\nabla w]\!]. \tag{4.6}$$

The local single layer boundary operator $\mathcal{S}_i$ can be introduced by restricting the single layer potential to Γ_i:

$$(\mathcal{S}_i\nu)(s) = \gamma_{D,i}(\tilde{\mathcal{S}}_i\nu)(s) = \int_{\Gamma_i} \frac{\nu(s')}{|s-s'|}\, ds', \qquad \forall s \in \Gamma_i,$$

where $\gamma_{D,i}$ denotes the Dirichlet trace onto Γ_i. In addition, the interior Neumann trace is given by

$$\nabla w|_{\Omega_i}\cdot n_i = (2\pi + \mathcal{D}_i^\star)\nu_i, \tag{4.7}$$

where $\mathcal{D}_i^\star$ is the adjoint operator for the double layer boundary operator which, in turn, is self-adjoint and equal to

$$\mathcal{D}_i^\star = \mathcal{D}_i = -\frac{1}{2a_i}\mathcal{S}_i \tag{4.8}$$

for the case of a sphere of radius a_i.

It follows from potential theory that any function satisfying Equations 4.3−4.5 can be represented by a global single layer potential

$$\Phi(r) = (\tilde{\mathcal{S}}_{\mathtt{G}}\sigma)(r) := \sum_{i\in\{1,\ldots,M\}} (\tilde{\mathcal{S}}_i\sigma_i)(r), \tag{4.9}$$

where $\tilde{\mathcal{S}}_{\mathtt{G}}$ is the global single layer potential and

$$\sigma_i = \sigma|_{\Gamma_i} = \frac{1}{4\pi}[\![\nabla\Phi]\!], \qquad \text{on each } \Gamma_i.$$

The evaluation of Φ at each boundary Γ_i, $i \in \{1,\ldots,M\}$, can be denoted by λ_i, i.e.

$$\lambda_i(s) = \mathcal{S}_{\mathtt{G}}\sigma(s), \qquad \forall s \in \Gamma_i. \tag{4.10}$$

where $\mathcal{S}_{\mathtt{G}}$ is the global single layer boundary operator. In addition, Φ can be locally represented in Ω_i by a local density ν_i which is supported only on Γ_i, such that

$$\Phi(r) = (\tilde{\mathcal{S}}_i\nu_i)(r) := \int_{\Gamma_i} \frac{\nu_i(s)}{|r-s|}ds, \tag{4.11}$$

for all $r \in \Omega_i$. The local density ν_i can be uniquely determined by the following local integral equation

$$\mathcal{S}_i\nu_i = \lambda_i,$$

assuming for now that λ_i is known. Having a representation for Φ in the interior of Ω_i, it follows from its Neumann trace, Equations 4.7 and 4.8:

$$\nabla\Phi|_{\Omega_i}\cdot n_i = \left(2\pi - \frac{1}{2a_i}\mathcal{S}_i\right)\nu_i.$$

Using the discontinuity condition, Equation 4.5, the exterior (to Ω_i) Neumann trace becomes

$$\nabla\Phi|_{\Omega_0}\cdot n_0 = \frac{1}{k_0}(4\pi K\sigma_{f,i} - k_i\nabla\Phi|_{\Omega_i}\cdot n_i),$$

on each Γ_i, $i \in \{1,\ldots,M\}$, where $K = 1$ hereafter in this section, as units can be imputed later, *vide* Section 2.5. However, it has already been shown in Equation 4.9 that the solution Φ can be represented globally by the density σ_i and therefore it holds locally on each Γ_i that

$$\begin{aligned}\sigma_i &= \frac{1}{4\pi}[\![\nabla\Phi]\!]|_{\Omega_i} \\ &= \frac{1}{k_0}\sigma_{f,i} + \frac{k_0-k_i}{4\pi k_0}\nabla\Phi|_{\Omega_i}\cdot n_i = \frac{1}{k_0}\sigma_{f,i} + \frac{k_0-k_i}{4\pi k_0}\left(2\pi - \frac{1}{2a_i}\mathcal{S}_i\right)\mathcal{S}_i^{-1}\lambda_i.\end{aligned}$$

Recalling Equation 4.10, a globally coupled integral equation can be given by

$$\left[I_{\mathrm{id}} - \frac{k_0-k_i}{4\pi k_0}\left(2\pi\mathcal{S}_i^{-1} - \frac{1}{2a_i}\right)\mathcal{S}_{\mathtt{G}}\right]\sigma = \frac{\sigma_{f,i}}{k_0} \tag{4.12}$$

on each Γ_i.

Considering the energy expression, Equation 4.2, it can be observed that

$$\begin{aligned}U(\Phi,\sigma_f) &= \frac{1}{2}\int_{\Gamma_0}\sigma_f(s)\Phi(s)ds \\ &= \frac{1}{2}\int_{\Gamma_0}\sigma_f(s)\lambda(s)ds = \frac{1}{2}\sum_{i=1}^{M}\int_{\Gamma_i}\sigma_{f,i}(s)\lambda_i(s)ds,\end{aligned} \tag{4.13}$$

The energy is computed starting from $\lambda = \mathcal{S}_{\mathtt{G}}\sigma$ and not from σ, which is an unknown quantity in Equation 4.12. Accordingly, an equivalent equation for σ

can be defined by applying $\mathcal{S}_{\mathtt{G}}$ to both sides in Equation 4.12:

$$\lambda - \mathcal{S}_{\mathtt{G}}\mathcal{L}\lambda = \frac{1}{k_0}\mathcal{S}_{\mathtt{G}}\sigma_f, \tag{4.14}$$

where the local operator $\mathcal{L}_j$ is defined by

$$(\mathcal{L}\lambda)|_{\Gamma_j} := \mathcal{L}_j\lambda_j, \tag{4.15}$$

$$\mathcal{L}_j\lambda_j := \frac{k_0 - k_j}{4\pi k_0}\left(2\pi\mathcal{S}_j^{-1} - \frac{1}{2a_j}\right)\lambda_j. \tag{4.16}$$

The problem consists of solving Equation 4.14 and then computing the energy following Equation 4.13. The electrostatic force acting on each of the particles Ω_i follows as the negative gradient of the energy with respect to changes in the location of the position $r_i = (r_{i,x}, r_{i,y}, r_{i,z}) = (r_i^1, r_i^2, r_i^3)$ of Ω_i.

4.1.2 Discretisation

Let $\mathbb{V}_{N,i}$ be the set of functions spanned by spherical harmonics on Γ_i of maximum degree N:

$$\mathbb{V}_{N,i} = \left\{ \sum_{\ell=0}^{N} \sum_{m=-\ell}^{\ell} [v]_\ell^m \, \mathcal{Y}_{\ell m}\left(\frac{r - r_i}{a_i}\right) \right\},$$

where

$$[v]_\ell^m = \int_{\mathbb{S}^2} v(r_i + a_i s)\mathcal{Y}_{\ell m}(s)\, ds. \tag{4.17}$$

Since the integral in Equation 4.17 can not always be computed exactly, a quadrature (numerical integration) scheme is therefore introduced, by a set $\{s_n, \omega_n\}_{n=1}^{N_g}$ of integration points and weights, respectively, on the unit sphere $\mathbb{S}^2$, defined by

$$\langle u, v\rangle_{n,i} := \sum_{n=1}^{N_g} \omega_n u(r_i + a_i s_n)\, v(r_i + a_i s_n). \tag{4.18}$$

In practice, the Lebedev quadrature [118] is used, as it can integrate couples of spherical harmonics very accurately depending on the number of integration points.

The Galerkin approximation to Equation 4.14 is then given by: on each Γ_i, find $\lambda_N|_{\Gamma_i} = \lambda_{N,i} \in \mathbb{V}_{N,i}$ such that

$$\forall v_{N,i} \in \mathbb{V}_{N,i} : \qquad \langle \lambda_{N,i} - \mathcal{S}_{\mathtt{G}} \mathcal{L} \lambda_N, v_{N,i} \rangle_{n,i} = \left\langle \frac{1}{k_0} \mathcal{S}_{\mathtt{G}} \sigma_f, v_{N,i} \right\rangle_{n,i} . \tag{4.19}$$

Since each $\lambda_{N,i} \in \mathbb{V}_{N,i}$, it is represented by a set of coefficients $[\lambda_i]_\ell^m$ so that

$$\lambda_N|_{\Gamma_i}(r) = \lambda_{N,i}(r) = \sum_{\ell=0}^{N} \sum_{m=-\ell}^{\ell} [\lambda_i]_\ell^m \, \mathcal{Y}_{\ell m} \left(\frac{r - r_i}{a_i} \right) . \tag{4.20}$$

Therefore the function λ_N has a discrete representation by means of a vector $\boldsymbol{\lambda} \in \mathbb{R}^{M(N+1)^2}$ consisting of all coefficients $[\lambda_i]_\ell^m$. The corresponding linear system, denoted here by

$$L\boldsymbol{\lambda} = \boldsymbol{f}, \tag{4.21}$$

is characterized by the entries of the solution matrix and the right-hand side

$$[L_{ij}]_{\ell\ell'}^{mm'} = \langle \delta_{ij} \mathcal{Y}_{\ell' m'} - \mathcal{S}_{\mathtt{G}} \mathcal{L}_j \mathcal{Y}_{\ell' m'}, \mathcal{Y}_{\ell m} \rangle_{n,i} , \tag{4.22}$$

$$[f_i]_\ell^m = \left\langle \frac{1}{k_0} \mathcal{S}_{\mathtt{G}} \sigma_f, \mathcal{Y}_{\ell m} \right\rangle_{n,i} , \tag{4.23}$$

which are derived as follows.

Focusing on Equation 4.14, it is first observed that the spherical harmonics are eigenfunctions of the local single layer operator $\mathcal{S}_j$, i.e.

$$\mathcal{S}_j \mathcal{Y}_{\ell m} = \frac{4\pi a_j}{2\ell + 1} \mathcal{Y}_{\ell m}, \qquad \text{on } \Gamma_j.$$

As a consequence,

$$\begin{aligned}(\mathcal{L}_j\mathcal{Y}_{\ell'm'})\left(\frac{r-r_j}{a_j}\right) &= \left[\frac{k_0-k_j}{4\pi k_0}\left(2\pi\mathcal{S}_j^{-1}-\frac{1}{2a_j}\right)\mathcal{Y}_{\ell'm'}\right]\left(\frac{r-r_j}{a_j}\right)\\ &= \ell'\,\frac{k_0-k_j}{4\pi k_0 a_j}\,\mathcal{Y}_{\ell'm'}\left(\frac{r-r_j}{a_j}\right),\end{aligned} \tag{4.24}$$

for all $r \in \Gamma_j$. Second, the single layer potential of $\mathcal{Y}_{\ell'm'}\left(\frac{r-r_j}{a_j}\right)$ in $\mathbb{R}^3\backslash\Omega_i$ is given by

$$(\tilde{\mathcal{S}}_j\mathcal{Y}_{\ell'm'})(r) = \frac{4\pi a_j}{2\ell'+1}\left(\frac{a_j}{|r-r_j|}\right)^{\ell'+1}\mathcal{Y}_{\ell'm'}\left(\frac{r-r_j}{|r-r_j|}\right), \qquad \forall r \in \mathbb{R}^3\backslash\Omega_i. \tag{4.25}$$

Introducing

$$v_n^{ij} := r_i + a_i s_n - r_j, \qquad s_n^{ij} := \frac{v_n^{ij}}{|v_n^{ij}|} \qquad \text{and} \qquad t_n^{ij} := \frac{|v_n^{ij}|}{a_j},$$

and combining Equations 4.24 and 4.25 yields

$$(\mathcal{S}_{\mathtt{G}}\mathcal{L}_j\mathcal{Y}_{\ell'm'})(r_i + a_i s_n) = \frac{\ell'}{2\ell'+1}\frac{k_0-k_j}{k_0}(t_n^{ij})^{-(\ell'+1)}\mathcal{Y}_{\ell'm'}(s_n^{ij}). \tag{4.26}$$

The numerical integration becomes

$$\begin{aligned}\langle \mathcal{S}_{\mathtt{G}}\mathcal{L}_j\mathcal{Y}_{\ell'm'}, \mathcal{Y}_{\ell m}\rangle_{n,i} &= \sum_{n=1}^{N_g}\omega_n\,\mathcal{Y}_{\ell m}(s_n)\,(\mathcal{S}_{\mathtt{G}}\mathcal{L}_j\mathcal{Y}_{\ell'm'})(r_i+a_i s_n)\\ &= \frac{\ell'}{2\ell'+1}\frac{k_0-k_j}{k_0}\sum_{n=1}^{N_g}\omega_n\,\mathcal{Y}_{\ell m}(s_n)\,(t_n^{ij})^{-(\ell'+1)}\mathcal{Y}_{\ell'm'}(s_n^{ij}).\end{aligned}$$

Therefore, it holds that

$$[L_{ii}]_{\ell\ell'}^{mm'} = \delta_{\ell\ell'}\delta_{mm'}\left(1-\frac{\ell}{2\ell+1}\frac{k_0-k_i}{k_0}\right) \tag{4.27}$$

$$[L_{ij}]_{\ell\ell'}^{mm'} = -\sum_{n=1}^{N_g}[L_{ij}^n]_{\ell\ell'}^{mm'}\,(t_n^{ij})^{-(\ell'+1)}\,\mathcal{Y}_{\ell'm'}(s_n^{ij}), \qquad j \neq i, \tag{4.28}$$

with

$$[L_{ij}^{n}]_{\ell\ell'}^{mm'} := \omega_n \frac{\ell'}{2\ell'+1} \frac{k_0 - k_j}{k_0} \mathcal{Y}_{\ell m}(s_n).$$

For the right-hand side, it can be similarly obtained:

$$[f_i]_\ell^m = [\sigma_{f,i}]_0^0 \frac{4\pi a_i}{k_0}\delta_{\ell 0} + \frac{1}{k_0} \sum_{\substack{j\in\{1,\dots,M\}\\ j\neq i}} \sum_{n=1}^{N_g} \omega_n (\tilde{\mathcal{S}}_j \sigma_{f,j})(r_i + a_i s_n) \mathcal{Y}_{\ell m}(s_n) \tag{4.29}$$

$$= [\sigma_{f,i}]_0^0 \frac{4\pi a_i}{k_0}\delta_{\ell 0} + \sum_{\substack{j\in\{1,\dots,M\}\\ j\neq i}} \frac{4\pi a_j}{k_0} \sum_{n=1}^{N_g} \omega_n \mathcal{Y}_{\ell m}(s_n) [\sigma_{f,j}]_0^0 (t_n^{ij})^{-1} \mathcal{Y}_{00} \tag{4.30}$$

$$= [\sigma_{f,i}]_0^0 \frac{4\pi a_i}{k_0}\delta_{\ell 0} + \sum_{\substack{j\in\{1,\dots,M\}\\ j\neq i}} \sum_{n=1}^{N_g} [f_j^n]_\ell^m (t_n^{ij})^{-1}, \tag{4.31}$$

with

$$[f_j^n]_\ell^m := \frac{4\pi a_j}{k_0} \omega_n \mathcal{Y}_{\ell m}(s_n) [\sigma_{f,j}]_0^0 \mathcal{Y}_{00}..$$

4.1.3 Electrostatic potential energy

Having solved the linear system $L\boldsymbol{\lambda} = \boldsymbol{f}$, the energy can be computed following Equation 4.13 as

$$U(\lambda_N, \sigma_f) = \frac{1}{2} \sum_{i=1}^{M} \int_{\Gamma_i} \sigma_{f,i}(s) \lambda_{N,i}(s) ds,$$

First, $\sigma_{f,i}$ is written in terms of spherical harmonics of degree 0, i.e.

$$\sigma_{f,i} = [\sigma_{f,i}]_0^0 \mathcal{Y}_{00}\left(\frac{r - r_i}{a_i}\right), \qquad \text{with} \qquad [\sigma_{f,i}]_0^0 = 2\sqrt{\pi}\sigma_{f,i}. \tag{4.32}$$

Then

$$U(\lambda_N, \sigma_f) = \frac{1}{2} \sum_{i=1}^{M} \int_{\Gamma_i} \sigma_{f,i}(s) \lambda_i(s) ds = \langle \boldsymbol{\Psi}, \boldsymbol{\lambda} \rangle, \tag{4.33}$$

where entries for the vector $\boldsymbol{\Psi}$ are given by

$$[\Psi_i]_\ell^m = \delta_{\ell 0}\frac{a_i^2}{2}[\sigma_{f,i}]_0^0$$

and

$$\langle \boldsymbol{\Psi}, \boldsymbol{\lambda} \rangle := \sum_{i\in\{1,\dots,M\}} \sum_{\ell=0}^{N} \sum_{m=-\ell}^{\ell} [\Psi_i]_\ell^m [\lambda_i]_\ell^m.$$

This corresponds to the total electrostatic potential energy of the system. In order to determine the interaction energy, the solution can be defined only for a single particle, neglecting the presence of all other particles in the system. Thus, the solution on Γ_i, denoted here by $\lambda_{f,i}$, is given by

$$\lambda_{f,i} = \frac{1}{k_0}\mathcal{S}_i\sigma_{f,i},$$

such that the total self-energy of the system, given by the sum of the individual self-energies (Born energies), is defined as

$$U^{\text{self}}(\sigma_f) = \frac{1}{2}\sum_{i=1}^{M}\int_{\Gamma_i}\sigma_{f,i}(s)\lambda_{f,i}(s)ds = \langle \boldsymbol{\Psi}, \boldsymbol{\lambda}_f \rangle. \tag{4.34}$$

Here, entries for the vector $\boldsymbol{\lambda}_f$ are given by

$$[\lambda_{f,i}]_\ell^m = \delta_{\ell 0}\frac{4\pi a_i}{k_0}[\sigma_{f,i}]_0^0.$$

The interaction energy is then given as the difference between the total energy and the self-energy of the system:

$$U^{\text{int}}(\lambda_N, \sigma_f) = U(\lambda_N, \sigma_f) - U^{\text{self}}(\sigma_f).$$

4.1.4 Electrostatic force

The force acting on each of the particles Ω_i is the negative gradient of the energy with respect to changes in the location of the centre $r_i = (r_i^1, r_i^2, r_i^3)$ of Ω_i,

that is

$$F_i^\alpha = -\partial_{r_i^\alpha} U(\lambda_N, \sigma_f) = -\partial_{r_i^\alpha} \langle \boldsymbol{\Psi}, \boldsymbol{\lambda} \rangle = -\langle \boldsymbol{\Psi}, \partial_{r_i^\alpha} \boldsymbol{\lambda} \rangle,$$

where $\partial_{r_i^\alpha} = \frac{\partial}{\partial r_i^\alpha}$ for $\alpha = 1, 2, 3$. Note first that $\sigma_{f,i}$ and thus Ψ do not depend on the position r_i of the particle Ω_i, and second, the self-energy $U^{\text{self}}(\sigma_f)$ also is independent of r_i.

Considering now the linear system $L\boldsymbol{\lambda} = \boldsymbol{f}$, the derivative with respect to r_i on both sides yields

$$\partial_{r_i^\alpha}(L\boldsymbol{\lambda}) = (\partial_{r_i^\alpha} L)\boldsymbol{\lambda} + L(\partial_{r_i^\alpha} \boldsymbol{\lambda}) = \partial_{r_i^\alpha} \boldsymbol{f}.$$

Regrouping the terms gives

$$L(\partial_{r_i^\alpha} \boldsymbol{\lambda}) = \partial_{r_i^\alpha} \boldsymbol{f} - (\partial_{r_i^\alpha} L)\boldsymbol{\lambda} =: \boldsymbol{h}_i^\alpha. \tag{4.35}$$

Then,

$$F_i^\alpha = -\langle \boldsymbol{\Psi}, L^{-1} \boldsymbol{h}_i^\alpha \rangle = -\langle L^{-T} \boldsymbol{\Psi}, \boldsymbol{h}_i^\alpha \rangle = -\langle \boldsymbol{s}, \boldsymbol{h}_i^\alpha \rangle,$$

where $\boldsymbol{s}$ is a solution to the adjoint system

$$L^T \boldsymbol{s} = \boldsymbol{\Psi}. \tag{4.36}$$

Thus the force acting on the ith particle is given by

$$F_i = (F_i^1, F_i^2, F_i^3).$$

It remains to characterize the different coefficients of $\boldsymbol{h}_i^\alpha$. Applying the chain rule implies

$$\begin{aligned}
\partial_{r_i^\alpha}[L_{ii}]_{\ell\ell'}^{mm'} &= 0 \\
\partial_{r_i^\alpha}[L_{ij}]_{\ell\ell'}^{mm'} &= -\sum_{n=1}^{N_g}[L_{ij}^n]_{\ell\ell'}^{mm'}\,\partial_{r_i^\alpha}\left((t_n^{ij})^{-(\ell'+1)}\,\mathcal{Y}_{\ell'm'}(s_n^{ij})\right) \\
&= -\sum_{n=1}^{N_g}[L_{ij}^n]_{\ell\ell'}^{mm'}\,(t_n^{ij})^{-(\ell'+1)} \\
&\quad\times\left(\partial_{r_i^\alpha}\mathcal{Y}_{\ell'm'}(s_n^{ij}) - (\ell'+1)(t_n^{ij})^{-1}\,(\partial_{r_i^\alpha}t_n^{ij})\,\mathcal{Y}_{\ell'm'}(s_n^{ij})\right), \qquad j\neq i,
\end{aligned}$$

and

$$\partial_{r_i^\alpha}[f_i]_\ell^m = -\sum_{\substack{j\in\{1,\dots,M\}\\ j\neq i}}\sum_{n=1}^{N_g}[f_j^n]_\ell^m\,(t_n^{ij})^{-2}(\partial_{r_i^\alpha}t_n^{ij}).$$

Note that

$$\partial_{r_i^\alpha}t_n^{ij} = \frac{1}{a_j}\partial_{r_i^\alpha}|v_n^{ij}|,$$

and thus, using the notation $v_n^{ij} = ((v_n^{ij})_1, (v_n^{ij})_2, (v_n^{ij})_3)$, yields

$$\partial_{r_i^\alpha}|v_n^{ij}| = \partial_{r_i^\alpha}\left(\sum_{\beta=1}^{3}(v_n^{ij})_\beta^2\right)^{\frac{1}{2}} = \frac{(v_n^{ij})_\alpha}{|v_n^{ij}|}\partial_{r_i^\alpha}(r_i + a_i s_n - r_j)_\alpha = \frac{(v_n^{ij})_\alpha}{|v_n^{ij}|}f_{ijk},$$

where

$$f_{ijk} = \begin{cases} 1 & \text{if } k = i \neq j \\ -1 & \text{if } k = j \neq j \\ 0 & \text{if } k = i = j \\ 0 & \text{if } k \neq i, j \end{cases}.$$

Further

$$\partial_{r_i^\alpha}\mathcal{Y}_{\ell'm'}(s_n^{ij}) = \frac{1}{|v_n^{ij}|}\partial_{s^\alpha}\mathcal{Y}_{\ell'm'}(s_n^{ij})\partial_{r_i^\alpha}v_n^{ij} = \frac{1}{|v_n^{ij}|}\partial_{s^\alpha}\mathcal{Y}_{\ell'm'}(s_n^{ij})f_{ijk},$$

where $\partial_{s^\alpha}\mathcal{Y}_{\ell' m'}(s_n^{ij})$ denotes the α-component of the gradient in Cartesian coordinates of $\mathcal{Y}_{\ell' m'}(s)$ for $s \in \mathbb{S}^2$.

4.2 General numerical results

In this section the focus is turned to the presentation of a number of many-body interaction cases that illustrate the capability of this new model. Once again, the various physical quantities are considered to be dimensionless in this initial calculations, unless otherwise stated. In this first few examples, the number of particles has been restricted to $M = 3$, so that physical intuition regarding the problem can be preserved as part of the interpretation.

As already discussed in the previous chapters, in a system containing a neutral particle and a charged particle, the existence of an electrostatic interaction depends upon the electric susceptibility of the former, i.e. the neutral particle must have a corresponding dielectric constant that is greater than unity. Consider the case shown in Figure 4.2, where three interacting particles are displaced in a linear geometry; the central particle carries a positive charge and two neutral particles sit equidistant either side. When each particle have a dielectric constant equal to unity, i.e. when they are non-polarisable, no bound charges are induced and there is a complete absence of any type of electrostatic interaction. As the value of k_i $(i = 1, 2, 3)$ is increased, i.e. as the particles become more polarisable, bound charges are induced and the interaction becomes progressively more attractive. As can be seen from the surface charge density map (inset in Figure 4.2), the electric field created by the positive free charge on the central particle induces the appearance of negative bound charge on the left- and right-hand particles, particularly on the two sides adjacent to the central charged particle. Since the left and right particles are neutral, their total charge should remain zero, hence positive bound charge emerge on the two sides farthest from the central particle. As it is an iterative process, the electric field created by the induced bound

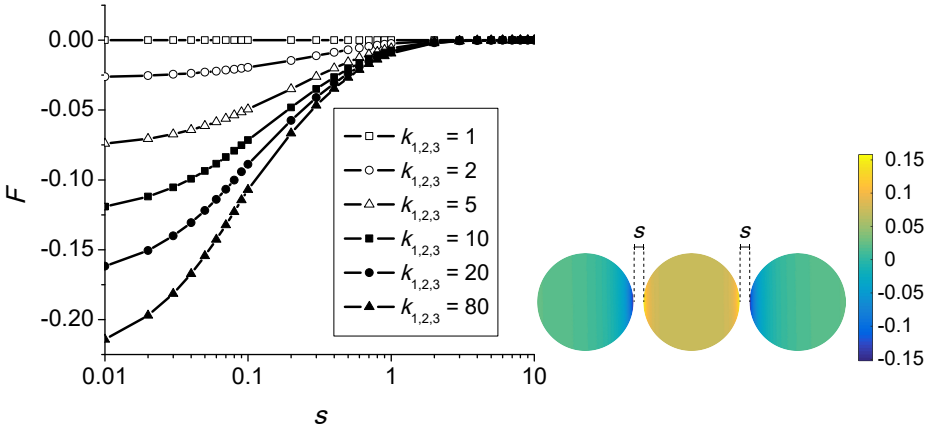


Fig. 4.2 Plot of the total electrostatic force F acting on the left-hand particle as function of the surface-to-surface separation s, for a case of charged particle − neutral particle interaction. The particle in the centre has a nominal charge of +1, whilst the left- and right-hand particles are neutral. The three particles are equal-sized, with nominal radii of 1 and each curve corresponds to a distinct value of the particles's dielectric constants, $k_1 = k_2 = k_3$. Also shown is a geometrical representation of the problem, with the total surface charge density (charge per unit area) mapped out for each of the particles, corresponding to the curve where $k_1 = k_2 = k_3 = 20$ and $s = 0.2$.

charges on the left and right particles also polarises the central particle, which then becomes more positively charged at the two ends closest to the adjacent neutral particles. The overall effect is that the total force on the left-hand particle is attractive and directed towards the other two particles. By symmetry, the total force on the right-hand particle is also attractive, acting with equal magnitude in the opposite direction; accordingly the total force on the central particle is zero.

In a second example, illustrated in Figure 4.3(a), there are again three interacting particles in a linear configuration, but this time they are all charged. The central particle is positively charged and the other two particles are equidistant and carry negatives charges. When the particles are non-polarisable, i.e. $k_i = 1$ $(i = 1, 2, 3)$, the electrostatic interaction is always attractive and described entirely by Coulomb's law. In this particular example, attraction is due to an opposite-charge interaction between the positive free charge on the central particle and the negative free charges on the two other particles. When k_i becomes larger than unity, bound charges are induced on the particles in a manner similar to the case depicted in Figure 4.2, such that, as the value of k_i increases, the interaction

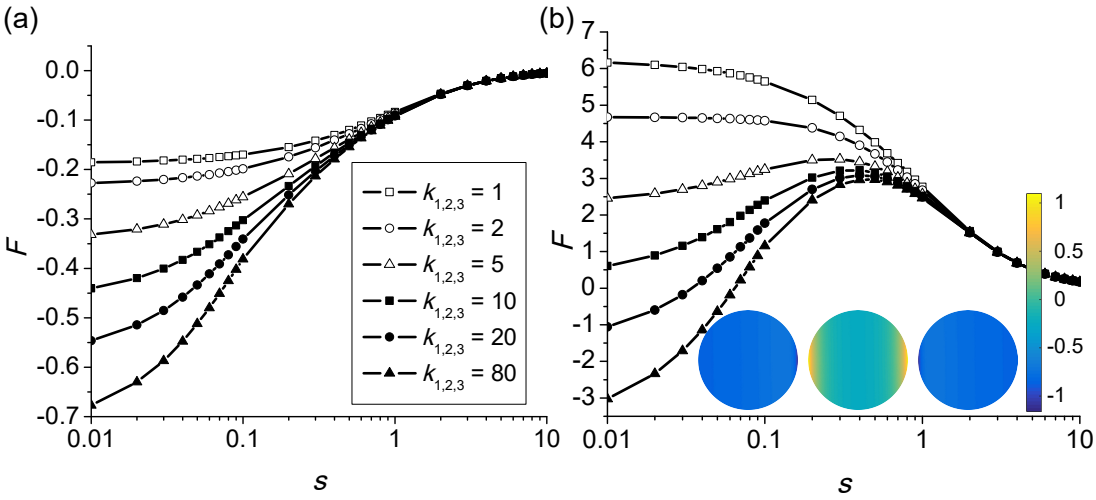


Fig. 4.3 Plot of the total electrostatic force F acting on the left-hand particle as function of the surface-to-surface separation s, for a case of opposite-charge interaction. In (a) the particle at the centre has a nominal charge of +1, while the left- and right-hand particles have nominal charges of -1. In (b) the particle at the centre has a nominal charge of +0.01, whilst the left and right particles have nominal charges of -10. In all cases the particles are equal-sized, with nominal radii of 1 and each curve corresponds to a distinct value of the particles's dielectric constants, $k_1 = k_2 = k_3$. Inset shows a geometrical representation of the problem, with the total surface charge density mapped out for each of the particles, corresponding to the curve in (b) where $k_1 = k_2 = k_3 = 20$ and $s = 0.2$.

becomes more attractive. In the case shown in Figure 4.3(b), the central particle carries significantly less charge than the other two particles in a way that a critical value of k_i is now necessary for the onset of an attractive interaction. As shown by the calculations, if $k_i \leq 10$, the combination of an opposite (free) charge interaction and additional attraction due to polarisation effects is not sufficient to balance the repulsion between the negative free charges on the left- and right-hand particles; therefore the overall force on the left-hand particle is repulsive. However, when $k_i \geq 20$, polarisation effects become stronger and can now promote the onset of an overall attractive interaction at sufficiently short inter-particle separation distances. As in the previous example, by symmetry, the total force on central particle is zero in all cases and what is changing are the forces on the left- and right-hand particles, which have the same magnitude but act in opposite directions.

Finally, consider again the case of three interacting particles placed in a linear configuration, but here the difference is that all carry a net positive charge, i.e. they are like-charged. Figure 4.4(a) shows that when the particles are identical, which includes a consideration of the magnitude and sign of charge, the electrostatic interaction will be always repulsive, no matter how polarisable the particles are; polarisation effects merely serve to weaken the electrostatic repulsion between particles, so as $k_i = 1$ $(i = 1, 2, 3)$ increases, the magnitude of the repulsive force decreases. However by changing one of the parameters, such that the polarisation effects become stronger, this scenario can be modulated. For example, in Figure 4.4(b), the central particle has been made three times larger than the left- and right-hand particles, such that they now have different surface charge densities. As can be inferred from the inset, the higher charge density on the two smaller particles induces negative bound charge on the central particle, specifically on the surfaces that are closest to either particle. In contrast, the left-

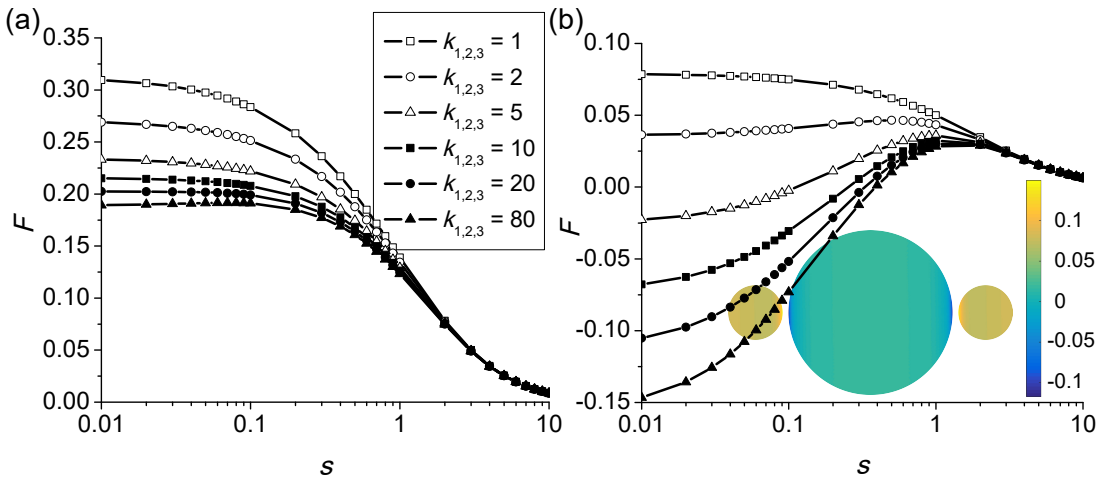


Fig. 4.4 Plot of the total electrostatic force F acting on the left-hand particle as function of the surface-to-surface separation s, for a case of like-charge interaction. In (a) all particles are identical, with a nominal charge of $+1$ and nominal radius of 1. In (b) all particles have a nominal charge of $+1$, the central particle has a nominal radius of 3, whilst the left- and right-hand particles have a nominal radius of 1. Each curve corresponds to a distinct value of the particles's dielectric constants, $k_1 = k_2 = k_3$, and the inset shows a geometrical representation of the problem, with the total surface charge density mapped out for each of the particles, corresponding to the curve in (b) where $k_1 = k_2 = k_3 = 20$ and $s = 0.2$. Note that the visual scale differs from that employed in the two previous figures.

and right-hand particles become more positively charged at those sides nearest to the central particle. The overall effect is that, at sufficiently short separations, an overall attractive interaction exists between the particles, even though they are all like-charged; a scenario comparable to that involving only two like-charged particles, presented in Section 2.2.

Figure 4.5 addresses another example of like-charge interaction, but this time the particles are displaced in a triangular geometry. Similarly to the previous case, shown in Figure 4.4, the particles in (a) are identical, and therefore the electrostatic interaction is always repulsive, with polarisation merely weakening its magnitude. However, when there is an asymmetry in one of the parameters, which in this case is the amount of charge on each particle, then as shown in Figure 4.5(b), an attractive interaction can emerge at sufficiently short separations.

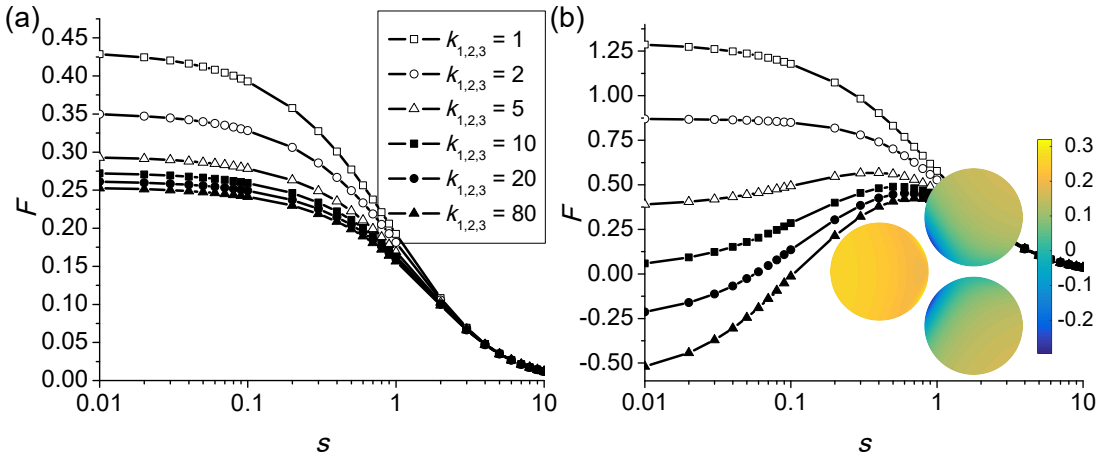


Fig. 4.5 Plot of the total electrostatic force F acting on the left-hand particle as function of the surface-to-surface separation s, for another case of like-charge interaction. In (a) all particles are identical, with a nominal charge of $+1$ and nominal radius of 1. In (b) all particles have a nominal radius of 1, but the left-hand particle has a nominal charge of $+3$, whilst the particles on the right-hand each have a nominal charge of $+1$. Each curve corresponds to a distinct value of the particles's dielectric constants, $k_1 = k_2 = k_3$, and the inset shows a geometrical representation of the problem, with the total surface charge density mapped out for each of the particles, corresponding to the curve in (b) where $k_1 = k_2 = k_3 = 20$ and $s = 0.2$.

4.3 Nonadditivity of the electrostatic force in many-body systems

As Coulomb's law obeys the principle of superposition (recall Equation 2.17), in the case of a system containing any number of uniformly charged non-polarisable spherical particles, or equivalent point charges at the centre of each respective particle, it is straightforward to recognise that the total electrostatic force acting on a specific particle is equal to the sum of forces corresponding to pairwise interactions between such particle and all other particles in the system.

Consider then the case depicted in Figure 4.6, which has the same geometry of the system previously considered in Figure 4.5, where each particle is positioned at a different vertex of an equilateral triangle. All particles are non-polarisable ($k_1 = k_2 = k_3 = 1$), equal-sized with nominal radii of 1, and separated by a distance $s = 1$; the left-hand particle has a nominal charge of 10, and both right-hand particles have a nominal charge of -10. The three upper representations in Figure 4.6 denote each isolated pairwise interaction, while the representation on the bottom shows the overall interaction between all three particles. As can be seen, the x and y components of the total force acting on each particle is simply the sum of the x and y components of the force due to the two corresponding pairwise interactions with the other particles. Therefore, for a system containing non-polarisable particles, likewise as for a collection of point charges, the principle of superposition holds and the force can be said to be additive.

Consider now the case illustrated in Figure 4.7, which has the same parameters of the system addressed in Figure 4.6, except for the dielectric constants of the particles, that now are equal to 20. Contrarily to the previous case, where the particles are non-polarisable, Figure 4.7 shows that when the particles have the ability to be polarised, the electrostatic force ceases to obey the principle of superposition and becomes nonadditive. Accordingly, in each of the isolated pairwise interactions, depicted in the three upper representations in Figure 4.7,

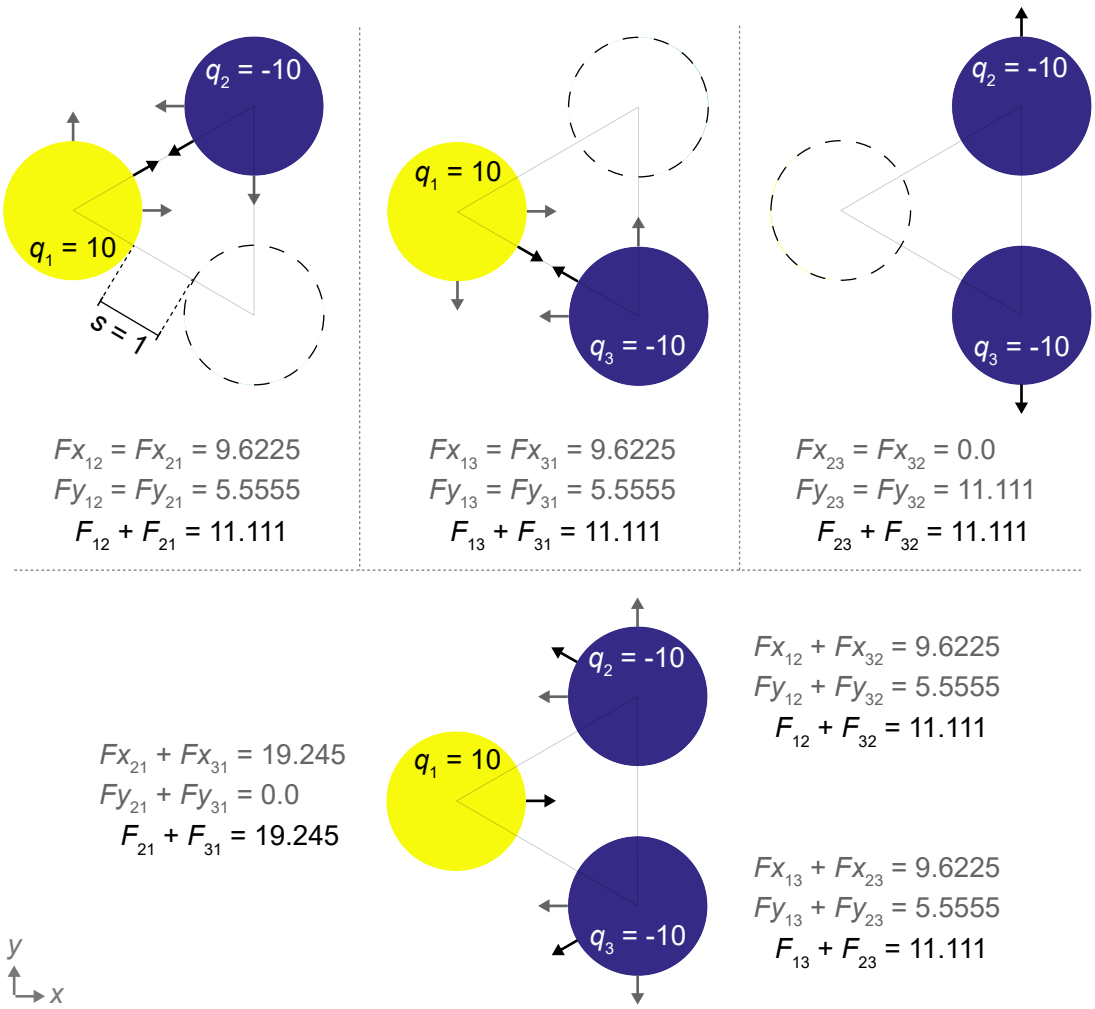


Fig. 4.6 Schematic illustration of the electrostatic interaction between three non-polarisable particles placed at the vertices of an equilateral triangle of side $h = 3$. The three upper diagrams represent an isolated pairwise interaction in the absence of the third particle, whose phantom location is shown as a dashed circle, and the bottom diagram represents the overall interaction, involving all three particles. The x and y components of the force are shaded in grey, while the total force is denoted in black. Accordingly, the arrows represent unit vectors (not in the same scale of the other length quantities, for clarity), portraying the direction of each force, whose corresponding absolute magnitude is displayed right below in each case.

the two particles become polarised by one another in such a way that they assume a static surface charge distribution that corresponds to the equilibrium configuration for each particular scenario. However, when a third particle is added to the system, it disrupts the static charge distributions on the two previously isolated interacting particles, and the system as whole, now composed by three particles, assumes a new equilibrium static surface charge distribution, as shown

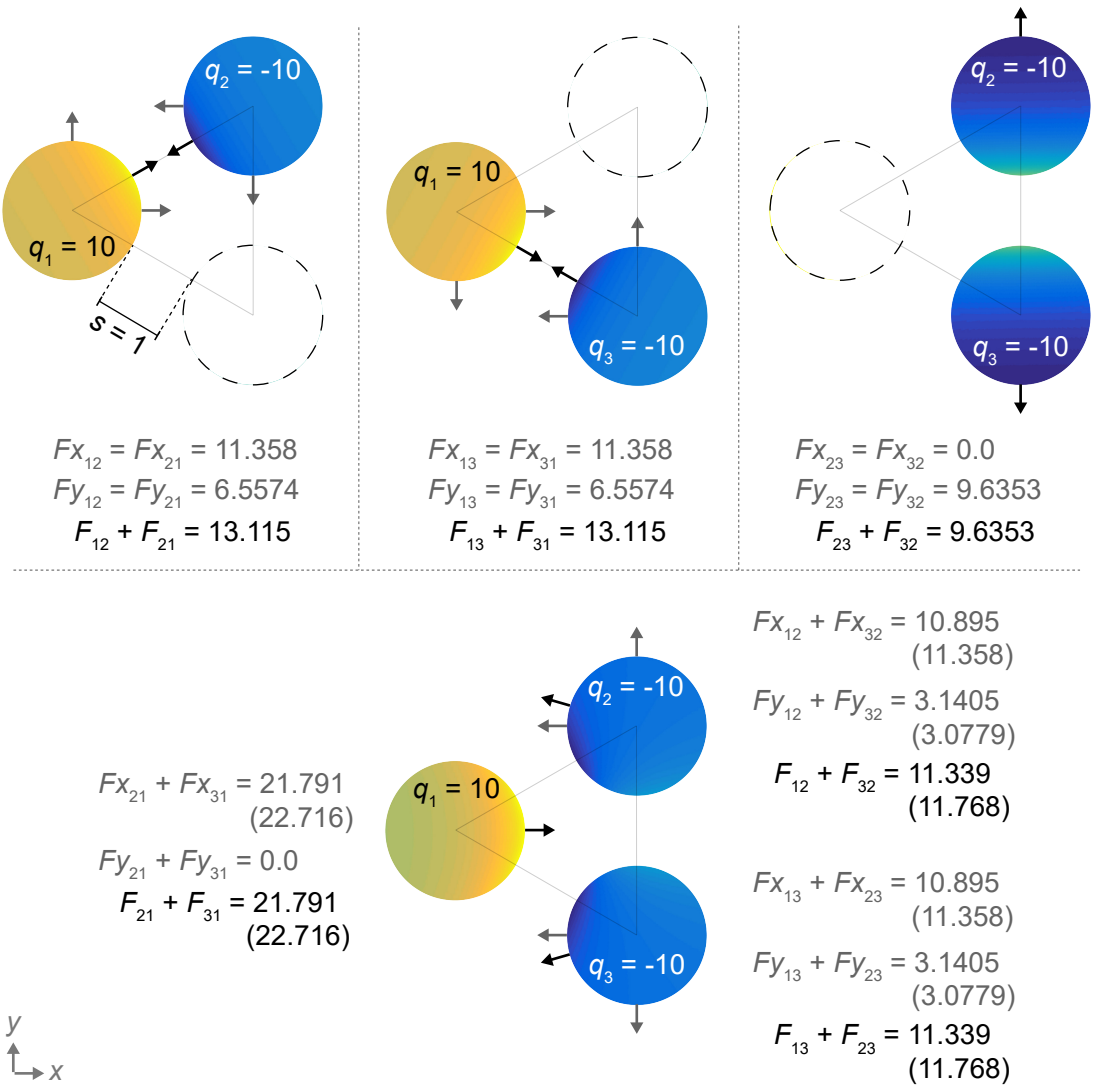


Fig. 4.7 Schematic illustration of the same system considered in Figure 4.6, but with the key difference that the particles are polarisable, with dielectric constants $k_1 = k_2 = k_3 = 20$. Clearly shown is the total surface charge density, mapped out for the particles, assuming a different distribution for each of the depicted diagrams. Values within brackets denote absolute force magnitudes that would be obtained if such interaction obeyed the principle of superposition, while values without brackets denotes the real force.

by the lower representation. In other words, the charge distribution on a specific particle in an isolated pairwise interaction is different from the charge distribution on the same particle when it is placed under influence of additional particles. As a consequence of such kind of change in a system, the various force components are also modified and the electrostatic force is characterized as nonadditive. This is evident from Figure 4.7 when one compares the force that would be obtained if the interaction obeyed the principle of superposition (within brackets) to the

real force resulting from the interaction. This effect is similar to that involving the induction component of intermolecular forces, which is recognised as being strongly nonadditive, since the fields of the different interacting neighbouring molecules may reinforce or cancel out each other. [119]

4.4 Calculations for systems with a larger number of particles

A couple of examples where the system contains a large number of particles are addressed next, in the form of calculations for the crystal structure of sodium chloride (NaCl) and estimation of its correspondent Madelung constant, and calculations for an electrostatic self-assembly process involving charged polystyrene microspheres.

4.4.1 Halite lattice and estimation of Madelung constant

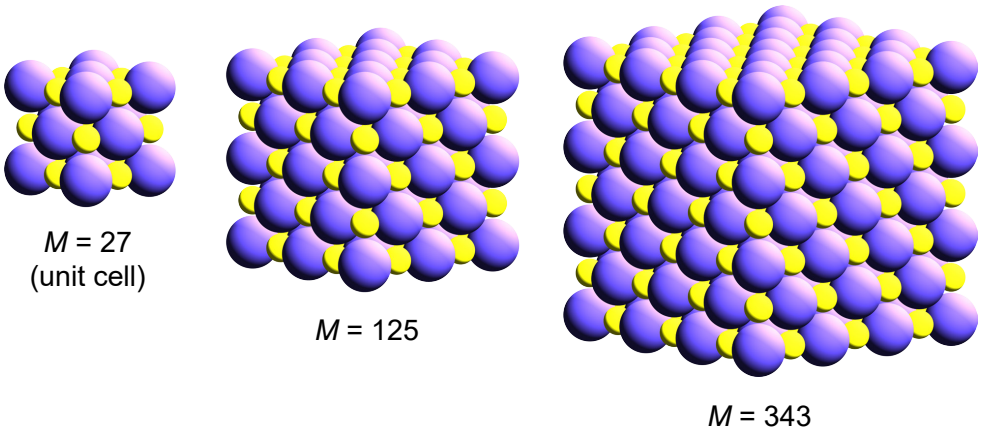


Fig. 4.8 Halite ('rock-salt') structure of sodium chloride (NaCl), where the sodium cation is depicted in yellow and the chlorine anion in blue. Shown are the first three possible cubic structures starting with the unit cell.

Sodium chloride (NaCl) occurs naturally in a (6,6)-coordinate halite ('rock-salt'), cubic structure, where each cation is surrounded by six anions and vice versa [120], as illustrated in Figure 4.8. As for any crystal, the lattice energy is defined as the difference in electrostatic potential energy between the salt

packed in a solid form and its isolated constituents, in this case Na^+ and Cl^-. If the constituents interacted to form ion pairs instead of the usual lattice then the energy released when the pairs form would be considerably smaller than that observed for the lattice energy. This difference is reflected in the Madelung constant, which is defined as the ratio between the lattice energy per mol of a substance in crystal form and the potential energy per mol of isolated ion pairs [121]. A knowledge of Madelung constants for crystals is important as they can be used to estimate lattice energies directly by treating a crystal's constituents as point charges. The Madelung constant also reflects geometric features of a crystal as, for example, the type of lattice present in a crystalline structure.

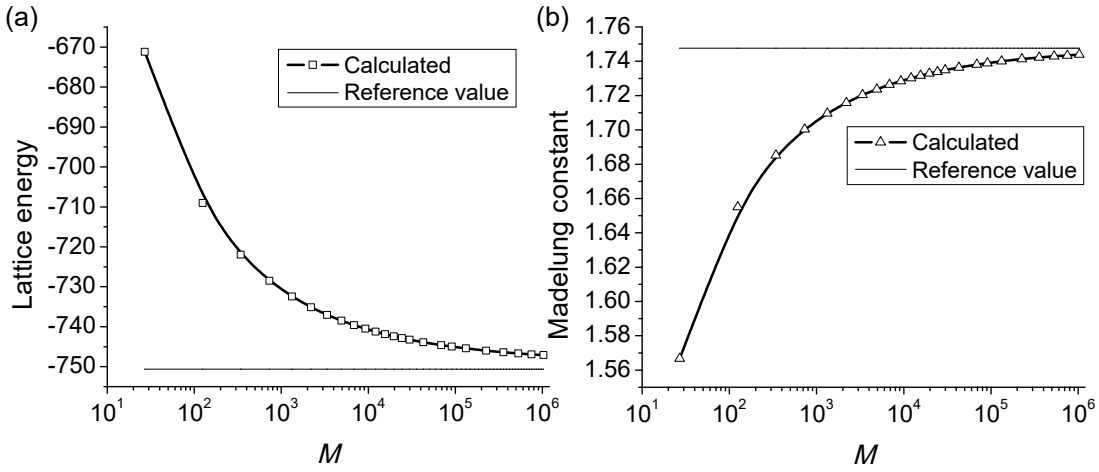


Fig. 4.9 (a) Semi-log plot of the estimated lattice energy and (b) estimated Madelung constant, as function of the number of particles M in the structure. The sodium cation is represented by a sphere of radius 1.02 Å [122] carrying a positive elementary charge, and the chlorine anion is represented by a sphere of radius 1.81 Å [122] carrying a negative elementary charge. Unlike some previous calculations, these results are not dimensionless, hence, the actual value of Coulomb's constant has been used. The lattice energy is presented as the Coulomb interaction added by the Born forces component from Born-Landé equation [123].

The potential energy of a single unit cell of a crystal is naturally expected to differ from the correspondent crystal lattice energy since the unit cell is not sufficiently large as to be representative of a crystal and edge effects cannot be appropriately smoothed, i.e. the pairwise interaction between any two of the constituents is significant enough to be neglected. As the unit cell is allowed to

grow in composition towards the structure of a larger crystal, interactions between distant ions becomes progressively smaller to a point where their contribution to the lattice energy becomes insignificant and the potential energy of the growing structure approximates that of the lattice energy. This is precisely what can be observed in Figure 4.9, where the estimated lattice energy and Madelung constant are plotted as function of the number of particles M in the evolving crystalline structure. As M increases, the estimated lattice energy and Madelung constant asymptotically approach their corresponding reference values [124, 125] of 750.619 kJ mol-1 and 1.74756, respectively.

4.4.2 Electrostatic self-assembly of polystyrene microspheres

About a decade ago, McCarty et al. [126] have described a process whereby polystyrene microspheres with opposite charges and different sizes self-assemble to form uniform multilayered microstructures. The microspheres are charged by means of a chemically directed contact electrification technique; some of the particles are covalently bound to tetraalkylammonium groups, which renders an uniformly distributed positive charge at the surface upon contact with an appropriated material that carries away negative charges, while others are covalently bound to sulfonate groups, oppositely rendering an uniformly distributed negative charge on the surface, upon contact with another type of material, that carries away positive charges. Information about the amount of charge on the largest of the manipulated particles, with 100 μm-radius, has been obtained through a device that essentially consists of an aluminium tube connected to an electrometer.

In one example, several of these 100 μm-radius sulfonate-functionalised microspheres with -0.01 nC of charge were placed in an aluminium dish with 10 μm-radius tetraalkylammonium-functionalised microspheres of undisclosed charge, and the arrangement was subsequently agitated until the particles were thoroughly mixed. Within seconds it was observed that each of the large 100 μm microspheres

were surrounded by the smaller, oppositely charged 10 μm microspheres, which effectively formed a layer of particles around the former. The authors estimated that the interaction energy for such kind of system is negative, by considering each microsphere as a non-polarisable spherical particle with a corresponding point charge at its centre, therefore showing that the assembly can be stable as a result of interactions of Coulombic nature alone. The obtained energy values can be in fact readily reproduced with the formalism introduced in this chapter, by considering only the spherical harmonic of degree zero in the truncated series utilised in its solution or, alternatively, by assigning dielectric constants equal to unity to all particles in the system. However, it is not strictly accurate to consider materials made of polystyrene as being non-polarisable; indeed polystyrene has a dielectric constant equal to 2.6 [127] and therefore it's possible that polarisation effects can make a significant contribution towards the overall stability of the assembly. To investigate such possibility, calculations have been undertaken where the charge $q_{central}$ on the central 100 μm-radius microsphere has been fixed to -0.01 nC, while the charge q_{1layer} on each of the 339 10 μm-radius microspheres that form the outer layer has been allowed to vary from 10^{-6} nC to 10^{-4} nC. Figure 4.10 shows the results, where the various energy curves, each corresponding to a different degree N of spherical harmonics, has been plotted as function of q_{1layer}. Since the maximum considered degree is $N = 10$, only the polarisation of the 339 smaller microspheres is accurately accounted for. Accordingly, a much higher degree would be necessary to properly describe the polarisation of the larger central particle, characterised by spots of high charge density each related to one of the 339 smaller microspheres, but that would require a calculation that is currently not viable in terms of computation time for this particular system.

As can be seen from the figure, polarisation effects are only significant when the amount of charge on the smaller particles is small. This is especially true due to the low value of the particles's dielectric constant. Accordingly, for most of the plot regions, opposite-charge attraction between the negative free charges

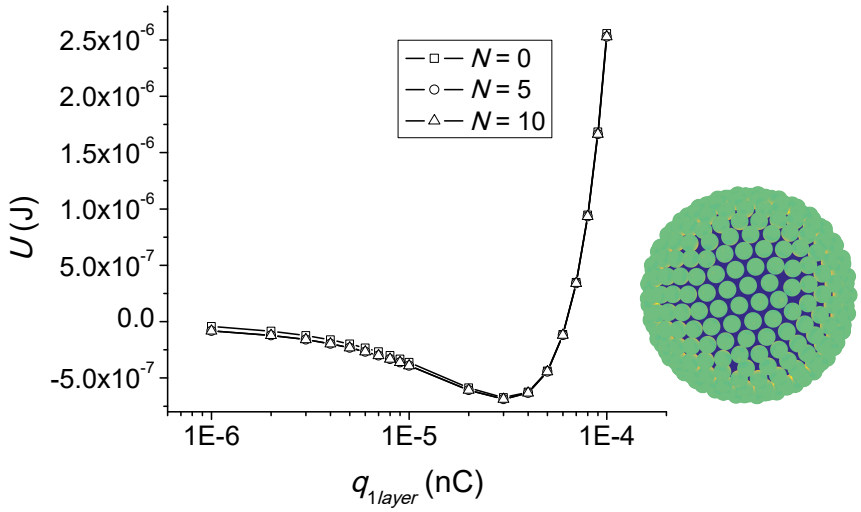


Fig. 4.10 Plot of the interaction energy U (J) as function of the amount of charge q_{1layer} (nC) on each of the 339 10 μm-radius microspheres that constitute the particles layer, for three different degrees N of spherical harmonics utilised in the truncated series. Placed on the right is an illustration of the system, with the total surface charge density mapped out for each of the particles.

on the central particle and the positive free charges on each of the particles in the layer dominates the overall interaction. It is only when the smaller particles are weakly charged that a residual attraction particularly due to interactions involving the induced bound charges on the smaller particles becomes significant enough so that the different curves in the plot do not superimpose one another. It can also be noted from the plot that, for a central particle carrying -0.01 nC of negative charge, the assembly is at the lowest energy configuration when the amount of positive charge on each of the 339 smaller particles is about 3×10^{-5} nC. Indeed, when the magnitude of charge on such particles decreases from the lowest energy point, the interaction energy goes to zero in the case of non-polarisable particles ($N = 0$), or it plateaus at a value close to zero, corresponding to the residual attractive interaction due to polarisation effects, when $N > 0$. Conversely, as such magnitude of charge increases from the lowest energy point, the energy increases continuously, eventually becoming positive at the point where the mutual repulsion between the positive smaller particles dominates over the atractive interation between these particles and the central microsphere.

In a second scenario, the authors have shown that when 35 μm-radius sulfonate-functionalised microspheres were added to the system, in addition to the other two types of microspheres considered in the previous case, a second layer of particles, constituted by these 35 μm-radius microspheres, was formed, effectively producing a multilayered assembly of alternating charges. Figure 4.11 shows electrostatic potential energy surfaces calculated for this case, where the charges q_{1layer} and q_{2layer} on each particle, respectively corresponding to the first layer made of 339 microspheres of 10 μm-radius, and the second layer constituted by 60 microspheres of 35 μm-radius, were allowed to vary. Each surface correspond to a different degree N of spherical harmonics, so polarisation effects can be also gauged in this case. Similarly to the previous case, since the maximum considered degree of spherical harmonics is $N = 10$, only the polarisation of the particles that form the first and second layers is accurately accounted for.

As illustrated in Figure 4.11, the three cases show a distinct "valley" where the interaction energy is close to the minimum, corresponding to an approximately constant value for the charge on the 10 μm-radius microspheres that constitute the first layer, except when the magnitude of charge on the 35 μm-radius microspheres in the second layer assumes a particular value of about -4×10^{-4} nC, which causes the "valley" to shift towards larger magnitudes of charge in the first layer. When the magnitude of charge on the 10 μm-radius microspheres is small, the assembly is predominantly unstable due to the repulsive interaction between the like charges in the 100 μm-radius central particle and in the particles that constitute the second layer, which is reflected in the positive value of the energy, especially if the particles are treated as being non-polarisable ($N = 0$). As the magnitude of charge on the microspheres in the first layer increases, the interaction energy shifts towards the above-mentioned "valley" until increasing again when such magnitude of charge is sufficiently large. At this latter condition, the interaction is mostly unstable due to either repulsion between the 10 μm-radius microspheres or repulsion between the 35 μm-radius microspheres, and also between these

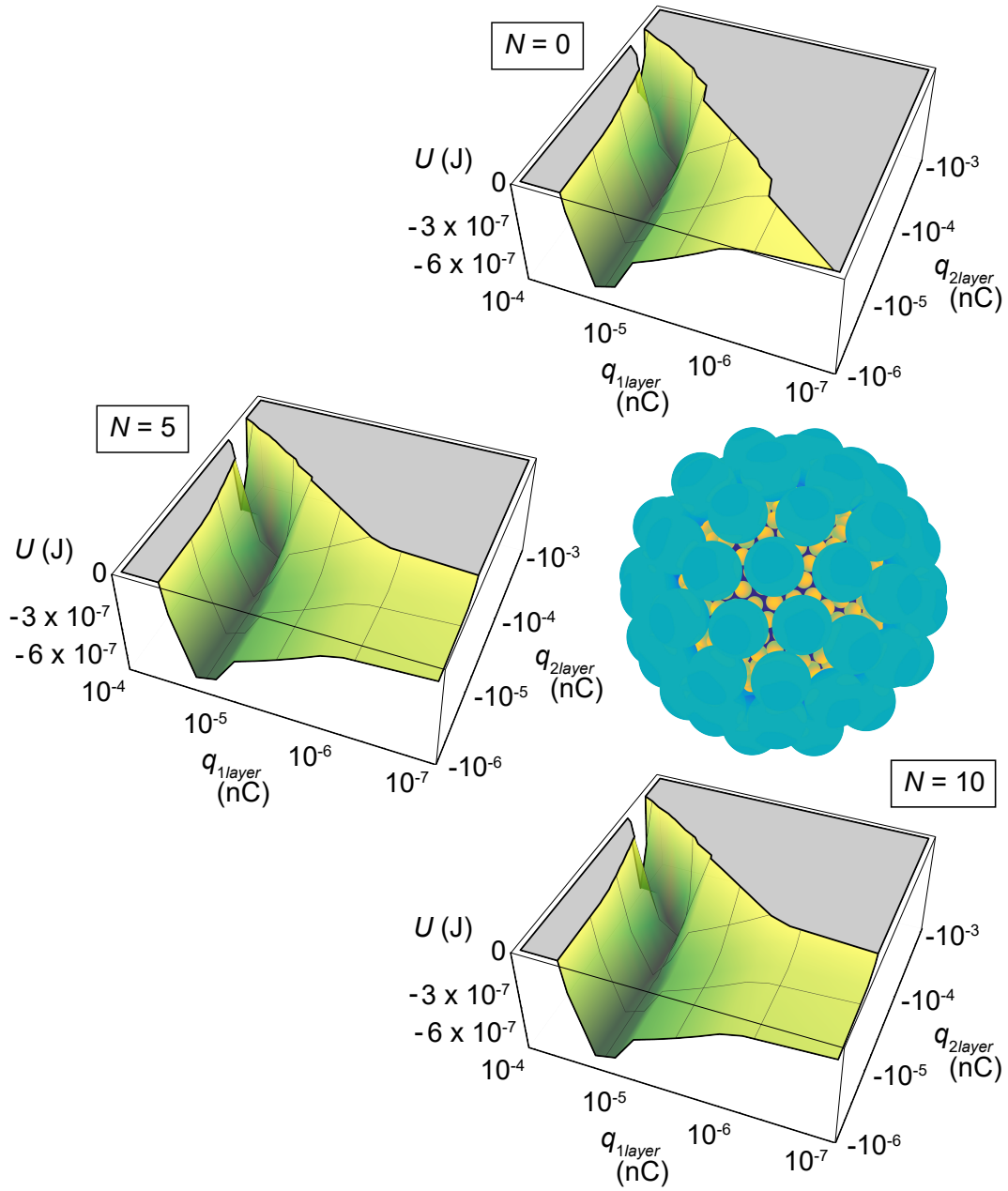


Fig. 4.11 Interaction potential energy U (J) surfaces, calculated as function of the amount of charge, q_{1layer} and q_{2layer}, on each particle that constitutes the first and second layer, respectively, for three different degrees N of spherical harmonics utilised in the truncated series. Shown are only the regions of surfaces where the energy is negative, so accordingly the flat parts represent regions of positive energy that have been clipped out, for clarity. Placed on the centre-right is an illustration of the system, with the total surface charge density mapped out for each of the particles.

latter particles and the central particle, apart from where the microspheres on the second layer aquire the already mentioned particular value of charge of about -4×10^{-4} nC, by which the "valley" passes. Figure 4.11 also shows that the

difference between the surfaces calculated with $N = 5$ and $N = 10$ are virtually non-existent, indirectly revealing that the accounted polarisation effects are not very significant for most of the graph, particularly because of the low dielectric constant of the microspheres.

Even though the stabilising effects in these cases addressed by McCarty et al. [126] are mainly of Coulomb nature, especially due to the low dielectric constant of the microspheres, the calculations suggest that, by considering particles that are able to be more strongly polarised, such stabilising effects can be pushed further due to a corresponding contribution made by polarisation effects.

4.5 Newtonian particle dynamics

As the last development addressed in this thesis, next it is demonstrated how the new formalism for calculating electrostatic interactions in many-body systems, introduced earlier in this chapter, can be implemented as a force field for Newtonian dynamics of many particles.

4.5.1 Physics engine

In the simple physics engine that has been initially developed for such dynamics simulations, a system that is composed by a given number of non-overlapping particles, each with a determined dielectric constant, charge, radius, mass, initial three-dimensional velocity and position, is considered. It is recognised that, since electric charges are effectively moving during a simulation, magnetic fields and hence magnetic forces also exist in the system. Accordingly, the total electromagnetic force corresponding to each pairwise interaction between charge elements can be obtained by [128]

$$\mathbf{F}_{12} = K\frac{q_1 q_2}{h^2}\left[\hat{\mathbf{h}} + \frac{\mathbf{v}_2 \times \left(\mathbf{v}_1 \times \hat{\mathbf{h}}\right)}{c^2}\right]. \tag{4.37}$$

where $\mathbf{v}_i$ $(i = 1, 2)$ is the particles's velocity and c is the speed of light. However, unless the speeds of the moving charged particles are close to that of light ($c \approx 3.0 \times 10^8$ m/s), which does not apply in what is presented next, the second term within square brackets in Equation 4.37 is considerably smaller than the first. Consequently, the magnetic component of the force can be safely neglected and any interaction can be accurately described by only considering the electric component. It is assumed that the particles are also not subject to any gravitational field, from either internal or external sources. Therefore, the only force acting on each particle is the electrostatic force due to the presence of charge on other particles.

The motion of the particles is governed by Newton's laws of motion, [129] especially the second law, $\mathbf{F}_i = m_i\ \mathbf{a}_i$, which relates the acceleration $\mathbf{a}_i$ experienced by a given particle i of mass m_i, with the total force $\mathbf{F}_i$ acting on it. Since the acceleration is subjected to any changes in total force, both the velocity and corresponding displacement of a particle are appropriately updated at each time step, according to the so-called Euler method. [130] In addition, as there should be no overlapping between particles, a serial collision handler, which is responsible for processing detection and response of any collision, has also been integrated in the engine.

4.5.2 Bouncing frequency of attracting particles

To investigate how polarisation effects can influence the progression of a dynamics simulation, consider a system composed by two equal-sized particles of varying dielectric constants, with nominal radii $a_1 = a_2 = 1$, nominal charges $q_1 = 1$ and $q_2 = 0$, and nominal masses $m_1 = m_2 = 1$. The charged particle is centred at the origin, i.e. with coordinates $(r_{1,x}, r_{1,y}, r_{1,z}) = (0,0,0)$, while the neutral particle is initially placed at the position $(r_{2,x}, r_{2,y}, r_{2,z}) = (h,0,0)$, where $h = 3$. The simulation starts with the particles at rest and the system is then allowed to evolve over time. Each collision is at first treated as being perfectly

elastic, wherefore the conservation of both the corresponding linear momentum and (translational) kinetic energy are observed.

In such simple scenario, the free charge on the first particle induces the appearance of bound charges on the second particle, which in response also induces the appearance of bound charges on the first particle, in an iterative process that is familiar from previous chapters. The net result is that a total electrostatic force of equal magnitude acts on both particles, accelerating them towards each other. With increasing acceleration, the particles collide elastically at halfway of their initial centre-to-centre separation distance, namely at the point $(h/2,0,0)$, leading to an inversion in the direction of their linear momentum. After collision, the particles move away from each other, being decelerated by a restoring electrostatic force, until assuming a velocity of magnitude zero once they reach their initial positions, therefore completing a cycle.

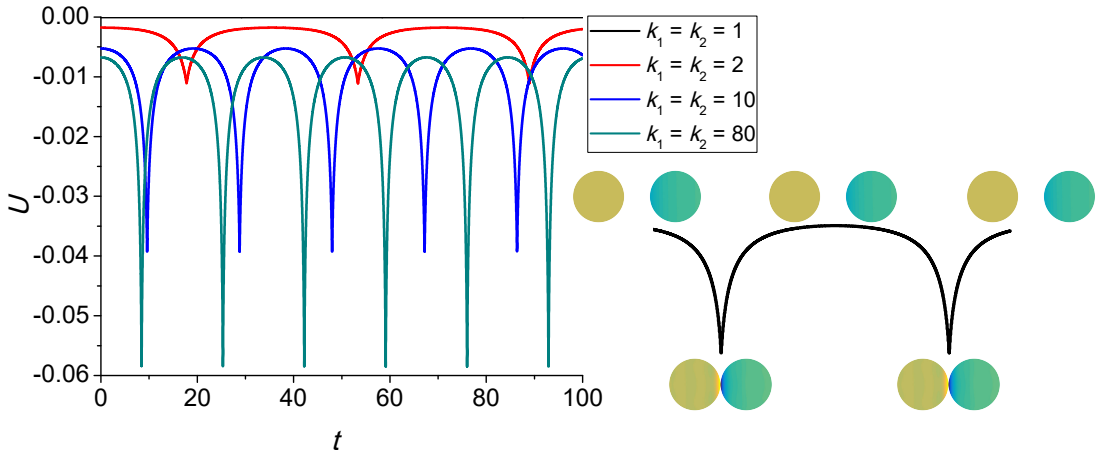


Fig. 4.12 Plot of the interaction energy U as function of simulation time t for distinct values of the particles's dielectric constants, $k_1 = k_2$. Each collision is treated as being perfectly elastic, where CR = 1. Diagram on the right shows a geometrical representation of the bouncing cycle.

Figure 4.12 illustrates how the electrostatic interaction energy varies as function of time, for distinct values of the particles's dielectric constants $k_1 = k_2$. As expected, lower interaction energies, especially at close proximity, are achieved as the particles become more able to be polarised, i.e. as their dielectric constants increase. Most interestingly for such time-evolving process is the fact that the

bouncing period, namely the time required to complete a cycle, is smaller for more polarisable particles. Understandably, higher dielectric constants results in stronger electrostatic forces between the particles, which consequently acquire faster speeds, allowing them to bounce in a higher frequency.

However, a real scenario collision can be rarely considered as being perfectly elastic, since the kinetic energies of the particles are generally converted into another form of energy in the process, such as thermal energy—in this scenario the kinetic energy can be absorbed either by surface vibrational modes or by internal vibrational modes associated with the constituent molecules of the colliding bodies; in return, the excess energy associated with these vibrational modes can be subsequently dissipated by a surrounding medium (e.g., air). [129] A more appropriate way of dealing with such problem is then to consider any given collision as being partially elastic, wherefore the linear momentum is still conserved, in contrast to the kinetic energy that is not. Such behaviour can be defined through a parameter known as the coefficient of restitution (CR), which relates the relative speeds of the colliding particles before and after the collision as

$$\mathrm{CR} = \frac{\text{relative speed after collision}}{\text{relative speed before collision}}. \tag{4.38}$$

Accordingly, for a perfectly elastic collision the coefficient of restitution assumes a value equal to unity, and for a perfectly inelastic collision it assumes a value equal to zero. Values of CR in-between 0 and 1 represents then a partially elastic collision (or partially inelastic collision, depending on one's point of view). In order to investigate the effects of treating collisions as belonging to the latter category, calculations for the same cases addressed in Figure 4.12 have been repeated with a coefficient of restitution equal to 0.9, and the new results are given in Figure 4.13. As can be seen, the main difference in such scenario is that, after each collision, the bouncing frequency increases as the particles don't return

to their previous initial cycle position, as a consequence of part of their kinetic energies being repeatedly lost in the process.

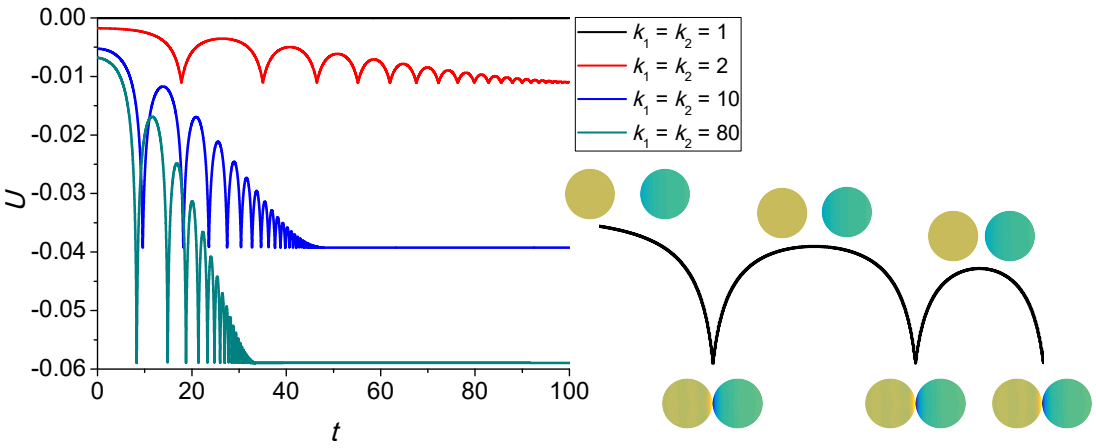


Fig. 4.13 Plot of the interaction energy U as function of simulation time t for distinct values of the particles's dielectric constants, $k_1 = k_2$. Each collision is treated as being partially elastic, where CR = 0.9. Diagram on the right shows a geometrical representation of the bouncing cycle.

The consideration of partially elastic collisions allows the simulation of processes where particles might aggregate, since no energy redistribution are explicitly taken into account in the current hard-sphere model. In the case of perfectly elastic collisions, attracting particles would bounce permanently and no aggregation would be observed, no matter how attractive the interaction. By making the collisions partially elastic, attracting particles are able to dissipate their kinetic energy at each collision, which makes their relative velocities go to zero, until a point they aggregate, i.e. until they are found in a configuration of constant contact with one another, if not perturbed by appropriate external forces, as it will be illustrated next.

4.5.3 A dynamics example of electrostatic self-assembly

As has already been thoroughly exposed in the previous sections and chapters, an attractive electrostatic regime can exist between particles that are oppositely charged, also between neutral but polarisable particles and charged particles, and even between like-charged polarisable particles, given the right circumstances.

However, until the present section, calculations have been performed by considering a static scenario, whereby parameters of the system are required at every single calculation step. For example, in the determination of a force − separation curve, like the ones presented in Figures 4.2 to 4.5, dielectric constants, radii and charge of the interacting particles are given and calculations are performed for a number of predetermined inter-particle separation distances, rendering a "snapshot" of the electrostatic interaction at each particular sub-configuration. Dynamics simulations, on the other hand, offer the extra information of how the system evolves over time, so in addition to knowing the regions of stability of a particular system through determination of potential energy curves or surfaces, for instance, dynamics calculations can also picture possible paths of how the system could transit from a particular configuration to another.

As an illustration, consider a system whose boundaries are defined by a cubic box which is effectively just an elastic boundary with fixed internal volume equal to 1.726×10^{10} nm^3, and a number of particles inside it, as depicted in Figure 4.14. Fixed at the centre of the box is a 500 nm-radius non-polarisable particle, bearing 25 elementary charges on its surface, that will serve as a constant source of radially distributed and spherically symmetric electric field. Surrounding this central particle are eight 100 nm-radius free to move particles, placed initially at positions corresponding to the vertices and half-sides of a square of side equal to 1414.2 nm, situated on the $x - y$ plane, whose centre also coincides with the one of the box. Such smaller particles have dielectric constants equal to 4.5, being then representative of materials that are of made of silica (silicon dioxide). [131]

An extrapolation of the kinetic theory of gases has been made for the system, so that the eight small particles can be given an initial speed that correspond to the root-mean-square (RMS) speed that the same collection of particles would have at a temperature $T = 298.15$ K. Note that there is no consideration of temperature in the simulation, and that such variable is utilised only for the calculation of an initial speed of the smaller particles. Accordingly, the particles

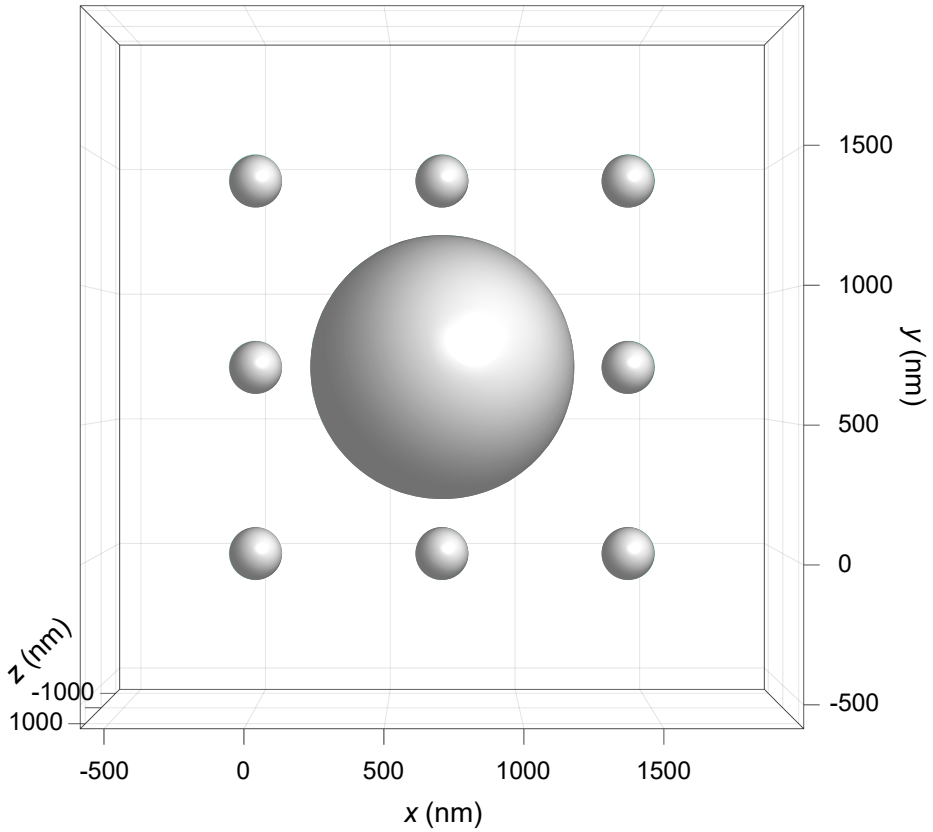


Fig. 4.14 Geometric representation of a system comprised of a 500 nm-radius particle fixed at the centre of a volume contained by a closed box, and eight surrounding 100 nm-radius free to move particles, placed initially at the vertices and half-sides of a virtual square situated on the $x-y$ plane and whose centre coincides with the one of the box.

are considered to be made of silica, having then a mass density of 2.21 g/cm^3, [132] which translates to a mass of 1.16×10^{-15} kg to the larger 500 nm-radius particle, and 9.26×10^{-18} kg to the smaller 100 nm-radius particles. As mentioned before, the former is fixed at the centre of the box but, in contrast, each of the latter have an initial velocity magnitude (speed) given by [120]

$$v_i=\sqrt{\frac{3RT}{\text{"molar mass"}}}, \tag{4.39}$$

where R is the universal gas constant, and the "molar mass" is determined as the product of the mass of the smaller particles with Avogadro's constant, relying then in the approximation of considering each particle as a spherical gas molecule. The directions of the particle's velocity are given by randomly

decomposed $(v_{i,x}, v_{i,y}, v_{i,z})$ components $(i = 1, 2, \ldots, 8)$, therefore inducing the small particles to permeate the whole box and not being restricted to the $x - y$ plane.

Note that such small system cannot be considered to be ergodic and it is not represented by an ensemble. The simulation simply constitutes an evolution of the system over time according to Newton's laws of motion, with the electrostatic force experienced by the particles acting as a modulator of their velocities through $\mathbf{F} = m\ \mathbf{a}$. The box merely acts as an elastic boundary that serves to contain the particles within the considered volume. The consideration of CR < 1 allows the kinetic energy to be partially lost with each particle−particle collision, as explained in Subsection 4.5.2, so if the electrostatic interactions are attractive, aggregation is expected to occur given sufficient time. For consistence, it could also be considered that the box is filled with an inert gas, that does not impose any mechanical resistance to the moving particles, and that can aid in the dissipation of the kinetic energy released during partially elastic collisions, through the mechanism mentioned in Subsection 4.5.2.

Figure 4.15 gives equally time-spaced snapshots of a 1000 μs simulation, calculated through 4000 steps of 0.25 μs, where each of the 100 nm-radius particles carry -1 e, which corresponds to the same absolute surface charge density of the larger 500 nm-radius particle. Any particle−particle collision has been treated as being partially elastic, with CR = 0.9, and collisions with the box wall has been treated as being perfectly elastic. As can be seen from this figure, the small particles progressively gather around the central particle as time evolves, until aggregation is virtually complete by the last frame. Note that the small particle tend to be displaced over the central one in a way that the system's energy is minimised, i.e. apart from being attracted to the central particle, the small particles generally assume positions that further minimise the repulsion that exists between one another. Additionally, Figure 4.15 also illustrates the path travelled by the particle that is initially placed at the origin, projected on

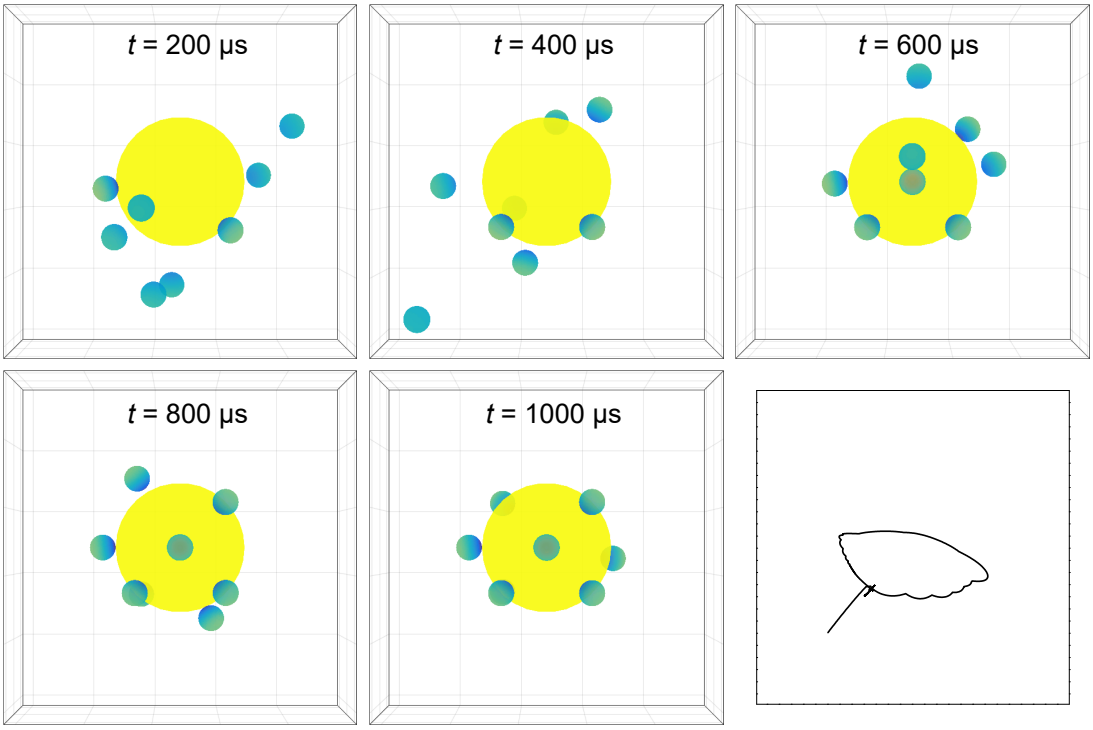


Fig. 4.15 Snapshots of a 1000 μs dynamics simulation involving a 500 nm-radius particle with 25 e of charge, and eight 100 nm-radius particles, each with -1 e of charge. Diagram in the bottom right corner shows the path traced by the particle that is initially placed at the origin. The spectrum of colours goes from deep blue to bright yellow, respectively representing the smallest and largest value of surface charge density in each frame.

the $x - y$ plane, showing that such particle is attracted by the oppositely charged central particle, bounces around it, as can be noted from some convolutions in the path trace, effectively loosing its kinetic energy and speed at each collision, until the point where aggregation occurs.

Such dynamics events are also reflected on Figure 4.16. Accordingly, Figure 4.16(a) shows that, as a consequence of the small particles progressively loosing speed and becoming, in average, closer to the central particle, the electrostatic interaction energy (U) decreases as the simulation evolves, due to the favourable attractive interaction that exists between the small particles and the oppositely charged central particle. Figure 4.16(b) shows that such events are naturally accompanied by a decrease in the RMS speed of the moving particles in the system, which assumes a value that approximates zero by the end of the simulation.

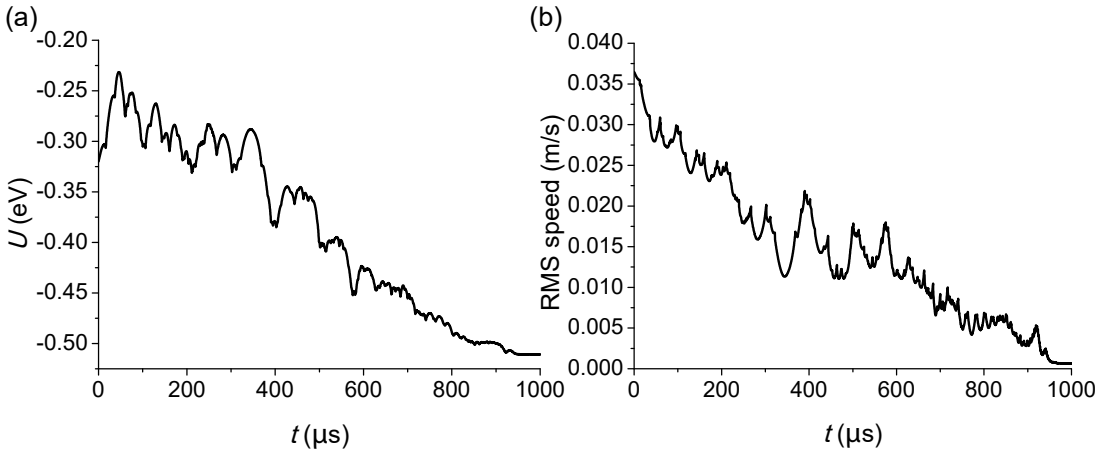


Fig. 4.16 Plots of the (a) electrostatic interaction energy U (eV), and (b) RMS speed (m/s), as function of time t (μs) for the simulation presented in Figure 4.15.

Aggregation is also possible if the 100 nm-radius particles are neutral, as illustrated in Figure 4.17. Even though such particles are not strongly polarisable, having a dielectric constant of just 4.5, the induced bound charges allied with a reduced coefficient of restitution of CR = 0.4 in this particular case, is sufficient to allow some aggregation to happen within the considered time frame. Differently from the previous case, attractive interactions rely entirely on the existence of polarisation of the small particles in the current example. However, since polarisation effects fade away quickly as the neutral particles get distanced from the central charged particle, the trajectories of each of the former become less influenced by the latter and shaped more like straight lines, as indicated by the traced path shown in Figure 4.17. Nevertheless, once any of the neutral particles collide with the central one, the low coefficient of restitution assures a considerable loss of kinetic energy, making the 100 nm-radius particles more susceptible to the attractive forces exerted by the central one, as evidenced by Figure 4.18, which shows an average decrease with a step-like pattern of both the electrostatic interaction energy and RMS speed, reflecting such more sharp losses of kinetic energy with the occurrence of a collision.

Interestingly, it can be noted that the distribution of the 100 nm-radius particles over the larger one in the current example does not result in the same

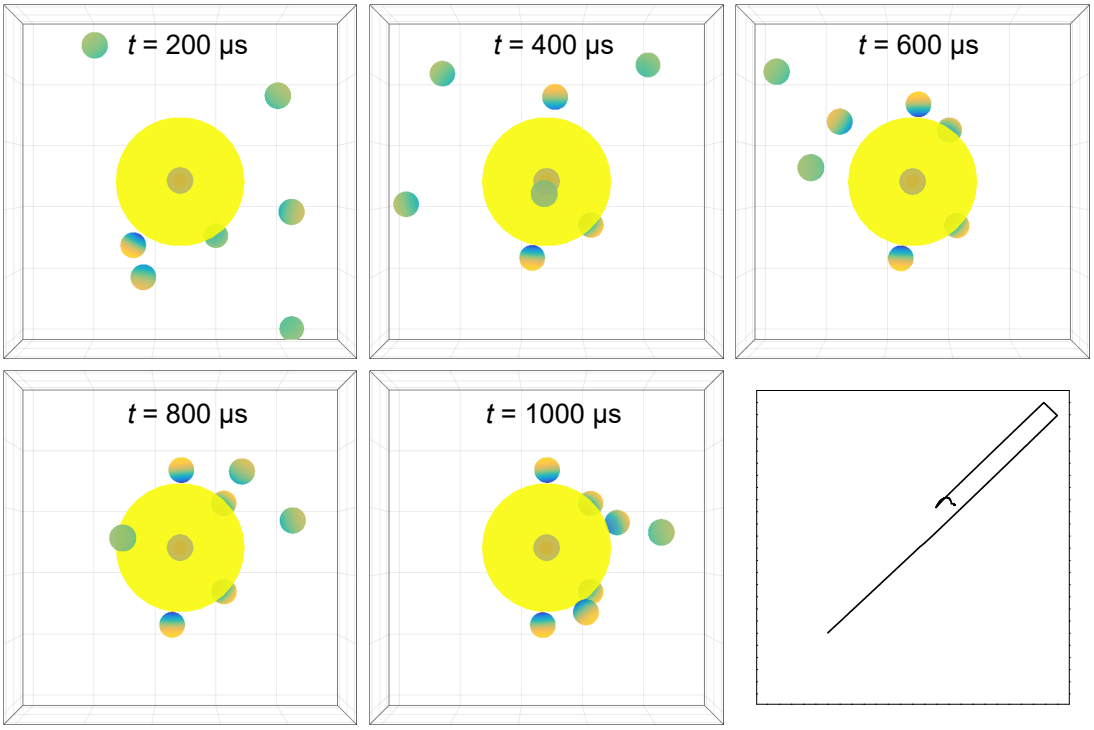


Fig. 4.17 Snapshots of a 1000 μs dynamics simulation involving a 500 nm-radius particle with 25 e of charge, and eight neutral 100 nm-radius particles. Diagram in the bottom right corner shows the path traced by the particle that is initially placed at the origin. The spectrum of colours goes from deep blue to bright yellow, respectively representing the lowest and highest value of surface charge density in each frame.

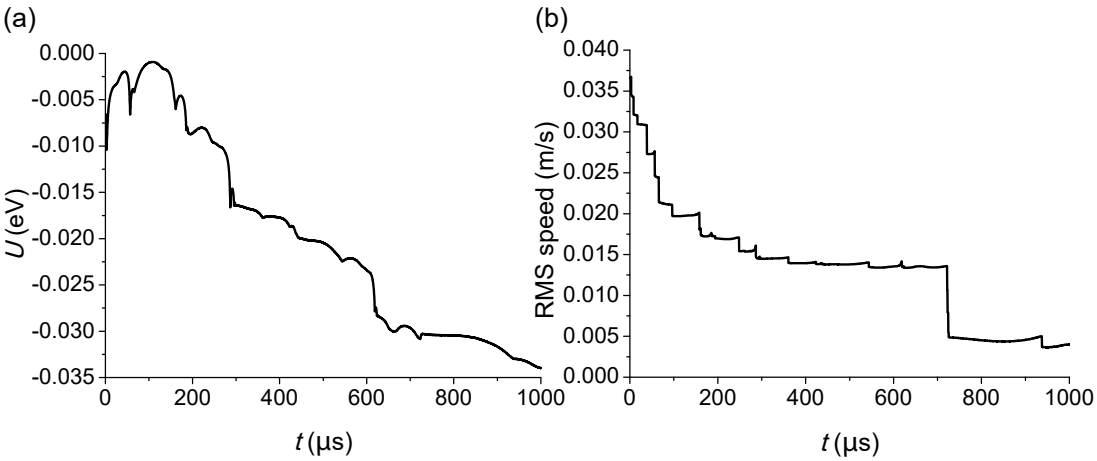


Fig. 4.18 Plots of the (a) electrostatic interaction energy U (eV), and (b) RMS speed (m/s), as function of time t (μs) for the simulation presented in Figure 4.17.

configuration that has been assumed by the equivalent particles in the previous case (see Figure 4.15). The difference here is that the repulsion between the bound charges induced in each of the neutral particles are virtually non-existent.

Effectively, the total charge on their surfaces is still zero, so it's only when they are at sufficiently close distances from each other that any interaction between them become significant.

Figure 4.19 reveals that no aggregation occurs when the 100 nm-radius particles have the same sign of charge in addition to the same absolute surface charge density as the 500 nm-radius central particle, i.e. when each carry 1 e. Clearly evidenced in this figure is the fact that through each frame the small particles are, in average, thoroughly dispersed within the box. In essence, such particles experience a constant cycle that consists of being accelerated when repealed by one another and especially by the central particle, and subsequently decelerated after colliding elastically with the wall and returning towards the latter, tracing generally curved trajectories, as depicted in the specific traced path also shown in Figure 4.19. As the coefficient of restitution in this case is equal to to 0.9, part

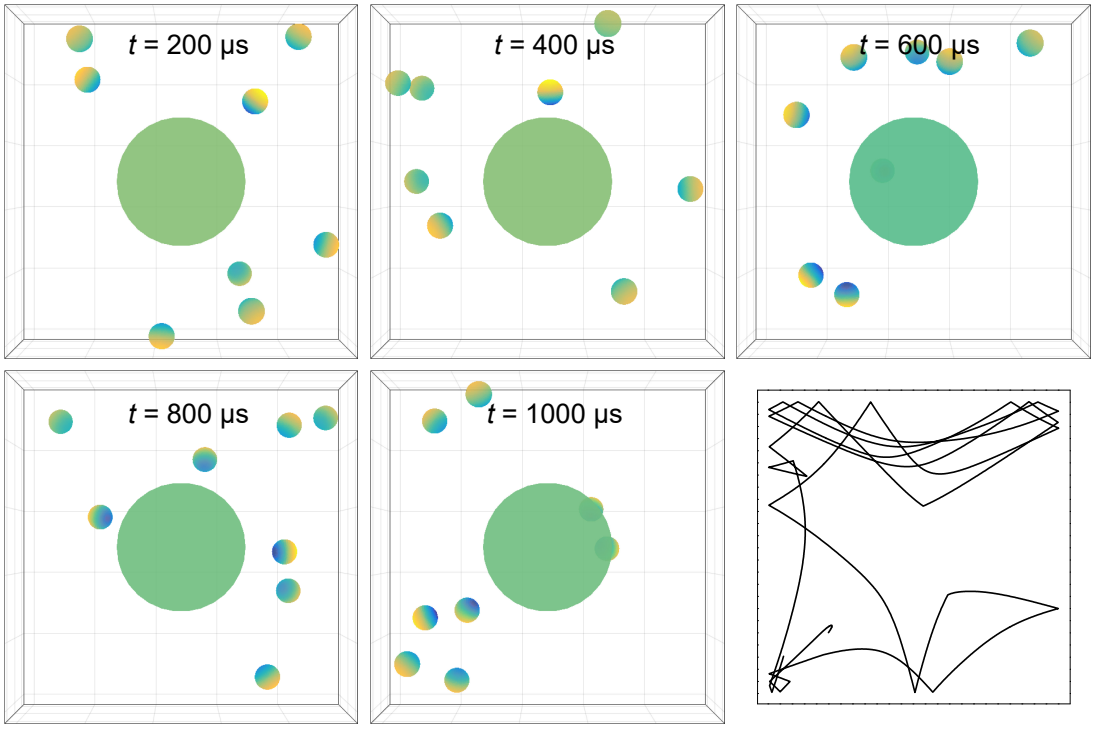


Fig. 4.19 Snapshots of a 1000 μs dynamics simulation involving a 500 nm-radius particle with 25 e of charge, and eight 100 nm-radius particles, each with 1 e of charge. Diagram in the bottom right corner shows the path traced by the particle that is initially placed at the origin. The spectrum of colours goes from deep blue to bright yellow, respectively representing the lowest and highest value of surface charge density in each frame.

of the kinetic energies is lost during each particle−particle collision, process that is reflected in Figure 4.20, which shows that, in average, both the interaction energy and the RMS speed decreases with time, but oscillates sharply along the way, reflecting the cycle of acceleration/deceleration experienced by the small particles.

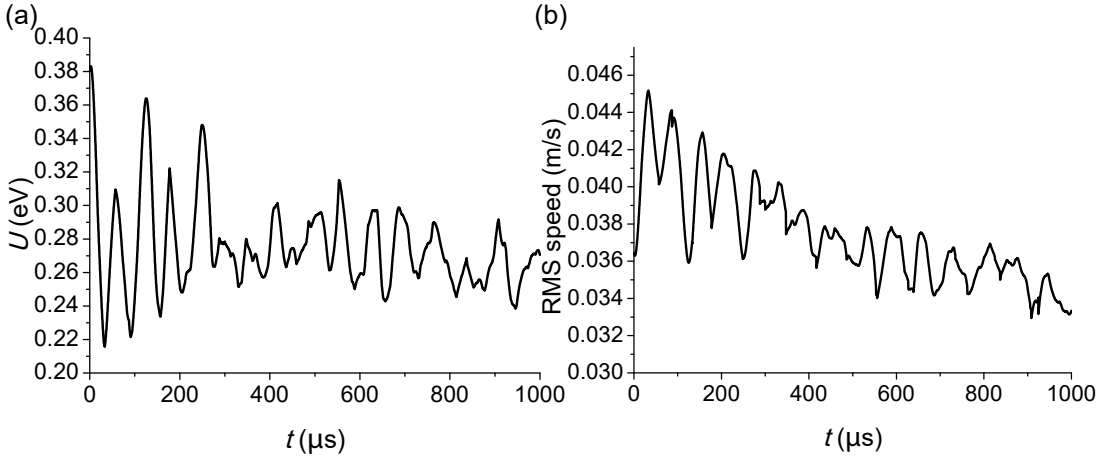


Fig. 4.20 Plots of the (a) electrostatic interaction energy U (eV), and (b) RMS speed (m/s), as function of time t (μs) for the simulation presented in Figure 4.19.

Aggregation when particles are like-charged is nevertheless possible to occur, given favourable circumstances. One of these circumstances is characterised by an inversion in the polarisation pattern, where it is the central 500 nm-radius particle that has a dielectric constant of 4.5 and gets polarised by the 100 nm-radius, turned non-polarisable particles. Figure 4.21 presents simulation snapshots for such case where, in addition, the central particle is singly charged and the surrounding particles are each charged with 4 e. Accordingly, as the particles are like-charged, it's only at sufficiently short separations distances that attraction can occur between each of the small particles and the central one. As the process evolves over time, each collision, where CR = 0.9, is followed by a loss of kinetic energy of the colliding particle. Consequently, in the event of any of the small particles having lost sufficient kinetic energy and also being situated at a distance where the interaction with the central particle is attractive, then aggregation is most likely to occur.

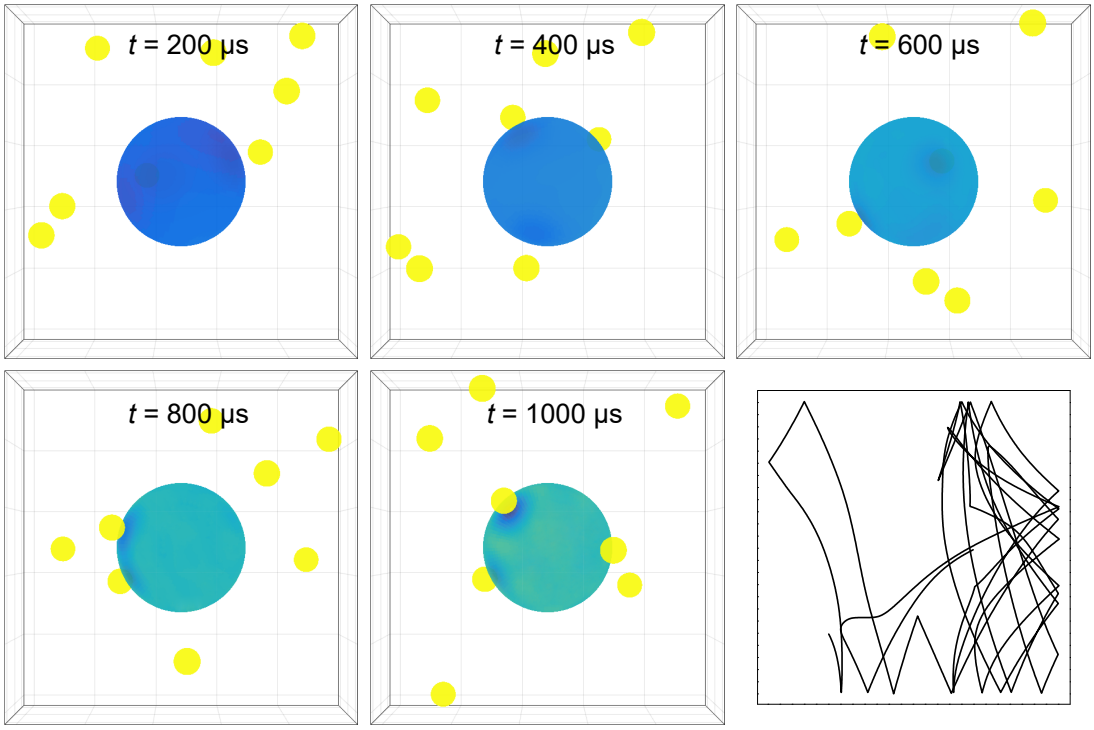


Fig. 4.21 Snapshots of a 1000 μs dynamics simulation involving a 500 nm-radius polarisable particle with 1 e of charge, and eight 100 nm-radius particles, each with 4 e of charge. Diagram in the bottom right corner shows the path traced by the particle that is initially placed at the origin. The spectrum of colours goes from deep blue to bright yellow, respectively representing the lowest and highest value of surface charge density in each frame.

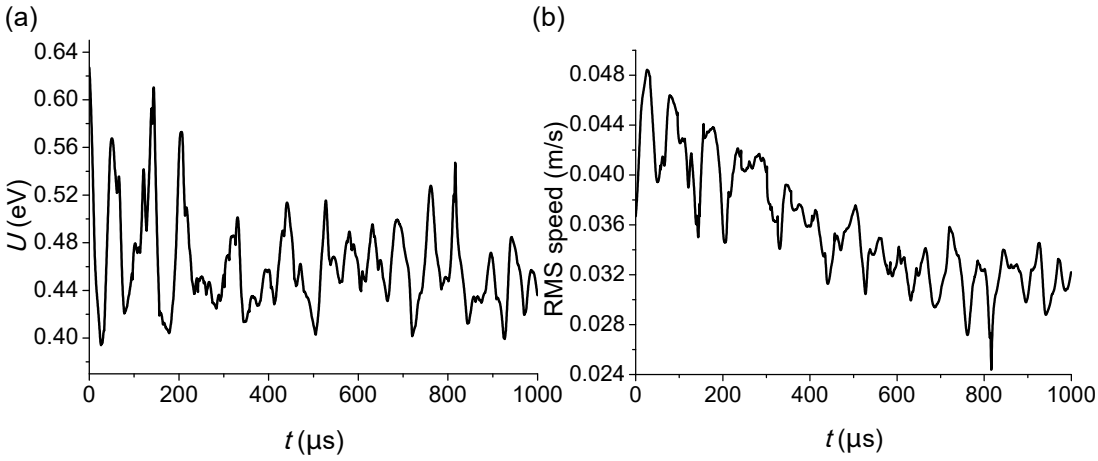


Fig. 4.22 Plots of the (a) electrostatic interaction energy U (eV), and (b) RMS speed (m/s), as function of time t (μs) for the simulation presented in Figure 4.21.

The trajectories traced by the smaller particles in this situation is in fact similar to the ones traced in the last example (see corresponding diagrams in Figure 4.19 and 4.21), as for most separation distances, the interaction is

repulsive. Figure 4.22 reveals that the interaction energy and RMS speed also evolves similarly to the previous example, decreasing in average but oscillating over time. Fundamentally, the systems addressed in the previous (Figures 4.19 and 4.20) and present (Figures 4.21 and 4.22) cases behave similarly in a great part of its corresponding possible configurations. It only when the small particles are at sufficiently close distances to the central particle in the present case that the possibility of aggregation exists, event that is impossible in the former.

4.5.4 Effusion through a charged array

In the next and final example, it is investigated whether same-sized but differently charged particles are able to effuse through a two-dimensional positively charged array. As depicted in Figure 4.23, the corresponding system for this case consists of a box with an opening in its far right side, that encloses an unmovable array of equally spaced 200 nm-radius non-polarisable particles, and four different 100 nm-radius particles. The array is positioned through the opening of the box, effectively constituting an interface across which the 100 nm-radius particles should pass in order to effuse to the outside. Similarly to the previous cases addressed in Subsection 4.5.3, the present system also can not be considered to be ergodic and it is not represented by an ensemble. In addition, the box merely acts as an elastic boundary and an inert air is considered to permeate the interior and exterior of the box, so that it can aid in the dissipation of the kinetic energy released during particle−particle collisions.

This case closely resembles the process of effusion of perfect gas molecules from a container, classically explained by the kinetic theory of gases. From such theory, it is known that lighter particles effuse more rapidly than heavier counterparts. [120] Therefore, in order to eliminate such variable, all four moving, 100 nm-radius particles have been assigned the same mass density of 2.21 g/cm^3 and a dielectric constant of 4.5, being then representative of silica made materials. Initial speeds were also assigned for each of them in a similar fashion to the

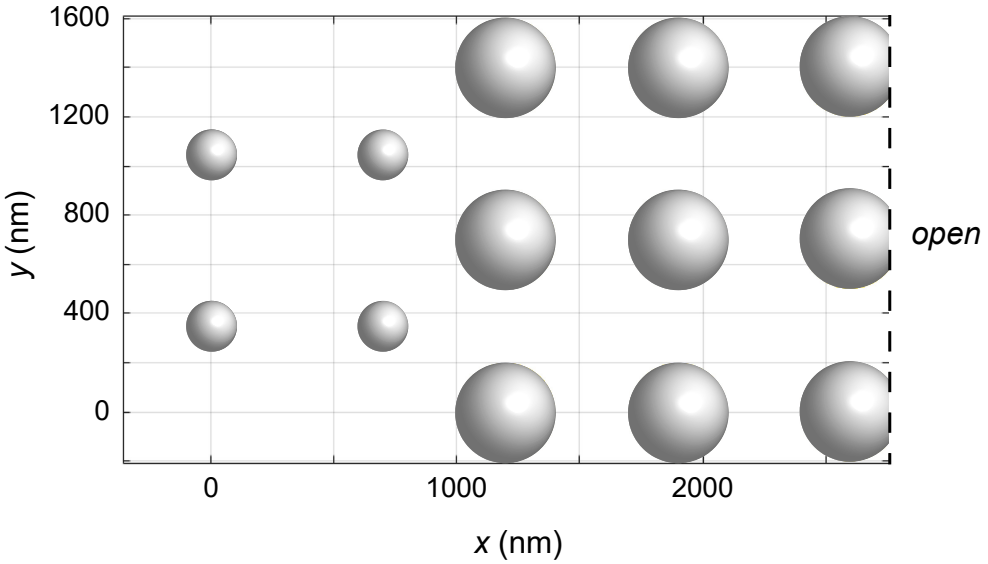


Fig. 4.23 Geometric representation of a system comprised of a box with an opening in its far right side, a two-dimensional fixed array consisted of nine 200 nm-radius particles, and 4 different, free to move 100 nm-radius particles, initially positioned at the innermost side of the box.

previous subsection, with directions that are randomly decomposed in $(v_{i,x}, v_{i,y}, 0)$ components $(i = 1, 2, 3, 4)$, therefore restricting their positions to the $x - y$ plane. In addition, such particles are also considered to be charged in different ways; a key difference that directly influences the way they interact with the unmovable array and the possibility they have to effuse.

Figure 4.24 shows selected snapshots of a 1000 μs simulation, where the particles in the array are each charged with 4 e, and the set of four moving particles are composed by a neutral particle, a negatively charged particle with -1 e, and two positively charged particles, one with 0.1 e and the other with 1 e. Appropriately, the walls are considered to be elastic, and each particle−particle collision has been treated as being partially elastic, with CR = 0.9. In the course of the simulation, it can be seen that the neutral and the slightly charged particle are able to effuse to the outside of the box, the negatively charged particle is sucked in and gets entrapped inside the attracting array, and the positively charged particle is unable to penetrate, let alone pass through the like-charged array. Further information is given in Figure 4.25, which shows corresponding plots of the electrostatic interaction energy and RMS speed of the moving particles

as function of time. Accordingly, it can be noted that until about 400 μs have passed, period of time in which two of the moving particles are able to effuse out of the box, both plotted quantities decrease in average, reflecting some losses of kinetic energy due to the occurrence of collisions, and the energetically favourable entrapment of the negatively charged particle. By the end of the simulation, as the latter assumes a stable position inside the array, the plots become dominated by the movement of the positively charged particle that remains trapped inside

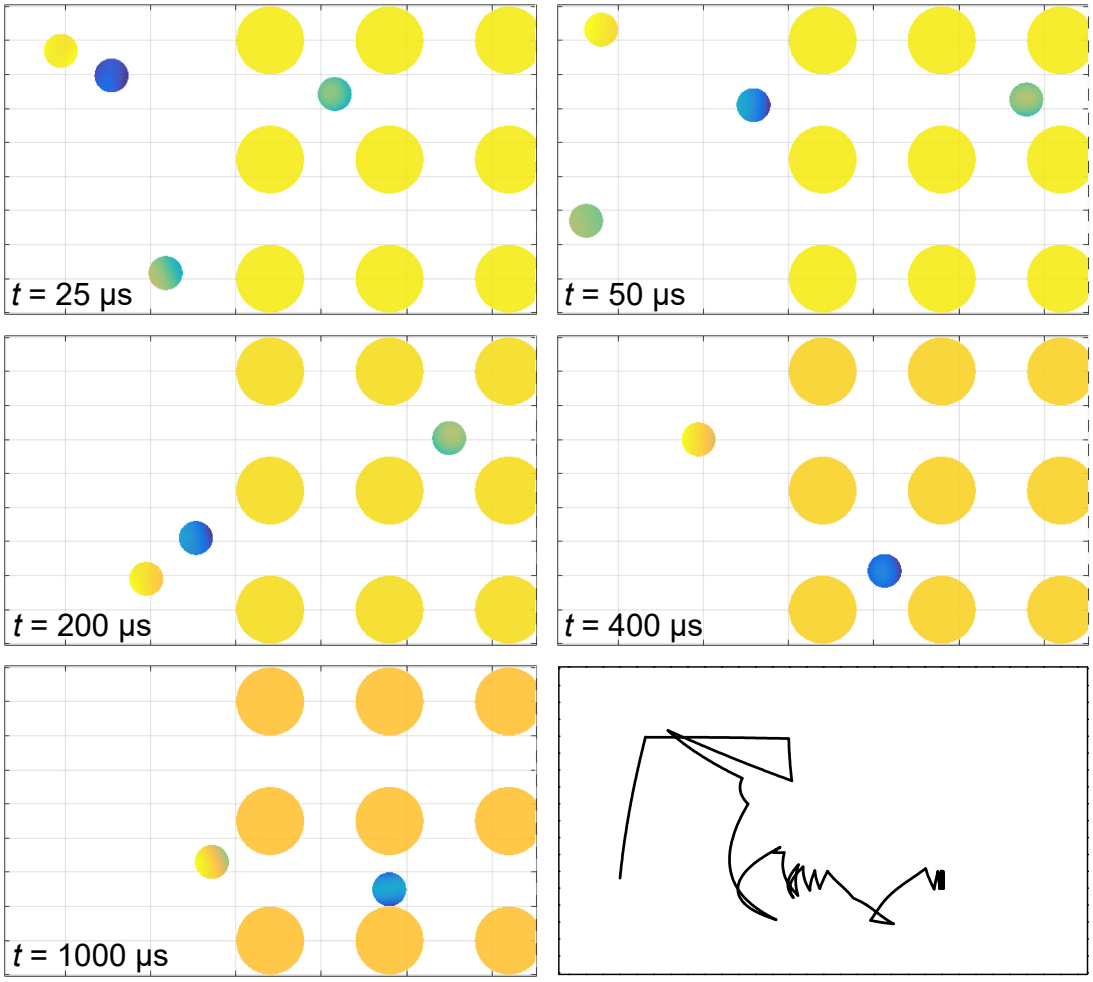


Fig. 4.24 Selected snapshots of a 1000 μs dynamics simulation involving an unmovable array of equally spaced 200 nm-radius non-polarisable particles, each carrying 4 e of charge, and a set of four different 100 nm-radius polarisable particles, with constituents carrying -1, 0, 0.1, and 1 e of charge, all placed in a box with an opening in its far right side. Diagram in the bottom right corner shows the path traced by the particle that is initially placed at a position that is closest to the origin. The spectrum of colours goes from deep blue to bright yellow, respectively representing the lowest and highest value of surface charge density in each frame.

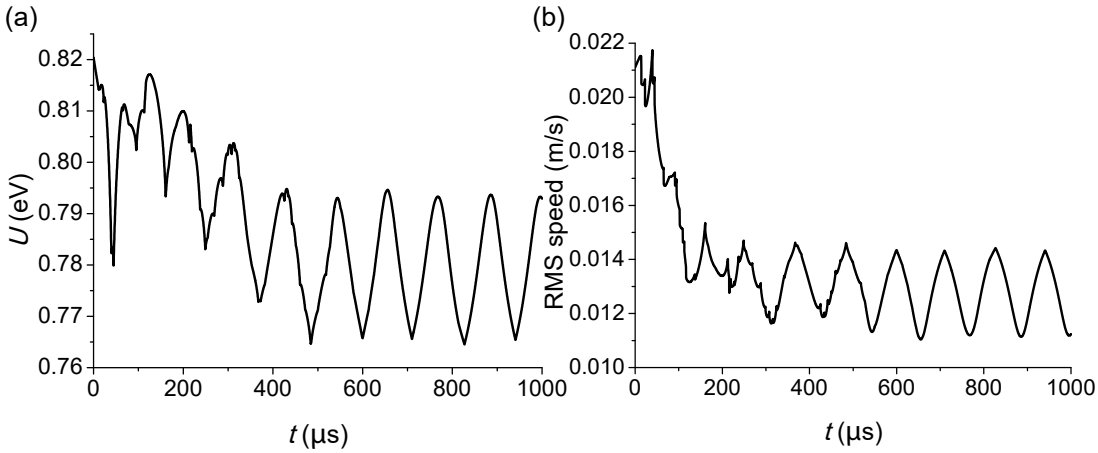


Fig. 4.25 Plots of the (a) electrostatic interaction energy U (eV), and (b) RMS speed (m/s), as function of time t (μs) for the simulation presented in Figure 4.24.

the box, being constantly repelled by the charged array, in a vicious cycle of alternating acceleration and deceleration in-between elastic collisions with the left side wall. In this example, the charged array acts effectively like a particle "sieve", favouring or disfavouring the transit of distinct types of particles, in this case by promoting appropriate electrostatic interactions, but also with potential to be size-selective through the adjustment of the spacing between its constituent particles.

Chapter 5

Outlook

Theoretical models for calculating electrostatic interactions between charged particles, henceforth named M1 and M2, have been presented. The first model (M1), based on a multipole expansion of the electric potential due to a pair of charged particles and originally introduced by Bichoutskaia et al. [37], has been extensively scrutinised, mathematically and computationally optimised, and later adapted to take into account the presence of a dielectric medium. In the context of M1, it has been described how dielectric particles are polarised when under influence of an external electric field, phenomenon that can be quantitatively accounted for by the dielectric constant of the material that the particles are made of. Accordingly, it has been shown that polarisation leads to creation of bound charges, that are in fact real charges originated from the displacement of nuclei and electron clouds of the atoms that constitute the material being polarised. Such charges are dynamically dependant on the configuration of the system and, when summed to the free charges that might be present on each particle, accounts for the total charge of each respective particle. Since it's a dynamic quantity, it can modulate the nature of an electrostatic interaction that would be otherwise slightly different or, in some cases, completely different if the particles were not able to be polarised. Correspondingly, the occurrence of rather counterintuitive phenomena have been theoretically shown to be possible, namely the so-called

like-charge attraction, that happens between particles bearing the same sign of charge, and opposite-charge repulsion, that occurs between particles with opposite signs of charge in the presence of a medium. The circumstances under which the former happens generally involves some sort of asymmetry between interacting particles, while the latter requires the presence of a sufficiently polarisable medium and magnitudes of charge that are below some critical limit.

It has been shown, through introduction of a general geometric parameter based on the bispherical coordinate system, that the initially assumed geometry of two interacting spherical particles can be actually extended to combinations of spheres, point particles and surface planes, by considering appropriate values of the objects's radii and surface-to-surface separation distance, according to what is determined by the parameter. The assessment of convergence has also been performed in terms of M1, where it has been determined how the various parameters of the system influence the number of terms that are needed to be employed in the perturbative solution in order to achieve a converged result that is in accordance with a chosen criterion. Accordingly, it has been illustrated that critical to some cases is the use of a sufficiently large number of terms that goes beyond the usual low order multipoles, such as the corresponding monopole, dipole and quadrupoles, commonly considered in some alternative approaches.

Calculations for experimental cases have also been performed by employing M1, with the respective results revealing significant information and new insights about the peculiarities of each problem. In the calculations for the process of aerosol formation in the atmosphere of Saturn's moon Titan, it has been suggested that aggregates can grow by a process of charge scavenging, whereby a large particle grows by assimilating smaller ones, even if they are like charged. In the calculations for electrostatic self-assembly processes, explanation for experimental findings have been given, where it has been show that by choosing a particular characteristic of the solvent (medium) in which the self-assembling particles are

dispersed, namely its dielectric constant, and the magnitude of charge on the interacting particles, the process might be suppressed or allowed to happen.

Introduction to a new model (M2) for calculating electrostatic interactions in many-body systems, developed by means of an integral equation approach, has been presented in Chapter 4. In practice, M1 and M2 can be used interchangeably in cases that involve two interacting dielectric particles as their numerics agree perfectly with each other. However, it is for scenarios where three or more particles interact that M2 is differentiated. Accordingly, it has been shown that the addition of a third body in an originally two-body system has the potential of significantly altering the pairwise interaction between the two original particles, and it is in situations of this nature that a model like M2 appears necessary. The conclusions drawn from the extensive analysis of M1 can be, in general, extrapolated in the context M2, as the physics of the problem remains unchanged. Particularly, the guidelines that were underlined in the convergence studies of M1 are also useful in the application of M2.

A simple physics engine has been developed for dynamics simulations of many particles, where M2 has been implemented as the force field, that is accompanied by a collision handler and a numerical integrator of classical equations of motion. It has been shown that dynamics calculations, in contrast to determination of static configurations, can provide the extra information of how a system evolves over time and, particularly, can also show paths a system can take to go from a particular configuration to another. Such calculations have in fact a far-reaching applicability potential, as it can be used as a powerful tool in the study of many processes that involve charged particles of size magnitudes that are too large to be considered by usual classical and quantum chemistry based molecular methods.

Future work

As presented, both M1 and M2 are very robust and well-behaved models, capable of accurately determining electrostatic interactions in a range of different

systems, that involve dielectric particles with relevant adjustable characteristics and the optional presence of a dielectric medium. Notwithstanding, the addition of other features, that would make their applicability more universal, would be greatly advantageous. Examples of desirable features are: the consideration of magnetic forces, so that systems involving high-speed charged particles can be also addressed; the addition of components that accounts for non-fundamental forces, such as van der Waals dispersion forces, [23] extremely relevant for a number of problems in physics and chemistry; the ability to treat particles of a variety of other shapes, like ellipsoids and cylinders, making the solutions more appropriate for systems that can be better approximated by considering other types of geometry, as for instance the asymmetric breaking of magnetically levitated ethanol droplets with different degrees of charge [Dr Richard J. A. Hill, personal communication, 2015-2016], that assume shapes ranging from spheres to prolate spheroids during the process; the consideration of charge exchange between any combination of particles and the medium, especially relevant in the treatment of the limiting case involving particles of conducting character; incorporation of a method capable of considering the presence of electrolytes in the medium, such as the proposed by Derbenev et al. [133], particularly in the presented many-body formalism.

Likewise, the introduced physics engine for dynamics simulations would benefit from a number of upgrades, such as: the consideration of ergodic systems and appropriate statistical ensembles so that relevant thermodynamic properties of such systems can be extracted; the consideration of the angular momentum of particles, an important component for a more realistic modelling of collisions and very concentrated systems, as it would allow, for instance, the rolling of particles over one another; a certain degree of allowed particle deformation, which, coupled with the electrostatic treatment of other shapes of particles, would further approximate the solution to real soft-matter systems; the consideration of the possibility of coalescence between particles, particularly relevant to some

aggregation processes; the consideration of drag forces and other fluid-related properties, for a better description of dynamics involving the presence of a medium; the implementation of more general collision solvers and more accurate algorithms for the equations of motion, such as the Runge-Kutta method.

References

[1] Feynman, R. P, Leighton, R. B, & Sands, M. L. (1964) *The Feynman lectures on physics: Mainly electromagnetism and matter.* (Addison-Wesley, Reading, MA) Vol. 2, 1st edition.

[2] Lilley, J. (2001) *Nuclear physics: Principles and applications.* (Wiley, Chichester), 1st edition.

[3] Griffiths, D. J. (2013) *Introduction to electrodynamics.* (Pearson, New York, NY), 4th edition.

[4] B. R. Martin, G. S. (2013) *Particle physics.* (Wiley, Chichester), 3rd edition.

[5] Maxwell, J. C. On physical lines of force; part I: The theory of molecular vortices applied to magnetic phenomena. *Philosophical Magazine* **21**, 161–175 (1961).

[6] Maxwell, J. C. On physical lines of force; part II: The theory of molecular vortices applied to electric currents. *Philosophical Magazine* **21**, 281–348 (1961).

[7] Maxwell, J. C. On physical lines of force; part III: The theory of molecular vortices applied to statical electricity. *Philosophical Magazine* **23**, 12–24 (1962).

[8] Maxwell, J. C. On physical lines of force; part IV: The theory of molecular vortices applied to the action of magnetism on polarized light. *Philosophical Magazine* **23**, 85–95 (1962).

[9] Fleisch, D. (2008) *A student's guide to Maxwell's equations.* (Cambridge University Press, Cambridge), 1st edition.

[10] Tinsley, B, Rohrbaugh, R, Hei, M, & Beard, K. Effects of image charges on the scavenging of aerosol particles by cloud droplets and on droplet charging and possible ice nucleation processes. *Journal of the Atmospheric Sciences* **57**, 2118–2134 (2000). DOI: 10.1175/1520-0469(2000)057<2118:EOICOT>2.0.CO;2.

[11] Tinsley, B. The global atmospheric electric circuit and its effects on cloud microphysics. *Reports on Progress in Physics* **71**, 066801 (2008). DOI: 10.1088/0034-4885/71/6/066801.

[12] Mather, T & Harrison, R. Electrification of volcanic plumes. *Surveys in Geophysics* **27**, 387–432 (2006). DOI: 10.1007/s10712-006-9007-2.

[13] Harrison, R. G, Nicoll, K, Ulanowski, Z, & Mather, T. Self-charging of the Eyjafjallajökull volcanic ash plume. *Environmental Research Letters* **5**, 024004 (2010). DOI: 10.1088/1748-9326/5/2/024004.

[14] Horányi, M. Charged dust dynamics in the solar system. *Annual Review of Astronomy and Astrophysics* **34**, 383–418 (1996). DOI: 10.1146/annurev.astro.34.1.383.

[15] Poppe, T & Schräpler, R. Further experiments on collisional tribocharging of cosmic grains. *Astronomy & Astrophysics* **438**, 1–9 (2005). DOI: 10.1051/0004-6361:20042327.

[16] Tuinier, R & De Kruif, C. Stability of casein micelles in milk. *Journal of Chemical Physics* **117**, 1290–1295 (2002). DOI: 10.1063/1.1484379.

[17] Jaworek, A, Krupa, A, & Czech, T. Modern electrostatic devices and methods for exhaust gas cleaning: A brief review. *Journal of Electrostatics* **65**, 133–155 (2007). DOI: 10.1016/j.elstat.2006.07.012.

[18] Khan, M. K. I, Schutyser, M. A, Schroën, K, & Boom, R. M. Electrostatic powder coating of foods–state of the art and opportunities. *Journal of Food Engineering* **111**, 1–5 (2012). DOI: 10.1016/j.jfoodeng.2012.02.002.

[19] Meng, X, Zhu, J. J, & Zhang, H. The characteristics of particle charging and deposition during powder coating processes with ultrafine powder. *Journal of Physics D: Applied Physics* **42**, 065201 (2009). DOI: 10.1088/0022-3727/41/19/195207.

[20] Jiang, H & Lu, L. Measurement of the surface charge of ultrafine particles from laser printers and analysis of their electrostatic force. *Atmospheric Environment* **44**, 3347–3351 (2010). DOI: 10.1016/j.atmosenv.2010.06.025.

[21] Comiskey, B, Albert, J, Yoshizawa, H, & Jacobson, J. An electrophoretic ink for all-printed reflective electronic displays. *Nature* **394**, 253–255 (1998). DOI: 10.1038/28349.

[22] Mazumder, M, Sims, R, Biris, A, Srirama, P, Saini, D, Yurteri, C, Trigwell, S, De, S, & Sharma, R. Twenty-first century research needs in electrostatic processes applied to industry and medicine. *Chemical Engineering Science* **61**, 2192–2211 (2006). DOI: 10.1016/j.ces.2005.05.002.

[23] Israelachvili, J. N. (2011) *Intermolecular and surface forces.* (Academic press, Burlington, MA).

[24] Miller, T. M. Atomic and molecular polarizabilities (2016) in *CRC Handbook of Chemistry and Physics*, ed. Haynes, W. M. (CRC Press/Taylor & Francis, Boca Raton, FL), 97th edition, pp. 188–203.

[25] Thomson, W. Extrait d'une lettre de M. William Thomson à M. Liouville. *Journal de Mathématiques Pures et Appliquées* pp. 364–367 (1845).

[26] Thomson, W. Extraits de deux lettres adressées à M. Liouville. *Journal de Mathématiques Pures et Appliquées* pp. 256–264 (1847).

[27] Davis, M. H. Two charged spherical conductors in a uniform electric field: Forces and field strength. *The Quarterly Journal of Mechanics and Applied Mathematics* **17**, 499–511 (1964). DOI: 10.1093/qjmam/17.4.499.

[28] Liang, Y, Hilal, N, Langston, P, & Starov, V. Interaction forces between colloidal particles in liquid: Theory and experiment. *Advances in Colloid and Interface Science* **134**, 151–166 (2007). DOI: 10.1016/j.cis.2007.04.003.

[29] Czarnecki, W. S & Schein, L. The contribution of the electrostatic proximity force to atomic force microscopy with insulators. *Physics Letters A* **339**, 145–151 (2005). DOI: 10.1016/j.physleta.2005.03.021.

[30] Zettergren, H, Forsberg, B. O, & Cederquist, H. Are single C_{60} fullerenes dielectric or metallic? *Physical Chemistry Chemical Physics* **14**, 16360–16364 (2012). DOI: 10.1039/c2cp42884a.

[31] Ohshima, H. Electrostatic interaction between a sphere and a planar surface: Generalization of point-charge/surface image interaction to particle/surface image interaction. *Journal of Colloid and Interface Science* **198**, 42–52 (1998). DOI: 10.1006/jcis.1997.5240.

[32] Messina, R. Image charges in spherical geometry: Application to colloidal systems. *Journal of Chemical Physics* **117**, 11062–11074 (2002). DOI: 10.1063/1.1521935.

[33] Feng, J. Q & Hays, D. A. Relative importance of electrostatic forces on powder particles. *Powder Technology* **135**, 65–75 (2003). DOI: 10.1016/j.powtec.2003.08.005.

[34] Kolikov, K, Ivanov, D, Krastev, G, Epitropov, Y, & Bozhkov, S. Electrostatic interaction between two conducting spheres. *Journal of Electrostatics* **70**, 91–96 (2012). DOI: 10.1016/j.elstat.2011.10.008.

[35] Xu, Z. Electrostatic interaction in the presence of dielectric interfaces and polarization-induced like-charge attraction. *Physical Review E* **87**, 013307 (2013). DOI: 10.1103/PhysRevE.87.013307.

[36] Washizu, M & Techaumnat, B. Analysis of general multipolar images on dielectric layers for the calculation of DEP force. *Journal of Electrostatics* **71**, 854–861 (2013). DOI: 10.1016/j.elstat.2013.06.010.

[37] Bichoutskaia, E, Boatwright, A. L, Khachatourian, A, & Stace, A. J. Electrostatic analysis of the interactions between charged particles of dielectric materials. *Journal of Chemical Physics* **133**, 024105 (2010). DOI: 10.1063/1.3457157.

[38] Khachatourian, A, Chan, H.-K, Stace, A. J, & Bichoutskaia, E. Electrostatic force between a charged sphere and a planar surface: A general solution for dielectric materials. *Journal of Chemical Physics* **140**, 074107 (2014). DOI: 10.1063/1.4862897.

[39] Raggi, G, Stace, A. J, & Bichoutskaia, E. Surface-charge distribution on a dielectric sphere due to an external point charge: Examples of C_{60} and C_{240} fullerenes. *Physical Chemistry Chemical Physics* **15**, 20115–20119 (2013). DOI: 10.1039/c3cp53522c.

[40] Linse, P. Electrostatics in the presence of spherical dielectric discontinuities. *Journal of Chemical Physics* **128**, 214505 (2008). DOI: 10.1063/1.2908077.

[41] Jackson, J. D. (1999) *Classical electrodynamics.* (Wiley, New York, NY), 3rd edition.

[42] Smythe, W. R. (1950) *Static and dynamic electricity.* (McGraw-Hill, New York), 2nd edition.

[43] Franklin, J. (2005) *Classical electromagnetism.* (Pearson, New York, NY), 1st edition.

[44] Lekner, J. Electrostatics of two charged conducting spheres. *Proceedings of the Royal Society A* **468**, 2829–2848 (2012). DOI: 10.1098/rspa.2012.0133.

[45] Wohlfarth, C. Permittivity (dielectric constant) of liquids (2016) in *CRC Handbook of Chemistry and Physics*, ed. Haynes, W. M. (CRC Press/Taylor & Francis, Boca Raton, FL), 97th edition, pp. 187–208.

[46] Tripathi, S. N & Harrison, R. G. Enhancement of contact nucleation by scavenging of charged aerosol particles. *Atmospheric Research* **62**, 57–70 (2002). DOI: 10.1016/S0169-8095(02)00020-0.

[47] Benz, W. Sphere geometries of Möbius and Lie (2012) in *Classical Geometries in Modern Contexts.* (Springer, Basel), 3rd edition, pp. 93 – 174.

[48] Jeffery, G. On a form of the solution of Laplace's equation suitable for problems relating to two spheres. *Proceedings of the Royal Society of London. Series A, Containing Papers of a Mathematical and Physical Character* **87**, 109–120 (1912). DOI: 10.1098/rspa.1912.0063.

[49] Morse, P. M & Feshbach, H. (1953) *Methods of theoretical physics.* (McGrawHill, New York) Vol. 2, 1sd edition.

[50] Flasar, F. M, Achterberg, R. K, Conrath, B. J, Gierasch, P. J, Kunde, V. G, Nixon, C. A, Bjoraker, G. L, Jennings, D. E, Romani, P. N, Simon-Miller, A. A, Bézard, B, Coustenis, A, Irwin, P. G. J, Teanby, N. A, Brasunas, J, Pearl, J. C, Segura, M. E, Carlson, R. C, Mamoutkine, A, Schinder, P. J, Barucci, A, Courtin, R, Fouchet, T, Gautier, D, Lellouch, E, Marten, A, Prangé, R, Vinatier, S, Strobel, D. F, Calcutt, S. B, Read, P. L, Taylor, F. W, Bowles, N, Samuelson, R. E, Orton, G. S, Spilker, L. J, Owen, T. C, Spencer, J. R, Showalter, M. R, Ferrari, C, Abbas, M. M, Raulin, F, Edgington, S, Ade, P, & Wishnow, E. H. Titan's atmospheric temperatures, winds, and composition. *Science* **308**, 975–978 (2005). DOI: 10.1126/science.1111150.

[51] Benner, S. A, Ricardo, A, & Carrigan, M. A. Is there a common chemical model for life in the universe? *Current Opinion in Chemical Biology* **8**, 672–689 (2004). DOI: 10.1016/j.cbpa.2004.10.003.

[52] McKay, C & Smith, H. Possibilities for methanogenic life in liquid methane on the surface of Titan. *Icarus* **178**, 274–276 (2005). DOI: 10.1016/j.icarus.2005.05.018.

[53] Raulin, F, Brasse, C, Poch, O, & Coll, P. Prebiotic-like chemistry on Titan. *Chemical Society Reviews* **41**, 5380–5393 (2012). DOI: 10.1039/C2CS35014A.

[54] Stevenson, J, Lunine, J, & Clancy, P. Membrane alternatives in worlds without oxygen: Creation of an azotosome. *Science Advances* **1**, e1400067 (2015). DOI: 10.1126/sciadv.1400067.

[55] Coates, A, Crary, F, Lewis, G, Young, D, Waite, J, & Sittler, E. Discovery of heavy negative ions in Titan's ionosphere. *Geophysical Research Letters* **34** (2007). DOI: 10.1029/2007GL030978.

[56] Cable, M. L, Hörst, S. M, Hodyss, R, Beauchamp, P. M, Smith, M. A, & Willis, P. A. Titan tholins: Simulating Titan organic chemistry in the Cassini-Huygens era. *Chemical Reviews* **112**, 1882–1909 (2011). DOI: 10.1021/cr200221x.

[57] Lavvas, P, Yelle, R. V, Koskinen, T, Bazin, A, Vuitton, V, Vigren, E, Galand, M, Wellbrock, A, Coates, A. J, Wahlund, J.-E, et al. Aerosol growth in Titan's ionosphere. *Proceedings of the National Academy of Sciences* **110**, 2729–2734 (2013). DOI: 10.1073/pnas.1217059110.

[58] Waite, J, Young, D, Cravens, T, Coates, A, Crary, F, Magee, B, & Westlake, J. The process of tholin formation in Titan's upper atmosphere. *Science* **316**, 870–875 (2007). DOI: 10.1126/science.1139727.

[59] Wahlund, J.-E, Galand, M, Müller-Wodarg, I, Cui, J, Yelle, R. V, Crary, F. J, Mandt, K, Magee, B, Waite Jr., J. H, Young, D. T, Coates, A. J, Garnier, P, Ågren, K, André, M, Eriksson, A. I, Cravens, T. E, Vuitton, V, Gurnett, D. A, & Kurth, W. S. On the amount of heavy molecular ions in Titan's ionosphere. *Planetary and Space Science* **57**, 1857–1865 (2009). DOI: 10.1016/j.pss.2009.07.014.

[60] Ågren, K, Edberg, N, & Wahlund, J.-E. Detection of negative ions in the deep ionosphere of Titan during the Cassini T70 flyby. *Geophysical Research Letters* **39**, L10201 (2012). DOI: 10.1029/2012GL051714.

[61] Lavvas, P, Yelle, R. V, & Vuitton, V. The detached haze layer in Titan's mesosphere. *Icarus* **201**, 626–633 (2009). DOI: 10.1016/j.icarus.2009.01.004.

[62] Lavvas, P, Yelle, R, & Griffith, C. Titan's vertical aerosol structure at the Huygens landing site: Constraints on particle size, density, charge, and refractive index. *Icarus* **210**, 832–842 (2010). DOI: 10.1016/j.icarus.2010.07.025.

[63] Lavvas, P, Sander, M, Kraft, M, & Imanaka, H. Surface chemistry and particle shape: Processes for the evolution of aerosols in Titan's atmosphere. *The Astrophysical Journal* **728**, 80 (2011). DOI: 10.1088/0004-637X/728/2/80.

[64] Vuitton, V, Yelle, R, & McEwan, M. Ion chemistry and N-containing molecules in Titan's upper atmosphere. *Icarus* **191**, 722–742 (2007). DOI: 10.1016/j.icarus.2007.06.023.

[65] Skorov, Y. V, Keller, H, & Rodin, A. Optical properties of aerosols in Titan's atmosphere. *Planetary and Space Science* **56**, 660–668 (2008). DOI: 10.1016/j.pss.2007.11.013.

[66] Coates, A. J, Wellbrock, A, Lewis, G. R, Jones, G. H, Young, D, Crary, F, & Waite, J. Heavy negative ions in Titan's ionosphere: Altitude and latitude dependence. *Planetary and Space Science* **57**, 1866–1871 (2009). DOI: 10.1016/j.pss.2009.05.009.

[67] Vuitton, V, Lavvas, P, Yelle, R, Galand, M, Wellbrock, A, Lewis, G, Coates, A, & Wahlund, J.-E. Negative ion chemistry in Titan's upper atmosphere. *Planetary and Space Science* **57**, 1558–1572 (2009). DOI: 10.1016/j.pss.2009.04.004.

[68] Imanaka, H & Smith, M. A. Formation of nitrogenated organic aerosols in the Titan upper atmosphere. *Proceedings of the National Academy of Sciences* **107**, 12423–12428 (2010). DOI: 10.1073/pnas.0913353107.

[69] Skorov, Y. V, Keller, H, & Rodin, A. Optical properties of aerosols in Titan's atmosphere: Large fluffy aggregates. *Planetary and Space Science* **58**, 1802–1810 (2010). DOI: 10.1016/j.pss.2010.08.002.

[70] Sittler, E, Ali, A, Cooper, J, Hartle, R, Johnson, R, Coates, A, & Young, D. Heavy ion formation in Titan's ionosphere: Magnetospheric introduction of free oxygen and a source of Titan's aerosols? *Planetary and Space Science* **57**, 1547–1557 (2009). DOI: 10.1016/j.pss.2009.07.017.

[71] Tomasko, M & West, R. Aerosols in Titan's atmosphere (2010) in *Titan from Cassini-Huygens*, eds. Brown, R. H, Lebreton, J.-P, & Waite, J. H. (Springer, Dordrecht), 1st edition, pp. 297–321.

[72] Michael, M, Tripathi, S. N, Arya, P, Coates, A, Wellbrock, A, & Young, D. T. High-altitude charged aerosols in the atmosphere of Titan. *Planetary and Space Science* **59**, 880–885 (2011). DOI: 10.1016/j.pss.2011.03.010.

[73] Tomasko, M, Doose, L, Engel, S, Dafoe, L, West, R, Lemmon, M, Karkoschka, E, & See, C. A model of Titan's aerosols based on measurements made inside the atmosphere. *Planetary and Space Science* **56**, 669–707 (2008). DOI: 10.1016/j.pss.2007.11.019.

[74] Tomasko, M, Doose, L, Dafoe, L, & See, C. Limits on the size of aerosols from measurements of linear polarization in Titan's atmosphere. *Icarus* **204**, 271–283 (2009). DOI: 10.1016/j.icarus.2009.05.034.

[75] Snowden, D, Yelle, R, Cui, J, Wahlund, J.-E, Edberg, N, & Ågren, K. The thermal structure of Titan's upper atmosphere, I: Temperature profiles from Cassini INMS observations. *Icarus* **226**, 552–582 (2013). DOI: 10.1016/j.icarus.2013.06.006.

[76] Carslaw, K, Harrison, R, & Kirkby, J. Cosmic rays, clouds, and climate. *Science* **298**, 1732–1737 (2002). DOI: 10.1126/science.1076964.

[77] Coates, A. J, Wellbrock, A, Lewis, G. R, Jones, G. H, Young, D. T, Crary, F. J, Waite, J. H, Johnson, R. E, Hill, T. W, & Sittler Jr, E. C. Negative ions at Titan and Enceladus: Recent results. *Faraday Discussions* **147**, 293–305 (2010). DOI: 10.1039/c004700g.

[78] Shebanits, O, Wahlund, J.-E, Mandt, K, Ågren, K, Edberg, N. J, & Waite, J. Negative ion densities in the ionosphere of Titan–Cassini RPWS/LP results. *Planetary and Space Science* **84**, 153–162 (2013). DOI: 10.1016/j.pss.2013.05.021.

[79] Wellbrock, A, Coates, A. J, Jones, G. H, Lewis, G. R, & Waite, J. Cassini CAPS-ELS observations of negative ions in Titan's ionosphere: Trends of density with altitude. *Geophysical Research Letters* **40**, 4481–4485 (2013). DOI: 10.1002/grl.50751.

[80] Wang, P & Anderko, A. Computation of dielectric constants of solvent mixtures and electrolyte solutions. *Fluid Phase Equilibria* **186**, 103–122 (2001). DOI: 10.1016/S0378-3812(01)00507-6.

[81] Khain, A, Arkhipov, V, Pinsky, M, Feldman, Y, & Ryabov, Y. Rain enhancement and fog elimination by seeding with charged droplets. Part I: Theory and numerical simulations. *Journal of Applied Meteorology* **43**, 1513–1529 (2004). DOI: 10.1175/JAM2131.1.

[82] Liu, S, Kurth, D. G, Bredenkötter, B, & Volkmer, D. The structure of self-assembled multilayers with polyoxometalate nanoclusters. *Journal of the American Chemical Society* **124**, 12279–12287 (2002). DOI: 10.1021/ja026946l.

[83] Verveniotis, E, Kromka, A, Ledinskỳ, M, Čermák, J, & Rezek, B. Guided assembly of nanoparticles on electrostatically charged nanocrystalline diamond thin films. *Nanoscale Research Letters* **6**, 1–6 (2011). DOI: 10.1186/1556-276X-6-144.

[84] Yin, P, Li, D, & Liu, T. Solution behaviors and self-assembly of polyoxometalates as models of macroions and amphiphilic polyoxometalate–organic hybrids as novel surfactants. *Chemical Society Reviews* **41**, 7368–7383 (2012). DOI: 10.1039/c2cs35176e.

[85] Stace, A. J, Boatwright, A. L, Khachatourian, A, & Bichoutskaia, E. Why like-charged particles of dielectric materials can be attracted to one another. *Journal of Colloid and Interface Science* **354**, 417–420 (2011). DOI: 10.1016/j.jcis.2010.11.030.

[86] Decher, G. Fuzzy nanoassemblies: Toward layered polymeric multicomposites. *Science* **277**, 1232–1237 (1997). DOI: 10.1126/science.277.5330.1232.

[87] Hyeon, T. Chemical synthesis of magnetic nanoparticles. *Chemical Communications* **8**, 927–934 (2003). DOI: 10.1039/B207789B.

[88] Yin, Y & Alivisatos, A. P. Colloidal nanocrystal synthesis and the organic-inorganic interface. *Nature* **437**, 664–670 (2005). DOI: 10.1038/nature04165.

[89] Tettey, K. E, Yee, M. Q, & Lee, D. Layer-by-layer assembly of charged particles in nonpolar media. *Langmuir* **26**, 9974–9980 (2010). DOI: 10.1021/la1000655.

[90] Murray, C. B, Kagan, C, & Bawendi, M. Synthesis and characterization of monodisperse nanocrystals and close-packed nanocrystal assemblies. *Annual Review of Materials Science* **30**, 545–610 (2000). DOI: 10.1146/annurev.matsci.30.1.545.

[91] Bishop, K. J, Wilmer, C. E, Soh, S, & Grzybowski, B. A. Nanoscale forces and their uses in self-assembly. *Small* **5**, 1600–1630 (2009). DOI: 10.1002/smll.200900358.

[92] Caruso, F, Lichtenfeld, H, Giersig, M, & Möhwald, H. Electrostatic self-assembly of silica nanoparticle-polyelectrolyte multilayers on polystyrene latex particles. *Journal of the American Chemical Society* **120**, 8523–8524 (1998). DOI: 10.1021/ja9815024.

[93] Smoukov, S. K, Bishop, K. J, Kowalczyk, B, Kalsin, A. M, & Grzybowski, B. A. Electrostatically "patchy" coatings via cooperative adsorption of charged nanoparticles. *Journal of the American Chemical Society* **129**, 15623–15630 (2007). DOI: 10.1021/ja075456w.

[94] Walker, D. A, Kowalczyk, B, de La Cruz, M. O, & Grzybowski, B. A. Electrostatics at the nanoscale. *Nanoscale* **3**, 1316–1344 (2011). DOI: 10.1039/C0NR00698J.

[95] Lee, H, You, S, Pikhitsa, P. V, Kim, J, Kwon, S, Woo, C. G, & Choi, M. Three-dimensional assembly of nanoparticles from charged aerosols. *Nano Letters* **11**, 119–124 (2011). DOI: 10.1021/nl103787k.

[96] Fudouzi, H, Kobayashi, M, & Shinya, N. Site-controlled deposition of microsized particles using an electrostatic assembly. *Advanced Materials* **14**, 1649–1652 (2002). DOI: 10.1002/1521-4095(20021118)14:22<1649::AID-ADMA1649>3.0.CO;2-Z.

[97] Grzybowski, B. A, Winkleman, A, Wiles, J. A, Brumer, Y, & Whitesides, G. M. Electrostatic self-assembly of macroscopic crystals using contact electrification. *Nature Materials* **2**, 241–245 (2003). DOI: 10.1038/nmat860.

[98] Borges, J. a & Mano, J. a. F. Molecular interactions driving the layer-by-layer assembly of multilayers. *Chemical Reviews* **114**, 8883–8942 (2014). DOI: 10.1021/cr400531v.

[99] Tien, J, Terfort, A, & Whitesides, G. M. Microfabrication through electrostatic self-assembly. *Langmuir* **13**, 5349–5355 (1997). DOI: 10.1021/la970454i.

[100] Serizawa, T, Hamada, K.-i, Kitayama, T, Fujimoto, N, Hatada, K, & Akashi, M. Stepwise stereocomplex assembly of stereoregular poly (methyl methacrylate)s on a substrate. *Journal of the American Chemical Society* **122**, 1891–1899 (2000). DOI: 10.1021/ja9913535.

[101] Tang, J, Li, X.-Y, Wu, H, Ren, L.-J, Zhang, Y.-Q, Yao, H.-X, Hu, M.-B, & Wang, W. Tube-graft-sheet nano-objects created by a stepwise self-assembly of polymer-polyoxometalate hybrids. *Langmuir* **32**, 460–467 (2016). DOI: 10.1021/acs.langmuir.5b04504.

[102] Liu, S, Kurth, D. G, Möhwald, H, & Volkmer, D. A thin-film electrochromic device based on a polyoxometalate cluster. *Advanced Materials* **14**, 225 (2002). DOI: 10.1002/1521-4095(20020205)14:3<225::AID-ADMA225>3.0.CO;2-F.

[103] Proust, A, Matt, B, Villanneau, R, Guillemot, G, Gouzerh, P, & Izzet, G. Functionalization and post-functionalization: A step towards polyoxometalate-based materials. *Chemical Society Reviews* **41**, 7605–7622 (2012). DOI: 10.1039/C2CS35119F.

[104] Durstock, M. F & Rubner, M. F. Dielectric properties of polyelectrolyte multilayers. *Langmuir* **17**, 7865–7872 (2001). DOI: 10.1021/la010954i.

[105] Robertson, J. High dielectric constant oxides. *European Physical Journal Applied Physics* **28**, 265–291 (2004). DOI: 10.1051/epjap:2004206.

[106] Xia, Y, Nguyen, T. D, Yang, M, Lee, B, Santos, A, Podsiadlo, P, Tang, Z, Glotzer, S. C, & Kotov, N. A. Self-assembly of self-limiting monodisperse supraparticles from polydisperse nanoparticles. *Nature Nanotechnology* **6**, 580–587 (2011). DOI: 10.1038/nnano.2011.121.

[107] Schoeler, B, Kumaraswamy, G, & Caruso, F. Investigation of the influence of polyelectrolyte charge density on the growth of multilayer thin films prepared by the layer-by-layer technique. *Macromolecules* **35**, 889–897 (2002). DOI: 10.1021/ma011349p.

[108] Hoogeveen, N. G, Cohen Stuart, M. A, Fleer, G. J, & Böhmer, M. R. Formation and stability of multilayers of polyelectrolytes. *Langmuir* **12**, 3675–3681 (1996). DOI: 10.1021/la951574y.

[109] Serizawa, T, Kamimura, S, & Akashi, M. Electrostatic adsorption of polystyrene particles with different surface charges onto the surface of an ultrathin polymer film. *Colloids and Surfaces A: Physicochemical and Engineering Aspects* **164**, 237–245 (2000). DOI: 10.1016/S0927-7757(99)00399-4.

[110] Brunner, M, Dobnikar, J, von Grünberg, H.-H, & Bechinger, C. Direct measurement of three-body interactions amongst charged colloids. *Physical Review Letters* **92**, 078301 (2004). DOI: 10.1103/PhysRevLett.92.078301.

[111] Shevchenko, E. V, Talapin, D. V, Kotov, N. A, O'Brien, S, & Murray, C. B. Structural diversity in binary nanoparticle superlattices. *Nature* **439**, 55–59 (2006). DOI: 10.1038/nature04414.

[112] Qin, J, Li, J, Lee, V, Jaeger, H, de Pablo, J. J, & Freed, K. F. A theory of interactions between polarizable dielectric spheres. *Journal of Colloid and Interface Science* **469**, 237–241 (2016). DOI: 10.1016/j.jcis.2016.02.033.

[113] Metzger, P. T & Lane, J. E. Electric potential due to a system of conducting spheres. *The Open Applied Physics Journal* **2**, 32–48 (2009). DOI: 10.2174/1874183500902010032.

[114] Kemp, B & Whitney, J. Electrostatic adhesion of multiple non-uniformly charged dielectric particles. *Journal of Applied Physics* **113**, 044903 (2013). DOI: 10.1063/1.4789014.

[115] Clercx, H & Bossis, G. Many-body electrostatic interactions in electrorheological fluids. *Physical Review E* **48**, 2721 (1993). DOI: 10.1103/PhysRevE.48.2721.

[116] Cancès, E. Integral equation approaches for continuum models (2008) in *Continuum solvation models in chemical physics: From theory to applications*, eds. Mennucci, B & Cammi, R. (John Wiley Sons, Chichester), pp. 29–48.

[117] Cancès, E, Maday, Y, & Stamm, B. Domain decomposition for implicit solvation models. *Journal of Chemical Physics* **139**, 054111 (2013). DOI: 10.1063/1.4816767.

[118] Lebedev, V & Laikov, D. A quadrature formula for the sphere of the 131st algebraic order of accuracy. *Doklady Mathematics* **59**, 477–481 (1999).

[119] Stone, A. J. (2013) *The theory of intermolecular forces.* (Oxford, Oxford), 2nd edition.

[120] Atkins, P & de Paula, J. (2010) *Physical chemistry.* (W. H. Freeman, New York, NY), 9th edition.

[121] House, J. E. (2013) *Inorganic chemistry.* (Academic Press, London), 2nd edition.

[122] Haynes, W. M. Ionic radii in crystals (2016) in *CRC Handbook of Chemistry and Physics*, ed. Haynes, W. M. (CRC Press/Taylor & Francis, Boca Raton, FL), 97th edition, pp. 12–13.

[123] Housecroft, C. E & Sharpe, A. G. (2005) *Inorganic chemistry.* (Pearson, Harlow), 2nd edition.

[124] Jenkins, H. D. B & Roobottom, H. K. Lattice energies (2016) in *CRC Handbook of Chemistry and Physics*, ed. Haynes, W. M. (CRC Press/Taylor & Francis, Boca Raton, FL), 97th edition, pp. 21–33.

[125] Haynes, W. M. The madelung constant and crystal lattice energy (2016) in *CRC Handbook of Chemistry and Physics*, ed. Haynes, W. M. (CRC Press/Taylor & Francis, Boca Raton, FL), 97th edition, p. 34.

[126] McCarty, L. S, Winkleman, A, & Whitesides, G. M. Electrostatic self-assembly of polystyrene microspheres by using chemically directed contact electrification. *Angewandte Chemie International Edition* **46**, 206–209 (2007). DOI: 10.1002/anie.200602914.

[127] Wohlfarth, C. Permittivity (dielectric constant) of selected polymers (2016) in *CRC Handbook of Chemistry and Physics*, ed. Haynes, W. M. (CRC Press/Taylor & Francis, Boca Raton, FL), 97th edition, p. 17.

[128] Mazur, E. (2014) *The principles and practice of physics.* (Pearson, New York, NY), 1st edition.

[129] Feynman, R. P, Leighton, R. B, & Sands, M. L. (1964) *The Feynman lectures on physics: Mainly mechanics, radiation, and heat.* (Addison-Wesley, Reading, MA) Vol. 1, 1st edition.

[130] Press, W. H, Teukolsky, S. A, Vetterling, W. T, & Flannery, B. P. (1992) *Numerical recipes in Fortran 77: The art of scientific computing.* (Cambridge University Press, Cambridge), 2nd edition.

[131] Frederikse, H. P. R. Permittivity (dielectric constant) of inorganic solids (2016) in *CRC Handbook of Chemistry and Physics*, ed. Haynes, W. M. (CRC Press/Taylor & Francis, Boca Raton, FL), 97th edition, pp. 47–55.

[132] Haynes, W. M. Density of various solids (2016) in *CRC Handbook of Chemistry and Physics*, ed. Haynes, W. M. (CRC Press/Taylor & Francis, Boca Raton, FL), 97th edition, p. 39.

[133] Derbenev, I. N, Filippov, A. V, Stace, A. J, & Besley, E. Electrostatic interactions between charged dielectric particles in an electrolyte solution. *Journal of Chemical Physics* **145**, 084103 (2016). DOI: 10.1063/1.4961091.

[134] Wolfram Research, Inc. Mathematica. (2016). (Champaign, IL), 10.4 edition.

[135] Wolfram Research, Inc. Wolfram Language & System: Documentation center. (2017).

[136] The MathWorks, Inc. Matlab. (2016). (Natick, MA), R2016b edition.

Appendix A

A.1 Matrix solution for the multipole moment coefficients

Equations 2.14 and 2.15 can be rewritten in the following form:

$$4\pi K a_1 \sigma_{f,1} \delta_{l,0} = \tilde{A}_{1,l} + \frac{(k_1 - 1)l}{(k_1 + 1)l + 1} \sum_{m=0}^{N} \tilde{A}_{2,m} \frac{(l+m)!}{l!\, m!} \frac{a_1^l a_2^{m+1}}{h^{l+m+1}}, \tag{A.1}$$

$$4\pi K a_2 \sigma_{f,2} \delta_{l,0} = \tilde{A}_{2,l} + \frac{(k_2 - 1)l}{(k_2 + 1)l + 1} \sum_{m=0}^{N} \tilde{A}_{1,m} \frac{(l+m)!}{l!\, m!} \frac{a_2^l a_1^{m+1}}{h^{l+m+1}}, \tag{A.2}$$

where

$$\tilde{A}_{i,(l \vee m)} = \frac{A_{i,(l \vee m)}}{a_i^{(l \vee m)+1}} \qquad (i = 1, 2), \tag{A.3}$$

which allows Equations A.1 and A.2 to be represented in matrix notation as:

$$b_1 = \tilde{C}_1 \tilde{A}_1 + \tilde{D}_1 \tilde{A}_2, \tag{A.4}$$

and

$$b_2 = \tilde{D}_2 \tilde{A}_1 + \tilde{C}_2 \tilde{A}_2, \tag{A.5}$$

where

$$\begin{aligned}(b_i) &= 4\pi K a_i \sigma_{f,i} \delta_{l,0},\\ (\tilde{C}_i)_{l,m} &= \delta_{l,m},\\ (\tilde{D}_i)_{l,m} &= \frac{a_j}{h}\frac{(k_i-1)l}{(k_i+1)l+1}\frac{(l+m)!}{l!\,m!}\left(\frac{a_i}{h}\right)^l\left(\frac{a_j}{h}\right)^m\\ &= \frac{a_j}{h}\frac{(k_i-1)l}{(k_i+1)l+1}(\tilde{d}_i)_{l,m},\end{aligned} \tag{A.6}$$

$$\text{and} \quad (\tilde{d}_i)_{l,m} = \frac{(l+m)!}{l!\,m!}\left(\frac{a_i}{h}\right)^l\left(\frac{a_j}{h}\right)^m.$$

Equation A.5 can be rearranged to give

$$\tilde{A}_2 = \tilde{C}_2^{-1}\left(b_2 - \tilde{D}_2\tilde{A}_1\right), \tag{A.7}$$

which can then be substituted into Equation A.4 resulting in

$$b_1 = \tilde{C}_1\tilde{A}_1 + \tilde{D}_1\left[\tilde{C}_2^{-1}(b_2 - \tilde{D}_2\tilde{A}_1)\right]. \tag{A.8}$$

Similarly, Equation A.4 can also be rearranged, giving

$$\tilde{A}_1 = \tilde{C}_1^{-1}\left(b_1 - \tilde{D}_1\tilde{A}_2\right), \tag{A.9}$$

which can then be substituted into Equation A.5 resulting in

$$b_2 = \tilde{C}_2\tilde{A}_2 + \tilde{D}_2\left[\tilde{C}_1^{-1}(b_1 - \tilde{D}_1\tilde{A}_2)\right]. \tag{A.10}$$

From Equation A.8, the multipole moment coefficient for sphere 1 when $l = 0$ is

$$\tilde{A}_{1,0} = b_1 = 4\pi K a_1 \sigma_{f,1} = \frac{Kq_1}{a_1}. \tag{A.11}$$

Similarly, from Equation A.10, the multipole moment coefficient for sphere 2 when $l = 0$ is

$$\tilde{A}_{2,0} = b_2 = 4\pi K a_2 \sigma_{f,2} = V_2 = \frac{K q_2}{a_2}. \tag{A.12}$$

Now, when $l > 0$ the Kronecker delta function makes $b_1 = 0$, so that Equation A.4 gives

$$b_1 = \tilde{C}_1 \tilde{A}_1 + \tilde{D}_1 \tilde{A}_2 = 0. \tag{A.13}$$

Substituting the expressions for $\tilde{C}_1$ and $\tilde{D}_1$, as given by Equation A.6, on Eq. A.13 gives

$$\delta_{l,m} \cdot \tilde{A}_{1,l} + \left(\frac{a_2}{h} \frac{(k_1 - 1)l}{(k_1 + 1)l + 1} \right) \sum_{m=0}^{N} \tilde{d}_{1_{lm}} \tilde{A}_{2,m} = 0. \tag{A.14}$$

The first term inside the summation is known and therefore can be isolated in the right-hand side of the equation:

$$\frac{1}{\left(\frac{a_2}{h} \frac{(k_1 - 1)l}{(k_1 + 1)l + 1} \right)} \delta_{l,m} \cdot \tilde{A}_{1,l} + \sum_{m=1}^{N} \tilde{d}_{1_{lm}} \tilde{A}_{2,m} = -\tilde{d}_{1_{l0}} \tilde{A}_{2,0}. \tag{A.15}$$

Similarly, when $l > 0$ the delta function makes $b_2 = 0$, so that Eq. A.5 gives

$$b_2 = \tilde{D}_2 \tilde{A}_1 + \tilde{C}_2 \tilde{A}_2 = 0. \tag{A.16}$$

Substituting the expressions for $\tilde{C}_1$ and $\tilde{D}_1$ on Eq. A.16 gives

$$\delta_{l,m} \cdot \tilde{A}_{2,m} + \left(\frac{a_1}{h} \frac{(k_2 - 1)l}{(k_2 + 1)l + 1} \right) \sum_{m=0}^{N} \tilde{d}_{2_{lm}} \tilde{A}_{1,l} = 0. \tag{A.17}$$

Isolating the first term in the summation (which is also known) in the right-hand side of the equation gives

$$\frac{1}{\left(\frac{a_1}{h} \frac{(k_2 - 1)l}{(k_2 + 1)l + 1} \right)} \delta_{l,m} \cdot \tilde{A}_{2,m} + \sum_{m=1}^{N} \tilde{d}_{2_{lm}} \tilde{A}_{1,l} = -\tilde{d}_{2_{0m}} \tilde{A}_{1,0}. \tag{A.18}$$

Equations A.15 and Eq. A.18 can then be written in the following matrix form:

$$\begin{pmatrix} \dfrac{1}{\left(\dfrac{a_2}{h}\dfrac{(k_1-1)l}{(k_1+1)l+1}\right)}\delta_{l,m} & \tilde{d}_{1_{lm}} \\ \tilde{d}_{2_{lm}} & \dfrac{1}{\left(\dfrac{a_1}{h}\dfrac{(k_2-1)l}{(k_2+1)l+1}\right)}\delta_{l,m} \end{pmatrix} \cdot \begin{pmatrix} \tilde{A}_{1,l} \\ \tilde{A}_{2,m} \end{pmatrix} \tag{A.19}$$

$$= \begin{pmatrix} -\tilde{d}_{1_{l0}}\tilde{A}_{2,0} \\ -\tilde{d}_{2_{0m}}\tilde{A}_{1,0} \end{pmatrix},$$

which consists of a system of linear equations $A\,x = b$ that can be solved by iterative methods. As $\tilde{d}_{2_{lm}}$ is the transpose of $\tilde{d}_{1_{lm}}$, the block matrix is symmetric with respect to the main diagonal. Besides that, the block matrix is also positive-definite, which makes it suitable to be efficiently solved by the conjugate gradient method. Once all elements of the column vector x are determined, then it's straightforward to obtain the multipole coefficients for each sphere through Equation A.3.

Equation A.20 illustrates the general case of the linear system that is Equation A.19, when the series expansion in Equation 2.16 needs to be evaluated to an upper value of $N = 2$.

$$\begin{pmatrix} \frac{h\,(2+k_1)}{a_2\,(-1+k_1)} & 0 & \frac{2a_1a_2}{h^2} & \frac{3a_1a_2^2}{h^3} \\ 0 & \frac{h\,(1+2\,(1+k_1))}{2a_2\,(-1+k_1)} & \frac{3a_1^2a_2}{h^3} & \frac{6a_1^2a_2^2}{h^4} \\ \frac{2a_1a_2}{h^2} & \frac{3a_1^2a_2}{h^3} & \frac{h\,(2+k_2)}{a_1\,(-1+k_2)} & 0 \\ \frac{3a_1a_2^2}{h^3} & \frac{6a_1^2a_2^2}{h^4} & 0 & \frac{h\,(1+2\,(1+k_2))}{2a_1\,(-1+k_2)} \end{pmatrix} \cdot \begin{pmatrix} \tilde{A}_{1,1} \\ \tilde{A}_{1,2} \\ \tilde{A}_{2,1} \\ \tilde{A}_{2,2} \end{pmatrix}$$

$$= \begin{pmatrix} -\frac{Ka_1q_2}{h\,a_2} \\ -\frac{Ka_1^2q_2}{h^2a_2} \\ -\frac{Ka_2q_1}{h\,a_1} \\ -\frac{Ka_2^2q_1}{h^2a_1} \end{pmatrix} \tag{A.20}$$

A.2 Benchmark of the two-body formalism related computer program

The two-body formalism [37] has been implemented in *Mathematica* [134] and the performance of the code is presented next, particularly with respect to its scaling properties as function of the number of terms N in the multipole expansion of Equation 2.16, and the computation time to build and solve the linear system, i.e. Equation A.19. All timing calculations have been performed on a single desktop-class computer, with an Intel Core i7-3820@3.60 GHz processor, 16 GB of DDR3@1333 MHz, running a Linux based operating system. Since computation time can be sensitive to background activities of the operating system, the calculations were repeated ten times, hence standard deviations are shown as error bars in the resulting figures.

The code can be divided in two main parts:

(i) Computation of the multipole moment coefficients through computation and evaluation of the linear system shown in Equation A.19;

(ii) Evaluation of Equation 2.16.

Part (i) is by far the most computationally expensive and benefits if each expression that is present on it is constructed as compiled functions in the Wolfram Language (the programming language of *Mathematica*), which are then evaluated by the program assuming that all the parameters which appear are numbers (or logical variables). The compilation of a function in *Mathematica* creates an object that contains a sequence of simple instructions for evaluating the compiled function. These instructions are chosen in such a way that they are close to those found in the machine code of a typical computer, and therefore are executed more rapidly. [135] Pre-computation of the factorials present at $\tilde{d}_{i_{lm}}$ $(i = 1, 2)$ (Equation A.6) also helps increasing the performance of the code.

The timing and scaling of the code with respect to the number of terms N are shown in Figure A.1. As can be seen, the code is very efficient, considering in takes less than ten seconds to perform a calculation where $N = 1000$ and that, in most circumstances, a value of N with considerably smaller magnitude is sufficient. Figure A.1 also reveals that the code scales with the number of terms in an approximately quadratic manner, therefore allowing it to be pushed up to higher orders of N as convenient.

Figure A.2 shows a breakdown of the time to build and evaluate the linear system (Equation A.19), in terms of its components, (a)−(g), as defined in the figure. Interestingly, it is shown that the time required to build some elements of the block matrix is greater than the time to solve the actual linear system. One can also note the advantage of such matrix being symmetric, which allows component (d) to be computed very efficiently, since it is just the transpose of component (c), the latter being the most computationally expensive component.

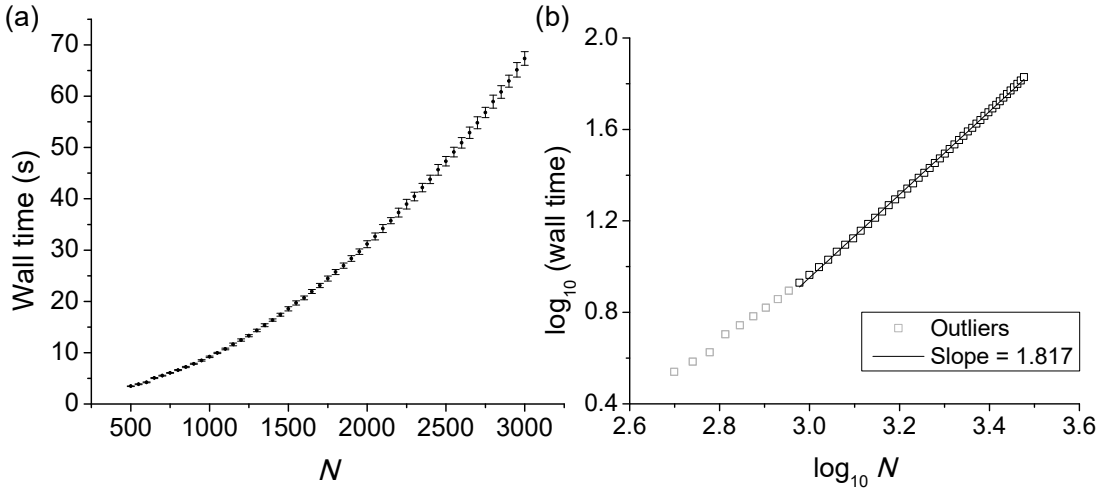
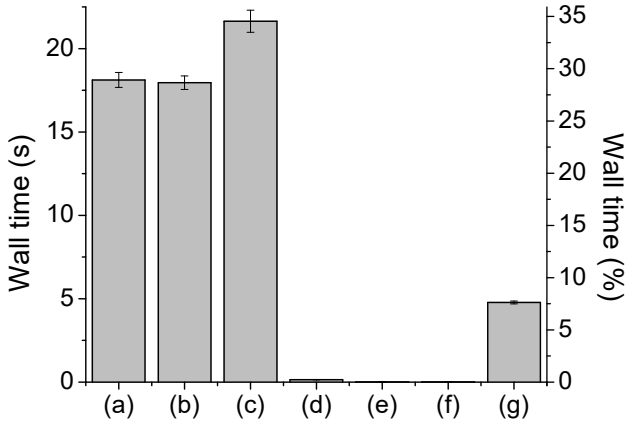


Fig. A.1 (a) Plot of the wall time (s) as function of the number of terms N in the multipole expansion. (b) Equivalent log-log plot, showing the approximately quadratic scaling behaviour.



where

(a) $\dfrac{1}{\dfrac{a_2}{h}\dfrac{(k_1-1)l}{(k_1+1)\,l+1}}\delta_{l,m}$ (b) $\dfrac{1}{\dfrac{a_1}{h}\dfrac{(k_2-1)l}{(k_2+1)\,l+1}}\delta_{l,m}$ (c) $\tilde{d}_{1_{lm}}$ (d) $\tilde{d}_{2_{lm}} = (\tilde{d}_{1_{lm}})^{\mathsf{T}}$

(e) $-\tilde{d}_{1_{l0}}\tilde{A}_{2,0}$ (f) $-\tilde{d}_{2_{0m}}\tilde{A}_{1,0}$ (g) evaluation of the linear system (Equation A.19) using the conjugate gradient method

Fig. A.2 Plot of the wall time (s) to compute each component and solve the linear system (Equation A.19). The y-axis in the right-hand side reflects the percentage of computation time with respect to the total wall time.

Appendix B

B.1 Effective electric dipole moment of a polarised particle

For some examples addressed in Chapter 3, where a neutral dielectric particle interacts with a second object that is charged, the former, under the influence of an electric field generated by latter, becomes polarised, which leads to the appearance of a dipolar distribution of positive and negative bound charge on its surface such that:

$$\int dq_{\mathrm{b}} = \int dq_{\mathrm{b}+} + \int dq_{\mathrm{b}-} = 0.$$

The averages of the position vectors $\mathbf{r}_{\mathrm{b}+}$ and $\mathbf{r}_{\mathrm{b}-}$ of the respective bound charge elements, $dq_{\mathrm{b}+}$ and $dq_{\mathrm{b}-}$, are given by

$$\langle \mathbf{r}_{\mathrm{b}+} \rangle \equiv \frac{\int \mathbf{r}_{\mathrm{b}+}\, dq_{\mathrm{b}+}}{\int dq_{\mathrm{b}+}} = \frac{\int \mathbf{r}_{\mathrm{b}+}\, dq_{\mathrm{b}+}}{\delta q},$$

and

$$\langle \mathbf{r}_{\mathrm{b}-} \rangle \equiv \frac{\int \mathbf{r}_{\mathrm{b}-}\, dq_{\mathrm{b}-}}{\int dq_{\mathrm{b}-}} = \frac{\int \mathbf{r}_{\mathrm{b}-}\, dq_{\mathrm{b}-}}{-\delta q},$$

where

$$\delta q \equiv \int dq_{\mathrm{b}+} = -\int dq_{\mathrm{b}-} \therefore \int dq_{\mathrm{b}-} = -\delta q.$$

By definition, the effective dipole moment on the neutral polarised sphere can be written as:

$$\begin{aligned}\mathbf{p}_{\mathrm{eff}} \equiv \delta q\ [\langle \mathbf{r}_{\mathrm{b}+} \rangle - \langle \mathbf{r}_{\mathrm{b}-} \rangle] &= \int \mathbf{r}_{\mathrm{b}+} dq_{\mathrm{b}+} + \int \mathbf{r}_{\mathrm{b}-} dq_{\mathrm{b}-} \\ &= \int \mathbf{r}_{\mathrm{b}} dq_{\mathrm{b}}.\end{aligned}$$

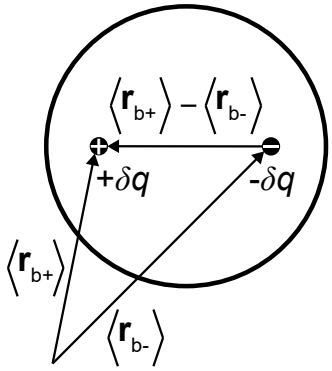


Fig. B.1 Geometric representation of the various relevant quantities to the calculation of the effective dipole moment of a polarised spherical particle.

With the origin of the spherical coordinate system at the center of the sphere, positions at the surface of the sphere are defined as follows: $r = a_s$ (sphere radius), $\theta \in \{0, \pi\}$ and $\varphi \in \{0, 2\pi\}$. For a bound charge element $dq_{\mathrm{b}} = \sigma_{\mathrm{b}} dS$, where σ_{b} is the surface bound charge density and $dS = a_s^2\ \sin\theta\, d\theta\, d\varphi$ is the surface element, an effective dipole moment on the polarised sphere can be derived as follows:

$$\begin{aligned}\mathbf{p}_{\text{eff}} &= \int r_{\text{b}} dq_{\text{b}} \\ &= a_s^3 \left[\int_{\varphi=0}^{\varphi=2\pi} \int_{\theta=0}^{\theta=\pi} \sigma_{\text{b}}(\theta,\varphi) \sin\theta \cos\theta \, d\theta \, d\varphi \, \hat{\mathbf{k}} \right. \\ &+ \int_{\varphi=0}^{\varphi=2\pi} \int_{\theta=0}^{\theta=\pi} \sigma_{\text{b}}(\theta,\varphi) \sin^2 d\theta \cos\varphi \, d\varphi \, \hat{\mathbf{i}} \\ &\left. + \int_{\varphi=0}^{\varphi=2\pi} \int_{\theta=0}^{\theta=\pi} \sigma_{\text{b}}(\theta,\varphi) \sin^2 d\theta \cos\varphi \, d\varphi \, \hat{\mathbf{j}} \right].\end{aligned} \tag{B.1}$$

The azimuthal symmetry inherent in this two-body problem allows a cancellation of the dependence of surface-bound charge density on the azimuthal angle φ, such that the second and third terms inside the brackets in Equation B.1 become zero and the expression for the effective dipole moment can be simplified to

$$\begin{aligned}\mathbf{p}_{\text{eff}} &= a_s^3 \int_{\theta=0}^{\theta=\pi} \sigma_{\text{b}}(\theta) \sin\theta \cos\theta \, d\theta \int_{\varphi=0}^{\varphi=2\pi} d\varphi \, \hat{\mathbf{k}} \\ &= 2\pi a_s^3 \int_{\theta=0}^{\theta=\pi} \sigma_{\text{b}}(\theta) \sin\theta \cos\theta \, d\theta \, \hat{\mathbf{k}}.\end{aligned} \tag{B.2}$$

Accordingly, the effective polarisation (dipole moment per unit volume) can then be defined as

$$\mathbf{P}_{\text{eff}} \equiv \frac{3}{4} \frac{\mathbf{p}_{\text{eff}}}{\pi a_s^3} = \frac{3}{2} \int_{\theta=0}^{\theta=\pi} \sigma_{\text{b}}(\theta) \sin\theta \cos\theta \, d\theta \, \hat{\mathbf{k}}. \tag{B.3}$$

Appendix C

C.1 Benchmark of the many-body formalism related computer program

The new solution to the problem of calculating electrostatic interactions in many-body system, briefly introduced in Chapter 4, has been implemented in a *Matlab* [136] code and the performance of the latter is presented next, particularly with respect to its scaling properties as function of the number of particles M in the system and the degree of spherical harmonics N utilized in the truncated series. In a similar way to the benchmark of the two-body formalism code, all timing calculations, performed on a single desktop-class computer with an Intel Core i7-3820@3.60 GHz processor, 16 GB of DDR3@1333 MHz, were repeated ten times, hence standard deviations are shown as error bars in the resulting figures.

In order to address the behaviour of the code with respect to the number of particles, initially a system that grows linearly with the progressive addition of identical particles is considered, and the corresponding results are plotted in Figure C.1. As can be seen from Figure C.1(a), it is clear that the calculation of systems with a large number of particles benefits from the implementation of the fast multipole method (FMM). When the number of particles is sufficiently small, the calculation that does not implement the FMM performs better. However, as the number of particles in the system increases, a crossover between the two curves happens at about $M = 50$ (for this particular example), and the FMM calculation

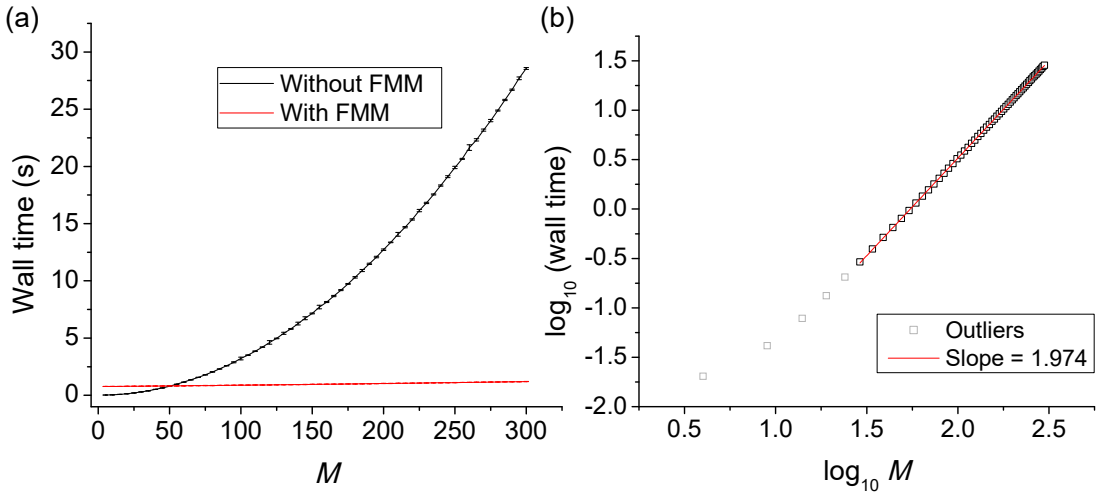


Fig. C.1 (a) Plot of the wall time (s) as function of the number of particles M in the system. Although visually indistinguishable, the elapsed time in the FMM calculation varies from ≈ 0.8 to 1.2 seconds. (b) Log-log plot of the calculation performed without the FMM, showing its quadratic scaling profile.

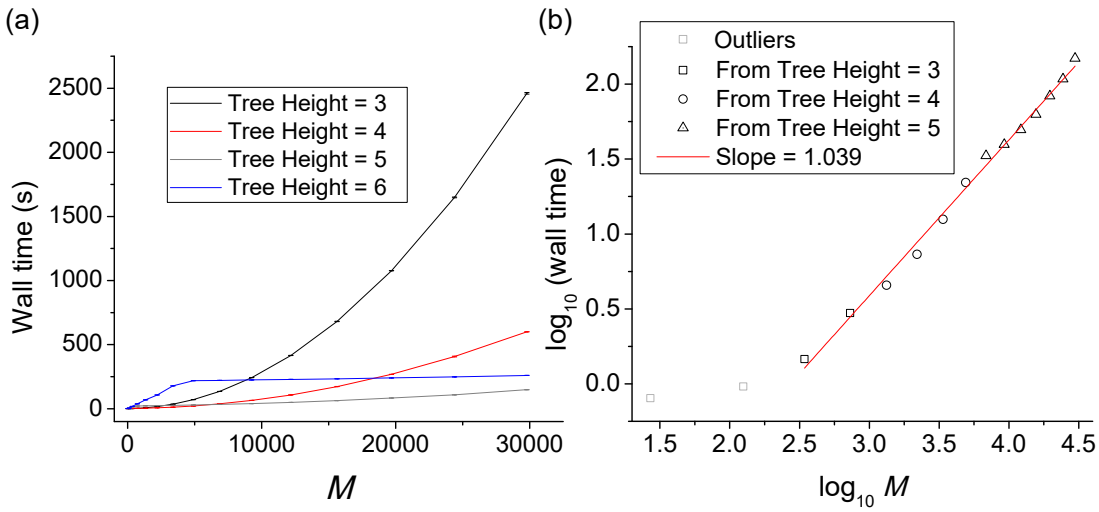


Fig. C.2 (a) Plot of the wall time (s) as function of the number of particles M in the system, for various curves representing different Tree Heights in the FMM calculation. (b) Log-log plot of the piecewise composition of parabolic profiles, each corresponding to a particular value of Tree Height, showing that a regular effective linear scaling can be obtained.

becomes the fastest. Figure C.1(b) shows that the calculation scales quadratically when FMM is not used. In fact, the FMM calculations also scales quadratically, but an approximately linear scaling in computational cost can be achieved, by adapting the Tree Height[1] to the magnitude of M. Accordingly, a quasi-linear

[1]In the FMM, particles are distributed in small boxes that belong to the finest level of an oct-tree. When the number of particles in such boxes increases, the calculation presents an asymptotically quadratic scaling behaviour.

curve that is in reality a piecewise composition of parabolic (quadratic) profiles, each corresponding to a different Tree Height, can be obtained. To illustrate this fact, consider next a system that assumes the halite cubic structure of sodium chloride, where each positive particle is surrounded by six negative particles and vice versa. For simplicity, the particles were made identical with regard to their dielectric constant, size and charge magnitudes. As shown in Figure C.2(a), each level of Tree Height performs best at a particular segment of the graph, being surpassed by the next level when the magnitude of M has increased sufficiently. Figure C.2(b) shows then the quasi-linear curve obtained by combining each segment, calculated with the optimum corresponding Tree Height.

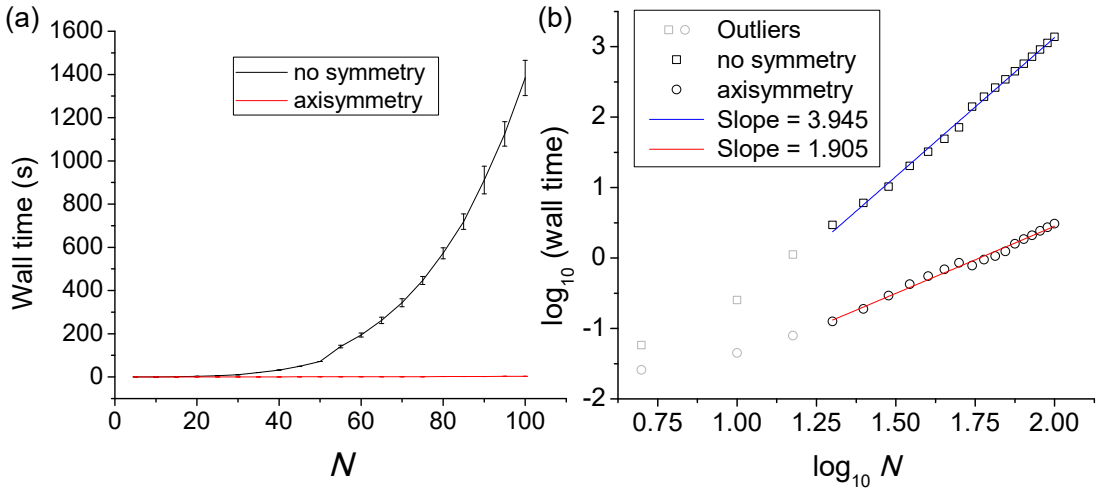


Fig. C.3 (a) Plot of the wall time (s) as function of the degree of spherical harmonics N utilized in the truncated series. Although visually indistinguishable, the elapsed time in the axisymmetric calculation varies from ≈ 0.03 to 3 seconds. (b) Log-log plot of both curves, showing that an imposition of symmetry reduces the scaling profile from $\approx N^4$ to N^2.

The behaviour of the code with respect to the degree of spherical harmonics N utilized in the truncated series is accessed in Figure C.3, where the case portrayed in Figure 4.2 is considered. Since this particular case exhibits a perfect linear geometry, an additional simplication can be imposed from the azimuthal symmetry of the system, which is that the spherical harmonics $Y_l^m{}_{(l\in N,\,-l\leq m\leq l)}(\beta,\varphi)$ utilized in the truncated series present no φ-dependance so that $m=0$. For the majority of problems, however, this later simplication cannot be made and the full set

of spherical harmonics needs to be considered. As shown in Figure C.3(a), the calculation where the axisymmetric simplication is adopted is considerably faster. Moreover, while the the calculation where the full set of spherical harmonics is applied scales as N^4, the use of symmetry reduces it to a quadratic scaling, as shown in Figure C.3(b). In absolute terms, the use of high orders of spherical harmonics inevitably causes the code to run considerably slower, especially when no symmetry can be imposed. However, the situations where the use of such high orders are necessary are, in fact, limited. It has already been shown for two-body systems, more specifically at Section 2.6, how the necessary number of terms in a truncated series generally depends on parameters of the system, namely the particles's dielectric constant, charge and radius, and the inter-particle separation distance. The conclusions drawn from this investigation can actually be extrapolated to a many-body system, if one takes into account each pairwise interaction separately.